UGAMP Newsletter

UGAMP: A network of excellence in climate modelling and research

Issue 27
October 2003

UGAMP Coordinator:
Prof. Julia Slingo

J.M.Slingo@rdg.ac.uk

Newsletter Editor:
Dr. Glenn Carver

Glenn.Carver@atm.ch.cam.ac.uk

Newsletter website:

acmsu.nerc.ac.uk/newsletter.html

Contents

(for full contents see listing on
the inside back cover)

NERC Centres for Atmospheric Science, NCAS

Alan Thorpe (a.j.thorpe@reading.ac.uk): Director NCAS

Since the last UGAMP Newsletter there have been a significant number of NCAS developments relevant to the UK atmospheric science community. These include the following, which are particularly pertinent to the UGAMP community:

- NERC have agreed to fund a new directed (new name for thematic) programme called "Surface Ocean – Lower Atmosphere Study" or SOLAS for short.

- NERC have agreed to fund a "pump-priming" activity for a proposed new directed programme called Flood Risk from Extreme Events, FREE. The full proposal for FREE will be considered by NERC early in 2004.

- NCAS is supporting a project to develop a new chemistry module for the HadGEM model. This is called UK-CHEM and Olaf Morgenstern at ACMSU is collaborating closely with the Hadley Centre on the project.

- NCAS is supporting a project to develop the science for a new aerosol module for HadGEM. This is being led by Ken Carslaw at Leeds and is in collaboration with the Hadley Centre.

- NCAS supported an experts workshop on Future Chemical Threats at the Royal Society in February and on Earth System Modelling at Cambridge in October. There are further workshops planned on Aerosols in global models and on Convection over the next few months.

- The RMS Conference 2003 at UEA attracted 415 attendees and in my view it was an excellent start to what I hope will be a long-standing and important conference series bringing together the whole atmospheric science community on a biennial basis.

- A group of 34 universities and allied organizations became NCAS Affiliated Institutions this year and representatives held the first of regular annual meetings to discuss the development of atmospheric science in the academic sector in the UK. Hopefully your university is an Affiliated Institution and please get to know who the lead and deputy contact people are so that you can input your views on the development of NCAS at the appropriate times.

- A draft of the Atmospheric Science Strategy that underpins NCAS research has been circulated widely for consultation. Comments on the Strategy are welcomed, preferably by end of October. This Strategy will be the back-drop to forming the proposal to NERC for funding for NCAS from April 2006 onwards. This proposal will be submitted in October 2004 for final consideration by NERC in February 2005.

- I'm sure Julia Slingo will be describing the Earth Simulator initiative elsewhere in the newsletter. This is an exciting opportunity which as well as its great potential for promoting UK-Japan collaboration is strongly supported by the Government Chief Scientific Adviser, the Director-General of the Research Councils and by NERC.

- There are many challenges ahead for the UGAMP community. Not least amongst these is continued access to sufficient high performance computing for climate modelling. I would also mention how important I think it is that we develop further the good collaboration with the Hadley Centre. It is also worth noting that UGAMP can play a central role within NERC in the developing use of Earth System models. Given the breath of processes that have to be represented in such models, the need for our interaction and collaboration with scientists right across the NERC community has never been stronger. The new NERC programme QUEST is a good opportunity for UGAMP to be centrally involved in the modelling aspects.

- Some NCAS research studentships have been advertised for the academic community to bid for. This emphasizes the importance we need to place on bringing the best students into atmospheric science research. The deadline for submission of proposal by supervisors is 21 November 2003.

- The NCAS Management Group of directors and heads of NCAS centres and facilities had their most recent meeting by Access Grid. This involved people located at the University of Leeds, Cambridge and Reading and at RAL. Increasingly universities are installing Access Grid facilities and it seems to be an effective way to have meetings and scientific interactions minimizing travel time and costs.

NCAS Centres and Facilities

CGAM:	Centre for Global Atmospheric Modelling – Climate processes
ACMSU:	Atmospheric Chemistry Modelling Support Unit – Chemistry-climate
UWERN:	Universities Weather Research Network – High-impact weather
DIAC:	Distributed Institute for Atmospheric Composition – Chemistry/physics of composition
BADC:	British Atmospheric Data Centre
UFAM:	University Facilities for Atmospheric Measurement – Ground based observations
FAAM:	Facility for Airborne Atmospheric Measurements – Aircraft observations

Editorial

Glenn Carver (Glenn.Carver@atm.ch.cam.ac.uk), ACMSU, Centre for Atmospheric Science, Dept. of Chemistry, University of Cambridge

This issue of the newsletter is in the main a compilation of posters and presentations from the RMS Conference at UEA in 2003 as well as regularly contributed articles. I'd just like to say a big thank you to everyone who took the time to submit an article for the newsletter. I'd also like to say thank you to Kirsten at CGAM who took a great load off my shoulders for this issue by receiving all the articles, checking them and collating them. I hope everyone enjoys reading this issue of the newsletter.

UGAMP Coordinator

Julia Slingo (J.M.Slingo@rdg.ac.uk), CGAM, Dept. of Meteorology, University of Reading.

Another bumper issue of the UGAMP Newsletter! Thank you to all who contributed and particularly to Glenn Carver for being Editor and Kirsten Wilmer-Becker for her help with bringing it all together.

It is evident from the breadth and depth of the science presented here that UGAMP continues to go from strength to strength. New groups are represented (a welcome to Sheffield University and Grant Bigg, and to Liverpool University and Ric Williams) and we are branching out into new areas of earth system science, in particular with more contributions on ocean processes and their impact on climate. And it's good to see that the new ERA-40 reanalysis, completed earlier this year is already being exploited.

This year we combined the UGAMP annual conference with the RMS National Conference at Norwich. It was an experiment, but one which seems to have worked extremely well. Next year we will have our own meeting, which will be held at Oxford, 8-10 September. UGAMP studentships are again on offer, this time through the wider NCAS scheme. Training the next generation of climate scientists is very important for us, and I'm glad to see so many contributions in this Newsletter from our PhD students.

In the coming year we will be going through a major period of change with new computers and a new model. In December, the T3E (Turing) will be retired from CSAR and we will need to transfer our runs to the SGI machines, including the new SGI Altix (Newton). Earlier this year, the new HPCx/IBM supercomputer came on line, which offers opportunities for running really big experiments. CGAM staff are working hard to ensure that UGAMP codes are ported to both facilities and that we can exploit the power of HPCx (see Jeff Cole and Paul Burton's articles). At the same time as dealing with these computing changes, we are also planning for UGAMP's use of the new Hadley Centre model (HadGEM1) which will be frozen shortly. This has a completely new dynamical core as well as major changes to the physics parametrizations, so we shall have a steep learning curve with this model in the coming months. I hope that the next edition of the Newsletter will feature articles on the performance and use of HadGEM1.

CGAM Director

Julia Slingo (J.M.Slingo@rdg.ac.uk), CGAM, Dept. of Meteorology, University of Reading.

This past year has seen some major changes at CGAM with the appointments of 2 Senior Scientists (Lesley Gray and Jonathan Gregory) and 2 Computational Scientists (Katherine Bouton and Paul Burton). Lesley has already started to revitalise and coordinate the UGAMP middle atmosphere modelling community, whilst Jonathan brings a welcome new focus for us on climate change processes and important links with the glaciology and earth system modelling communities. Jonathan's appointment is joint funded by the Hadley Centre and recognises the close links we have with them. CGAM's Computational Science team, led by Lois Steenman-Clark, is now very strong and beginning to make a real difference in modelling and data support activities. The new CGAM website was launched during the last year, which provides a much improved information service on all aspects of our research and our support for the UGAMP community.

Two important modelling programmes were proposed and funded in the last year which will both lead to major steps forward in the resolution and complexity of our climate models. UK-HiGEM (to develop, evaluate and exploit a high resolution version of HadGEM1) has been funded by NERC as a consortium programme. With partners drawn from across the NERC Centre/Surveys, University groups and the Hadley Centre, UK-HiGEM will be an important step towards a more integrated approach to global environment modelling in the UK. I'm delighted that Warwick Norton (a long term, and valued member of UGAMP) will be the UK-HiGEM Project Manager. The collaboration with the Japanese to use the Earth Simulator for high resolution, earth system modelling has also been formalised this year and we will shortly be recruiting 3 scientists to work on that project. I hope that there will be opportunities for UGAMP scientists to exploit the integrations, as well as to use the Earth Simulator and collaborate with our Japanese colleagues. We'll keep you all posted!

Both UK-HiGEM and the Earth Simulator projects involve a close collaboration with the Hadley Centre. I am delighted that our links with them are stronger than ever and that we have developed excellent working relationships with their scientists. With the establishment of a Hadley Centre Unit at Reading we are looking forward to an even stronger programme of joint research in the coming years.

ACMSU Director

John Pyle (John.Pyle@atm.ch.cam.ac.uk), ACMSU, Centre for Atmospheric Science, Dept. of Chemistry, University of Cambridge.

The main current aims at ACMSU in Cambridge continue to centre around major issues in stratospheric and tropospheric science. Two particular themes are to continue to develop models for process studies, using field data collected by the NERC community, and chemistry-climate studies. Many of these activities are described in more detail in this newsletter.

Glenn Carver, Fiona O'Connor and Nick Savage have developed a high resolution, parallelised version of the tropospheric chemical transport model, named p-TOMCAT. Preliminary runs have included studies at 0.5^o horizontal resolution. Our first scientific investigations with the new model will include a study of the tropical tropopause layer. We hope soon to have a version available for the community.

We are using the Met Office UM with our chemical schemes for tropospheric and stratospheric studies. Recent investigations led by Peter Braesicke, described elsewhere here, include the role of chemistry-climate interactions in the unusual development of ozone depletion in the Antarctic in 2002. Tropospheric studies also concentrate on chemistry-climate interactions. Guang Zeng has recently completed a study of the pre-industrial atmosphere to complement here earlier work looking at the 2100 atmosphere.

Glenn Carver, together with Howard Roscoe at the British Antarctic Survey, organised a very successful meeting in August 2003 on the events surrounding the unusual split ozone hole of the winter of 2002. This meeting was held as a Royal Meteorological Society's Special Interest Group and was well attended with over 60 participants, including a number of attendees from Europe and the US. A particular coup was to have Gloria Manney, from JPL, speak at the meeting as it was her first ever visit to the UK! Glenn and Howard are working on producing a report of this meeting.

A major new NCAS initiative is a collaboration with the Met Office to develop the next generation chemistry-climate model for community use. This will be based on Met Office's new dynamics in HadGEM. Olaf Morgenstern is a new ACMSU member, warmly welcomed back to Cambridge after a stint in Hamburg working with Guy Brasseur, who will be implementing chemistry into this model. The University of Leeds (led by Ken Carslaw and Martyn Chipperfield) are also playing a major role in this initiative, being funded by NCAS to develop aerosol code for the model.

The "New Dynamics" Unified Model is now the first non-hydrostatic climate model (the same model is also used for high-resolution, limited-area integrations) avoiding common approximations like the shallow-atmosphere assumption. Integrating a fully coupled Eulerian troposphere-stratosphere chemistry, the main thrust of the UCHEM project, is a major milestone towards building a comprehensive global environment model. Given the possibly large computational cost associated with atmospheric chemistry, we aim to provide ready-made schemes at different levels of complexity suitable for climate-chemistry integrations over a range of timescales. This will be facilitated by using the flexible ASAD chemical integrator already embedded in TOMCAT and other models. We anticipate that the model will become widely used in the UK community and therefore strive to provide a flexible environment which future users with limited in-depth knowledge of model internals can adjust to their particular needs.

Bristol Research Initiative for the Dynamic Global Environment (BRIDGE)

Paul Valdes, University of Bristol

A new part of UGAMP has just formed in Bristol. BRIDGE is hoping to become a leading centre for improving our understanding of natural climate/Earth system variability and to use this knowledge to better constrain uncertainty in future changes, including their impact on all aspects of human society. Our main research effort will be to test our understanding of the causes of Earth system change, and specifically to test the computer climate models used to predict future climate change. The group will have a strong focus on interdisciplinary aspects of the subject, bringing together expertise in atmosphere, ocean, biosphere, chemosphere, and cryosphere, and we are particularly interested in investigating the interactions and feedbacks between different components of the Earth system.

Major themes of the new research work will be:

• Quantifying environmental/climate change in the distant past through the combined use of data and models

• Rigorous evaluation of climate models with accurate proxy climate records, especially during periods of rapid climate change

• Improvements in climate models by incorporating additional components of the Earth System, and detailed analysis of these processes for past, present and future change

• Impact of future climate change on spatial and temporal scales relevant to society, and including timescales from decadal to millennial.

Faculty staff are currently Dr. Sandy Harrison and Prof. Paul Valdes but we are in the process of recruiting two further faculty. In addition, a number of postdocs will be joining the group. Two have already started; Dr. Dan Lunt (a former UGAMPer) is working on the GENIE project (Grid Enabled Integrated Earth System Model) studying past rapid climate change events, and Dr. Joy Singarayer is working on a COAPEC funded project about sea-ice variability. In November two new postdocs (John Hughes and Julia Tindall) will start work on an archaeological project examining the effects of climate change on human evolution and dispersal, and adding oxygen and deuterium isotope components to the Hadley Centre model and using it to model rapid climate change events in the past. Two further posts are to be advertised related to PMIPII.

Tropical Climate

The influence of Indian Ocean SST on East African rainfall: Insights from observations and GCMs

Emily Black (emily@met.rdg.ac.uk), CGAM, Centre for Global Atmospheric Modelling, Department of Meteorology, University of Reading

Introduction

Understanding the processes controlling East African rainfall is essential both for the development of seasonal forecasting systems and for understanding the climate of the Indian Ocean basin as a whole. The description of the Indian Ocean dipole (IOD) (see Saji *et al*. (1999)) has led to increased focus on the role of the Indian Ocean in controlling East African rainfall. The IOD, which peaks in the boreal autumn, is characterised by a reversal of the zonal SST gradient and low-level easterly wind anomalies in the central Indian Ocean. It is associated with rainfall anomalies in the Indian Ocean basin and in particular has been shown by several studies to trigger extremely strong boreal autumn precipitation in East Africa (see for example Black *et al*. (2003), Goddard and Graham (1999) and Latif *et al*. (1999)). Simulating this relationship in coupled models is vital for the successful seasonal forecasting of these extreme events. Moreover, comparisons between atmosphere-only global climate models (AGCMs), fully coupled global climate models (CGCMs) and observations have the potential to deepen our understanding of the East African climate as a whole.

This article summarises the results of a study that used both AGCM and CGCM integrations in conjunction with observed data to tackle the following questions:

- How well can the relationship between East African rainfall and the Indian Ocean Dipole be simulated by an AGCM?

- To what extent is the simulation affected by the lack of ocean-atmosphere coupling in an AGCM?

The simulation of IOD induced rainfall anomalies by HadAM3

Figure 1 compares observed October rainfall and wind fields with those obtained from a run of HadAM3 forced with observed SST (from the GISST dataset). The period used is 1958-1997. It is clear from Figure 1 that during dipole years high rainfall is observed in coastal equatorial East Africa. It can also be seen that these rainfall anomalies are associated with anomalous easterly flow in the central Indian Ocean, which has the effect of weakening the climatological westerlies and reducing the flow of moisture away from the African coast (for more details see Black (2003) and Black *et al*. (2003)). It also be seen from the lower panel of Figure 1 that the model captures some aspects of observed wind and rain fields quite well. For example, the low rainfall in Indonesia is well replicated and there are weak easterly anomalies in the central Indian Ocean. However, although rainfall is generated off the African coast in the model run, the observed excessive precipitation on land is not reproduced. Furthermore, although the long-term mean wind vectors are reasonably well simulated, the easterly anomalies during dipole years are far weaker than those observed. In summary therefore, although

HadAM3 captures some aspects of the Indian Ocean basin's climatic response to the IOD, it does not simulate the observed relationship between the IOD-induced weakening of the mean westerly flow in the central northern Indian Ocean and excessive precipitation in East Africa.

The effect of short time-scale ocean-atmosphere coupling on IOD induced rainfall

A possible reason for HadAM3's failure to simulate the observed relationship between East African rainfall and the IOD is that AGCMs cannot account for short time-scale coupling between the atmosphere and ocean. In order to explore this possibility, a fully coupled model integration (using HadCM3) was compared to HadAM3 forced with monthly SST values from HadCM3. By comparing these runs, it is possible to ascertain the impact of short time-scale coupling. In the 20-year integration, there was only one convincing dipole-like event. The precipitation and wind anomalies for this year are shown in Figure 2. It can be seen that the wind anomalies generated by the coupled model are considerably stronger than those generated by the atmosphere only model and, unlike the atmosphere only case, they are focused in the central Indian Ocean. Excessive rainfall also extends from the ocean to coastal East Africa in the coupled integration, while in contrast, rainfall anomalies are focused entirely in the Indian Ocean in the AGCM simulation. In both cases, there are strong anomalies in western and central tropical Africa.

Comparison of Figures 1 and 2 suggests that the coupled model simulates the observed climate system significantly better than the atmosphere-only model. In simulations forced with both GISST and HadCM3 SSTs, the atmosphere-only model failed to capture both the magnitude of the zonal wind anomalies in the central Indian Ocean and the observed excessive precipitation in East Africa. The coupled model, on the other hand, generates wind anomalies over the whole Indian Ocean basin and precipitation anomalies onshore in East Africa. Although these anomalies differ somewhat from those observed during dipole years, they are significantly more realistic than those generated by the atmosphere-only model. The observation that HadCM3 produces a more realistic simulation than HadAM3 forced with HadCM3 SST implies that the improvements noted in the coupled model are not purely due to compensation of errors. It can thus be concluded that lack of coupling in HadAM3 limits its ability to simulate the observed relationship between East African rainfall and the Indian Ocean dipole. This suggests that short time-scale coupling has a significant part in generating the wind and rain anomalies that are observed during dipole years.

Conclusions

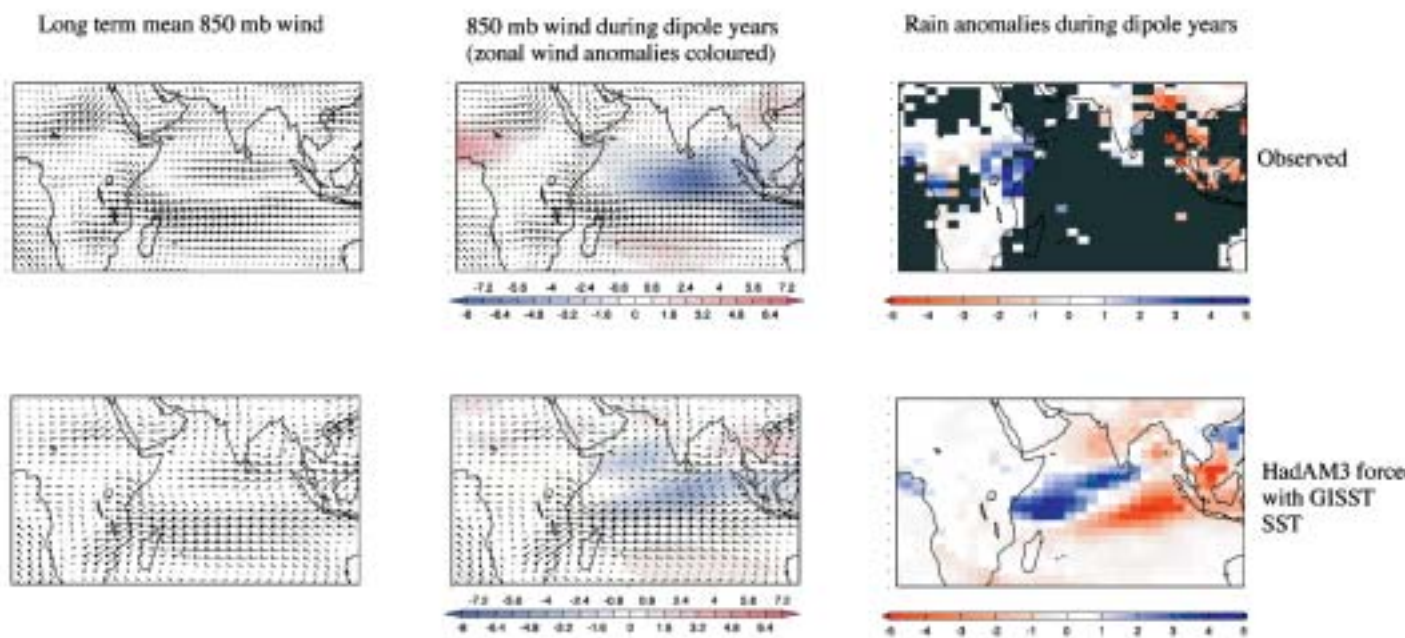- The observed relationship between the Indian Ocean dipole and

Figure 1. (above) Observed wind and precipitation (top line) compared to wind and precipitation obtained from an integration of HadAM3 forced with observed SST (second line). All data shown is from October. The left panel shows long term mean 850 mb vector wind. The middle panel shows mean 850 mb vector winds during dipole years with the zonal wind anomaly shaded.   The right panel shows mean rain anomalies during dipole years. Observed wind fields are taken from the NCEP reanalysis and observed rain from the CRU dataset.

Figure 2. As for Figure 1 but with the top line showing data for a single dipole year from a 20-year fully coupled run of HadCM3 and the bottom panel showing data taken from an integration of HadAM3 forced with HadCM3 SST during this dipole year.
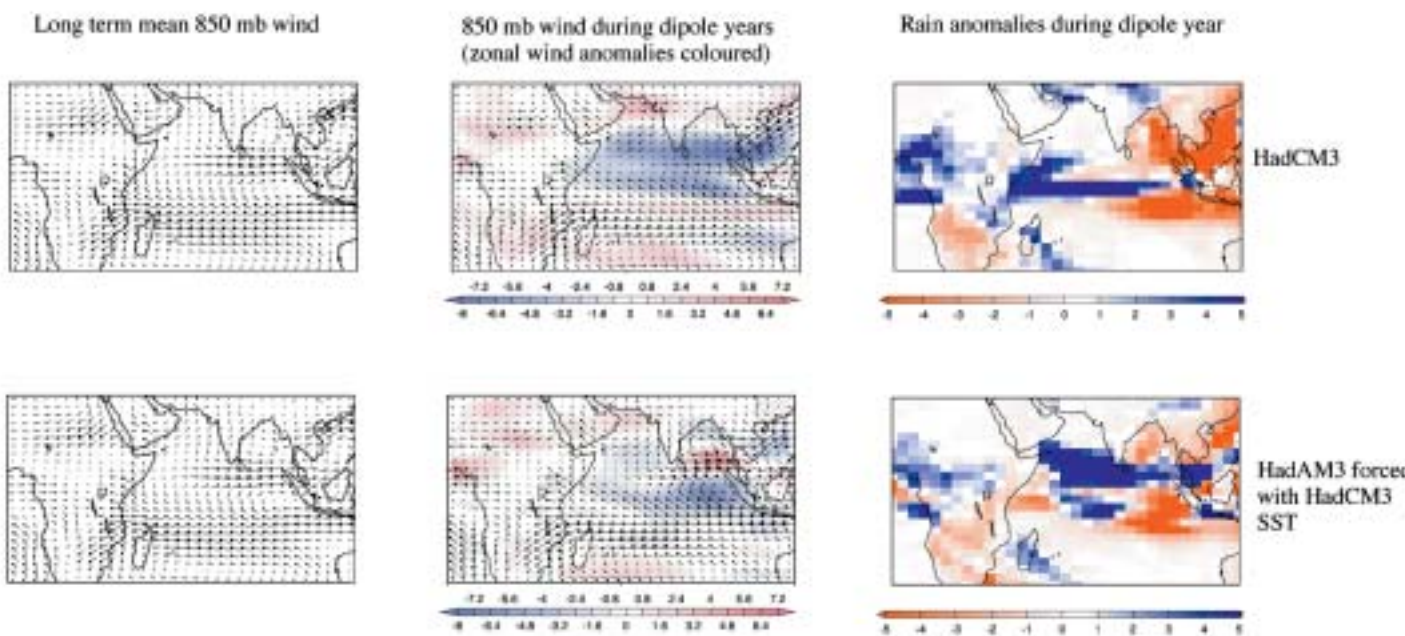
East African rainfall cannot be represented by an atmosphere only GCM

• A comparison between AGCM and CGCM simulations suggests that this may in part be due to the AGCM's lack of ocean-atmosphere coupling

References

Black, E., 2003: The impact of Indian and Pacific Ocean processes on the East African short rains. Clivar Exchanges, 8, 40-43.

Black, E., J. M. Slingo, and K. R. Sperber, 2003: An observational Study of the relationship between excessively strong short rains in Coastal East Africa and Indian Ocean SST. Monthly Weather Review, 103, 74-94.

Goddard, L. and N. E. Graham, 1999: Importance of the Indian Ocean for simulating rainfall anomalies over eastern and southern Africa. Journal of Geophysical Research-Atmospheres, 104, 19099-19116.

Latif, M., D. Dommenget, M. Dima, and A. Grotzner, 1999: The role of Indian Ocean sea surface temperature in forcing east African rainfall anomalies during December-January 1997/98. Journal of Climate, 12, 3497-3504.

Saji, N. H., B. N. Goswami, P. N. Vinayachandran, and T. Yamagata, 1999: A dipole mode in the tropical Indian Ocean. Nature, 401, 360-363.

Evaluation of hydrological components of GCM simulations of tropical hydrological processes

Nick A Chappell (n.chappell@lancaster.ac.uk) and Martin Fowell, Lancaster Environment Centre, Lancaster University, Lancaster LA1 4YQ, UK

The multi-disciplinary nature of the Lancaster Environment Centre has fostered links between the academic communities of tropical meteorology, humid tropical hydrology and biosphere-atmosphere interactions. One of our developing interests is the accurate description of tropical hydrological processes within climate models. Indeed, climate simulations by Global Circulation Models (GCMs) have been shown to be very sensitive to land-surfaces fluxes of water and energy (e.g., Polcher *et al.*, 1996, J. Hydrol., 180: 373-394). These fluxes (including latent heat flux and riverflow) are the greatest in the humid tropics. The latent heat flux comprises of the components of wet canopy evaporation and transpiration, with the latter being regulated by soil-water storage, which is itself regulated by rainfall-riverflow processes. Thus large-scale riverflow (Q) measurements are required by models that predict soil-water storage, though these also act as observations to evaluate inter-annual predictions of the residual of precipitation and evapotranspiration (P-E).

The accuracy of GCM predictions are, therefore, sensitive to the accuracy of the hydrological fluxes predicted for the humid tropics. Several studies over the past 10 years have evaluated the hydrological components of the 'Land-surface Parameterisation Schemes' (LPSs) within the GCMs. Two studies, namely Lau *et al.* (1996, Bull. Am. Meteor. Soc., 77: 2209-2227) and Pitman *et al.* (1999, Climate Dynamics, 15: 673-684) can be used to highlight the degree of uncertainty in current LPSs. Pitman *et al.* (1999) suggested a large range in latent heat flux of 106-186 Wm^{-2}, equivalent to 1,337-2,346 mm of actual evapotranspiration, for simulations of Amazonian rainforest from 16 GCM-LPS simulations (PILPS programme). Similarly large ranges in water flux resulting from model uncertainty were observed in the predictions of riverflow from the Amazon within the AMIP programme that involved the LPSs from 29 GCMs. Lau *et al.* (1996) found the simulations of the intra-annual cycle of Amazon riverflow varied between a highly uncertain +500 and –350 mm of the observed cycle. There are many reasons for these uncertainties - we would like to highlight three key water-related issues:

(1) The first issue to be addressed is the accuracy of the key components of rainfall-riverflow response. Outside the small research community of 'hillslope hydrologists', an unsupported assumption / misconception pervades. The notion that overland fl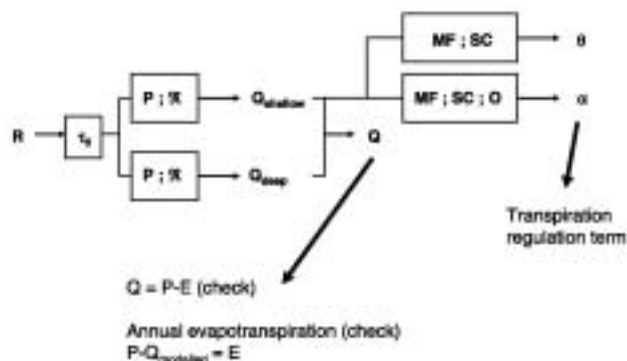ow on slopes generates most of the riverflow observed during storm periods, is widely held, but is unsupported by field research. Slopes in humid tropical regions of Africa (e.g., Dabin, 1957, Decret Permanent Bureau Sols AOF), South America (e.g., Callieux, 1959, Serv. Carte Geol. Fr.) and SE Asia (e.g., Chappell *et al.*, 1999, Phil. Trans. Roy. Soc. Lon. B., 354: 1831-1846) usually generate only a few percent overland flow per unit slope area. In some contrast, most of the LSPs studied by Pitman *et al.* (1999) generated much more than a few percent overland flow, even as much as 100%. If water only flows overland and does not enter the soil-water system, then simulation of the transpiration regulation process will be inaccurate.

(2) The second issue affecting LPS accuracy are the limitations of the theory describing rainfall-riverflow processes. Most LPS describe river generation processes either by: (a) an extension of the Manabe (1969) 'Bucket Model' or (b) the Darcy-Richards model. With the bucket model soil-water drainage (discharge from the system) is generated only after a threshold is reached. In reality, the 'pure time delays' between local rainfall and local river response are almost synchronous (see e.g. Chappell *et al.* 1999 op. cit.). With regard to the Darcy-Richards approach, hydrologists are increasingly questioning the validity of applying this approach at catchment scales, i.e., 0.1 km^2 and above (e.g., Beven, 2002, Hydrol. Process., 16: 189-206; Dumenil and Todini, 1992, Elsevier). One of the key reasons for the lack of applicability is the failure of the theory to adequately characterise the large-scale effects of pipeflow and pressure waves within what is a highly non-linear system. Further, measurements of the key catchment properties, e.g., permeability, are typically measured at scales of 0.1 to 1 m^2. The statistical distribution of values from this scale do not match those required to calculated rainfall-riverflow behaviour at the small catchment scale of 0.1 to 10 km^2 let alone the scale of GCM grid elements (3,000 to 70,000 km^2) – see for example, Chappell *et al.* (1998, Hydrol. Process., 12: 1507-1523).

(3) The third issue that may partly explain weakness in LPSs is the limited evaluation or validation of predicted hydrological fluxes. Fowell and Chappell (2003, PROMISE Conference, Trieste) demonstrated that while a GCM may explain a relatively high proportion of the variance in the zonal mean precipitation in SE Asia (e.g., r^2 0.537 for a GFDL model simulation), the variance explained falls dramatically when 0.5 degree pixels of observed and simulated data are correlated (e.g., r^2 0.300 for the same GFDL simulation). Validation (of precipitation, riverflow, latent heat flux or soil moisture) at scales larger than individual pixels may, therefore, mask fundamental problems in the model structure or parameterisations.

Given the limitations of the hydrological approximations within current GCMs, and of the need to keep this single component of a GCM's overall structure and parameterisation simple - what are the rules that should guide the development of an improved hydrology model? We would tentatively suggest that better hydrological models could be developed if the following criteria were kept in mind: (a) a high degree of parsimony in model structure (i.e., simple but efficient models which constrain

Figure 3.

Transpiration regulation term

Q = P-E (check)

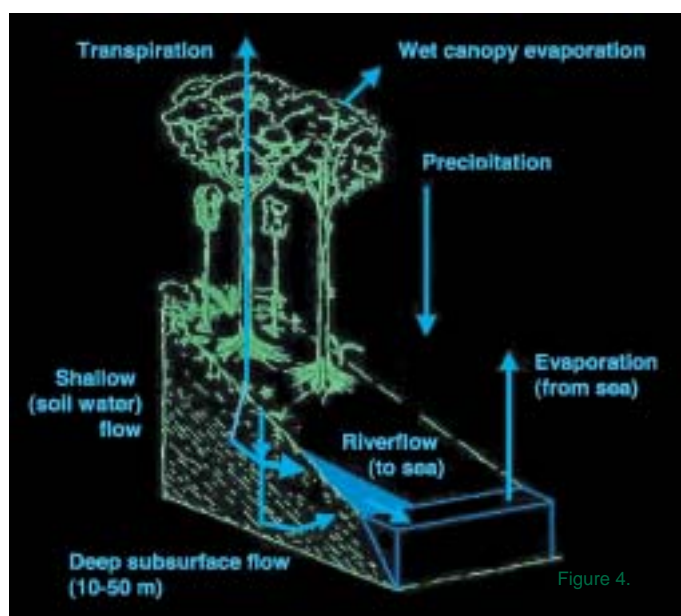Annual evapotranspiration (check)
P-Q$_{modelled}$ = E

Figure 4.

calibration uncertainty), (b) parameterisations directly at large scales (without the need for highly uncertain 'upscaling'), and (c) a focus on predicting the correct hydrological stores and fluxes (i.e., riverflow, latent heat flux / evapotranspiration, soil moisture storage) at large scales (e.g., 3,000 km^2 GCM pixel scale) rather trying to capture small-scale hydrological phenomena.

We are currently developing an alternative approach to the representation of GCM pixel-scale hydrology that is based on the use of Data-Based-Mechanistic (DBM) modelling. The DBM approach derives model structure and parameters of the rainfall-riverflow system from observed data using: (a) multiple model structure identification based on linear transfer functions and state-dependent (non-linear) modelling, (b) objective statistical inference to reject some model structures, and (c) further model structure rejection using physically-based understanding of system behaviour (Young *et al*., 1997, Wat. Sci. Tech., 36: 99-116). Thus far, we have been examined this large-scale hydrology problem as three steps:

(i) First, parsimonious parameters capturing rainfall-riverflow response are derived from large (>3,000 km^2) reference catchments, e.g., the 3,853 km^2 Mae Chaem catchment in Northwest Thailand (P14 river station). We have shown that a 3-parameter DBM model can capture most of these dynamics (Chappell *et al*., 2004, Cambridge University Press). With a small tropical catchment (say 0.1 to 5 km^2) with a shallow subsurface system (say < 10m), then riverflow (because it is almost entirely generated from the whole subsurface flow system) is likely to be a better predictor of catchment water content available to large rainforest trees than is surface (< 0.3m) water content. Within large catchments (> 3,000 km^2) some deeper (and longer residence time) moisture stores are likely to be present and expressed in the runoff response, but are too deep to regulate transpiration of tropical trees. The moisture present within the upper few metres of soil, therefore, needs to be identified separately from that in the whole subsurface system, if this critical regulator of transpiration is to be quantified.

(ii) The DBM approach allows the identification of these faster (i.e., shallower) component of flows separate from the slower components in the riverflow records.

(iii) The model-derived fast flow component (observed directly at large-scales) can then be ready related to the dynamics of the shallow (< 10 m) soil moisture store (see e.g., Fawcett *et al*., 1997, ICSE97), which can then be related to the term regulating large-scale transpiration. Alternatively, the fast flow components could be directly related to the transpiration regulation term, e.g., the α or β terms within the generalised evapotranspiration model of Polcher *et al*. (1996, *op. cit.*).

This simple approach could with a precipitation forcing and only 5 parameters, forecast: (a) GCM pixel-scale riverflow – which could provide a check on the model predicted P-E or if subtracted from the annual precipitation a check on the evapotranspiration, and (b) the fast component of GCM pixel-scale riverflow – which with a 2-3 further parameters, forecast the terms which regulate large-scale transpiration (Figure 3). By applying this approach it is also clear that the first part of the modelling generates riverflow which can be validated against large-scale observational data. The second part of the approach generates soil moisture and/or a transpiration regulation term. This highlights the need for observations of soil moisture or and/or the transpiration regulation term, which are currently not available for the scale of 3,000 km^2 in plan by several metres deep. Hydrologists need to be encouraged to develop new technologies to derive these estimates.

While the DBM model structure generated by this approach is simple, it is consistent with a hydrological model of the humid tropics derived from process research (Figure 4; see Bonell *et al*., 2004 Cambridge University Press). The aim of this overall approach to addressing current weakness in the hydrological components of GCM models is one of building models based on large-scale empiricism rather than over-extrapolation of small-scale physics. This work is at an early stage of development and we hope to report on progress over the coming months.

For further information, please contact Dr. Nick A Chappell at n.chappell@lancaster.ac.uk.

A spatio-temporal methodology for evaluating GCM simulations of tropical water fluxes

Martin Fowell (m.fowell@lancs.ac.uk), Nick Chappell, Rob MacKenzie, Lancaster Environment Centre, Lancaster University, LA1 4YQ

This article aims to present a new methodology for evaluating GCM model output against observed precipitation data. The poster presented at the RMS Conference 2003 can be downloaded from http://www.es.lancs.ac.uk/people/nickc/rms2003.ppt. This article includes some of the key steps within the methodology and some sample results. The results compare modelled (GFDL R30 model run; Alexander & Scott, 1995) with observed precipitation (Legates & Willmott, 1990) across SE Asia (90˚E to 160˚E and 20˚S to 30˚N) and Amazonia (14.5˚N to 25.5˚S and 90˚W to 30˚W).

There are several reasons for performing comprehensive and rigorous model evaluations, notably:

• A quantitative assessment is more objective and more informative than presenting plots of gridded observation and model output.

• Observational data sets are improving. Thus, more sophisticated types of evaluation are possible.

• Model performance is improving, therefore, more objective and sophisticated evaluation methods will be required to distinguish the more subtle differences

If GCMs are going to be used at the regional scale, for applied problems, such as the impact of land-use change on tropical rainfall (e.g. Polcher & Laval 1994a,b) we need to be sure that models can resolve the sub-regional (grid cell) variability of the current climate. In addition, if a robust model evaluation shows that the models have skill in representing the current climate, greater faith can be placed in the model forecasts of changing climates (Airey & Hulme, 1995).

1. There are three basic requirements for a quantitative model evaluation (adapted from Hulme 1992):

1. A suitable observed precipitation climatology.

These data sets need to be global in extent covering a long time period. Maximum temporal and spatial resolution are preferable, whilst over land, the gauge network should have maximum density.

2. Consistent spatial resolutions between the model and the gridded observations.

The observed data and the model output need to be transformed onto the lower of the grid resolutions.

3. Appropriate statistics to quantify model performance.

3. 1 A comparison of modelled and observed means, ranges and standard deviations.

3. 2 Graphical representation, such as scatter plots and difference plots.

3. 3 The distribution of the data must be examined for normality before the statistical analysis.

3. 4 At least one goodness-of-fit (relative error estimate) and one or more absolute error estimates should be calculated.

The analysis method proposed here is broken down into a series of steps, each of which will be discussed below.

1. Obtain suitable model output and gridded observations, and produce absolute and relative difference plots of the precipitation field. To quantitatively summarise the differences, error bounds for the region are calculated, e.g., the number of modelled grid boxes within +/- 0.5 mm/day of the observed data.

2. This methodology uses parametric statistics, therefore, the data must be normally distributed or transformed. The statistical distribution of the data is examined with a frequency histogram and a Kolmogorov-Smirnov test. Normalisation can be achieved with, for example, the square root, 2/3 power and $\log_{10}$ transformations. If the distribution contains excessive kurtosis, this may be corrected with a modified arcsine transformation. (When using this transformation the data must be converted so that the range lies between 0.0 and 1.0, without changing the relative ranges of the two distributions).

3. Once normally distributed, the data are displayed on a scatter plot and linear regression is performed. For a good model, the zero intercept regression equation should have a gradient close to unity.

4. The goodness-of-fit of the model output can be quantified with the coefficient of determination (r^2), which shows the proportion of the variance within the gridded observations that is explained by the variation within the model output. Despite its common use, r^2 has limitations. The magnitudes of r and r^2 are not consistently related to the accuracy of prediction (Willmott 1982). Further, r^2 is insensitive to additive and proportional differences between the model simulation and observations. Thus, r^2 will be 1.0 whenever $m_i=(Ao_i + B)$ for any non-zero value of A and any value of B, instead of being reserved for the occasion of interest when $m_i=o_i$ (Legates & Davis 1997). To enhance the evaluation, alternative goodness-of-fit estimates should be calculated, such as the coefficient of efficiency, E_2 (Nash & Sutcliffe 1970). It is preferable to calculate the modified coefficient of efficiency (E_1) rather than E_2, as this is less sensitive to outliers (Legates & McCabe 1999). The statistical analysis is concluded with a calculation of the error using dimensional measures such as the mean absolute error (MAE) and root mean square error (RMSE).

5. When this analysis is complete, one can compare results for the same model for different seasons or locations. Alternatively, different models can be compared. Thus far, only the GFDL R30 model has been tested with this methodology, but there are plans to test other GCMs from the AMIP programme. Table 1 gives a summary of the results that describe model performance, for the SE Asian and Amazonian annual precipitation budgets, for the GFDL R30 GCM.

The statistics in Table 1 show that while the modelled mean annual precipitation averaged over the whole region is within 0.5 mm/day of the gridded observations, the model is poor at simulating the spatial patterns for both the SE Asian and the Amazonian regions. For SE Asia, the variation within the model output can explain only 30% of the variation within the gridded observations. For both regions, both E_2 and E_1 are less than zero. Thus, for a given grid cell, the regional average precipitation (observed) will give a more accurate estimate of the rainfall for that particular cell than the corresponding modelled grid cell. The expected error, for a given grid cell, in either region, is 2.1 mm/day. Contrary to what may be expected, the model performs no better in Amazonia than SE Asia.

If the analysis at the grid scale reveals that all model simulations compared are equally poor, the analysis can be repeated with the zonal mean precipitation for the region. This is a less stringent test of model performance, therefore, it should be used as a secondary analysis tool, because too much detail is lost within the averaging process.

The analysis presented here is for the precipitation field but the method could be applied to other waterflux variables such as evaporation or riverflow as long as suitable (gridded) observations are available. The analysis method presented is still under development and will eventually include geostatistical and time-series tools.

Table 1: Parameters describing the annual precipitation field for SE Asia and Amazonia for the Legates and Willmott (1990) gridded observations and the GFDL R30 model run.

	SE Asia		Amazonia		
Parameter	LW (1990)	GFDL	LW (1990)	GFDL	Optimum value
Mean (mm/day)	5.652	5.173	3.989	3.385	
S.D (mm/day)	2.479	3.097	2.418	3.442	
Coefficient of determination (r^2)		0.300		0.342	+ 1
MAE (mm/day)		2.120		2.142	0
RMSE (mm/day)		2.752		3.068	0
Coefficient of efficiency (E_2)		-0.224		-0.227	+ 1
Modified coefficient of efficiency (E_1)		-0.048		-0.109	+ 1

References

Alexander, M.A. and Scott, J.D., 1995: Atlas of climatology and variability in the GFDL R30S14 GCM, University of Colorado, CIRES.

Legates, D.R. and Willmott, C.J.,1990: Mean Seasonal and Spatial Variability in Gauge-Corrected, Global Precipitation. International Journal of Climatology, 10(2): 111-127.

Polcher, J. and Laval, K., 1994a: A Statistical Study of the Regional Impact of Deforestation on Climate in the LMD GCM. Climate Dynamics, 10(4-5): 205-219.

Polcher, J. and Laval, K.,1994b: The Impact of African and Amazonian Deforestation on Tropical Climate. Journal of Hydrology, 155(3-4): 389-405.

Airey, M.J. and Hulme, M.,1995: Evaluating climate model simulations of precipitation: methods, problems, and performance. Progress in Physical Geography, 19(4): 427-448.

Hulme, M.,1992: A 1951-80 Global Land Precipitation Climatology for the Evaluation of General-Circulation Models. Climate Dynamics, 7(2): 57-72.

Willmott, C.J., 1982: Some Comments on the Evaluation of Model Performance. Bulletin of the American Meteorological Society, 63(11): 1309-1313.

Legates, D.R. and Davis, R.E., 1997: The continuing search for an anthropogenic climate change signal: Limitations of correlation-based approaches. Geophysical Research Letters, 24(18): 2319-2322.

Nash, J.E. and Sutcliffe, J.V., 1970: Riverflow forecasting through conceptual models, I, A discussion of Principles. Journal of Hydrology, 10: 282-290.

Legates, D.R. and McCabe, G.J., 1999: Evaluating the use of "goodness-of-fit" measures in hydrologic and hydroclimatic model validation. Water Resources Research, 35(1): 233-241.

Nonlinearity in the ENSO from observations and coupled model simulations

A. Hannachi, D.B. Stephenson, and K.R. Sperber, CGAM, Department of Meteorology, The University of Reading

A major feature of ENSO is the clear asymmetry between the positive and negative phases, El Nino and La Nina respectively, of the oscillation. This behaviour tends, however, to be overlooked (Penland and Sardeshmukh 1995a,b; Sardeshmukh *et al*. 2000.) We have addressed the question of quantifying nonlinearity in the ENSO using robust statistical tools. We adopted a probabilistic approach by using a simple stochastic nonlinear model, $Y = g(X)$ between thermocline depth X and the sea surface temperature (SST) Y. The SST data consists of the NCEP Nino-3 SST time series Jan 1950 - Dec. 2000, and the thermocline data consists of the monthly mean depth of the 20 degC isotherm at (0N, 140W) from April 1983 to December 2000.

The transfer g function is estimated by plotting the quantiles of SST versus the quantiles of the thermocline depth anomalies shown by the thick line in Figure 5 (see Hannachi *et al*. 2003 for details.) The saturation of the SST observed at deep thermocline starts when the (absolute) thermocline is approximately around 140m deep, where the SST becomes nearly independent of the thermocline as it deepens. When the thermocline is deep, stratification acts as a barrier between the surface and the thermocline and the link between them becomes very weak.

It is also interesting to note that the SST changes are most sensitive for thermocline depths between 120m and 140m with a rate of change around 1/8 degC/m. For depths less than 120m, the
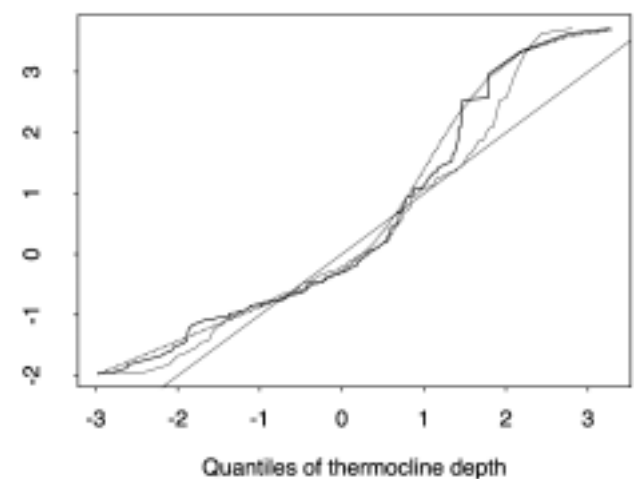

Quantiles of thermocline depth

Figure 5. Quantiles of Nino-3 SST versus quantiles of thermocline depth anomaly (thick line) along with a smooth piece-wise fit (dotted line). The diagonal line is expected from a normal distribution.
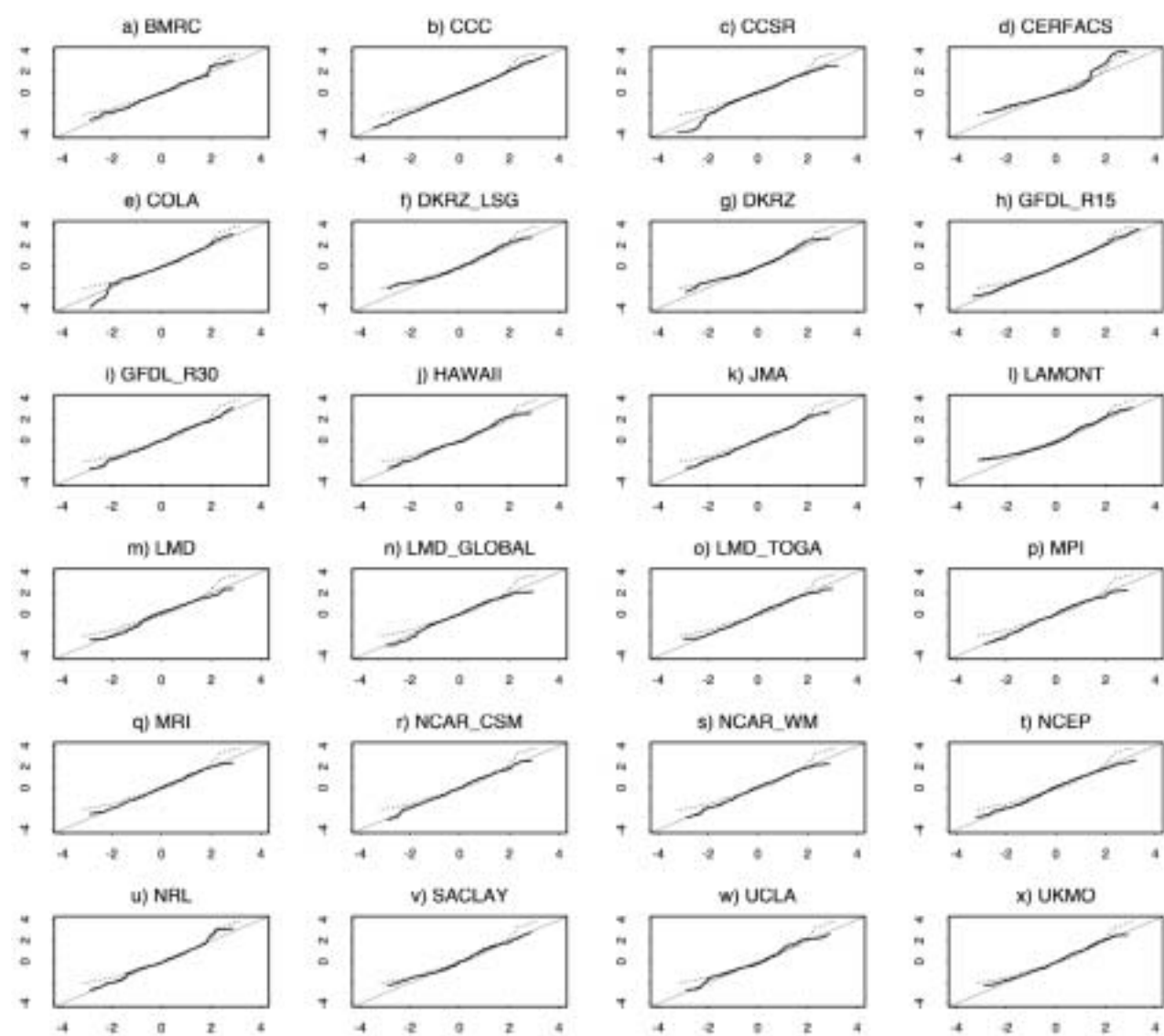
Figure 6. Quantiles of Nino-3 indices from 24 ENSIP coupled models versus quantiles of a normal distribution. The curve from the observed Nino-3 SST is also shown (dotted.)

rate is around 1/25 degC/m and the lower part of the curve does not saturate at least as sharply as the upper part. Although the 20C isotherm does not reach the surface it remains in constant contact with the mixed layer when the thermocline is shallow. In this case a slight change in the thermocline depth will not change the SST substantially. This makes the SST-thermocline depth sensitivity fairly linear because of the active mixing processes in the mixed layer and the absence of any barrier such as stratification when the thermocline is shallow (less than a 120m deep). This explains the observed weaker rate of change of 1/25 degC/m as opposed to the higher rate observed for depths between 120m and 140m. The dotted line in Figure 5 shows a smooth piecewise fit to the SST-thermocline depth curve obtained by fitting a tangent hyperbolic function to the upper half and a straight line fitted to the lower half.

The approach was then applied to Nino-3 indices from 24 coupled ocean-atmosphere models from ENSIP (see, Hannachi *et al*. 2003 for details). The result is shown in Figure 6. The majority of the 24 coupled models in ENSIP underestimate the nonlinearity noted in the transfer function of the observed Nino-3 index. Thirteen out of the 24 models gave Nino-3 indices that were normally distributed at 99% confidence. Of the remaining

non-normal models only 2 models show skewness. The detail of this skewness are however different from that observed (see Hannachi *et al.* 2003.) The most non-normal models did not correctly simulate the interannual spread although the phase of the annual cycle was reasonably well simulated. There are several possible explanations for this discrepancy. The thermocline depth in the coupled models is perhaps either deeper or shallower than in reality. Alternatively, The background vertical diffusivity may play an important role in ENSO SST variability, as shown by Meehl et al. (2001) where smaller values of the vertical diffusivity parameter could give larger ENSO variance due to the existence of a sharper thermocline.

References

Hannachi, A., D.B. Stephenson, and K.R. sperber (2003) Probability-based methods for quantifying nonlinearity in the ENSO. Clim Dyn 20: 241-256
Meehl GA, Gent PR, Arblaster JM, Otto-Bliesner BL, Brady EC, Craig A (2001) Factors that affect the amplitude of El Nino in global coupled climate models Clim Dyn 17: 515-526.
Penland C, Sardeshmukh P (1995a) The optimal growth of tropical sea surface temperature anomalies. J Clim 8: 1999-2024
Penland C, Sardeshmukh P (1995b) Error and sensitivity analysis of geophysical eigen-systems. J Clim 8: 1988-1998 Sardeshmukh PD, Compo GP, Penland C (2000) Changes of probability associated with El Nino. J Clim 13: 4268-4286

The Climate of the Maritime Continent

Pete Inness and Julia Slingo, CGAM, Dept. of Meteorology, University of Reading.

The climate of the Maritime Continent plays a key role in the global circulation. Deep convection over and around the islands of Indonesia and Papua New Guinea drives circulations which extend around the Tropics and into mid-latitudes. The complex topography of the islands means that convection is often driven by small-scale, local circulation patterns, but larger scale phenomena such as convectively coupled equatorial waves, the Madden-Julian oscillation (MJO) and El Nino all also have a role in determining the climate and climate variability of the region.

Neale and Slingo (2003) showed that the climate of the Maritime Continent was rather poorly simulated in HadAM3. By modifying the mean climate, (by removing the islands altogether and replacing them by ocean points) they showed that there was a positive impact on the climate simulation of the model, not only throughout the Tropics but on a global scale. Inness and Slingo (2003) found that the MJO in HadCM3 tended to break down at the Maritime Continent. These studies have highlighted the importance of the Maritime Continent in the tropical climate system, and indicate a need to improve the simulation of the climate of this region in our GCMs. Understanding the interactions between the different time- and space-scales of convective variability may hold the key to this problem.

A suite of experiments using an aquaplanet version of HadAM3, with various configurations of islands on the equator, with and without orography, is currently being developed and run in order to test the impact of the islands on a moving, MJO-like, convective anomaly. The convection is generated in the model by a moving SST anomaly, using the technique described in Woolnough *et al.* (2001). The SST anomaly propagates around the globe once every 60 days. Figure 7 shows a time-longitude section of the precipitation on the equator in the aqua-planet GCM, with the islands of the Maritime Continent as represented in the full GCM centred at 120 degrees east. At some times the enhanced precipitation is disrupted by the presence of the islands (e.g. around day 120) whereas at other times the islands seem to have little impact on the strength of the anomaly (e.g. around day 420).
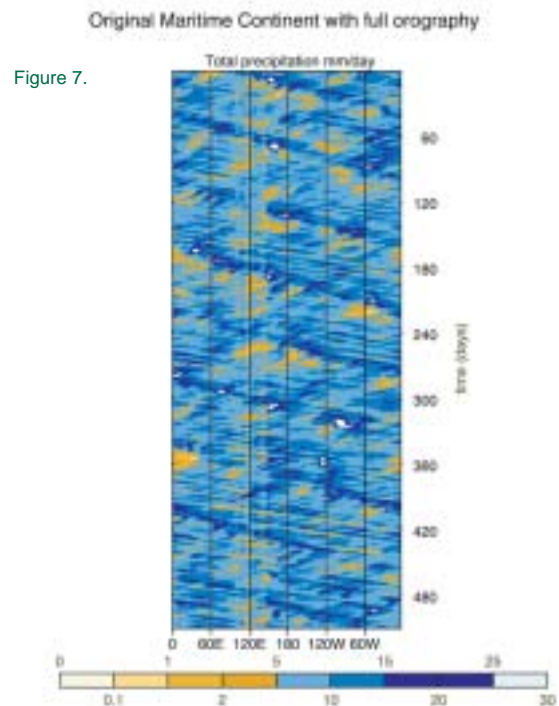
Figure 7.

other scales of variability are also apparent in the figure, with a strong eastward propagating Kelvin wave signature at higher frequencies than the MJO, and a lower frequency westward propagating signal.

By analysing the full set of aquaplanet experiments, together with full atmosphere-only and coupled GCM results, we hope to gain a better idea of how the convection associated with the MJO interacts with and is affected by the presence of the Maritime Continent islands. We will also study the small, island-scale processes that may result in enhanced convective activity in this region, with the aim of developing a way of parameterizing them in GCMs.

The atmospheric response to tropical intraseasonal sea surface temperature anomalies

Adrian Matthews, Schools of Environmental Sciences and Mathematics, University of East Anglia

The Madden-Julian oscillation (MJO) is the dominant mode of intraseasonal variability in the tropical atmosphere, and is manifested by large-scale tropical convective and associated circulation anomalies that propagate eastward from the Indian Ocean to the western Pacific on a time scale of 30 to 60 days. Recently, the role of ocean-atmosphere coupling in the MJO has been emphasised, with observed positive sea surface temperature (SST) anomalies leading the enhanced convection by a quarter of a cycle. The SST anomalies are thermodynamical in origin, arising through changes to the surface shortwave radiation and latent heat fluxes during the MJO cycle (Shinoda *et al*. 1998). The inclusion of ocean-atmosphere coupling in GCMs generally leads to a more

realistic simulation of the MJO in terms of organisation and eastward propagation of convective anomalies (e.g., Inness and Slingo 2003) but this is not always the case (Hendon 2000).

An intermediate step between an atmosphere-only model and a fully coupled GCM is the impact of intraseasonal SST anomalies on the atmospheric MJO and the implied feedback onto the ocean. Woolnough *et al*. (2001) analysed the equilibrium response of an aquaplanet AGCM to an idealised eastward propagating tropical SST dipole and found a good agreement between the model and observations in the phasing of the convection to the SST anomalies. Here, the response of a more realistic atmospheric
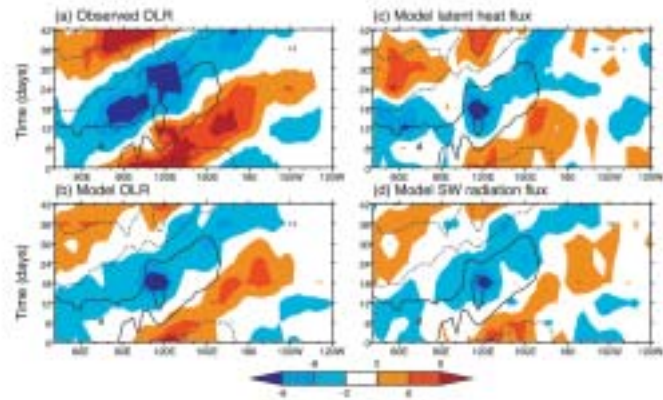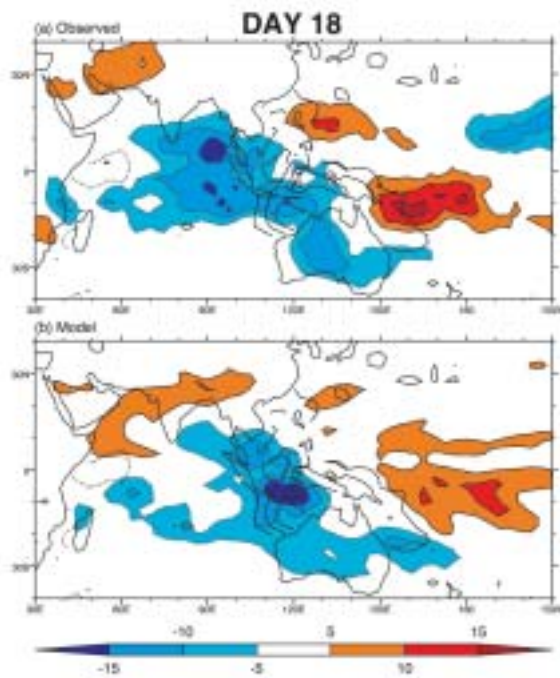
DAY 18

Figure 8. SST and OLR anomalies on day 18 of the MJO cycle. (a) observations, (b) model. SST contour interval is 0.15 C; positive contours are heavy solid lines and negative contours are heavy dashed lines. OLR interval is 5 W m-2 and shading is shown by the legend.

Figure 9. hovmöller diagrams, averaged from 15S to 5N. The time through the MJO cycle is on the vertical axis. SST anomalies are shown in all panels by the heavy contours; contour interval is 0.2 C and the first positive contour is at 0.1 C; positive contours are solid and negative contours are dashed. Anomalous (a) observed OLR, (b) model OLR, (c) model surface latent heat flux, (d) model surface shortwave radiation flux. All fluxes are shaded according to the legend.

model to observed MJO SST anomalies and the implied feedback onto the ocean are investigated.

The Hadley Centre AGCM (HadAM3 configuration) was forced by the Reynolds observed SSTs from 1982 to 2002. The weekly time resolution of the data set includes the MJO signal. The MJO was then extracted using a standard EOF analysis of 20-200-day filtered SST over the tropical warm pool domain. The leading two EOFs defined the MJO and a life cycle based on the phase of these EOFs was constructed, following Matthews (2000). By basing the analysis on the SST anomalies, a direct comparison can be made between the observed MJO and the modelled MJO, which by design is the forced response to the intraseasonal SST anomalies.

The observed and modelled convective anomalies are shown for a selected phase (day 18) of the MJO cycle in Figure 8. The model (forced response) is in good agreement with the observations with convective anomalies spatially lagging (i.e., to the west of) the SST anomalies. Hence, to a large extent the MJO can be characterised as a coupled phenomenon, as any atmospheric-only MJO component that was independent of the SSTs would not be picked out by this analysis. However, the exact phasing of the convective anomalies and the SST forcing in the model does not agree with the phasing in the observations. The enhanced convection (negative OLR anomalies) in the observed MJO lags the warm SST anomalies by about 12 days or a quarter cycle (Figure 9a) while in the model the enhanced convective response

lags the SST forcing by only four days (Figure 9b). It is not clear whether this "fast" response in the model is due to model deficiencies or a difference between the forced (model) and fully coupled (observed) systems. The model also still underestimates the overall MJO convective signal, as diagnosed by the OLR variance in the intraseasonal 20-200-day band (not shown). However, the model MJO forced by the weekly SSTs shows an improvement over the MJO in a control integration in which the intraseasonal SST forcing was removed by a 90-day low pass filter.

The implied feedback onto the ocean can be diagnosed in the integration forced by the full weekly SSTs. The surface latent heat flux anomalies are due to changes in the surface wind field arising as a response to the MJO convection. As this latent heat flux depends on the total wind speed, an accurate simulation of the mean surface winds as well as the anomalous MJO winds is necessary, if the MJO latent heat flux anomalies are to be modelled correctly. The surface latent heat flux (Figure 9c) and shortwave radiation flux (Figure 9d) anomalies in the model lag the SST forcing by only four days (consistent with the convection), rather than the quarter cycle as in the observations. Hence, it appears that if the model atmosphere was coupled to the ocean, the surface flux anomalies would act to damp out the intraseasonal SST anomalies. These findings will be tested in the fully coupled system.

The Role of the Equatorial Pacific Ocean Mean State in Modulating the Oceanic Response to Westerly Wind Event Forcing

Anna Pirani (ap698@soc.soton.ac.uk), Southampton Oceanography Centre

Westerly Wind Events (WWEs) are a climatological feature of the Western Equatorial Pacific and are observed at intraseasonal timescales. These high frequency, localised wind events generate a basin-wide planetary wave response, affecting the evolution of the background ocean mean state. Studies looking at the performance of general circulation models (GCMs) in forecasting recent El Niño Southern Oscillation (ENSO) events have concluded that one of the limitations of these systems is their difficulty in capturing intraseasonal atmospheric variability in the western Pacific (Slingo *et al.*, 1996, Landsea and Knaff, 2000). It is believed that ENSO is an oscillating system, as proposed by Suarez and Schopf (1988), but that its intensity is modulated by WWEs acting as random disturbances (Fedorov *et al.*, 2003). Recent work has shown that the inclusion of WWEs in a coupled forecasting system improved the forecast of the 1997-98 El Niño event (Vitart *et al.*, 2003).

Process studies are performed with the Océan Parallélisé (OPA) ocean GCM to examine the sensitivity of the WWE oceanic response to the variability of the background state of the equatorial ocean and to elucidate what temporal and spatial scale interactions need to be resolved when considering such adjustment processes in the Equatorial Pacific region. Different ocean conditions are generated in an idealised equatorial ocean basin, depending on the strength of the background Trade winds (Hellerman and Rosenstein, 1983) and the settings for horizontal viscosity (as in Maes et al., 1997). This modifies the principal components of the equatorial circulation that we are considering; the strength of the zonal circulation, the equatorial thermocline gradient and the Tropical Instability Wave (TIW) activity. An analytical WWE is applied (Zhang, 1998) and the propagation of the wind-generated Kelvin wave through these different ocean conditions is studied.

The hovmöller plots in Figure 10 of the depth of the 20˚C isotherm anomaly and sea surface temperature (SST) anomaly, show the planetary wave response to a WWE that takes place over ten days at 30˚ longitude at the Equator. A Rossby wave propagates westward and a Kelvin wave propagates eastward away from the WWE source. We are particularly interested in the propagation of the Kelvin wave and a modal decomposition of the signal is carried out by projecting the zonal velocity anomaly onto the vertical baroclinic modes, as in Killworth *et al*. (1997). From this we find that the Kelvin wave signal visible in Figure 10 is predominantly due to the second baroclinic mode.

Figure 11 and Figure 12 show the modal decomposition of the Kelvin wave at 80˚ longitude on the Equator for different oceanic conditions. In Figure 11 the background Trade winds (Hellerman and Rosenstein, 1983) have been used (standard), and then doubled (f2) and quadrupled (f4) over the whole domain, and in Figure 12 the level of horizontal viscosity has been set at $10^2 m^2 s^{-1}$ (low), $10^3 m^2 s^{-1}$ (standard) and $10^4 m^2 s^{-1}$ (high). The Kelvin wave propagating through the standard ocean configuration (Figure 11(a), Figure 12(b)) has a bi-modal structure with an even distribution of energy between the first and second baroclinic
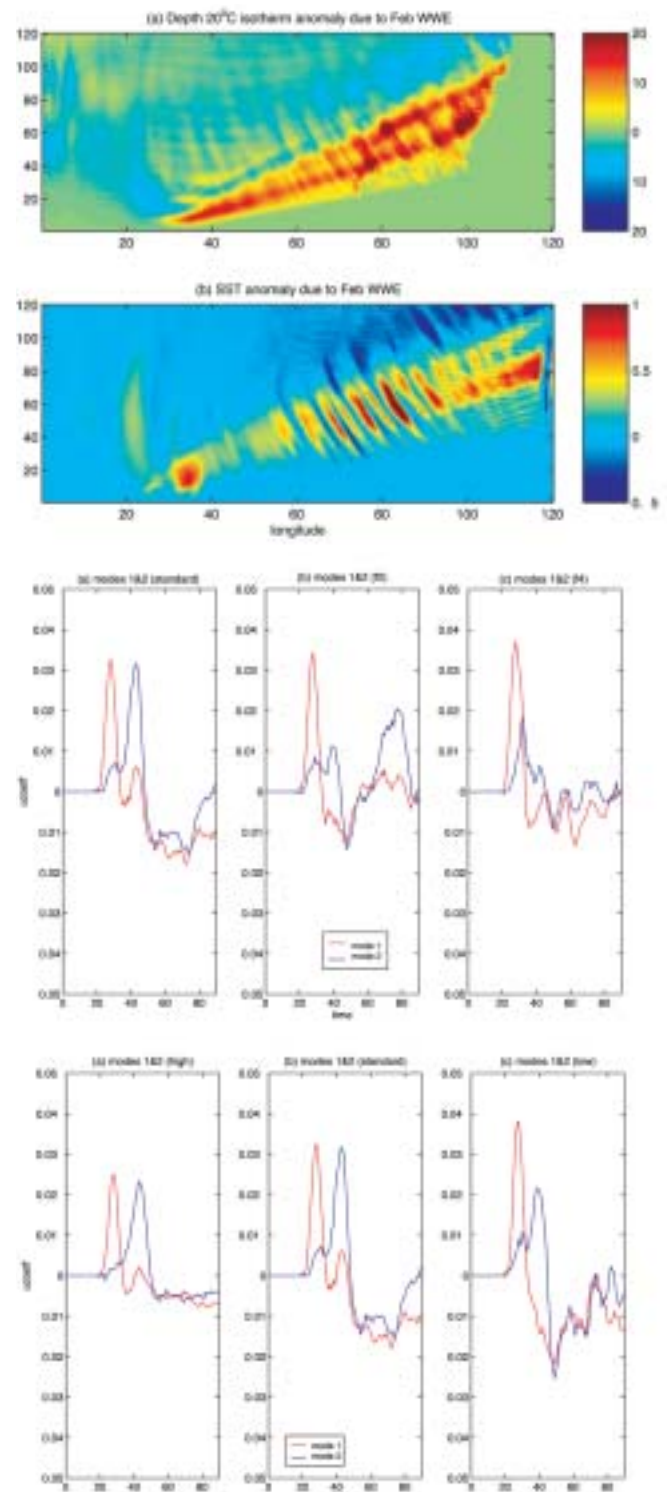

Figure 10. (top) Hovmöller plots of the evolution of (a) the depth of the 20˚C isotherm anomaly in meters, and (b) the sea surface temperature anomaly in ˚C, after a WWE has occurred at 30˚ longitude at the Equator.

Figure 11. (middle) Modal decomposition of the zonal velocity anomaly at 80˚ longitude at the Equator where a WWE has occurred in three different background conditions where the strength of the Hellerman and Rosenstein (1983) wind field has been varied. (a) is the standard wind field, (b) is the wind field doubled and (c) quadrupled all over the domain. The first baroclinic mode is shown in red and the second baroclinic mode in blue over a period of 90 days since the WWE occurred at 30˚ longitude at the Equator.

Figure 12. (bottom) As in Figure 11, but the standard wind field is used and the horizontal viscosity coefficient is varied from (a) $10^4 m^2 s^{-1}$ (high viscosity), (b) $10^3 m^2 s^{-1}$ (standard viscosity setting), to (c) $10^2 m^2 s^{-1}$ (low viscosity).

modes. This is also the case in the high viscosity case, in Figure 12(a), though the amplitude of the modal coefficient is weaker. The amplitude of the second baroclinic mode is significantly diminished by the strengthened equatorial circulation and steepened thermocline generated in the increased background wind field experiments, in Figure 11(b,c), and the low viscosity regime in Figure 12(c).

Another aspect of the Kelvin wave adjustment is its impact on the background TIW field, that exhibits considerable seasonal variability in terms of spatial distribution and level of activity. TIW-like velocity and SST anomalies are generated when the Kelvin wave, in particular the second baroclinic mode, encounters the TIW field, as seen in Figure 10(b) The Kelvin wave leads to a phase shift of the TIW field. The background state is in turn affected through interactions with the TIWs and SST anomalies are generated that persist after the adjustment to a WWE that could have implications for a coupled response.

We have shown that the Kelvin wave generated by a WWE consists mainly of the first and second baroclinic modes and that the second baroclinic mode is sensitive to the background ocean conditions, including the level of horizontal viscosity. Experiments where the wind stress has been successively increased are analogous to the development of La Nina conditions. Benestad et al. (2002) found that La Nina conditions strongly damp intraseasonal Kelvin waves. Here we suggest this is the result of the reduction in amplitude of the second baroclinic mode. The results show that the ocean response to a WWE and its impact on the ocean state depends on the oceanic conditions at the time of the wind perturbation. The full resolution of all the processes described here is necessary to model the adjustment process to a WWE. The resolution of the Kelvin wave propagation characteristics should be fully captured, with particular attention on the second baroclinic mode as this leads to the strongest oceanic signal.

References

Benestad, R, E, R. T. Sutton, and D. L. T. Anderson, 2002: The effect of El Niño on intraseasonal Kelvin waves. Quart. J. Royal. Met. Soc., 128, 1277-1291.

Fedorov, A. V., S. G. Philander, B. Winter and A. Wittenberg, 2003: How predictable is El Niño? Bull. Amer. Meteor. Soc., 84, 911-919.

Hellerman, S., and M. Rosenstein, 1983: Normal monthly wind stress over the World Ocean with error estimates. J. Phys. Oceanogr., 13, 1093-1104.

Landsea, C. W., and J. A. Knaff, 2000: How much skill was there in forecasting the very strong 1997-1998 El Niño? Bull. Amer. Meteor. Soc., 81, 2107-2120.

Maes, C., G. Madec, and P. Delecluse, 1997: Sensitivity of an Equatorial Pacific OGCM to lateral diffusion. Mon. Wea. Rev., 125, 958-972.

Killworth, P. D., D. B. Chelton, and R. A. De Szoeke, 1997: The speed of observed and theoretical long extra-tropical planetary waves. J. Phys. Oceanogr., 27, 1946-1966.

Slingo, J. M., K. R. Sperber, J. S. Boyle, J. P. Ceron, M. Dix, B. Dugas, W. Ebisuzaki, J. Fyfe, D. Gregory, J. F. Gueremy, J. Hack, A. Harzallah, P. Inness, A. Kitoh, W. K. M. Lau, B. McAvaney, R. Madden, A. Mathews, T. N. Palmer, C. K. Park, D. Randall, and N. Renno, 1996: Intraseasonal oscillations in 15 atmospheric general circulation models: results from an AMIP diagnostic subproject. Clim. Dynamics, 12, 325-357.

Vitart, F., M. Alonso Balmaseda, L. Ferranti, and D. Anderson, 2003: Westerly Wind Events and the 1997/98 El Niño event in the ECMWF Seasonal Forecasting System: A case study. J. Climate, 16, 3153-3170.

Zhang, K. Q., and L. M. Rothstein, 1998: Modelling the oceanic response to Westerly Wind Bursts in the Western Equatorial Pacific. J. Phys. Oceanogr., 28, 2227-2249.

The Indian Ocean Dipole in Two Coupled GCMs

Dr. Hilary Spencer, Prof. Julia Slingo, Dr. Rowan Sutton, Dr. Emily Black and Dr. Malcolm Roberts, CGAM, Dept. of Meteorology, Univ. of Reading.

Introduction

The Indian Ocean dipole is a coupled ocean-atmospheric phenomenon that was described by Saji et al., 1999 and Webster et al., 1999. It is related to the climate of many regions surrounding the Indian Ocean (e.g., Black et al., 2002, Guan and Yamagata, 2003) but these teleconnections can be hard to detect since the dipole is weakly correlated with El Niño. The dipole consists of cool sea surface temperature anomalies (SSTAs) in the southeast tropical Indian Ocean (SE) and warm SSTAs in the west (W) and occurs most strongly during the Boreal autumn (SON). Figure 13a shows 95% significant composite SST and 10m wind anomalies in SON of five observed dipoles from the past 50 years that were not accompanied by strong El Niños. These events are 1961, 1963, 1967, 1977 and 1994.

The dipole in SSTA is accompanied by southeasterly surface wind anomalies in the SE and easterly wind anomalies on the equator. This is consistent with the Gill atmospheric response to tropical heating. Between April and November the climatological winds in the SE are southeasterly. Therefore there are a number of possible positive feedbacks of the strengthened southeasterlies in the S back onto the cool SSTAs. There is the wind-evaporation-SST feedback, the equatorial Bjerknes wind-thermocline-SST feedback and a feedback involving upwelling along the coast of Sumatra (Fischer et al., 2003). Due to a lack of direct measurements and to model uncertainties, it is controversial which processes dominate.

Due to these model uncertainties and since it is important to predict the evolution of these dipoles, the accuracies of two coupled models in representing the dipole are assessed. This study is restricted to dipoles that are not accompanied by strong El Niños so that the remote affects of El Niño do not dominate the Indian Ocean processes.

Models and Data

The coupled models studied are the Hadley Centre ocean-atmosphere models, HadCM3 (Gordon, 2000) and HadCEM (Roberts et al., 2003). Both have the same atmospheric component, HadAM3 with 3.75^o by 2.5^o horizontal resolution and 19 vertical levels. HadCM3 has a 1.25^o ocean with 20 vertical levels and HadCEM has a $1/3^o$ ocean with 40 vertical levels. These are compared with the GISST SST dataset (Parker et al., 1995) and the NCEP reanalysis winds (Kalnay et al., 1996).
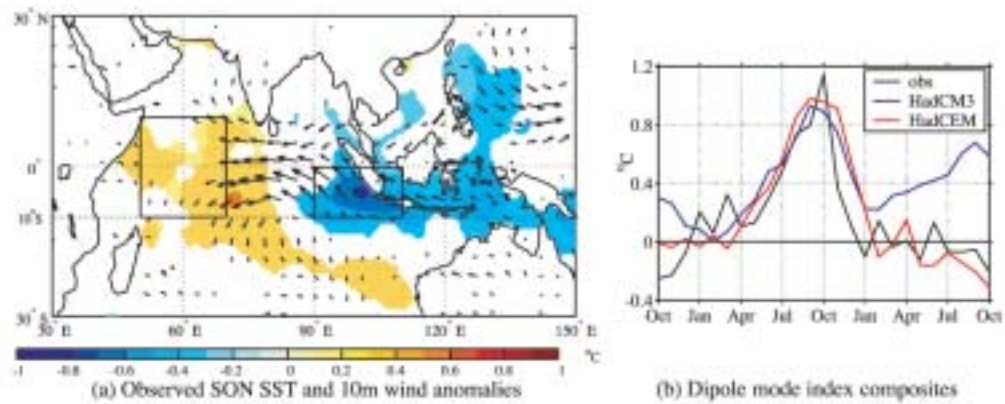
Figure 13. (top) Indian Ocean dipole composite anomalies. (a) 95% significant observed SST and 10m wind for SON. Boxes indicate regions for definition of dipole mode index (DMI) (b) Time series of DMI for observed and model composites.
Figure 14. (bottom) Total and anomalous temperature through a section of the Indian Ocean at 10°S for the two models. 95% significant anomalies are coloured and total temperature is contoured with an interval of 1°C. Contours ≤23°C dashed.
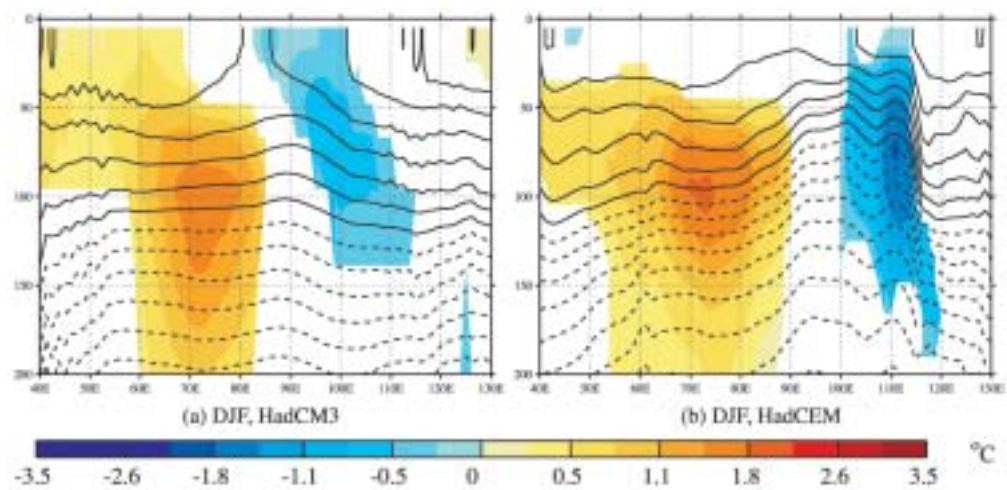
Results

The dipole mode index (DMI) is the difference in SSTA between the W and SE in the regions shown in Figure 13a. The composite DMI timeseries for the observations and the coupled models are shown in Figure 13b. The composites consist of strong, persistent, October dipoles that are not strong El Niños. Figure 13b shows that both models have realistic timing and strength of the onset and peak of the dipoles. The observed termination is very rapid between October and January. Both models simulate the correct timing of the termination but with insufficient speed. In fact, the HadCM3 dipoles do not terminate completely. The anomalies decay slightly but then re-invigorate the following year once the climatological winds return to southeasterlies in the SE. This leads to dipoles in HadCM3 that persist for 2-3 years, unlike observed and HadCEM dipoles.

A possible reason why the HadCM3 dipoles persist through DJF is found in cross sections of the Indian Ocean temperature through 10°S (shown as a line in Figure 13a). The total and anomalous composite ocean temperatures in DJF for both models are shown in Figure 14. These show the shoaling of the thermocline in the east and the deepening in the west. In HadCEM, the temperature anomalies in the ocean interior do not extend to the surface in DJF and hence the SSTAs decay. However, in HadCM3, with a diffuse thermocline, the temperature anomalies do extend to the surface. It is hypothesised that, with the low vertical resolution in HadCM3, the surface and the thermocline are too closely connected and the memory of the ocean interior is transmitted to the surface. Whereas, in reality and in HadCEM, the sharper thermocline can become disconnected from the surface and hence surface features can disappear while deeper anomalies persist. Therefore, the very expensive, fine horizontal resolution may not be required in order to simulate the dipole accurately; enhanced vertical resolution may be sufficient. Results from the coupled model with a 1.25° horizontal resolution and the same 40 vertical levels as HadCEM (partly) confirm this hypothesis.

References

Black, E., J. Slingo, and K. Sperber, 2003. An observational study of the relationship between excessively strong short rains in coastal East Africa and Indian Ocean SST. Mon. Wea. Rev., 131(1):74 94.

Fischer, A.S., P. Terray, E. Guilyardi, S. Gualdi, and P. Delecluse, 2003. Triggers for the Indian Ocean dipole/zonal mode and links to ENSO in a constrained coupled GCM. submitted to J. Clim.

Gordon, C., C. Cooper, C. Senior, H. Banks, J. Gregory, T. Johns, J. Mitchell, and R. Wood, 2000. The simulation of SST, sea ice extents and ocean heat transports in a version of the Hadley Centre coupled model without flux adjustments. Climate Dyn., 16(2-3):147 168.

Guan, Z.Y. and T. Yamagata, 2003. The unusual summer of 1994 in East Asia: IOD teleconnections. Geophys. Res. Lett., 30(10).

Roberts, M.J., H. Banks, N. Gedney, J. Gregory, R. Hill, S. Mullerworth, A. Pardaens, G. Rickard, R. Thorpe, and W. R., 2003. Impact of an eddy-permitting ocean resolution on control and climate change simulations with a global coupled GCM. To appear in J. Clim.

Saji, N.H., B. Goswami, P. Vinayachandran, and T. Yamagata, 1999. A dipole mode in the tropical Indian Ocean. Nature, 401(6751):360 363.

Webster, P.J., A.Moore, J. Loschnigg, and R. Leben, 1999. Coupled ocean-atmosphere dynamics in the Indian Ocean during 1997-98. Nature, 401(6751):356 360.

The role of the basic state in determining the predictability of the tropical climate system, with particular reference to the Asian summer monsoon

Andrew Turner, Pete Inness, and Julia Slingo, CGAM, Dept. of Meteorology, University of Reading

The basic state errors in the tropical Pacific of the UK Met Office Hadley Centre Model (HadCM3) are partially corrected by the use of a flux adjusted version of the model (HadCM3FA), originally devised by Inness *et. al*. (2003). The anomalous summer zonal temperature gradient in the equatorial Pacific is reduced, correcting the excessive trade winds prevalent there in HadCM3. The strength of the Pacific trades is a well-known signature of the Asian summer monsoon circulation (see, e.g. Webster *et al*. 1998). Consequently, their reduction in HadCM3FA is coupled with a reduction in the strength of the broad-scale monsoon over Asia, as measured by the dynamical monsoon index (DMI), first used by Webster and Yang (1992). The index covers 5-20°N, 40-110°E and is a measure of the anomalous zonal wind-shear in summer. A reduced south-westerly monsoon flow is observed in the summer HadCM3FA climate. However, monsoon variability in the Hadley Centre model increases with flux adjustments, observed as an increase in the standard deviation of the DMI in 40 year integrations of the model: 1.20 for HadCM3, 2.19 for HadCM3FA, 1.60 for ERA40, (used as an indicator of the real-world scenario). The increased variability is also observed in strong minus weak monsoon difference composites of lower tropospheric wind, surface temperature and precipitation. Differences of strong and weak monsoon summers therefore show stronger monsoon flow into India with the flux-adjusted version of the model, and this is also represented in the equatorial Pacific with increased easterly trade winds during strong monsoon summers. Possible sampling errors were accounted for by extending integrations to 100 years, to no effect on the overall circulation variability or summer mean climate. That the use of a seasonal cycle of flux-adjustments to force sea surface temperatures in a coupled GCM increases the interannual variability is somewhat surprising. The adjustments have altered the ENSO cycle to the extent that the standard deviation of the Nino-3 timeseries has increased (0.87, 1.29, 0.85 for HadCM3, HadCM3FA, and ERA40 respectively). Correlations between the Nino-3 timeseries and the DMI for ERA40 and the 100 year model integrations (see Figure 15) show a stronger ENSO teleconnection in the flux adjusted model. This is to be expected with the mean state correction, extending the warm pool further

eastward. The spring predictability barrier becomes evident with flux adjustments, represented by the steep nature of the HadCM3FA correlation curve around March/April time of the same year prior to the summer monsoon. Stronger ENSO forcing in HadCM3FA may explain this, but its lack in HadCM3 is not yet understood.
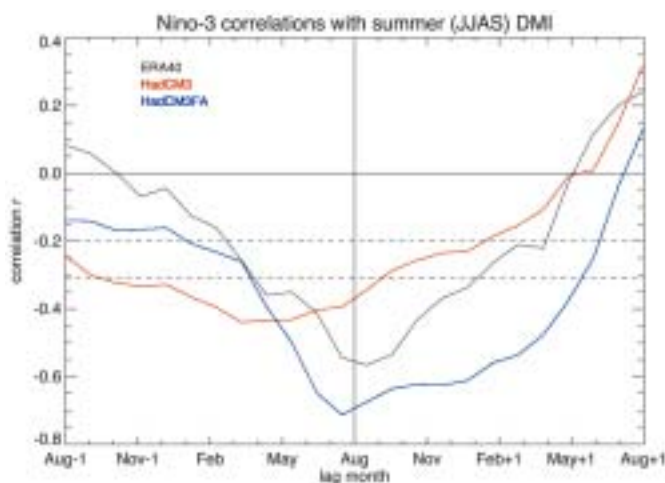

Figure 15. Correlation between Nino-3 and summer (JJAS) DMI plotted against lag in months. 'Aug-1' indicates the August Nino-3 anomaly the year before DMI. Correlations significant in all but 5% of cases are indicated outside the dashed lines: |r|>0.31 for the 40 year dataset, |r|>0.20 for the 100 year datasets.

References

Inness, P.M., Slingo, J.M., Guilyardi, E., and Cole, J. (2003). Simulation of the Madden-Julian Oscillation in a coupled general circulation model II: the role of the basic state. J. Climate, 16, 365-382

Webster, P.J., Magana, V.O., Palmer, T.N., Shukla, J., Tomas, R.A., Yanai, M., and Yasunari, T. (1998) Monsoons: Processes, predictability, and the prospects for prediction. J. Geophys. Res. (Oceans), 103, 14451-14510

Webster, P.J. and Yang, S. (1992). Monsoon and ENSO: Selectively interactive systems. Q. J. R. Meteorol. Soc., 118, 877-926
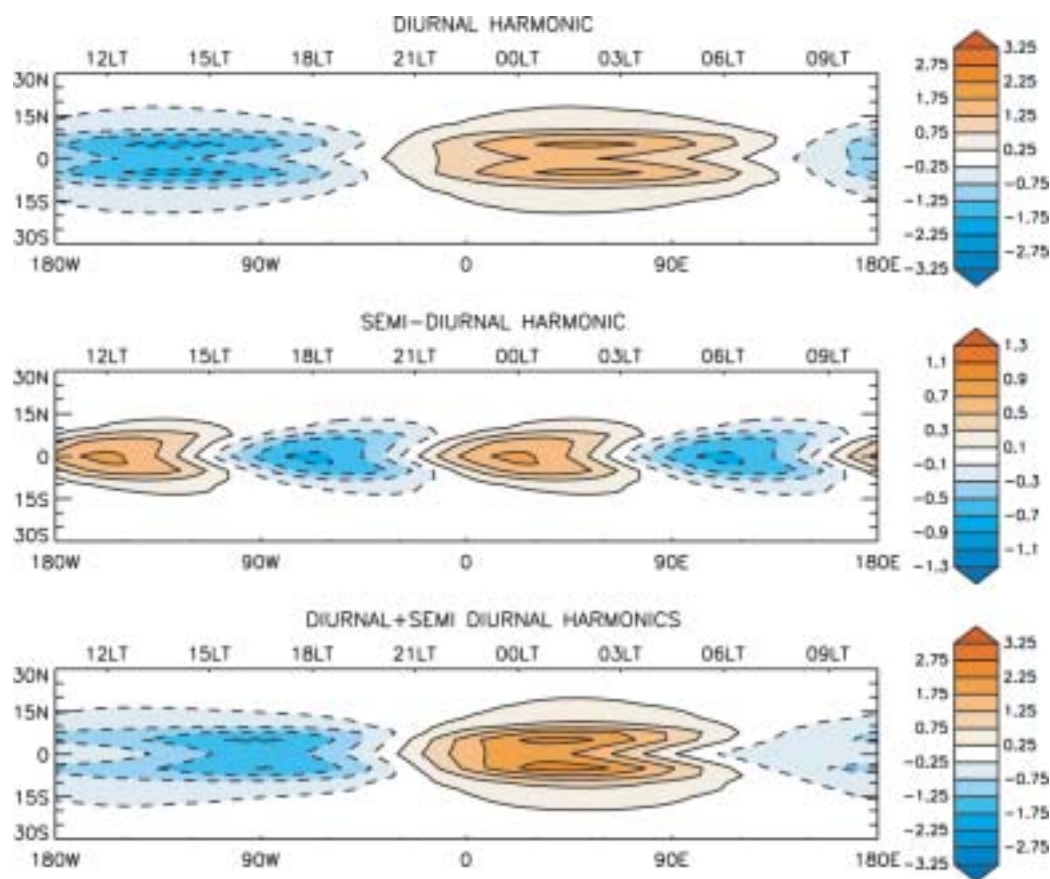
Figure 16. Composite diurnal and semi-diurnal harmonics of precipitation from an aquaplanet version of the UM, and their sum. The lower horizontal axis represents longitude for the averaging period 21Z-00Z. The upper axis represents local time for a particular longitude.

The diurnal cycle of tropical convection in an aquaplanet GCM.

Steve Woolnough (s.j.woolnough:rdg.ac.uk), Julia Slingo (CGAM, University of Reading) and Brian Hoskins (Dept. of Meteorology, University of Reading)

The diurnal[1] cycle of tropical convection over land and oceans is very different. Over land the diurnal cycle of convection is driven by the destabilization of the surface by the strong daytime solar heating, and typically peaks in the early evening, and the magnitude of the diurnal cycle is comparable to the mean. In contrast, over the open ocean the amplitude of the diurnal cycle is typically 10-15% of the daily mean precipitation and the maximum tends to occur in the early hours of the morning. The process which drive the diurnal cycle of convection over ocean are less certain and suggest mechanisms include: night-time destabilization of the profile by infrared cooling of clouds at night as opposed to daytime stabilization of the profile by shortwave warming during the day (Randall *et al*. 1991), vertical circulations induced by differences in cloudy and cloud-free heating rates (Gray and Jacobsen 1977), and the lifetime associated with convective systems triggered in the afternoon by near surface heating (Chen and Houze 1997).

Atmospheric GCMs typically have a very poor representation of the diurnal cycle of convection over land, with the maximum in precipitation occurring too early in the day. This error almost certainly arises because most GCM convective parametrizations take no account of the temporal development of convective cloud

systems and so tend to produce deep convection to early in the day. In contrast over the oceans, GCMs tend to be able to capture the early morning peak in convection, despite the absence of any representation of some of the proposed mechanisms for driving the oceanic diurnal cycle (e.g. subgrid scale vertical circulations).

In this article the diurnal cycle of convection in an aquaplanet version of the Met Office Unified Model (UM) is discussed. The aquaplanet configuration provides a relatively simple framework for studying the mechanism which drive the diurnal cycle of convection over the open oceans in the UM. As well as improving our understanding of the diurnal cycle of the model, studies such as these can improve our understanding of the processes which drive convective variability in the model in general.

Figure 16 shows diurnal and semi-diurnal harmonics of precipitation in an aquaplanet version of the UM, forced by zonally symmetric sea surface temperature distribution, representative of the West Pacific Warm Pool. Both the diurnal and semi-diurnal harmonics make a strong contribution to the diurnal cycle of convection in this model. The diurnal harmonic has a maximum at around 0130LT with a magnitude of about 1.5mm/day. The semi-diurnal harmonic peaks at around noon and midnight with a magnitude of about 0.7mm/day on the equator. The resultant sum of these harmonics (bottom panel in Figure 16), which describes around 80% of the variability in precipitation diurnal timescales, has a maximum between 00-03LT of about 2mm/day with a

---

1.   The word diurnal will be used here to describe variations with periods of 24 hours or less, except in the phrases 'diurnal harmonic' or 'diurnal tide' where it will refer to variations with a period of 24 hours only.

broader, weaker minimum between about 15-18LT with a magnitude of about 1.25mm/day. This diurnal cycle of convection in the aquaplanet is in broad agreement with the observed diurnal cycle over the open ocean and with that in the full version of the GCM.

Detailed analysis of the behaviour of the convection scheme in this integration revealed that the convective precipitation is strongly determined by the boundary layer properties through the following mechanism. The boundary layer T,q determine the parcel buoyancy at the top of the boundary layer, which determines whether any convection is shallow or deep. If there is deep convection, the convective mass flux is strongly influenced by the amount of forced detrainment, if any required to maintain the positive buoyancy of the parcel at the top of the boundary layer. The convective precipitation, in turn is strongly correlated with the mid-level mass flux, which itself is largely determined by the mass flux at the top of the boundary layer.

These relationships mean that the diurnal and semi-diurnal harmonics of convective precipitation in this model are largely determined by the variations in the boundary layer T,q on these timescales.

The diurnal and semi-diurnal harmonics of temperature have nearly uniform vertical profiles, so the effect of the temperature perturbations on the buoyancy of a parcel lifted from the surface to the top of the boundary layer, is to increase the parcel buoyancy when the temperature perturbation is negative, through the lowering of the lifting condensation level.

For the semi-diurnal harmonic these boundary layer temperature variations are driven almost entirely by the adiabatic cooling/warming associated with the pressure variations of the semi-diurnal tide. In contrast, the diurnal temperature variations are not dominated by a single process The shortwave and

longwave heating, and the convection all drive variations of similar magnitudes, but of different phases. The diurnal tide has a very small boundary layer temperature signal. The moisture variations are driven by the convection, and act to reduce the magnitude of the variations in precipitation compared to those which would arise in the absence of this feedback and alter the phase of these harmonics.

A further series of experiments in which the standard closure for the convection scheme was replaced by one in which the mass flux was scaled to remove CAPE from the profile on a given timescale were performed. These experiments showed some sensitivity of the diurnal cycle of convection to the choice of timescale, although not necessarily the choice of closure scheme. However, because of the changes to the mean climate of the model produced by the changes in the convection scheme it was not possible to determine whether this sensitivity of the diurnal cycle arises from a sensitivity to the mean climate or to the closure of the convection scheme directly.

The large number of processes which can influence the diurnal cycle of convection, even under these simplified conditions and with a good knowledge of the behaviour of the convection scheme, would make priori prediction of the diurnal cycle of convection difficult.

References

Chen, S.S. and R.A. Houze (1997) Diurnal variation and life-cycle of deep convective systems over the Tropical Pacific Warm Pool. Quart. J. R. Met. Soc., 123, 357-388

Gray, W.M. and R.W. Jacobsen (1977). Diurnal variation of deep cumulus convection. Mon. Wea. Rev., 105, 1171-1188.

Randall, D.A., Harshvardhan and D.A. Dazlich, (1991). Diurnal variability of the hydrological cycle in a general circulation model. J. Atmos. Sci., 48, 40-62.

The Structures of Observed Convectively Coupled Equatorial Waves

Gui-Ying Yang, Brian Hoskins and Julia Slingo, University of Reading

Convectively coupled equatorial waves are a key part of the tropical climate system. A faithful representation of these wave modes is needed for predictions on all time-scales. In Yang *et al*. (2003), a new methodology, which isolates individual equatorial modes based on theoretical structures, has been developed and applied to two independent data sources, ERA 15 and satellite observed window brightness temperature (T_b) for May-October of 1992. The study shows that this method has been successful in identifying equatorial wave structures and provides a powerful diagnostic tool for investigating convectively coupled equatorial waves. It is shown that for convectively coupled waves, most off-equatorial convection is closely associated with the low level convergence of these waves, as suggested by simple equatorial wave theory. In addition, it is also found that wind-dependent surface fluxes of moist entropy may play an important organizational role for equatorial convection, particularly where the SSTs are sufficiently warm to support convection. Such conditions potentially occur in the Kelvin and n=1 Rossby (R1) waves which have maximum zonal winds on the equator. In this

study the methodology is applied to multi-level ERA 15 data and results of the seasonal statistical analysis will be shown.

Westward moving waves coupled with off-equatorial convection

Figure 17 shows seasonal (May-October 1992) statistical analysis of westward moving convectively coupled WMRG and R1 waves. It is seen that the westward moving coupled MRG waves show good agreement with the theory, with a well-defined first internal vertical mode structure in the eastern hemisphere (Figure 17a,b). The coupled wavelength is typically between 45° and 60°, as estimated from successive correlation peaks, and significant coupling can occur for at least at one wavelength. Given the eastward group velocity of WMRG waves, the eastward bias of the pattern indicates weaker convective coupling in new WMRG waves formed to the east. The low-level regressed structure (Figure 17b) is similar to the theoretical structure given in Figure 3 of Yang *et al*.2003. However the upper-level structure shows some differences, particularly the zonal wind in the region of convection.
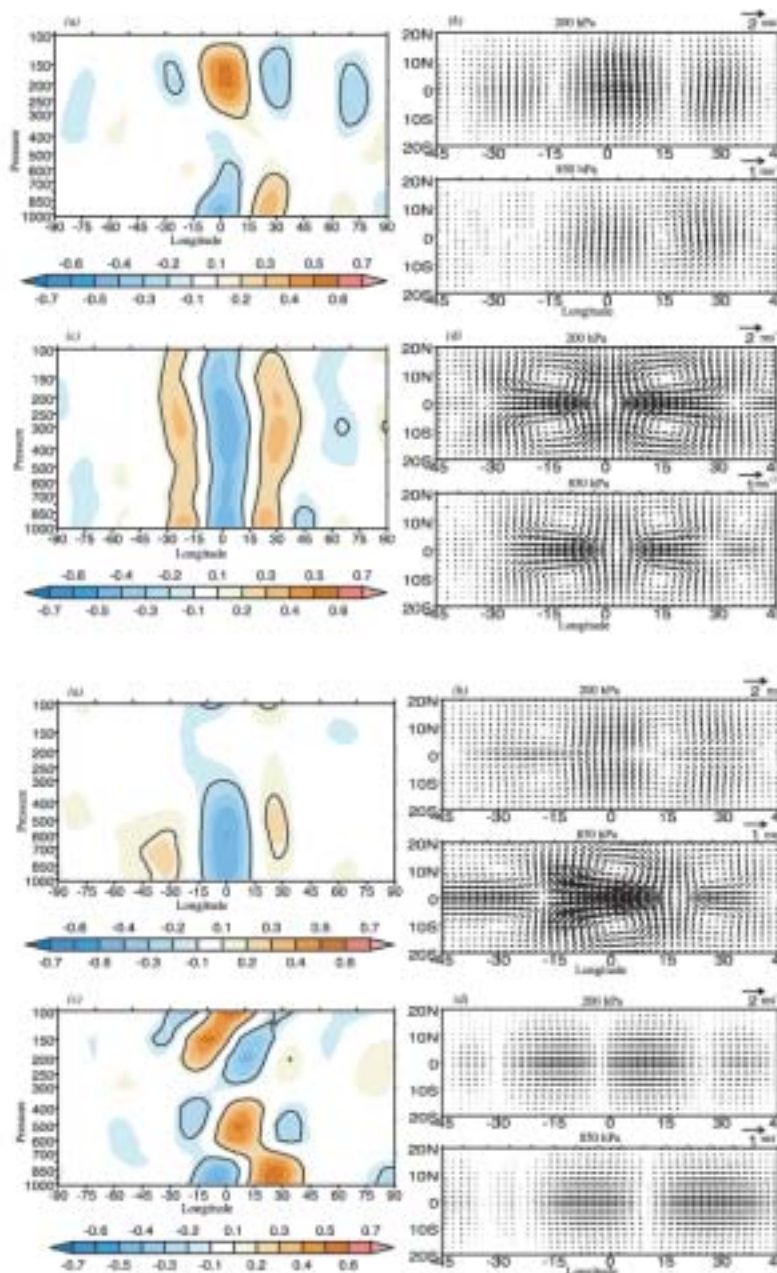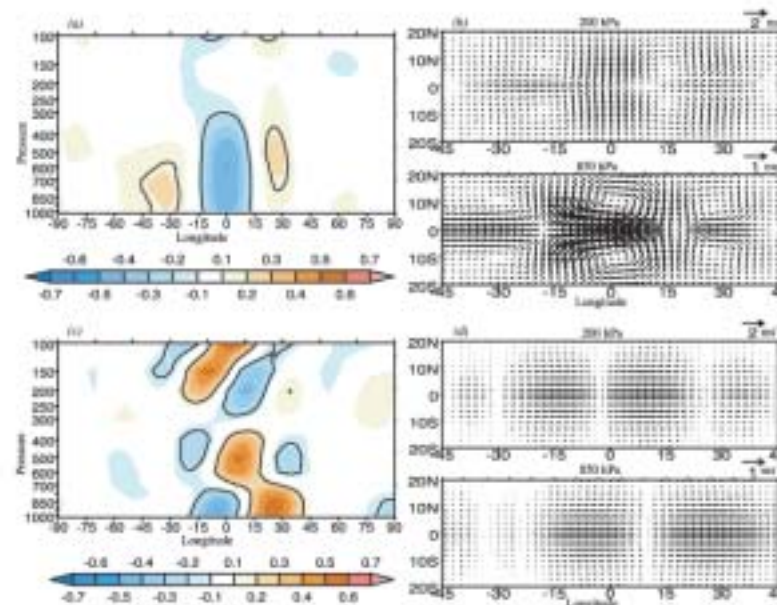
Figure 17. (a) Correlation between off-equatorial convection (T_b extrema at 6°N-16°N) and equatorial meridional winds (v) for WMRG waves in the eastern hemisphere, as a function of longitude and height. The convective maximum is displaced to 0° longitude. Note that according to theory, the divergent and convergent centres are coincident with the v extrema, so that convective extrema should be correlated with the v field. Solid contours indicate significance exceeding 95%. (b) Corresponding horizontal winds of the MRG wave at 200 and 850 hPa regressed with T_b = -7.6K at 0° longitude. The T_b value is 1.5 times the peak standard deviation in the eastern hemisphere, 6°N-16°N. (c) As for (a) but for westward moving R1 waves (v at 8°N) correlated with T_b extrema at 8°N-18°N in the western hemisphere. (d) As for (b) but for R1waves regressed with T_b = -7.5K.

Figure 18. (a) Correlation between equatorial convection (T_b extrema at 6°N-6°S) and equatorial zonal winds for westward moving R1 waves in the eastern hemisphere. (b) Corresponding horizontal winds of R1waves regressed with T_b = -7.2K at 0° longitude. (c) As for (a) but for eastward moving Kelvin waves. (d) As for (b) but for eastward moving Kelvin waves regressed with T_b = -8.7K.

Westward moving R1 waves coupled with off-equatorial convection also exhibit the first internal mode structure in the eastern hemisphere (not shown). However in the western hemisphere they are dominated by a barotropic structure (Figure 17c,d). The barotropic structure is more significant in the transition season where the basic zonal wind has a strong westerly vertical shear. This structure is thought to be associated with upper level forcing by midlatitude Rossby waves.

R1 and Kelvin waves coupled with equatorial convection

The potential for equatorial convection to be influenced by wind-induced surface fluxes of moist entropy is shown in observed R1 and Kelvin waves coupled with equatorial convection, especially for R1 waves.

It is clear that enhanced equatorial convection is closely related to low-level westerly winds for R1 waves (Figure 18a,b), in line with the mean low- level westerly background state in the eastern hemisphere. This convective response to equatorial zonal winds modifies the structure of R1 waves so that they no longer closely resemble their theoretical counterpart which is expected to be

associated only with off-equatorial convection. The low-level equatorial westerly wind anomalies are considerably strengthened by a positive feedback between the convection and the wind field. As in the WMRG case, the upper-level equatorial divergence above the equatorial convection modifies the equatorial zonal winds.

For Kelvin waves (Figure 18c,d), there is a closer association between convection and low-level zonal winds, than with the low-level convergence expected from some theory. This is consistent with a westward tilt with height below 300 hPa, with the 200 hPa divergence being closely associated with convection. Above 300 hPa the wave tilts eastwards with height (Figure 18c), suggesting propagation into the stratosphere.

Reference

Yang G. -Y, B. Hoskins, and J. Slingo, 2003: Convectively coupled equatorial waves: A new methodology for identifying wave structures in observational data. J. Atmos. Sci., 60,1637-1654.

Climate Change

Ocean dynamical influence on climate sensitivity

Ben Booth (booth@atm.ox.ac.uk), Climate and Oceanography Group, Atmospheric, Oceanic and Planetary Physics, Clarendon Laboratory,

Understanding the sensitivity of climate to radiative changes is an ongoing thread in the climate research. Much of this research goes into characterising and understanding individual feedback mechanisms (some of which are better understood than others) which contribute to the overall climate response. The traditional approach to this has focused on atmospheric and oceanic processes while the ocean is considered to only influence the timescale of response. On closer consideration however, you might expect changes in ocean circulation to affect the climate sensitivity. The ocean is responsible for the pole ward transport of the heating at the equator. The resulting pattern of land surface temperatures determine the pattern of cloud formation, precipitation, surface albedo and many other aspects of climate which contribute feedbacks. Conventional assumptions of climate sensitivity assume that oceans circulation patterns in radiatively forced equilibrium climate are not significantly different from the control climate. Recently, however, long integrations of radiatively forced fully coupled ocean atmosphere climate models have been run. This allows us to start to investigate the influence of the long term ocean changes on climate sensitivity. In this case we look at the impact of changes observed in a 1700 year integration of the coupled model, HadCM3.

Comparisons between the response of the atmosphere model coupled to thermodynamic slab ocean (HadSM3 known as the slab model) and the response of the coupled model (HadCM3) allows us to tease out the role the ocean plays. Differences in warming between these two models can be attributed to ocean changes in the coupled model which aren't represented in the slab model. First off it becomes apparent that the pattern of ocean circulation changes through the first 300 years of the coupled simulation. By the end of the coupled simulation (1700 years) the ocean has a new and stable circulation. Although the coupled model hasn't reach equilibrium we can investigated the impact of these circulation changes by imposing changes in sea surface heat fluxes diagnosed from the coupled simulation, on to the simpler model, HadSM3. The slab model rapidly reaches equilibrium to changes so we can use this feature to explore the equilibrium response. Through a series of experiments we are able to quantify the impact of the heat flux changes (on the global mean temperature response in the model) with quadrupling of the CO_2 levels. The standard slab model has an global mean equilibrium temperature response of 7.1 degrees. We can carry out the same experiment with the slab model with the imposed changes in ocean surface heat flux from the coupled run. This model gives a warming of 10.4 degrees, 3.3 degrees warmer than the slab with no ocean changes. To put this into context, current estimates of uncertainty in climate sensitivity give a range of values between 1.5 and 4.5 with perhaps the largest uncertainty in the impact of the cloud response (roughly 2 degrees). Assuming that the temperature response in linear with forcing, neglecting the impact of ocean changes on climate sensitivity would under represent the climate sensitivity by 1.6 degrees (for a doubling of CO_2) in the Unified Model.

On further analysis we can separate the difference between the standard model and the model with the imposed ocean surface heat flux changes (from the coupled model) into a direct effect and a indirect effect. By imposing the surface heat flux changes on to a unforced slab model we observe a warming of 1.2 degrees. Changes in the resultant land sea temperature contrast produce changes in the atmospheric and land surface patterns. The dominate change is to the pattern of cloud formation. These changes are sufficient to cause the warming which is observed. We can refer to this as the direct influence of ocean dynamical changes on climate sensitivity however it doesn't explain the total difference (3.3 degrees). To explain this we need to look at the climate sensitivity of the slab model with the surface heat fluxes changes (the difference between the perturbed equilibrium response and the control temperature). The global mean temperature difference of the adjusted slab model (with representation of the ocean changes) to quadrupling of CO_2 is 9.2 degrees (larger than the standard temperature response). Due to the changes in ocean circulation, the distribution of many feedback mechanisms has changed. The strengths of these feedbacks in a radiative forced scenario are no longer the same as the standard model/climate and the response is more sensitive. This change in the sensitivity of the model can be seen as the indirect influence of ocean dynamical changes.

This is a significant result and should change the way we view uncertainty in climate sensitivity, however it is dangerous to draw too strong conclusions about the impact of ocean dynamical changes on the climate response. There is the suggestion that other models show a different ocean response to radiative forcing (Watterson, 2003). What this work does do is highlight that ocean impacts can be highly significant. Clearly the role of ocean dynamics needs to be considered but further work needs to be done to better understand the nature of the ocean's impact.

References

I. G. Watterson, (2003): Effects of a dynamical ocean on simulated climate sensitivity to greenhouse gases. Climate Dynamics 21 197-209
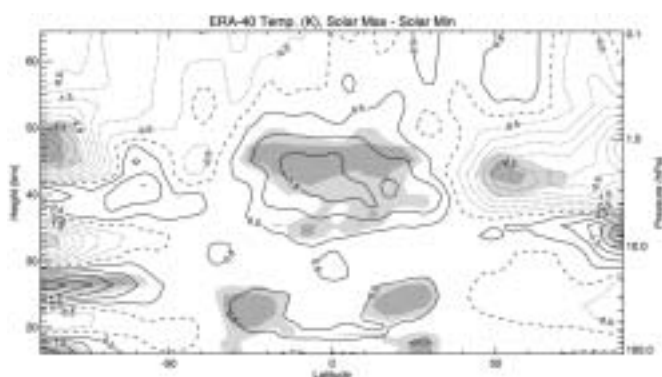
Figure 19. Amplitude of solar signal in zonal mean temperatures in units of Kelvin per solar cycle. Shaded areas denote statistical significance at the 5% (light shading) and the 1% (dark shading) levels.
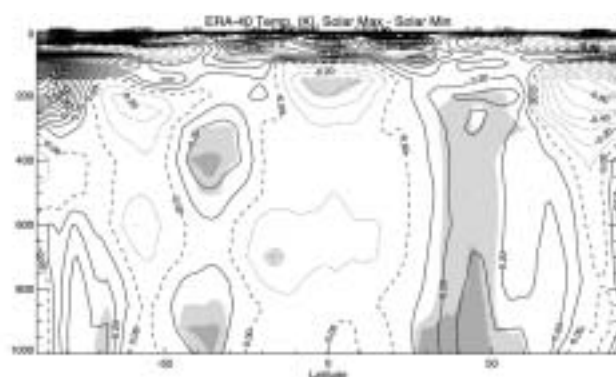

Figure 20. Solar signal in zonal mean tropospheric temperatures in units of Kelvin per solar cycle.

Describing the solar signal in ERA-40 zonal mean temperatures

Simon Crooks, University of Oxford, Lesley Gray, Reading University

One of the fundamental problems in attributing atmospheric changes to changes in solar activity is that the magnitudes and locations of these solar induced changes are largely unknown, as is the true nature of the mechanism, or mechanisms that facilitate these changes. Knowledge of such matters would enable modelling and mathematical analysis of datasets to be much more accessible, and alongside an insight into the impacts that other forcings have on the atmosphere, would provide a platform from which to base future analysis of naturally induced climate change. An ordinary least squares multiple regression analysis was performed to disentangle various specific components of temperature change and to illustrate that each individual forcing scenario would produce an individual pattern of response dissimilar to that of the others.

The ECMWF, ERA-40 re-analyses of zonally averaged monthly mean data covering 1979-2001 are used in this analysis. A standard linear multiple regression technique using an auto-regressive model of order three was used to separate various climatic effects in the temperature and zonal wind datasets. The data, whether it be, temperature or zonal wind, was deseasonalized by removing the climatology derived from 1979-2001, before fitting it to twenty independent indices via an ordinary linear least-squares regression model. Twelve of the indices represent any re-current annual and semi-annual variations in the other indices (and the data), and in effect deseasonalize (if necessary) the remaining indices. The regression model also incorporated: a linear trend term, the solar 10.7cm flux (which is highly positively correlated with the sunspot solar cycle), optical depth (related to volcanic eruptions) (Sato *et al*., 1993), North Atlantic Oscillation (NAO) (Jones *et al*., 1997), Cold Tongue Index (highly correlated to El Niño Southern Oscillation (ENSO)), and two orthogonal quasi-biennial oscillation (QBO) timeseries. The last remaining index is a step function (step before April 1986) which accounts for a discontinuity in the ERA-40 re-analyses due to a blip in the data owing to the joining together at the end of March 1986 of two independently run analysis streams (Agathe Untch, personal communication). The 10.7cm solar flux was scaled to represent the average difference between solar minimum and solar maximum,

(based on over 40 years of observations). Thus the slope of the regression onto the solar timeseries will show the change in the diagnostic (temperature or zonal wind) for a standard change in flux between solar minimum and solar maximum.

Figure 19 presents the latitudinal-vertical structure of the solar signal in temperature (K per mean change in flux over a solar cycle) in the ERA-40 data. The spatial pattern of temperature increases is maximized over low latitudes with an approximate symmetry about the equator within the tropics. A statistically significant warming is shown in the tropical (30˚S-30˚N) upper stratosphere peaking at an amplitude of over 1.75K at 42km (≈2.5hPa). A large negative component is seen in high northern latitudes at equivalent altitudes but peaking more strongly at over -3.5K at 55˚N, leaving a region of large anomalous meridional shear across the mid-latitudes. Two significant lobes of positive temperature response appear in the lower stratosphere, each centred ≈25˚ from the equator, with the lobe in the northern hemisphere being ≈0.25K warmer than the lobe in the opposing hemisphere. These lobes are not present in the work of any other author performing similar analyses on datasets of middle atmosphere temperatures. The temperature response throughout the whole of the tropical stratosphere is positive with a null value at 16km (≈100hPa), implying that increasing stratospheric temperatures follow an increase in solar insolation. This is undoubtedly linked with increased UV absorption by ozone.

Figure 20 shows the solar signal in tropospheric temperatures. There are also two regions of positive response; one in each hemisphere between 30-50°N, extending vertically through the troposphere. These features are very similar to the response presented by Haigh (2003).

In summary it is possible to separate the solar signal in atmospheric temperatures from other signals, e.g. volcanic, and based on this dataset of ERA-40 re-analyses there appears to be a solar signal in the troposphere and lower stratosphere as well as in upper stratosphere temperatures. The analysis also shows that the solar signal is dependent upon location and time of year. Solar changes also induce a large significant temperature change in the mid-stratosphere at the pole in northern hemisphere winter (not

shown) thus suggesting that the response is dynamical and not just radiative.

References

Sato, M., Hansen, J.E., McCormick,M.P. and Pollack, J. B. Stratospheric aerosol optical depth (1850-1990) Journal of Geophysical Research, year: 1993, vol.: 98, pages: 22987-22994

Jones, P. D., Jonsson, T. and Wheeler, D. Extension to the North Atlantic Oscillation using early instrumental pressure observations from Gibraltar and South-West Iceland Int J. Climatol., year: 1997, vol.: 17, pages: 1433-1450

Haigh, J. D. The effects of solar variability on the Earth's climate Phil. Trans. Roy. Soc., year: 2003, vol.: 361, pages: 95-111

Seasonal Predictability of North Atlantic Climate in the ECMWF System II Forecasting System

Steve George and Rowan Sutton, Dept. of Meteorology, University of Reading

The European Centre for Medium-Range Weather Forecasts (ECMWF) has developed a seasonal forecast model (System II), and provides monthly operational seasonal forecasts out to six months ahead. The system employs a variant of the ECMWF medium-range atmosphere model, coupled to the HOPE ocean model from the Max-Planck Institute for Meteorology. Forecasts from the 1st November consist of 40 ensemble members, with perturbations being applied to both the sea surface temperature (SST) and wind fields. In addition to two years of operational runs, the system has also been run in hindcast mode from 1987 onwards.

One of the objectives of this project is to use the model as research tool for investigating ocean atmosphere interactions on seasonal timescales. Before such work can be undertaken, one must have confidence that the model is performing in a similar manner to the real ocean/atmosphere system. A general methodology for addressing how well an ensemble forecasts is performing has not as yet been developed, and this article describes some of the work that is trying to address this problem.

For the purposes of this article, analysis is limited to the DJF season 500mb geopotential height fields. Verification is made with respect to ERA15 data and recent operational analysis. Initially, it is important to define exactly what is meant by a forecast performing "well". In the context of seasonal forecasting, model performance can be devolved into two components:

• Skill: Is the model consistent with observations?

• Predictability: Is the ocean influence (signal) strong by comparison with weather noise.

The model is known to exhibit consistent spatial biases, thus the analysis is performed with anomaly fields (rather than raw data).

Model Skill: Interval Test

It can be hypothesised that reality is but one possible solution to the integration of weather noise in the climate system, and that a real world ensemble exists until the moment of observations. As such, the model intra-ensemble variability can be employed as an estimate of weather noise. Assuming a perfect model and gaussian statistics, the observations for a particular year would expect to be described by the model population distribution $X \sim N(\upsilon, \sigma)$, where υ and σ are the mean and standard deviation respectively. If the observations are consistent with the model, it is expected that on average they will fall within the central 95% of the model population distribution 95% of the time. It should be noted that the population parameters are estimated and thus there are appropriate uncertainties included in the analysis.

The interval test was applied to the region defined as the North Atlantic (110W:35E, 20N:85N). In addition to the observational
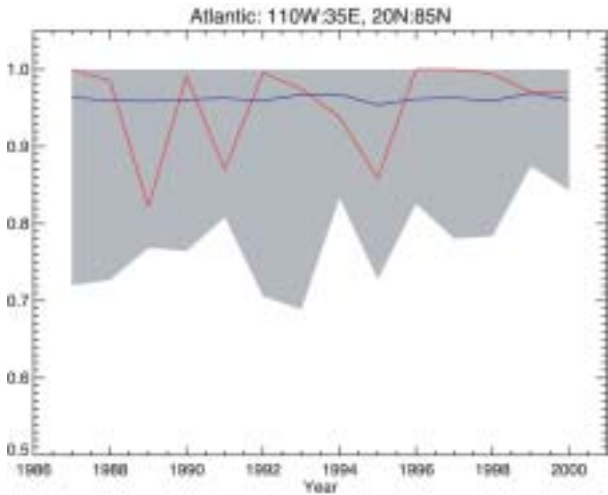

Figure 21. Time series of interval test (95% level) applied to the Atlantic region (110W:35E,20N:85N), with y-axis indicating percentage areal cover. The grey area represent the spread of coverage obtained from individual ensemble members, red line observations and blue line the average of all ensemble members. The expected coverage is 95%.
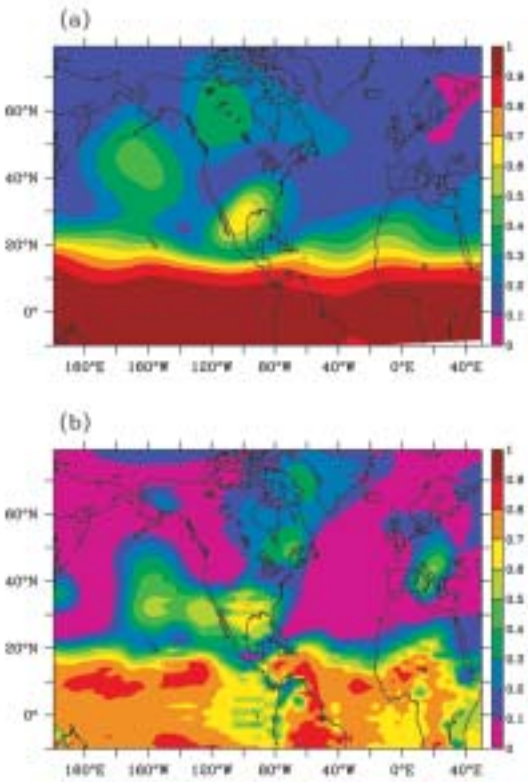

Figure 22. (a): Average R^2 (variance explained) from the regression of each ensemble member onto the ensemble mean. (b) Variance explained by regressing observations onto the ensemble mean. High R^2 values signify high signal-to-noise.

study, the calculations were repeated for each ensemble member, and Figure 21 displays the results, the grey shaded areas indicating the range of coverage from the ensemble members. It can be seen that, in a broad sense, the model is consistent with observations within these regions. The observational coverage timeseries is indistinguishable from that of an individual ensemble member.

Analysis of Variance: Regression Analysis

By regressing both the ensemble members and the observational timeseries onto the ensemble mean, comparisons can be made of the signal-to-noise ratio. This is achieved by calculating the coefficient of determination (or R^2), which is the ratio of the regression sum of squares to the total sum of squares. A high R^2 value indicates high signal-to-noise.

Figure 22(a) and (b) show the R^2 values for the model members and observations respectively. The model shows high signal-nose in tropics and some regions of the extra-tropics (North Pacific, SE USA and West Atlantic). The observations are similar, but data for NW South America (Ecuador Venezuela) and Western Canada (NW Territories/British Columbia) suggests that the model is not variable enough. Conversely, over Greenland and the Mediterranean/Southern Europe the model seems to be excessively variable. The latter result is interesting in that it suggests there may be more potential predictability available in these regions than the model suggests.

Conclusions

The analysis indicates that according to the measures considered the model is performing well, and can thus be employed as a tool for future mechanistic studies. The main points to note are as follows:

• Interval test shows that, in a broad sense, the model is consistent with the observations.

• Test for variance explained shows that the model exhibits significant predictability in tropical and some extra-tropical regions.

• There is evidence that the model may have too much variability (& hence too low signal-to-noise) over Mediterranean/Southern Europe.

Evaluating modelled and observed trends and variability in ocean heat content

Jonathan Gregory [1,2], Helene Banks [1], Peter Stott [1], Jason Lowe [1],
[1] Hadley Centre for Climate Prediction and Research, Met Office, Bracknell, United Kingdom,
[2] Centre for Global Atmospheric Modelling, Department of Meteorology, University of Reading, United Kingdom

Observational results have previously shown that ocean heat content has increased over the last fifty years. Models are generally able to reproduce the observed trend but not the substantial decadal variability seen in the observed timeseries (Levitus *et al.*, 2000, hereafter referred to as the "Levitus" results), as shown for instance in Figure 23 for the HadCM3 AOGCM (Gordon *et al.*, 2000). It is important to explain the discrepancy because variability of the size exhibited by the Levitus timeseries would have a substantial influence on the heat balance of the climate system and the interannual variability of climate, possibly affecting the conclusions of climate change detection and attribution studies. For example, the Levitus timeseries shows an increase of 7.5e22 J from 1988 to 1994, corresponding to a heat flux averaged over the world of 0.7 W m^{-2}, about half the size of the radiative forcing due to carbon dioxide.

Sampling can be very sparse in the World Ocean Database (WOD), on which the Levitus results are based. When interpolated onto the HadCM3 grid, data coverage reaches a maximum of 70% after 1970 in the upper 360 m in the Northern Hemisphere (0-65N). Coverage declines with increasing depth; below 1200 m it never exceeds 20%. Levitus *et al.* (2000) created almost globally complete data using interpolation methods. Our attempts to estimate global ocean heat content from the WOD data suggest that the trend and variability can be very sensitive to the method of filling in the data voids.

In the well-sampled NH upper ocean, we find that the model is able to reproduce both the trends and variability when HadCM3 includes both anthropogenic and natural forcings (ALL ensemble). While the trend is reproduced reasonably well in the ANTHRO ensemble, the variability appears to be underestimated. The
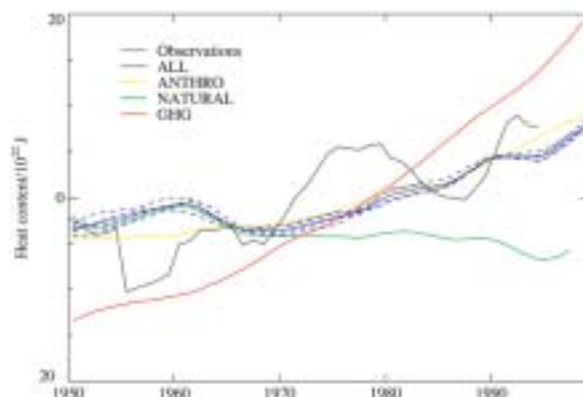

Figure 23. World ocean heat content as estimated by Levitus et al. (2000) and from the HadCM3 ensembles: GHG (greenhouse gases only), ANTHRO (greenhouse gases plus sulphate aerosols and tropospheric and stratospheric ozone changes), NATURAL (changes in solar output and stratospheric volcanic aerosols) and ALL (all the forcings included in ANTHRO and NATURAL). Solid lines show the mean of four ensemble members and the blue dashed lines show the values for individual members of the ALL ensemble.

NATURAL ensemble shows a slight decreasing trend in ocean heat content but has enhanced variability.

We have analysed the variability as a function of depth in the Levitus timeseries and the HadCM3 control, both detrended. We used a large number of portions of the control, each of the length of the Levitus timeseries, in order to evaluate the uncertainty in the estimate of the model variability. Figure 24 shows that the simulated and observed datasets agree rather well in the upper 50

m. Variability in the model generally declines monotonically with
increasing depth, but in the Levitus dataset there are marked peaks
in the approximate ranges 40-100 m and 200-600 m. Since the
source of variability is at the surface, we find these subsurface
maxima intriguing. Around 500 m Levitus has twice the variability
of the model. Below 200 m, imposing the observed data mask for
1947-1994 on the simulated data has a strong influence on the
estimated variability, doubling it at some levels. This sensitivity to
the data mask leads us to suggest that the sparseness of the
observed data could have made a contribution to inflating the
subsurface variability in the Levitus timeseries.

References

Gordon, C., C. Cooper, C. A. Senior, H. Banks, J. M. Gregory, T. C. Johns
and J. F. B. Mitchell, The simulation of SST, sea ice extents and ocean heat
transports in a version of the Hadley Centre coupled model without flux
adjustments, Climate Dyn, 16, 147-168, 2000.
Levitus, S., J. I. Antonov, T. P. Boyer, and C. Stephens, Warming of the
world ocean, Science, 287, 2225-2229, 2000.
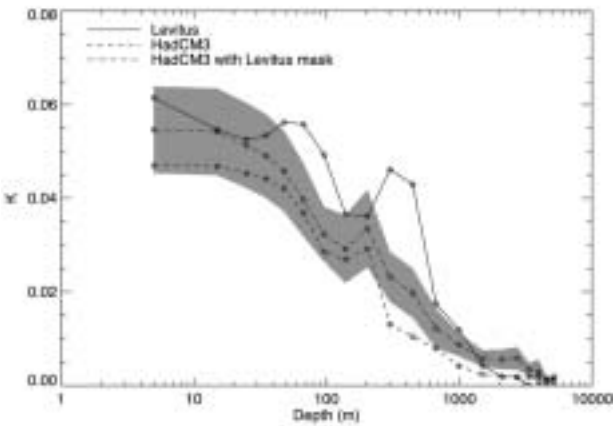
Figure 24. The interannual standard deviation of detrended
temperature as a function of depth for HadCM3 and Levitus. The
shaded region indicates the sampling uncertainty obtained by
taking a number of 50-year segments of the HadCM3 control
simulation.

Climate response to absorbing tropospheric aerosols

J. Cook and E. J. Highwood, Department of Meteorology, The University of Reading

Radiative forcing is a useful indicator of climate change
assuming that the climate sensitivity parameter, λ, is constant
regardless of the forcing mechanism. Hansen *et al.* 1997,
(hereinafter H97) suggested that while λ is consistent for forcings
such as $2xCO_2$ and increased solar irradiation, it differs for ozone
and aerosols. This was particularly true for absorbing aerosols,
where H97 proposed the existence of an aerosol "semi-direct
effect", whereby the absorption of solar radiation by aerosol
reduces large-scale cloud cover. This study aims to investigate
whether these results are corroborated in the Reading Intermediate
General Circulation model (IGCM) and to determine the
qualitative contribution of clouds to climate response to
tropospheric aerosols.

Multi-decadal integrations of the mixed layer, $5° \times 5°$ model with
22 levels in the vertical, simulated the climate response to globally
uniform distributions of five different aerosol types, characterised
only by their single-scattering albedo, ω. The aerosol was placed
in the lowest four model levels. We examine a range extending
from purely scattering aerosols ($\omega=1$) to strongly absorbing
aerosols ($\omega=0.8$). λ varied dramatically from the value for the
response to an increase in carbon dioxide when the aerosol was
only slightly absorbing of solar radiation. For ω of around 0.85 to
0.9, the climate sensitivity parameter was found to be negative,
with aerosol causing a negative radiative forcing but a positive
surface temperature change. Thus global mean radiative forcing
was found to be a poor predictor of even the sign of equilibrium
surface temperature change.

Cloud changes play a vital role in the IGCM response to aerosol.
The so-called semi-direct effect of H97 does exist in the IGCM but
can be split into two distinct parts. For aerosol with $\omega=0.8$, a
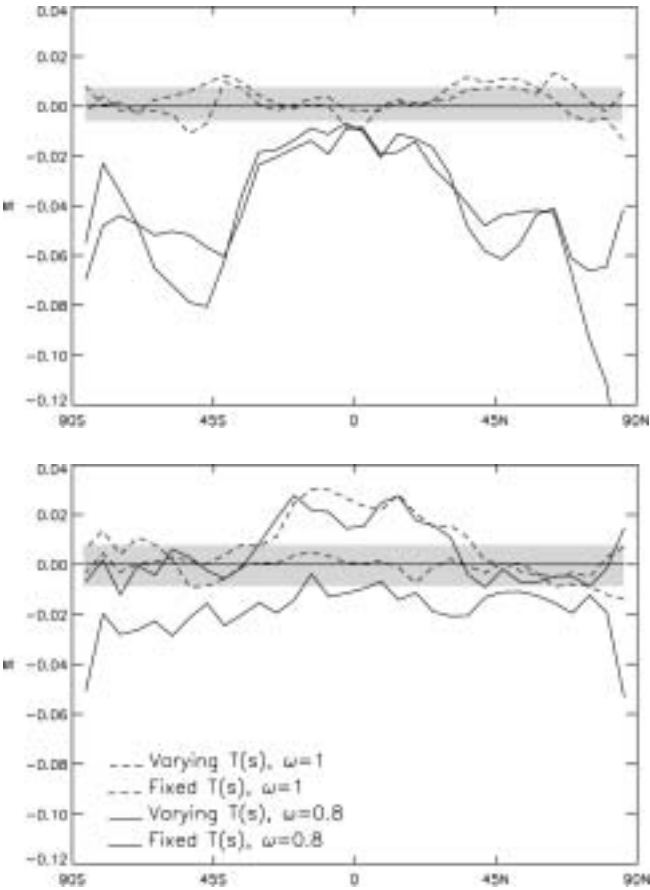significant decrease in low cloud amount was found at virtually

Figure 25. Zonal mean low cloud fraction responses (top) and
high cloud fraction responses (bottom) to scattering and
absorbing aerosol in model runs where the surface temperature
is allowed to vary (heavy), or remains fixed (light). Shading is
where changes are not significant at the 95% level.

every latitude as shown in the top panel of Figure 25 (heavy solid line). When the simulation was repeated but the surface temperature was not allowed to respond to the aerosol, these changes in cloud remained virtually unchanged (thin solid line). In the case of purely scattering aerosol, the low cloud changes were not significant at the 95% level (indicated by the shading) and remained insignificant in the simulation with fixed surface temperature. The first role of cloud in the IGCM response to aerosol, (the reduction in large-scale low cloud), is a result of the presence of the aerosol in the column and is not substantially mitigated by the surface temperature change. This result also suggests that it is an effect peculiar to aerosols.

However, there is also a change in the high cloud in the simulation. The bottom panel in Figure 25 shows a small reduction in high cloud fraction at all latitudes in the absorbing aerosol case, which becomes insignificant (or even an increase in the tropics) when the surface temperature is not allowed to respond. Similarly, changes in the scattering aerosol case become insignificant in the fixed surface temperature simulation. Thus we conclude that the

high cloud response to aerosol is partly due to the surface temperature change and could be generic to any mechanism producing a similar surface temperature change. Comparison with H97 shows that this is likely to be model dependent.

Whilst these experiments use highly idealised aerosol distributions, they demonstrate that the response of climate models to even such simple aerosol fields is not well understood. Since the response is heavily dependent on cloud changes, and clouds are somewhat troublesome to represent in climate models, we may be some way from defining the mechanisms of the aerosol semi-direct effect. Nonetheless, this effect exists, largely undiagnosed, in any model including absorbing aerosols. Further examination tells us not only about the model response to aerosol but also about the cloud feedbacks of the model in general.

This work is to appear in the Quarterly Journal of the Royal Meteorological Society early next year.

Reference

Hansen, J. Sato, M. and Ruedy, R., 1997: Radiative forcing and climate response. J. Geophys. Res., 102, 6831-6864.

External control of changes in global land precipitation

F. Hugo Lambert (1) (hlambert@atm.ox.ac.uk), Peter A. Stott (2), Myles R. Allen (1) and Michael A. Palmer (3)
1. Atmospheric, Oceanic and Planetary Physics, University of Oxford.
2. Hadley Centre for Climate Prediction and Research, Met. Office.
3. Space Science and Technology group, Rutherford Appleton Laboratory.

During the last few years, linear regression studies comparing General Circulation Model (GCM) output with observations have established that external factors, including human influences, have determined a proportion of 20th century climatic behaviour.Here, we demonstrate for the first time the formal detection of the influence of external forcing on global land precipitation at a high confidence level. Observed and HadCM3 model simulated precipitation are compared using an "optimal fingerprinting" (linear regression) method. It is found that 6-year mean observations for 1945-97, and to a lesser extent for 1900-97, are well described where the model is forced with anthropogenic and natural forcings. For 1945-97, we find an estimate of beta, the amount by which the model simulated signal must be multiplied to best represent observed behaviour, of 2.22 with 5-95% confidence limits spanning 0.96 to 5.61.

Precipitation is a variable that suffers much small-scale spatio-temporal variability. The generalisation of point-like precipitation gauge measurements to gridded data is difficult, and contains many possible sources of systematic and random error (e.g. Groisman and Legates, 1994). The modelling of precipitation relies on the parameterisation of processes which occur on scales smaller than GCM grid boxes. How then, are we able to attribute changes in global land 20th century rainfall? We believe the reason is that changes in global precipitation are well-constrained by the tropospheric energy budget, of which latent heating related to precipitation is an important part.

Following the work of Mitchell et al., 1987, we write down the perturbation energy budget of the troposphere to first order as,

$$L\Delta P \; = \; k_T \Delta T + \Delta R_c + \Delta R_s$$

where $L\Delta P$ represents changes in latent heating of the troposphere, $k_T \Delta T$ changes in tropospheric cooling due to changes in temperature, ΔR_c changes in tropospheric cooling due to changes in atmospheric composition and ΔR_s represents changes in tropospheric cooling due to changes in direct shortwave cooling. In the HadCM3 model simulation of the 20th century, precipitation changes over land areas corresponding to those
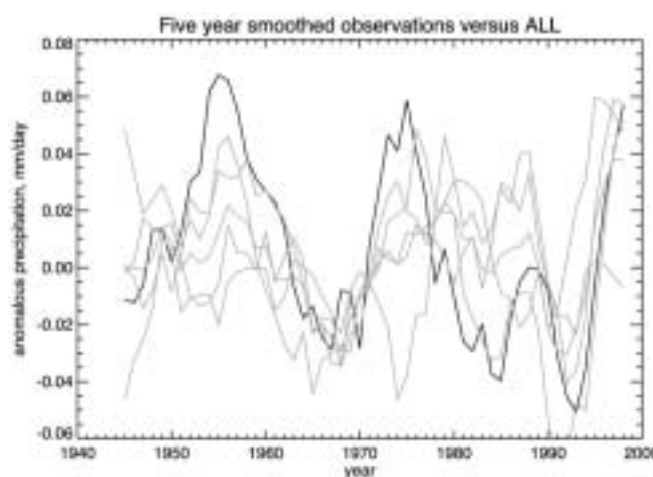

Figure 26. Observed and all forcings model-simulated mean time series compared for 1945-98. The thick black line represents observations and the thick grey line represents the model ensemble mean. The individual ensemble members are included as thin grey lines. All are series of anomalous precipitation and are smoothed with a 5-year boxcar filter. The model series are "masked" to include only the same areas for which there are data in the observations. The model simulation captures some of the form of the observations, but is possibly underestimating the response to forcing.

covered by the observed dataset were found to have a correlation of 0.63 with global precipitation. Global tropospheric conservation of energy in the model, therefore, may be sufficient to produce trends in precipitation of a similar shape over land areas to those observed where the model is appropriately forced.

Furthermore, the size of the precipitation response to a radiative forcing is dependent on the forcing's origin. In general, an external forcing causing an increase in tropospheric cooling due to an increase in global temperature, $k_T \Delta T$, cause an accompanying increase in precipitation subject to offsets introduced by the nature of the forcing, ΔR_c and ΔR_s. Immediately, we can see that the effects of natural and anthropogenic forcings on tropospheric cooling will be different. Whereas the natural forcings, predominantly changes in solar insolation and the effect of volcanic stratospheric aerosols, warm the climate system by direct shortwave absorption at the surface, changes in anthropogenic CO_2 warm the surface by reducing the ability of the troposphere to cool. Although a small amount of solar radiation is absorbed by the troposphere causing an instantaneous reduction in tropospheric cooling, ΔR_s, we expect from model studies a much larger instantaneous reduction in tropospheric cooling due to a change in CO_2, ΔR_c. Hence, a natural forcing that causes the same change in surface temperature as a CO_2 forcing will produce a larger change in global precipitation. The ratio of the precipitation response to a natural forcing to the precipitation response to anthropogenic CO_2, where both forcings produce the same change in global surface temperature, is estimated to be more than 1.5 from HadSM3 slab model experiments.

The aim of our future work is to investigate this more fully by estimating the size of each term in the perturbation energy budget equation by carrying out regression studies with the forced coupled model simulations and observations used here.

The work in this study has been submitted for publication in Geophysical Research Letters.

References

Groisman PY and Legates DR (1994): The accuracy of United States precipitation data. Bull. Am. Meteorol. Soc., 75:215-227.

Mitchell JFB, Wilson CA and Cunnington WM (1987): On CO_2 climate sensitivity and model dependence of results. Q.J.R. Meteorol. Soc., 113:293-322.

A Constraint on Future Changes in Extreme Precipitation

Pardeep Pall [a], Myles Allen [a], Jonathan Gregory [b], Steve Jewson [c]
[a] Atmospheric, Oceanic & Planetary Physics, University of Oxford, Clarendon Laboratory, Parks Road, Oxford, OX1 3PU, UK
[b] Hadley Centre, Met. Office, London Road, Bracknell, Berkshire, RG12 2SZ, UK
[c] Risk Management Solutions Inc.,10 Eastcheap, London, EC3M 1AJ, UK

The IPCC workshop on Changes in Extreme Weather and Climate Events (2002) recognised that understanding precipitation distribution is key to understanding the behaviour of its extremes. Concurrently it identified weaknesses in the IPCC TAR relating to the characterisation of extreme precipitation which were due to availability, quality and definition of data. What then can be said about future changes in extreme precipitation, and in particular, are there constraints that could potentially simplify the problem?

Whereas global-mean precipitation change under CO_2 warming is primarily constrained by the global energy budget, the heaviest events can be expected when effectively all the moisture in a volume of air is precipitated out – suggesting the intensity of these events increases with availability of moisture, that is, significantly faster than the global mean (Allen and Ingram, 2002). Further, under the regime of constant relative humidity one might expect the specific humidity, and hence moisture availability, to increase according to the Clausius-Clapeyron (C-C) relation (Boer, 1993) and hence for this relation to give a quantitative constraint on the change at uppermost quantiles of precipitation distributions. Indeed it appears this constraint on the extreme is emergent in at least one AOGCM, namely HadCM3, as shown in Figure 27.

This study shows how the phenomenon manifests on regional scales also. Zonal analysis of daily rainfall in HadCM3 under a transient CO_2 forcing scenario shows an increased probability of extreme precipitation in the tropics accompanied by increased drying at lower percentiles of the distribution. At mid- to high-latitudes there is increased probability of precipitation over all percentiles, with the greatest agreement with C-C prediction
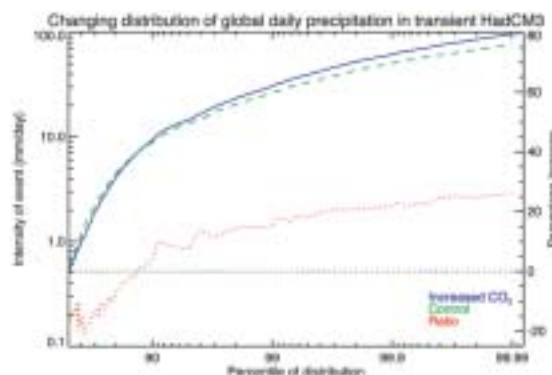

Figure 27. A return level plot (on a log-log scale) of daily precipitation in HadCM3 under a transient CO_2 forcing scenario, relative to a control, for the period 2070-2100. Extreme (99.99[th] percentile or 1/10,000 day event) precipitation intensity has increased by ~25% as shown by the ratio curve. Moreover, the C-C prediction on this change based on a global-mean temperature increase of 3.6K is ~22%. Furthermore, the discrepancy could be accounted for by 'Super C-C' conditions whereby flows that give rise to precipitation here are themselves driven by the latent heat released by that precipitation. Additionally, global energy considerations demand that there are decreases in precipitation intensity at lower percentiles.

occurring at mid-latitudes. The pattern is consistent with other climate model projections (Hennesy *et al.*, 1997) and suggests that the tropics dominate the global signal of extreme precipitation but regions in which the ambient flows change little give the greatest

Extreme precipitation change and Clausius-Clapeyron prediction at the gridbox level
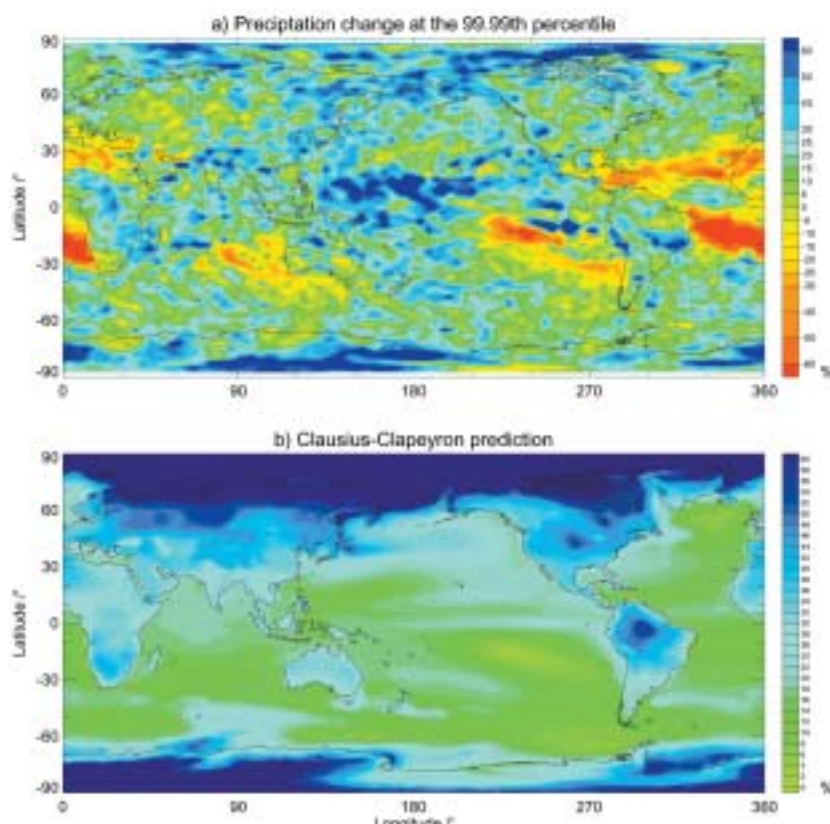

Figure 28. Maps at model gridbox resolution of:
a) Precipitation change at the 99.99[th] percentile (1/10,000 day event) in HadCM3 under the transient forcing scenario of Figure 27. The values shown here would correspond to the 'ratio' curve of Figure 27 at the 99.99[th] percentile, with the data now having been disaggregated by gridbox.
b) The C-C predicted change based on mean temperature increase at that gridbox.

agreement with C-C thermodynamics – i.e. that the phenomenon is local. This is borne out by a repeat of the global analyses at the gridbox level as shown in Figure 28.

It is evident from Figure 28a. that there are pronounced regions of enhanced tropical convergence and subsidence associated with stronger meridional circulations. Moreover, the C-C predicted changes are everywhere positive, so that agreement is best only in mid-latitudes, where ambient flows change relatively little. We conclude that one must expect changes in circulation, where they occur, to dominate our C-C prediction which is based on local

thermodynamics; but in regions where the constraint does apply it is arguably a better predictor of extreme precipitation change than more direct methods such as using the change in mean (not shown).

If the C-C prediction is indeed an emergent physical constraint, robust over both models and observations, then it would be powerful result of value for risk evaluation, where (better defined) predicted temperature changes could be used to constrain uncertainty on future extreme precipitation under climate change.

The QBO and climate change

Michael Palmer[1], Lesley Gray[2], Myles Allen[3],
[1]Rutherford Appleton Laboratory, [2]Reading University, [3]University of Oxford

Atmospheric carbon dioxide concentrations have increased by nearly 40% since the industrial revolution and, in combination with the other greenhouse gases, have produced a significant and detectable influence on global mean temperature (IPCC, 2001). The impact is not restricted to temperature, however, and a recent study has also been able to detect an anthropogenic influence on mean sea level pressure (Gillett *et al*., 2003a). The pressure response, seen in observations and models forced with elevated CO_2 levels, involves increasing pressure in the sub-tropics and reduced pressure over the north-pole. This pattern projects strongly onto the positive phase of the Arctic Oscillation (AO; Thompson and Wallace, 1998). However, it appears that the

response of many general circulation models (GCMs) significantly underestimates that in the observations (Gillett *et al*., 2003a).

Shindell *et al*. (1999) showed that forcing the stratosphere-resolving GISS GCM with increasing concentrations of CO_2 led to an AO response which was comparable in magnitude to that found in observational data. They argued that a key component of the response mechanism was a change in planetary wave propagation, made possible only by the high (~85km) vertical extent of the model. A follow up study (Gillett *et al*., 2002) showed, however, that increasing the vertical extent of the Unified Model made no significant impact on the AO response to doubled CO_2. We have extended this research by performing the first
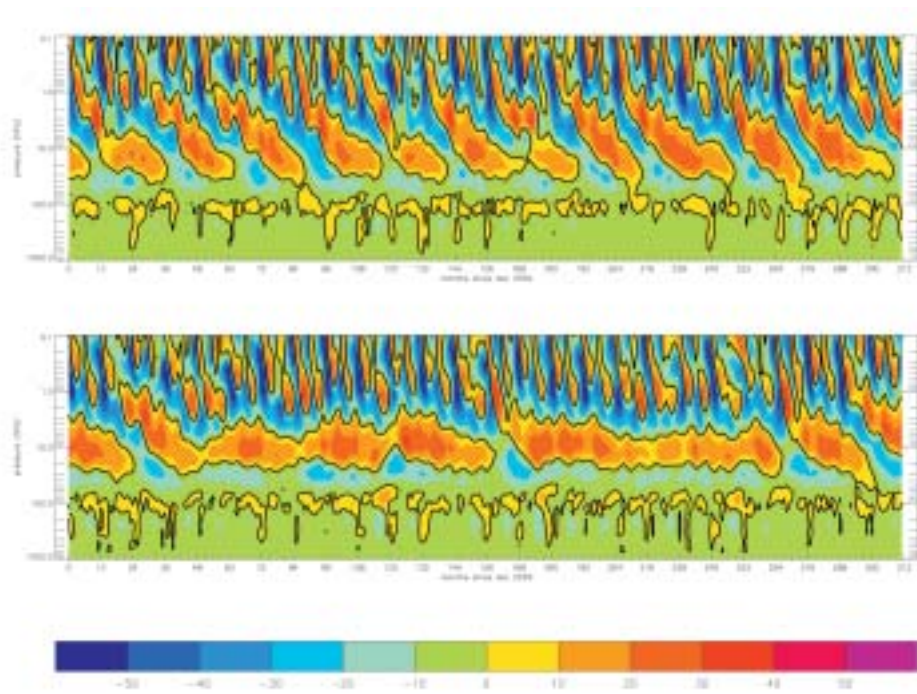
Figure 29. Absolute value of the equatorial zonal mean wind taken from the control integration (top panel) and from the doubled CO_2 integration after equilibration (bottom panel). The x-axis shows time (months) through the integration and the y-axis shows pressure (hPa). Contour interval is $10ms^{-1}$ and the zero contour is shown in black.

doubled CO_2 experiment in a stratosphere-resolving GCM with a self sustaining Quasi-Biennial Oscillation. The experiment performed is a direct extension of the work reported by Gillett *et al*. (2003b) to which we compare our findings. The results show that the stratosphere is important in determining the response of the lower atmosphere to increasing levels of carbon dioxide, and draw attention to the potential for tropical stratospheric changes to influence the climate response at higher latitudes.

Figure 29 (top) shows the QBO from the Unified Model incorporating the Hines' gravity wave parametrisation (Hines, 1997a; 1997b). The scheme produces a realistic QBO, with a mean period of approximately 26 months, which compares well to that of 28.2 (27.7) months found in observational data covering the period 1953-1995 (1953-1984) (Baldwin *et al*., 2001). The model QBO phases do not, however, penetrate to the lower-most stratosphere. This is primarily a result of a poorly simulated annual cycle in lower stratospheric zonal wind, giving a significant easterly bias in this region. De-seasonalising both model and reanalysis data shows considerably closer agreement than the absolute values of the winds shown here. However, we show the absolute values of the winds, as these are important in determining the potential effects on planetary wave propagation and hence on the extra-tropical circulation.

The parameters of the gravity wave scheme in the model are held constant for the doubled CO_2 experiment, and the resulting equatorial winds are shown in the bottom panel of Figure 29. Clearly the oscillation no longer has an approximately two year period, but shows persistent westerlies near to 10 hPa and easterlies both above and beneath. In addition, the difference between the experiment and the control simulation in DJF shows a strengthening of the mean meridional circulation and a weakening of the polar night jet. In comparison to the equivalent experiments, conducted with a rayleigh friction version of the model (Gillett *et*
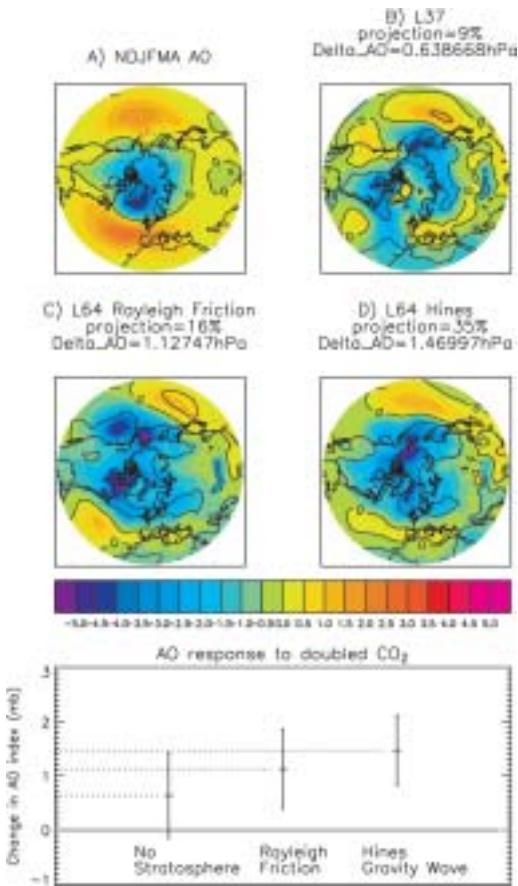

Figure 30. (top): Panel A shows the leading mode (EOF1) of sea level pressure variability from the Hines' control integration. Panels B and C (after Gillett *et al*., 2003b) show the difference between the doubled CO_2 atmosphere and the control for a model with a poorly resolved stratosphere (panel B) and a well resolved stratosphere with a rayleigh friction parametrisation (panel C). Panel D shows the difference between the doubled CO_2 case and the control for the stratosphere resolving model with the Hines' gravity wave scheme.
Bottom graph shows the value obtained by projecting the anomalies (panels C-E) onto EOF1 (panel A), normalized so that the pattern has an amplitude of 1hPa north of 60°N.

al., 2003b) we find that the strengthening of the mean meridional circulation and the weakening of the stratospheric polar night jet are less pronounced when the gravity wave scheme is included. The lower stratospheric and upper tropospheric winds are thus relatively more westerly in the doubled CO_2 Hines' case, and there is a corresponding impact at the surface.

Figure 30 (panel A) shows the leading mode of variability of the sea level pressure field from the Hines' model control run, the so-called Arctic Oscillation (AO; Thompson and Wallace, 1998). Also shown is the difference in surface pressure between doubled CO_2 experiments and the relevant control, for three separate cases: panels B and C (after Gillett et al., 2003b) show the results from a model with a poorly resolved stratosphere (panel B) and from an identical model with a well resolved stratosphere and a rayleigh friction parametrisation (panel C). The last picture (panel D) shows the result from the stratosphere resolving model with the Hines' gravity wave scheme. The graph below shows the change in AO index in these three cases, obtained by projecting the anomaly patterns onto the AO. Whilst it is impossible to differentiate statistically between the two stratosphere resolving models (panels C and D) there is a statistically significant increase in the magnitude of the AO change when the Hines' scheme is included compared to the model version with a poorly resolved stratosphere (panel B compared to panel D). In contrast to the results of Gillett et al., we therefore conclude that inclusion of a well resolved stratosphere can have a significant impact on the surface response to doubled CO_2. Moreover, we highlight the

potential for changes to occur in the equatorial QBO in response to increasing carbon dioxide levels, and hypothesize from these results that such changes may be important in determining the magnitude of any extra-tropical climate change signal. We note, however, that the parameters defined in the Hines' gravity wave scheme, such as the source strength of the gravity waves, are held constant in the two experiments. In reality, these are also likely to change with changing CO_2 concentrations, highlighting the need to couple the gravity wave parametrisation to the tropospheric wave source.

References

Baldwin M.P. et.al., 2001: The Quasi-Biennial Oscillation. Rev. Geophys., 39, p179-229.

Gillett, N.P., Zwiers, F.W., Weaver, A.J. and Stott, P.A., 2003a: Detection of human influence on sea-level pressure. Nature 422, p292-294.

Gillett, N.P., Allen, M.R. and Williams, K.D., 2003b: Modelling the atmospheric response to doubled CO2 and depleted stratospheric ozone using a stratosphere-resolving coupled GCM. Q. J. Roy. Meteorol. Soc. 129, p 947-966.

Hines C.O.,1997a: Doppler-spread parameterization of gravity-wave momentum deposition in the middle atmosphere. Part 1: basic formulation. J. Atmos. Solar Terr. Phys. 59, p371-386.

Hines C.O., 1997b: Doppler-spread parameterization of gravity-wave momentum deposition in the middle atmosphere. Part 2: Broad and quasi-monochromatic spectra, and implementation. J. Atmos. Solar Terr. Phys. 59, p387-400.

Thompson, D.W.J and Wallace, J.M., 1998: The Arctic Oscillation signature in the wintertime geopotential height and temperature fields. Geophys. Res. Lett., 25, p1297-1300.

Informing Adaptation: New Challenges for the Climate Modelling Community

Rowan Sutton, CGAM, University of Reading

In the climate change policy arena attention to date has focused primarily on mitigation measures such as the Kyoto agreement. Progress, however, has been notably slow, and it seems clear that we are already committed to significant climate change under all plausible emissions scenarios. It follows that in the decades to come the issues surrounding adaptation to climate change will demand increasing policy attention.

The policy agenda has, to a large extent, shaped developments in climate modelling. Driven by the need to inform policy on mitigation, efforts to forecast climate change have focused on time horizons of many decades or centuries, and on global mean temperatures as a crude proxy for harmful climate impacts. The information required to inform adaptation decisions is of a different nature. Regional and local details are essential, and information must be provided for the time horizons that are most relevant to strategic planning decisions. These time horizons vary considerably between sectors, but only rarely (such as for major infrastructure projects) do they extend toward centennial timescales.

The challenge to the climate science community is to provide the best possible information to inform adaptation decisions given the obvious constraints of uncertain science, uncertain data, and limited resources. Here I highlight three specific challenges:

1. The role of initial conditions

Initial conditions, especially in the oceans, cryosphere and land surface are an important constraint on the evolution of climate. This constraint has been largely ignored by IPCC because for time horizons of many decades or centuries other sources of uncertainty (model uncertainty and scenario uncertainty) are of greater importance. But for nearer time horizons ignoring information about the current climate state is likely to overestimate the true uncertainty in future climate. It follows that to provide the best possible information to inform adaptation decisions, the challenge of incorporating initial condition information must be faced.

2. Understanding the regional patterns of climate change

Confidence in projections of global mean temperature is based in large part on the existence of a simple mechanistic model with which the scientific community is generally content. By contrast there is very little mechanistic understanding, or consensus, concerning regional climate change. Existing "state-of-the-art" climate models show a wide range of regional climate change responses, and without a more developed mechanistic understanding it is difficult, if not impossible, to say which may be most trustworthy. A good example is provided by the land/sea temperature contrast. Climate models reliably suggest that the land warms more than the sea surface in response to greenhouse gas forcing, but in current climate models the ratio of warming over

land to warming over sea varies between about 1.2 and 1.9 (Jonathan Gregory, personal communication). There is as yet no theory that can explain, still less constrain, the factors that determine this ratio. There is a need for much more research to understand, at a mechanistic level, this and many other aspects of regional climate change.

3. Quantifying uncertainty

A systematic approach to estimating uncertainty is essential to meet the needs of decision makers concerned with adaptation to climate change. The hardest component of uncertainty to estimate is model uncertainty, associated with the fact that we will never have a perfect model of the climate system. Model uncertainty can be explored, to an extent, by making forecasts with a range of different climate models. However, decisions must be made about which set of models should be considered.

A basic but important insight is that the aspects of model uncertainty which it is most important to explore are those to which the forecast quantities of interest are most sensitive. This is clearly application/user specific, so we must be clear about our purposes. We must also recognise that in practice we don't know in advance where the greatest sensitivities may lie, so we must

exercise scientific judgement. For example, there are good reasons to expect that forecasts of precipitation over the UK may be very sensitive to the spatial resolution of a climate model, whereas forecasts of global mean temperature may be much less sensitive. More generally, we may reasonably anticipate that many aspects of regional climate change will be sensitive to resolution. The issues can be explored to a degree with regional climate models, but because the results from such models are very sensitive to the large scale driving fields, this approach alone is insufficient. To provide the best possible information to guide adaptation decisions it is important that the sensitivity of regional forecasts to global resolution is also investigated systematically.

Conclusions

• Adaptation to climate change promises to be one of the big issues of the 21st century.

• Informing adaptation presents different requirements to informing policy on mitigation.

• The climate modelling community must recognise and respond to these different requirements.

Palaeoclimate Model Intercomparison Project II (PMIPII)

Paul Valdes, School of Geographical Sciences, University of Bristol

Those of you who are regular readers of the UGAMP newsletter (and with long memories) will have frequently read about PMIP. This international project involves members of most of the major climate modelling groups worldwide and endorsed by the World Climate Research Programme (WCRP) and the International Geosphere-Biosphere Programme (IGBP) under the CLIVAR and PAGES core programs. The project was launched in 1994 with the dual aims of:

(a)   Understanding the mechanisms of climate change by examining such changes in the past, when the external forcings

were large and relatively well known and when various kinds of geological evidence provide evidence of what actually happened;

(b)   Providing a framework for the evaluation of climate models in order to determine how far they are able to reproduce climate states radically different from that of the present day.

In its initial phase, designed to test the atmospheric component of climate models (atmospheric general circulation models: AGCMs), the project focused on the last glacial maximum (LGM: ca 21,000 years before present, 21 ka. BP) and the mid-Holocene
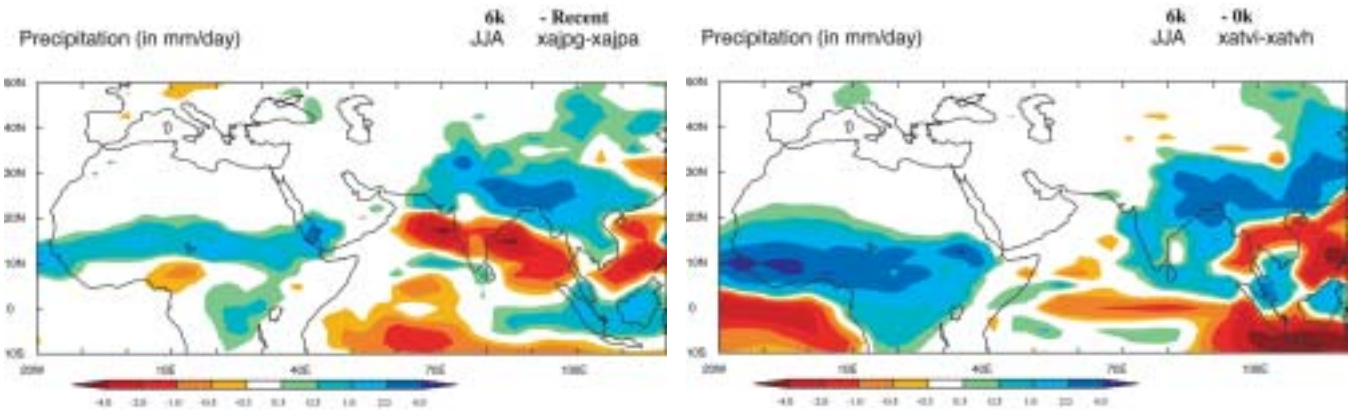

Figure 31. June-July-August mean precipitation changes for the mid-Holocene minus present day for (left) atmosphere only simulation (HadAM3) in which the orbital parameters are changes for the mid-Holocene but the sea surface temperatures and vegetation cover are held constant at present day conditions, and (right) coupled atmosphere-ocean-vegetation simulation (HadCM3 coupled to TRIFFID) in which ocean temperatures and vegetation cover are predicted to change. The enhancement of the monsoons is insufficient when compared to proxy data for the period.

(6000 years before present, 6 ka BP). The results showed that many features of the PMIP experiments are robust, including global cooling at the LGM and the expansion of the northern hemisphere summer monsoons during the mid-Holocene. However, differences in the magnitude of the response between individual models are large. This sort of analysis formed part of the evaluation of climate models in the Third Assessment Report of the Intergovernmental Panel on Climatic Change (IPCC).

One of the most important conclusions emerging from the first phase of PMIP was that inclusion of ocean and of vegetation feedbacks in model simulations was necessary in order to simulate the extent and magnitude of past climate changes correctly. Phase II of PMIP will address these issues. The main modelling foci will be to evaluate coupled models used for future climate simulations under the well documented past extreme climate conditions of the mid Holocene (6ka) and last glacial maximum (21ka). Coupled ocean atmosphere (OAGCM) and whenever possible ocean-atmosphere-vegetation (OAVGCM) will be used. Such experiments will also help to understand the role of ocean and land surface feedbacks by a series of complementary sensitivity experiments. Other time periods and experiments will also be considered in this PMIP second phase in order to better understand mechanisms of past climate changes and model responses to past forcings. These include the early Holocene, early glacial (115,000 calendar years BP, 115ka), and prescribed freshwater fluxes experiments.

As a preliminary, we have completed a coupled atmosphere-ocean-vegetation simulation for the mid-Holocene

(6000 years BP). This was a time period in which the key external change was to the Earth's orbit resulting in more solar energy in the Northern hemisphere summer. This causes warmer summers and enhanced land-sea temperature contrasts hence strengthening the monsoon. Figure 31 shows the change in precipitation (mid-Holocene, 6000 years ago minus present day conditions) for N. Hemisphere summer means (June-July-August). Figure 31(a) shows the results from a HadAM3 simulation using PMIPI boundary conditions, in which the orbital configuration is changed but the sea –surface temperature and the vegetation cover are held fixed at present day conditions. Both the African and Asian monsoons are stronger. Figure 31(b) shows the results from HadCM3 coupled with MOSES2 and TRIFFID so that the oceans and vegetation cover now change. The results show that the addition of ocean and vegetation feedbacks have amplified the response of the monsoon over Africa. It is substantially stronger and broader, which is in accord with the data. However, the extent of the monsoon is not sufficient. Data suggests that much of the Sahara was wetter in those periods, resulting in more vegetation cover (the so called "Green Sahara") but the model has not captured this expansion.

This work is still very preliminary. We are now beginning to examine these simulations in more details to improve our understanding of the processes and feedbacks. Another important aspect of the new project will be to examine the interannual variability of the climate, such as changes in ENSO and the NAO.

Chemistry-Climate Interactions

Southern Hemisphere Major Warmings: Observations and Model Results

P. Braesicke and J. A. Pyle, NCAS-ACMSU, Department of Chemistry, University of Cambridge, Cambridge

The unprecedented major warming in the southern hemisphere during 2002 which led to a split ozone hole by the end of September 2002 raises a number of questions: How likely is such an event; what is the role of chemistry in producing it and what exactly caused the warming? Major warmings in the northern hemisphere have been observed as far back as 1952 (Scherhag, 1952) and are a common feature in the interannual variability of this hemisphere during winter and are well understood in terms of their dynamical evolution, but major warmings on the southern hemisphere have not been observed since the start of our observational records (Roscoe *et al.*, 2003). In an attempt to answer some of the questions raised in the introduction we analysed four integrations of 20 years each with the Unified Model comprising a simple ozone chemistry. One integration used the modelled ozone interactively, whereas the other integrations used climatological ozone in the radiation. Even though there is no major warming in the SH (as defined by WMO) in the 80 years modelled, we find one exceptional early and strong warming in the integration with interactive chemistry. Here, we will just briefly discuss the interannual variability of wind and ozone in the southern hemisphere in spring in observations and our model.

Figure 32 shows a scatter plot for the October mean of zonal-mean zonal wind in 60ºN, 10 hPa (NCEP data) versus total ozone in 72.5ºS (TOMS data, detrended) for the years 1979-2002. There is no ozone data available from TOMS for the years 1993 and 1994. As expected, many years are in a high wind speed/low ozone regime. Nevertheless, some interannual variability can be seen easily. The winter 2002 (labelled) stands clearly out as the winter with the weakest wind and highest ozone (taking into account a linear decline in ozone from 1979 to 2002).

Figure 33 shows the corresponding plot from our model results. Again, a majority of winters is clustered in a high wind speed/low ozone regime. Overall the interannual variability of ozone in the model is smaller than observed (this is in part due to the fact that the model is not using a scenario for the chlorine and aerosol loading). One exceptional warming stands out in the scatter plot: in model year 1989 (labelled) the interactive chemistry run (results from the interactive run are indicated with green crosses) developed a very strong wavenumber 1 warming with anomalously high ozone.

The following conclusion can be drawn from these plots: The model is in good agreement with observations. It seems that the overall interannual variability in the model is determined by the run with interactive chemistry. If we define a strong warming by winds less than 10 m/s and ozone above 290 DU we find four warmings in our model results; if we define an exceptional warming by winds less than 0 m/s and ozone above 300 DU we are
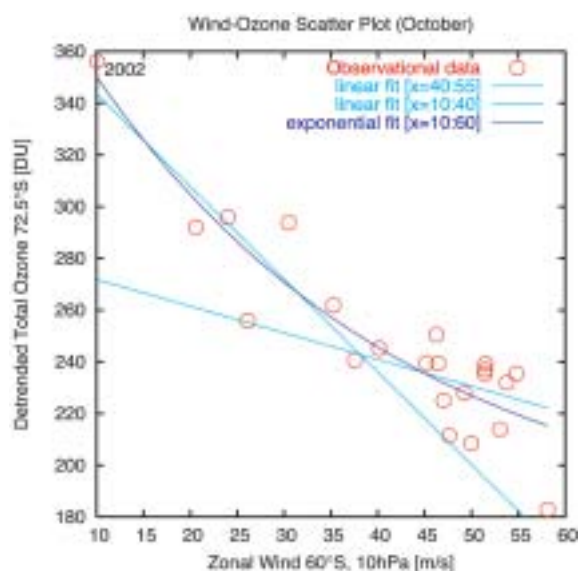

Figure 32. Scatter plot of October mean zonal-mean zonal wind in 60ºS, 10 hPa and total ozone in 80ºS from four twenty year integrations using the Unified Model with a simple ozone chemistry. Results from the interactive integration are marked with green crosses.
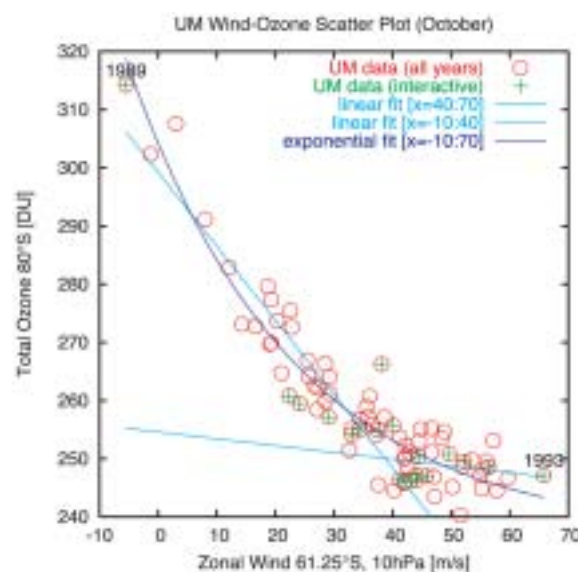

Figure 33. Scatter plot of October mean zonal-mean zonal wind in 60ºS, 10 hPa from NCEP data versus total ozone in 72.5ºS from TOMS data for the years 1979 to 2002. In 1993 and 1994 no ozone data is available.
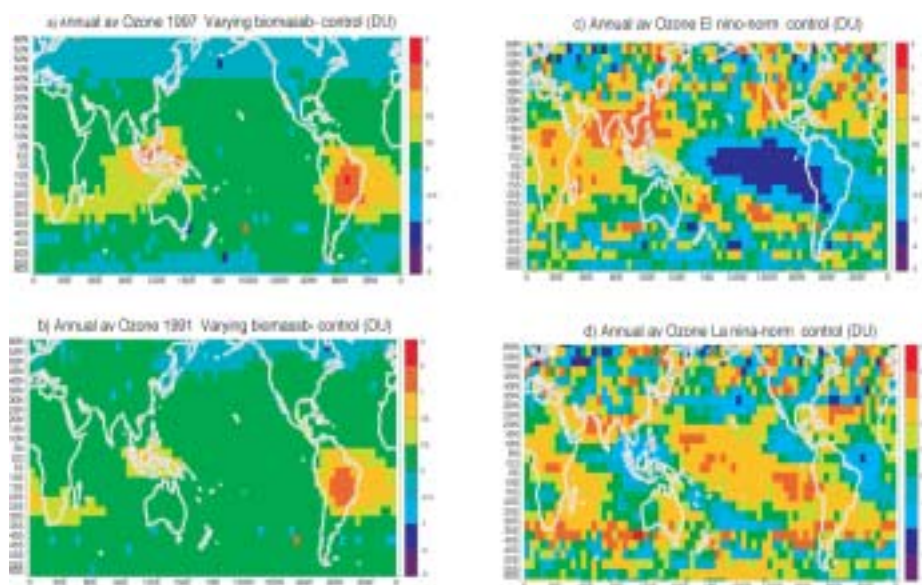
Figure 34. Annual average ozone changes for biomass burning events (a,b) and for ENSO composites (c,d)

down to two events in 80 years. This may already give us some idea about the probability of such events in nature.

A detailed discussion of the exceptional warming considering the development in daily data and a comparison to observations and model statistics has been submitted to the JAS special issue dedicated to the 2002 ozone hole split.

References

Braesicke, P. and J. A. Pyle, Long-term variability of the Antarctic vortex and ozone hole: how close is the UM to producing a SH major warming?, submitted to JAS, 2003.

Roscoe H. K., J. D. Shanklin and S. R. Colwell, Has the Antarctic vortex split before?, submitted to JAS, 2003.

Scherhag, R., Die explosionsartige Stratosphärenerwärmung des Spätwinters 1951-52, Berichte des Deutschen Wetterdienstes in der US-Zone, 38, 1952.

ENSO direct and indirect effects on Tropospheric Ozone over the Indonesian region

Ruth Doherty, David Stevenson, Institute of Atmospheric and Environmental Science, University of Edinburgh

Unified Model simulations were performed to ascertain the role of ENSO on tropospheric ozone variability in the HadAM3/STOCHEM coupled model over the period 1979-1999. STOCHEM is a detailed Lagrangian tropospheric chemistry model (Sanderson *et al*., 2003 and references therein) which is run fully coupled to the Unified Model. Previous analyses have shown ENSO to be the dominant mechanism influencing tropical interannual variability of tropospheric ozone. ENSO affects ozone in (at least) two ways. First, directly through changes in the Walker circulation, in particular convection, and secondly indirectly through changes in rainfall which produce changes in vegetation fire activity which in turn affect biomass burning emissions. During an El Niño increased convection over the central and eastern Pacific reduces Tropospheric Column Ozone (TCO), whilst reduced convection over Indonesia increases TCO. Over the Indonesian region, biomass burning events associated with El Niño-related drought have produced large increases in TCO; 1997 was a particularly noteworthy year (e.g., Thompson 2003).

Coupled model experiments were performed to investigate the importance of the direct and indirect effects of ENSO, as described above, on TCO over the Indonesian region. It should be noted that biomass burning events through vegetation fires have a strong anthropogenic component and are not solely related to drought conditions. Nevertheless, biomass burning emissions are still expected to be exacerbated in drought years. Two simulations were performed: a "control" run that used seasonally varying but annual invariant biomass mass burning emissions for 1979-99, and a "biomass burning" run that used seasonally and annually varying biomass burning emissions over this same period. The annually varying global biomass burning dataset was produced using scaling factors constructed from the TOMS Aerosol Index for 6 world regions by Duncan et al., (2003). Figure 34 a and b show the change in annual-average TCO for years 1997 (strongest El Niño year in period) and 1991 (a more "normal" El Niño). Figure 34c and d show the change in annual-average ozone for El Niño-Normal (c) and La Niña-normal (d) composites for the 1979-99 period. Over Indonesia the changes in TCO associated with biomass burning events for both years (0.5-2 DU) are comparable to the changes in TCO from ENSO-related dynamical changes (0.3-2 DU). These preliminary analyses indicate that both mechanisms of modulating TCO are important and through comparison with observations (e.g., Thompson 2003) may provide a useful method of validating the model in the tropics.

References

Duncan, B.N., Randall, R.V., Staudt, A.C., Yevich, R., and Logan, J.A., 2003, Interannual and seasonal variability of biomass burning emissions
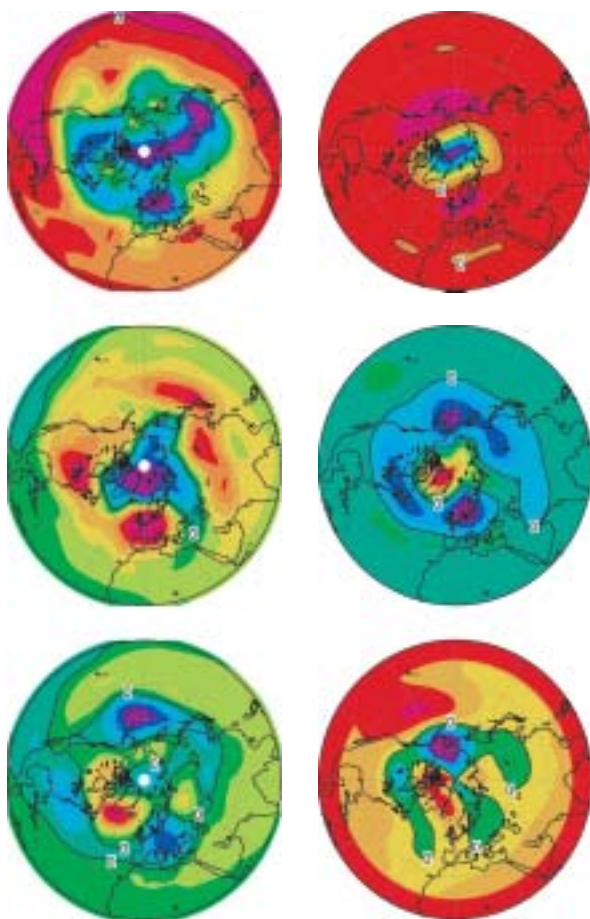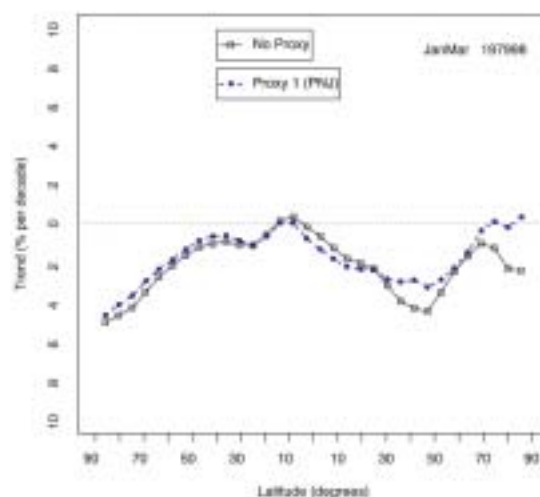
Figure 35. The three leading EOFs from ozone anomalies (left), and the correlated EOFs derived from the geopotential height anomalies (right), the monthly anomalies were averaged over January to March.

Figure 36. Winter trend (January to March) for the modelled ozone, with no proxy, and with the PNJ index as a proxy in MLR analysis.

constrained by satellite observations, J. Geophys. Res., 108, ACH 1-1 to 1-22.

Sanderson, M.G., Jones, C.D., Collins, W.J., Johnson, C.E, and Derwent, R.G., 2003, effect of climate change on isoprene emissions and surface ozone levels, Geophys. Res., Lett., 30, 18, 10.1029/2003GL017642.

Thompson, A.M., 2003, Tropical tropospheric ozone: A perspective on photochemical and dynamical interactions from observations in the past five years, IGAC newsletter, 28, 6-11.

Hadjinicolaou P., Jrrar A., Pyle J.A. and Bishop L., The dynamically-driven long-term trend in stratospheric ozone over northern middle latitudes, Q.J.R. Meteorol. Soc., 128, 1393-1412, 2002.

Model Study of Ozone Signatures of Climate Patterns over the Northern Hemisphere

Amna Jrrar, P. Braesicke, P. Hadjinicolaou and J. A. Pyle, Centre for Atmospheric Science, Chemistry Dept.,University of Cambridge, UK

The dynamical contribution to the observed downward trend in ozone in winter is investigated in a 20 year run. The SLIMCAT model was forced by ECMWF analyses from 1979 to 1998. The model uses a simple chemistry (Cariolle and Deque, 1986), which excludes variations in chlorine or aerosol loading, so any calculated trend or variability should be due to changes in meteorology.

There is an overall good agreement between the model and observations. An overall downward trend is observed especially during winter season (not shown) (Hadjinicolaou *et al.*, 2002). Winter model ozone averaged over January to March between 33N-60N, correlates with the North Atlantic Oscillation (NAO) index, the Arctic Oscillation (AO) index, and the Polar Night Jet (PNJ) index (r=0.42, r=0.65 and r=0.65 respectively).

At polar latitudes between 72N-90N, the winter model ozone correlates highly with the PNJ index (r=0.76). These relations were further investigated in a Singular Value Decomposition (SVD) analysis (Golub and Reinsch, 1970). SVD analysis has been performed for modelled total ozone and ECMWF analyses of

geopotential heights (Z) at 200 and 30 hPa for the period from 1979 to 1998 over the northern hemisphere. Seasonally averaged results (January to March) are presented in Figure 35. O_3 EOF1 explains 20% of the overall variance explained by the five leading EOFs. It has a dispersed centre over the pole and high latitudes, contrasted by a ring of positive anomalies. It has a similarity in the spatial pattern to the Z EOF1 at 30 hPa, and correlates highly with PC1 at this level (r=0.76). Z EOF1 at 30 hPa represents the strength of the vortex and therefore correlates highly with the PNJ index (r=0.98). The PNJ index here is defined as the zonal mean zonal wind at approximately 60 N and 50 mb (Kodera *et al.*, 1999). O_3 EOF2 explains 11% of the overall variance it has a centre of action over Scandinavia, contrasted by opposite anomalies over western Europe, North America, China, Japan and the Pacific. The O_3 PC2 correlates highest with the Scandinavia pattern (r=0.48), but the Arctic Oscillation (AO) and the East Atlantic pattern show correlations as well (r=-0.45, r=-0.40) respectively. Averaging over three months and applying the analysis for the whole northern
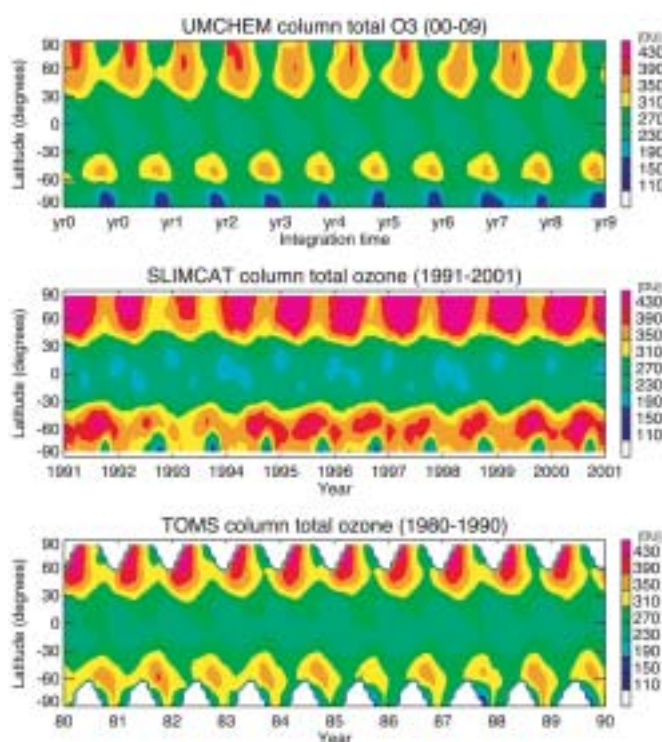
Figure 37. Zonal mean column ozone from (top) 10-year UM simulation, (middle) 10 years of SLIMCAT CTM simulation forced by ECMWF ERA-40 winds, and (bottom) TOMS observations 1980-1990. The coupled UM scheme is stable and captures the observed latitudinal gradients and seasonal variations. The Antarctic ozone hole is also reproduced.
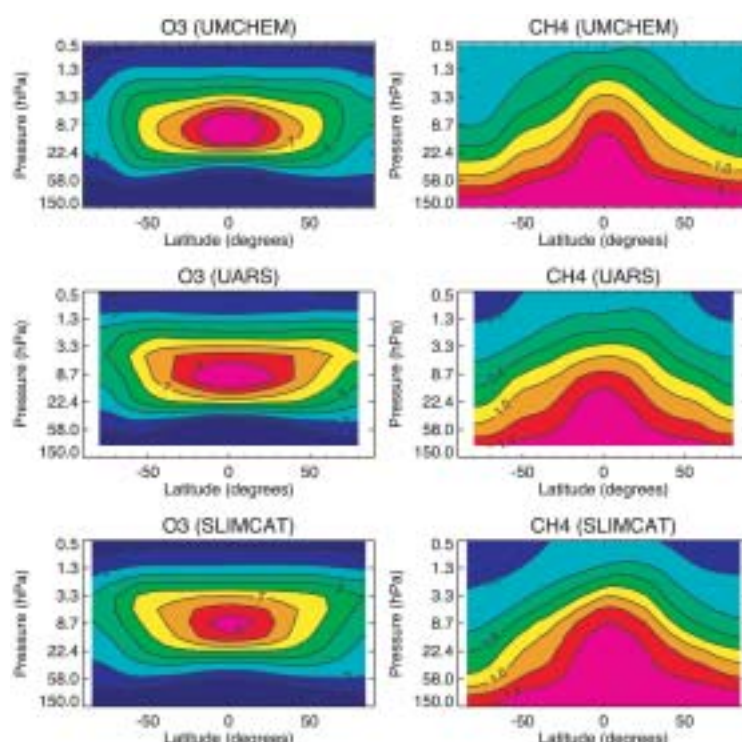

Figure 38. Latitude-height cross sections of zonal mean / annual mean O3 and CH4 fields from the UM (top), SPARC UARS climatology (middle) and SLIMCAT (bottom). The UM well reproduces the basic features of the observations.

hemisphere, allows more than one mode to appear in the same EOF (Barnston and Livezey, 1987).

O_3 EOF3 explains 9.4% of the overall variance. The spatial pattern for this EOF combines also more than one mode of variability, the Pacific North American (PNA) pattern (Z EOF2 at 200 hPa, r=0.83 with PNA index). The AO index, correlates with O_3 PC3 (r=0.89), while the PNA index correlates with r=0.87.The SVD analysis revealed the importance of the PNJ index in modulating winter model ozone variations, by including the PNJ index as a proxy in Multiple Linear Regression (MLR) analysis. The PNJ index, modifies the trend at middle latitudes and reduces the unexplained trend to zero at polar latitudes (Figure 36).

Conclusions

- There is high negative correlation between the model middle latitude ozone, the Arctic Oscillation and the polar night jet as seen in other studies using observations.

- SVD analysis applied to modelled winter ozone, reveals a

structure reminiscent of the AO/PNJ pattern. The signatures of other teleconnection patterns, such as the NAO, EA, and PNA are found in the three leading EOFs.

- Including the PNJ index as a proxy in MLR analysis, explains most of the trend at polar latitudes.

References

Barnston A. G. and R.E. Livezey, Classification, seasonality and persistence of low-frequency atmospheric circulation patterns, Mon. Weath. Rev., 115, 6, 1083-1126, 1987.

Cariolle, D., and M. Deque, Southern hemisphere medium-scale waves and total ozone disturbances in a spectral general circulation model, J. Geophys. Res., 90, 10825-10846, 1986.

Hadjinicolaou P., Jrrar A., J.A. Pyle and L. Bishop, The dynamically driven long-term trend in stratospheric ozone over northern middle latitudes, Q. J. R. Meteorol. Soc., 128, 1393-1412, 2002.

Kodera K.,H. Koide, and H. Yoshimura, Northern Hemisphere winter circulation associated with the North Atlantic Oscillation and stratospheric polar-night jet, Geophys. Res. Lett., 26, 443-446, 1999.

Coupled Full Stratospheric Chemistry in the Unified Model

Wenshou Tian and Martyn Chipperfield, Institute for Atmospheric Science, School of the Environment, University of Leeds

Many problems of interest in the atmosphere involve the coupling of chemistry and radiation/dynamics. To address these problems requires detailed models which include the whole range of relevant processes. We have recently included a full stratospheric chemistry scheme in the Unified Model (UM, L64 v4.5). John Austin and co-workers have pioneered the inclusion of

comprehensive chemistry schemes in the UM. However, for our work we have taken the full stratospheric scheme directly from our SLIMCAT off-line CTM (Chipperfield, 1999). This scheme has been developed and tested over a number of years and contains the important species and reactions required to simulate the stratosphere. It is difficult to validate and test coupled

chemistry-climate models but by using the identical chemistry scheme to SLIMCAT we can make use of our CTM/observations comparisons. Using the self-contained SLIMCAT modules also makes working with the UM somewhat easier.

Our UM chemistry scheme uses 28 tracers and includes the O_x, HO_x, NO_y, Cl_y and Br_y families, source gases and a full CH_4 oxidation scheme. The scheme contains a treatment of heterogeneous chemistry on sulphate aerosols and polar stratospheric clouds. The chemical O_3, CH_4, N_2O and H_2O fields are coupled to the UM radiation scheme.

So far we have performed a series of 10-year 'time-slice' experiments (i.e. with constant boundary conditions). Figure 62

shows the time series of zonal mean column O_3 for a 10-year '2000' simulation compared to TOMS observations and a SLIMCAT run. Figure 38 compares zonal mean O_3 and CH_4 also compared to SLIMCAT and an observed climatology. The coupled model performs well and will be used for future chemistry-climate studies.

References

Austin J., N. Butchart, and J. Knight, QJRMS, 127, 959-974, 2001.
Chipperfield, M.P., JGR, 104, 1781-1805, 1999.

Calculated changes of oxidation capacity of the Earth's atmosphere: From the past to future

Guang Zeng (Guang.Zeng@atm.ch.cam.ac.uk) and John A. Pyle, NCAS ACMSU, Centre for Atmospheric Science, University of Cambridge.

The hydroxyl radical (OH) is a principal oxidant in the troposphere, controlling the abundance of many species including some green house gases. The formation of OH is via O3 photolysis and its subsequent reaction with water vapour. The main sink of OH in the troposphere are reactions with CH4, CO and other organic compounds. The short lifetime of OH of about 1 second and its low concentration (daytime level $\sim 10^6$ molecules cm^{-3}) make the direct detection particularly difficult. Understanding changes of OH over time is highly important for our understanding the changes of the oxidation capacity of the Earth's atmosphere.

There is direct evidence that anthropogenic activities have changed the chemical composition of the atmosphere since pre-industrial times. Continuing increases of surface emissions of NO_x, CH_4, CO and NMHCs are inevitable. Changes in OH depend critically on changes of NO_x and hydrocarbons and are highly complex: Increases of NO_x and O_3 tend to increase OH and increases of CO and CH_4 depress OH. Here, we use a coupled climate/chemistry model (UM/CHEM) to calculate changes of tropospheric composition from pre-industrial time to the present and from the present to the future, assuming IPCC emission scenarios for the years 1850, 2000 and 2100. The model is the 19 level 4.4 version of the UM combined with a detailed tropospheric chemical scheme comprising 46 species and 186 reactions. Figure 39 shows the calculated changes of OH (a) from pre-industrial times to the present-day, (b) from the present to the future without changing the climate and (c) from the present to the future including a double-CO_2 climate forcing. The changes of OH can be either positive or negative as a result of increased emissions. Since the pre-industrial Age, the increase of OH has largely occurred in the northern hemisphere lower atmosphere as a result of increasing NO_x emissions due to intensified human activities. Away from source regions, OH decreases due to the increase of hydrocarbons which have a longer lifetime and experience more long-range transport than NO_x. Our model suggests that in the future, the increase of hydrocarbons will outweigh the increase of NO_x for the continents which leads to the decrease of OH in the extratropics. The increase of OH will mainly occur in the lower and upper tropical troposphere due to an assumed relatively larger
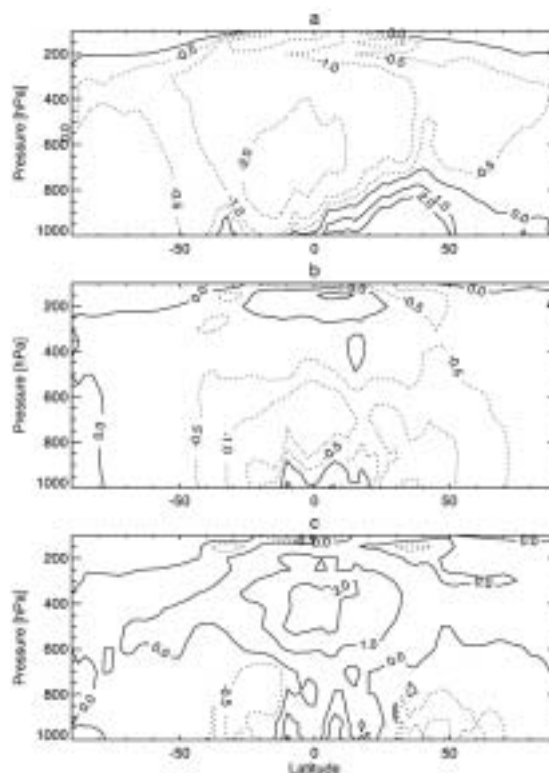

Figure 39. Annual and zonal mean changes of OH (10^5 molecules cm^{-3}; (a) from pre-industrial to present; (b) from present to future; and (c) from present to future including climate change.

increase of NO_x in the tropical region, which can be more effectively transported to the upper troposphere by convection. NO_x in the upper troposphere has a longer lifetime; therefore it tends to increase OH in that region. When climate changes are included in the future scenario, a substantial increase of OH is calculated due to an increase of water vapour in a warmer and wetter climate. The oxidation capacity of the atmosphere is evidently affected by a changed climate. This can lead to the change of lifetime of longer-lived species, such as methane, with its large global warming potential.

Ocean Influences on Climate

Modelling Diurnal to Intraseasonal Variability of the Ocean Mixed Layer

Daniel Bernie[1], Steve Woolnough[1], Eric Guilyardi[1,2], Julia Slingo[1],
[1]Centre for Global Atmospheric Modelling, Department of Meteorology, University of Reading, UK
[2]Laboratoire des Sciences du Climat et de l'Enviroment, CEA-CNRS, Gif-sur-Yvette, France

The intraseasonal variability of SST associated with the passage of the Madden-Julian Oscillation (MJO) is well documented, yet coupled model integrations generally under predict the magnitude of the SST variability.

Observations from the IMET mooring in the west Pacific during the Intensive Observing Period (IOP) of TOGA COARE showed a large diurnal signal in SST which is modulated by the passage of the MJO. In this study observations from the IOP of TOGA COARE and a 1-D mixed layer model incorporating the KPP vertical mixing scheme have been used to investigate the rectification of this diurnal signal onto the intraseasonal time scales and the implied impact of the absence of a representation of this process on the modelled intraseasonal variability in coupled GCMs.

Analysis of the SST observations has shown that the rectification of the diurnal cycle of SST onto the daily mean SST accounts for about one-third of the magnitude of intraseasonal variability of SST associated with the MJO in the west Pacific warm pool. Figure 40 shows a period intraseasonal SST warming associated with the quiescent phase of the MJO for model integrations forced with 1 hourly (red) and daily mean (black) surface fluxes. The rectification of diurnal cycle onto the daily mean SST can clearly be seen.

It is found that the representation of the diurnal cycle is sensitive to the temporal resolution of the surface fluxes and the local time of the flux averaging period. As models are forced at the same instant over a global domain this means that the local time of the flux averaging period is a function of longitude implying that a sub-diurnal flux resolution will introduce a geographical bias in the representation of the diurnal cycle. To capture 90% of the diurnal variability of SST over a global domain a temporal flux resolution of 3 hours is required.

During the calm suppressed phase of the MJO the ocean mixed layer is very shallow due to the characteristic light winds and high solar insolation. These conditions lead to the diurnal temperature variability being confined to the top few meters of the mixed layer. The typical mixed layer resolution in coupled models of 10m is therefore insufficient to resolve such variability. The importance of the resolution of the top model layer is shown in Figure 41 where the diurnal variability of the 1-D model is shown for a series of constant resolution grids (black) and stretched grids (red) where the top model layer resolution is fixed. The thickness of the top level is given by the numbers in the body of the figure and the resolution below is measured here by the number of levels in the top 25m.
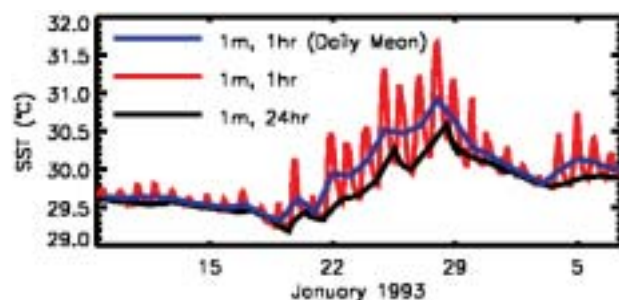

Figure 40. Sample of model SST from and integration forced with 1 hourly surface flux data (red) with the daily mean of this (blue) and an integration forced with daily mean fluxes (black)
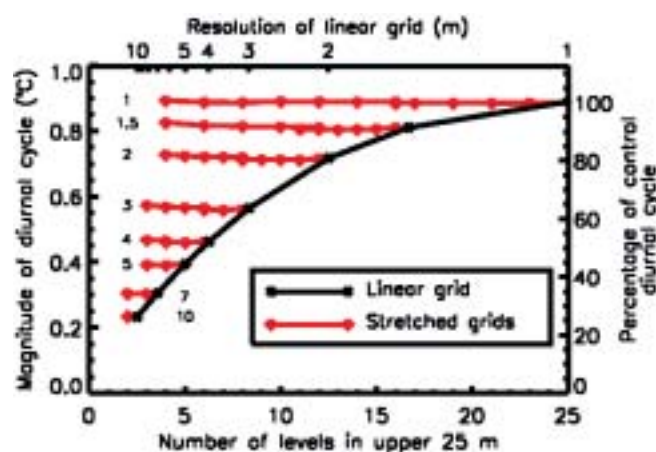

Figure 41. Magnitude of the diurnal variability of SST for integrations forced with 1 hourly data. The linear grids (black) have a constant resolution throughout, while the stretched grids (red) have a fixed uppermost level thickness, denoted by the numbers on the body of the figure, with different resolutions below.

In summary the rectification of the diurnal variability of SST in the warm pool accounts for some 35% of the intraseasonal variability and should be included in studies of the coupled nature of the MJO. It has be shown that to capture of 90% of this variability requires a flux resolution of 3 hr. and an uppermost model layer of the order of 1m thick. These results are currently under implementation in a full 3-D ocean model.
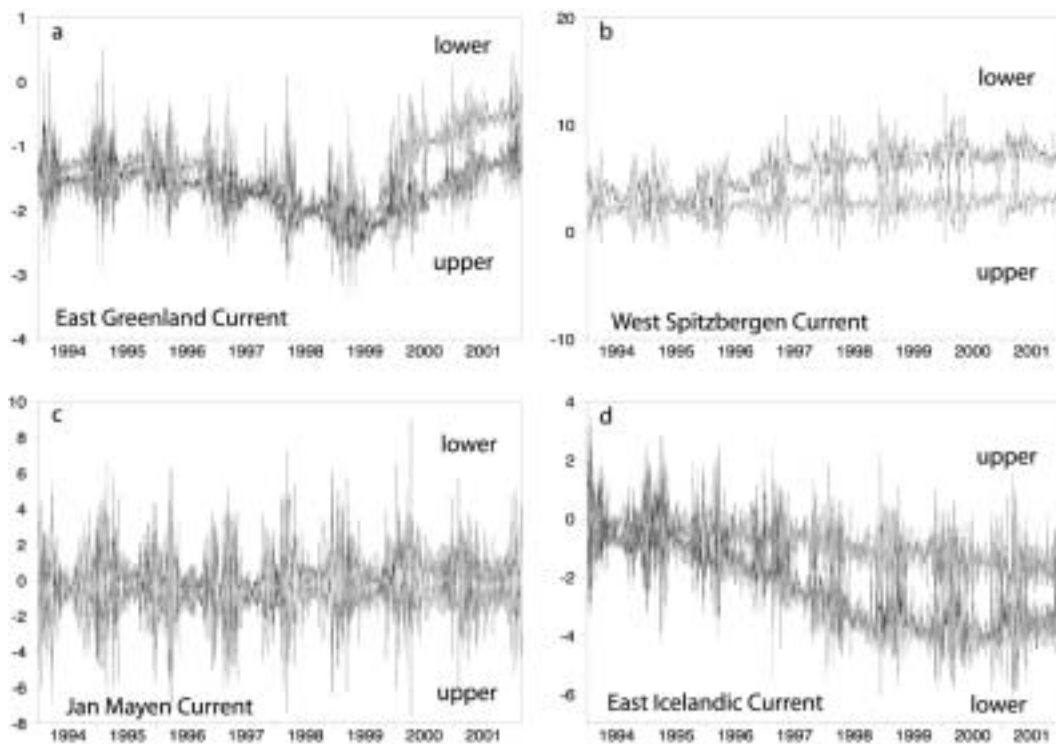
Figure 42. Volume fluxes (in Sv), at daily resolution, within principal currents internal to the Nordic Seas:
(a) East Greenland Current,
(b) West Spitzbergen Current,
(c) Jan Mayen Current,
(d) East Icelandic Current. The upper and lower layers of each are taken at ~ 150 m.

Oceanic variability during the 1990s in the Nordic Seas

Grant Bigg, Department of Geography, University of Sheffield

During the 1990s deep convection showed signs of switching from the Labrador Sea back to the Greenland Sea, re-establishing a pattern last occurring in the early 1970s (Lazier *et al*., 2002; Gascard *et al*., 2002; Wadhams *et al*., 2002). In addition, the North Atlantic Oscillation showed its largest recorded excursion from positive to negative index values during the middle of the decade. A fine resolution curvilinear ocean model, forced by NCEP Re-Analysis fluxes, was used to study changes in the circulation of the Nordic Seas and surrounding ocean basins during 1994-2001. The model fields exhibited regionally distinct temporal variability, mostly determined by atmospheric forcing but in regions of significant sea-ice a longer timescale variability is found. Some abrupt circulation changes accompany the relaxation of the westerlies following the peak North Atlantic Oscillation Index phase of the mid 1990s (Figure 42).

The Greenland gyre spins up over the following years, with the increased circulation partially exiting through the Denmark Strait into the northern Atlantic as well as re-circulating within the Nordic Seas. This resulted in a distinct freshening around northern Iceland and an increase in the East Icelandic Current. However,

these latter increases steadied after 1998, as the increased Greenland Sea gyre circulation led to a greater proportion of water leaving through the Denmark Strait, rather than re-circulating. Increased convection in the Icelandic Sea in the model in 1998-2001 acted to obliterate the anomalies that would otherwise have fed into the East Icelandic Current. A fresh, cold anomaly from the Arctic during 1998/1999 was shown to propagate through the system. Model and observations showed good agreement generally, but diverged at depth more in the last few years of the simulation.

This work was funded by COAPEC.

References

Gascard, J.-C., Watson, A.J., Messias, M.-J., Olsson, K.A., Johannessen, T., Simonsen, K., 2002. Long-lived vortices as a mode of deep ventilation in the Greenland Sea. Nature 416, 525-527.

Lazier, J., Hendry, R., Clarke, A., Yashayaev, I., Rhines, P., 2002. Convection and restratification in the Labrador Sea, 1990-2000. Deep-Sea Research Part I (49), 1819-1835.

Wadhams, P., Holfort, J., Hansen, E., Wilkinson, J.P., 2002. A deep convective chimney in the winter Greenland Sea. Geophysical Research Letters 29 (10), art. no. 1434.

Towards an Improved Description of the Air-Sea Heat Exchange

Jeremy P. Grist (jyg@soc.soton.ac.uk) and Simon A. Josey, Southampton Oceanography Centre

Quantifying the transfer of energy between the atmosphere and ocean is of fundamental importance to understanding the climate system. The Southampton Oceanography Centre (SOC) air-sea flux climatology provides estimates of ocean heat exchange in the form of monthly mean fields for the global ocean. The climatology was produced using meteorological observations from merchant ships that were corrected for biases in observing procedures. Estimates of the surface fluxes were obtained from the reports using various bulk formulae (Josey *et al.* 1999).

On decadal timescales, one would expect the global climatological mean heat flux to average to zero. However, in common, with other ship-based climatologies, the SOC climatology exhibits a global mean net heat gain of 30Wm^{-2}. Therefore, the goal of our Coupled Ocean-Atmosphere Processes and European Climate (COAPEC) project is to produce an improved version of the SOC climatology in which the ocean heat budget is balanced.

To balance the climatology, we have adopted the inverse analysis method of Isemer *et al.* (1989) and adjusted the meridional ocean heat transport implied by the SOC climatology to agree with hydrographic estimates at different latitudes. Isemer *et al.* (1989) were limited to estimates of heat transport at only three latitudes in the Atlantic. We have taken advantage of the increased number and geographical range of hydrographic sections during the period of the SOC climatology (1980-93), utilising up to 10 constraints throughout the Atlantic and the North Pacific (see Figure 43).

When all 10 constraints are applied, the magnitude of the bias in the heat budget is reduced substantially from 30 Wm^{-2} to 5 Wm^{-2}. Separate hydrographic observations indicate that this imbalance may still be too large. In particular, repeat hydrography at 24° N in the Atlantic has revealed a change in temperature of about 0.2^oC to a depth of approximately 1000m between sections taken in 1981 and 1992 (Bryden *et al.* 1996). This would imply a bias of no more than 2Wm^{-2} in the net heat flux over the same period. With this in mind we have repeated our analysis, including an additional constraint that the global heat budget should balance to within $\pm 2 \text{Wm}^{-2}$. The resulting solution required a 19% increase in the latent heat flux, a 6% reduction to the shortwave flux and less significant adjustments to the other components (Grist and Josey 2002; 2003).

The adjusted flux fields obtained with this solution have a global mean net heat flux of -2Wm^{-2} and are available from http://www.soc.soton.ac.uk/JRD/MET/coapec.php3. The new fields agree to within 7 Wm^{-2} with independent large scale area average heat flux estimates obtained from a more recent hydrographic section at 32° S. Good agreement is also found with recent estimates of the net heat flux obtained using residual techniques and from atmospheric model reanalyses (see Figure 44). However, comparisons of the adjusted fluxes with measurements from air-sea flux buoys have given more mixed results, discussed in detail in Grist and Josey (2003), which indicate that further improvements are required. Ongoing work in this project is focused on both extending the inverse analysis
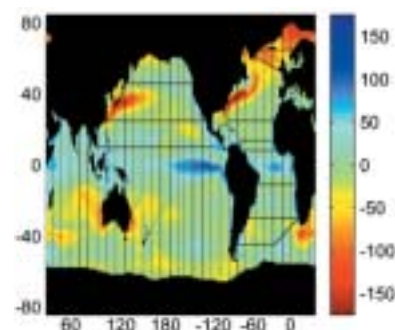

Figure 43. The net heat flux (Wm-2) from the adjusted version of the SOC climatology. Also shown are the locations of the 10 hydrographic constraints (solid lines) used in the inverse analysis.
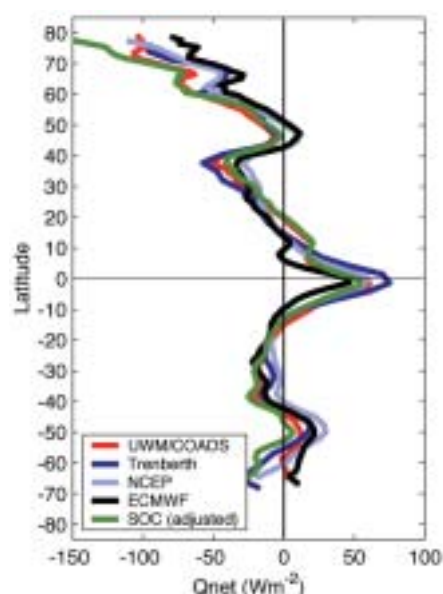

Figure 44. Zonally averaged annual mean net heat flux from the adjusted version of the SOC climatology and other recent climatologies.

method to include spatially dependent adjustments and applying recent improvements to the flux formulae (e.g. Josey *et al.* 2003) which should allow a significant proportion of the original bias to be removed without the need to constrain the fluxes.

References

Bryden, H. L, M. A. Griffiths, A. L. Lavin, R. C. Millard, G. Parrilla, and W. M. Smethie 1996: Decadal Changes in Water Mass Characteristics at 24 N in the Subtropical North Atlantic Ocean, Journal of Climate, 9, 3162-3186.

Grist, J. P. and S. A. Josey, 2002: Balancing the SOC climatology using inverse analysis with spatially fixed parameter adjustments, Southampton Oceanography Centre Internal Document No. 80, 38 pp. + figs.
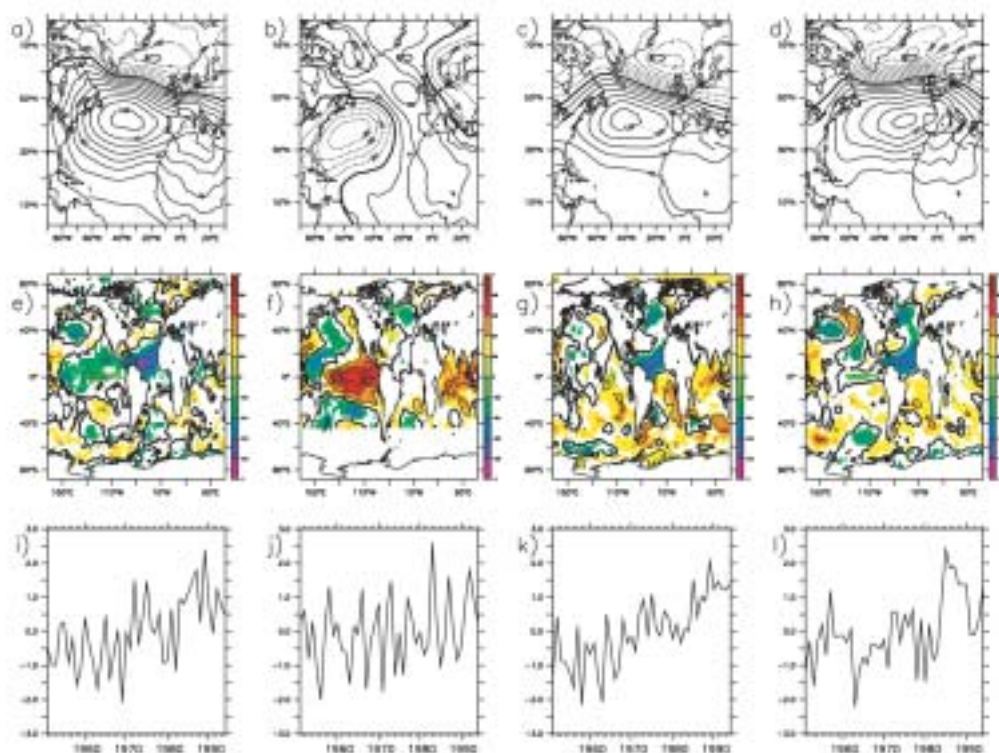
Figure 45. Shows the results for winter time (DJF) Mean Sea Level Pressure (MSLP). Panels a-d show the dominant mode of forced MSLP variability in the four models. Panels i-l show the time-series associated with these modes. Panels e-h show the regression of the SST forcing field onto these time series.

Grist, J. P. and S. A. Josey, 2003: Inverse Analysis Adjustment of the SOC Air-Sea Flux Climatology Using Ocean Heat Transport Constraints, J. Climate, 16, 3274-3295.

Isemer, H.-J., J. Willebrand and L. Hasse, 1989: Fine adjustment of large scale air-sea energy flux parameterizations by direct estimates of ocean heat transport. J. Climate., 2, 1173 – 1184.

Josey, S. A, E. C. Kent, P. K. Taylor, 1999: New Insights into the Ocean Heat Budget Closure Problem from Analysis of the SOC Air-Sea Flux Climatology. J. Climate, 12, 2856-2880.

Josey, S. A., R. W. Pascal, P. K. Taylor and M. J. Yelland, 2003: A New Formula For Determining the Atmospheric Longwave Flux at the Ocean Surface at Mid-High Latitudes J. Geophys. Res., 108 (C4) 10.1029/2002JC001418.

Influence of the Oceans on North Atlantic Climate Variability: A comparison of results from four atmospheric GCMs

Daniel Hodson and Rowan Sutton, Holger Pohlmann, Mark Rodwell, Martin Stendel, Laurent Terray, Centre for Global Atmospheric Modelling, Department of Meteorology, University of Reading

Atmospheric variability arises both from internal processes and from external influences. Amongst the external influences, the role of the oceans is of particular interest because the evolution of (large-scale) ocean conditions is predictable months or even years ahead. It follows that if we can understand the way in which changing ocean conditions impact climate, we may be able to provide useful climate predictions. Furthermore, knowledge about the influence of the ocean on climate variability will be crucial if we are to fully understand and quantify anthropogenic climate change.

The influence of the ocean on the climate of the North Atlantic region is has received considerable attention recently (e.g. Rodwell 1999; Mehta 2000; Czaja 2002). Many have focused on the ocean's influence on the North Atlantic Oscillation (NAO), the dominant mode of wintertime climate variability in the North Atlantic region (e.g. Hurrell 1995).

Previously, (Sutton et al. 2003) we investigated the impact of Sea Surface Temperatures (SSTs) between 1871-1999, on North

Atlantic climate variability using an ensemble of six simulations with HadAM3. These were analysed using an optimal detection algorithm (Venzke 1999) to separate the influence of the ocean from that of internal atmospheric variability. We concluded that: 1) on multi-decadal timescales the ocean influence is dominated by a single mode that is associated primarily with changes in the North Atlantic SST, has a strong projection on the NAO in wintertime, and may be a response to fluctuations in the thermohaline circulation; 2) on interannual timescales the climate of the North Atlantic region is influenced by the Pacific ENSO phenomenon but also by SST anomalies in the Atlantic, especially the Tropical North Atlantic (TNA) region.

Of course, these results may be entirely peculiar to HadAM3. Therefore we analysed similar simulations of forced North Atlantic climate variability using three other climate models: Arpege-climat (CERFACS/Meteo France), Echam4 and Echam 5 (MPI) together with HadAM3. Each model was forced with a reconstruction of historical global SST patterns between

1951-1999 (HadISST/GISST). As in Sutton et al. 2003 we used the Optimal Detection algorithm to identify the (common) dominant modes of forced atmospheric variability within each model ensemble.

Figure 45 shows the results of this analysis for winter time (DJF) Mean Sea Level Pressure (MSLP). Panels a-d show the dominant mode of forced MSLP variability in the four models. Panels i-l show the time-series associated with these modes. Panels e-h show the regression of the SST forcing field onto these time series. For three of the four models (HadAM3, Arpege and Echam5) the spatial pattern of the leading mode features a dipole structure in MSLP reminiscent of the NAO. The SST regression patterns (panels e,g,h) indicate that the largest fraction of SST variance explained by the time-series occurs in the TNA region; this suggests that the TNA is a likely source of forcing for this mode, with negative TNA SST anomalies being associated with a positive NAO. This result is consistent with our findings in Sutton 2003 and also other modelling studies (Sutton 2001, Cassou 2001). The results for Echam 4 (panels b,f,j) show a dominant mode of that is different from the other models. The SST pattern suggests that ENSO is the dominant influence on North Atlantic climate in this model.

Sensitivity studies of the Echam 4 results suggests, however, that the response of this model to TNA SST may be weaker relative to the ENSO influence than is found in the other models.

Conclusions

• The results from all models suggest that SSTs influenced North Atlantic Climate during the period 1951 to 1999.

• In three of the models the dominant winter time (DJF) mode of forced atmospheric variability appears to be an NAO-like dipole pattern.

• The same three models suggest that the Tropical North Atlantic region may play a key role in influencing the North Atlantic Climate.

A full discussion of these results will be contained in Hodson *et al.*, 2004

References

Cassou C and L Terray, 2001: Oceanic forcing of the wintertime low-frequency atmospheric variability in the North Atlantic European sector: A study with the ARPEGE model. J. Climate, 14, 22, 4266--4291.

Czaja A and C Frankignoul, 2002: Observed impact of atlantic sst anomalies on the north atlantic oscillation. J. Climate, 15, 606--615.

Hurrell JW, 1995:Decadal Trends in the North Atlantic Oscillation: Regional Temperatures and Precipitation, Science, 269, 676--679

Mehta VM, MJ Suarez, JV Manganello and TL Delworth, 2000: Oceanic influence on the North Atlantic Oscillation and associated Northern Hemisphere climate variations: 1959-1993. Geophys. Research. let., 27, 121--124

Rodwell M, DP Rowell, and C Folland, 1999: Oceanic forcing of the wintertime north atlantic oscillation and European climate. Nature, 398, 320--323.

Sutton RT and DLR Hodson, 2003: Influence of the Ocean on North Atlantic Climate Variability 1871-1999. J. Climate, 16, 3296--3313

Sutton RT and WA Norton and SP Jewson,2001:The North Atlantic Oscillation - What Role for the Ocean? Atmospheric Science Letters, 1, 2, 89--100

Venzke R, MR Allen, RT Sutton, and DP Rowell. The atmospheric response over the north atlantic to decadal changes in sea surface temperature. J. Climate, 12, 2562--2584.

Preliminary results from the CHIME Coupled Climate Model

Alex Megann, Bablu Sinha and Adrian New, SOC

The Coupled Hadley-Isopycnic Model Experiment (CHIME) is a new UK coupled climate model, developed to investigate the effects of the vertical representation of the ocean component of a climate model. The model is identical to the Hadley Centre's HadCM3 climate model, except for its use of a hybrid-coordinate ocean model instead of HadCM3's z-coordinate (constant depth levels) ocean model. The hybrid-coordinate model has layers of constant potential density in the ocean interior, transitioning to constant-depth levels near the surface. It is expected to maintain the advantages of purely isopycnic models (namely conservation of water properties over large length and time scales) while permitting the higher vertical resolution near the surface characteristic of traditional z-coordinate models.

The first main integration of CHIME has now reached twenty years, and we aim to complete the control run of two hundred years early in 2004. Preliminary analysis of the output shows markedly

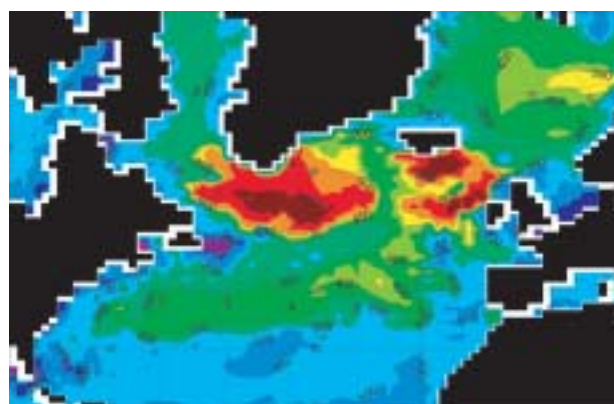Figure 46. Sea surface elevation in the North Atlantic in March

Figure 47. Mixed layer depth for March.

higher interannual variability compared with the same ocean model forced by climatological surface fluxes. In particular, an ENSO-like signal is present in the equatorial Pacific, which was absent in ocean-only runs. Overall, the ocean model shows a general slow warming (0.06˚C in the second decade), but is otherwise performing well in terms of circulation, seasonal cycle and ice cover.

Figure 46 shows the sea surface elevation in the North Atlantic in March, ten years into the model run. The North Atlantic Current can be clearly seen, approximately following the 90cm height contour from the Gulf Stream separation off the eastern seaboard

of the US, across the north Atlantic, and finally passing into the Norwegian Sea between Iceland and Scotland. Figure 47 shows the mixed layer depth, again in March of year 10. Wintertime deep mixing can be seen in the Labrador Sea and south of Iceland, which contributes to the formation of North Atlantic Bottom Water. Further south, a tongue of mixing down to 300-400 metres is visible across the Subtropical Gyre; this produces the characteristic mode waters in the gyre.

Reference
Bleck, R., 2002: An oceanic general circulation model framed in hybrid isopycnic-cartesian coordinates, Ocean Modelling, 4, 55-88.

Diagnosis of daily HadCM3 ocean-atmosphere coupling using a simple stochastic model

T.J.Mosedale (t.j.mosedale@rdg.ac.uk), D.B.Stephenson and M.Collins, Department of Meteorology, University of Reading

Extratropical effects of the ocean on the atmosphere are difficult to quantify in observational studies. Such coupling from the persistent ocean to the atmosphere can lead to long-term predictability of the atmosphere. Previous studies have used descriptive covariance techniques (e.g. SVD analysis) to estimate the association between oceanic and atmospheric fields. In this paper, a more model-based statistical approach is used in which a simple 2-variable stochastic model is employed to diagnose the atmosphere-ocean interaction in the North Atlantic in simulations of a state of the art coupled climate model (HadCM3).

The simple coupled model is a discrete time version of the model proposed by Barsugli and Battisti (1998) to represent local extratropical atmosphere-ocean interactions. The model is derived using an energy balance of a slab ocean and single layer atmosphere, driven by a stochastic noise forcing. This results in a linear first order vector autoregressive (VAR(1)) stochastic model for an atmospheric and an oceanic component. In this model the effect that the ocean has on the atmosphere is given by a single numericalvalue.

Daily data from HadCM3 (1.5m air temperature and 300m integrated ocean heat content) are interpreted in terms of this simple model to obtain estimates at each gridpoint for the parameter representing ocean to atmosphere influence. An OLS
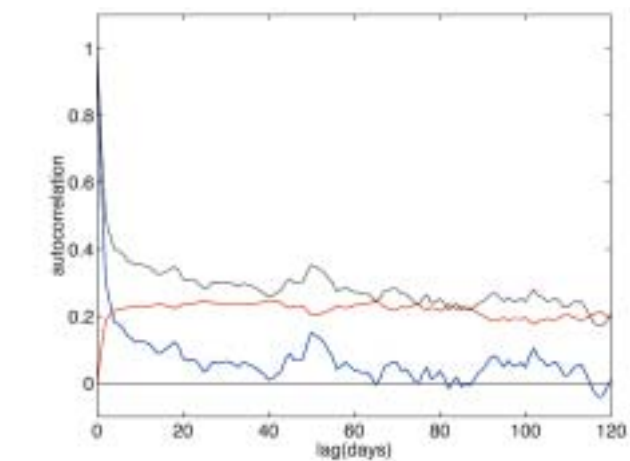

Figure 49. The autocorrelation of the atmospheric variable T at 47.5N, 26.25W for lags up to six months. The black line is the autocorrelation, which is split into an atmospheric direct part (blue line) which is from atmospheric interactions only, and an indirect part (red line) which arises due to interactions with the ocean.

estimation procedure is used. Figure 48 shows a map over the North Atlantic region of this parameter. A region of non-zero parameter is seen in the North Atlantic, in this region the ocean is affecting the ocean on a day to day time scale.

This ocean to atmosphere affect has an impact on the persistence of atmospheric temperature anomalies. Using the simple model, the autocorrelation in the atmosphere can be split into a direct and an indirect part, where the direct part is purely from the atmosphere, and the indirect part arises due to interactions with the ocean. Figure 49 shows the autocorrelation (black) of a point (47.5N, 26.25W) in the North Atlantic. Some persistence can be seen in the substantial autocorrelation at lags up to a few months. The blue line shows the direct atmospheric part, which decays to zero after about 20 days. The indirect part is shown by the red line to be the major contributor to this persistence in the atmosphere. So here the large ocean to atmosphere influence in HadCM3 increases the persistence of atmospheric temperature anomalies beyond a few days.

Reference
Barsugli and Battisti (1998), The basic effects of atmosphere-ocean thermal coupling on midlatitude variability. Journal of the Atmospheric Sciences 55(5) 477-493.
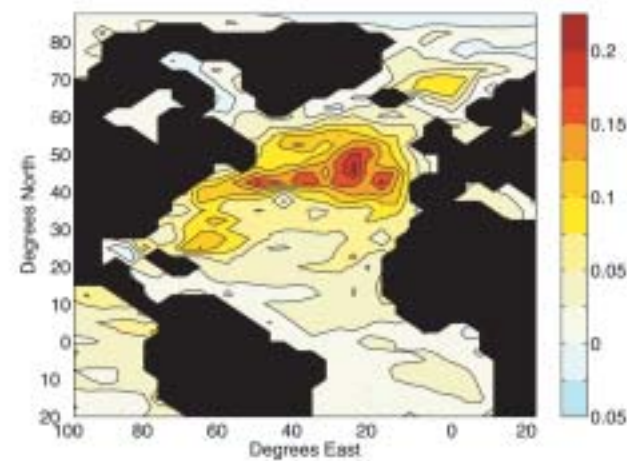

Figure 48. The complex model data is fitted to the simple model, giving an estimate for the parameter representing the influence of the ocean on the atmosphere, shown here.

Diagnosing the pathways of North Atlantic oceanic heat anomalies in HadCM3

Chris Old (cpo@mail.nerc-essc.ac.uk) and Keith Haines, ESSC, The University of Reading

Oceanic heat anomalies provide a memory of the changes in surface fluxes. Such anomalies are observed in the oceanographic record. By assimilation of the observations into a coupled ocean-atmosphere GCM it should be possible to track the anomalies and predict their impact on the ocean climate and the atmosphere. As a step towards this goal a set of diagnostics are being developed to study ocean heat pathways in the Hadley Centre's coupled climate model.

Heat anomalies are created and destroyed through the irreversible thermodynamic transformation of water masses by surface fluxes. Anomalies can be moved around by advection and mixing. Longer-lived anomalies are likely to be associated with water masses that are isolated from surface processes. This suggests that the subduction of water masses into the permanent thermocline plays a key role.

Water mass transformations in temperature space [G(T)] have been diagnosed for the N. Atlantic sector from 100 years of HadCM3 control run data using the method of Walin (1982). By considering the volumes above and below the maximum winter mixed layer base (WMLB) separately, the subduction has been included in the diagnostic (see Marshall *et al.*, 1999). From filtered (5yr Lanczos) time series of the transformations in temperature space, heat anomaly pathways have been identified using lag correlations between the processes involved at key classes.

Mean water formation processes for the volume above the WMLB in the North Atlantic are shown in Figure 50. The terms sum to zero at all temperatures indicating no long-term trend in the heat content above the WMLB. There are a number of obvious subduction and obduction (water returning to the mixed layer from the main thermocline below) classes. The two considered here are the subduction peak at 18ºC (subtropical mode waters) and the obduction peak at 12ºC (the warmer subpolar mode waters).

Lag correlations of subduction against surface transformations (Figure 51a) show that at the 12ºC obduction class, subduction leads the surface transformations by approximately 2 years with a positive correlation. Hence if obduction increases the surface transformations are forced to remove the anomaly, whereas a decrease in obduction causes the surface transformations to produce waters in this class. At 18ºC the surface transformations lead the subduction by approximately 2 years with a positive correlation. Hence an increase in mixed layer volume due to surface transformations at 18ºC precedes by 2 years an increase in subduction, i.e. the removal of the mixed layer anomaly.

The fate of an 18ºC mode water anomaly can be traced further by lag correlating the subduction at 18ºC with the processes at all other temperatures. Figure 51b and c show the subduction at 18ºC lag correlated at all temperatures with the mixing below the WMLB and the subduction respectively. The mixing correlations (2b) show a strong dipole between the 18ºC and the 21ºC classes where the subducted anomaly is moved to a warmer class by mixing below the WMLB over a 3-year period. The subduction correlations (Figure 51c) show the same dipole pattern where the anomaly subducted at 18ºC leads to an increase in obduction at
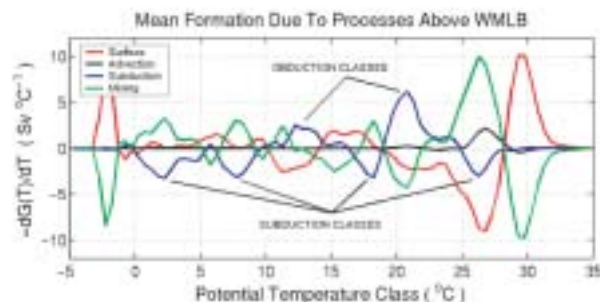

Figure 50. The 100-year mean formation due to the processes above the WMLB in the North Atlantic. The surface formation results from surface heating/cooling at the isotherm outcrops. The advection is the convergence through the open boundaries (Equator and Bering Strait) above the WMLB. The subduction is the convergence across the WMLB. The mixing is calculated as a residual from the conservation equations. Positive values indicate a net production by the process and negative values a net destruction. (Sv = 10^6 m^3 s^{-1})
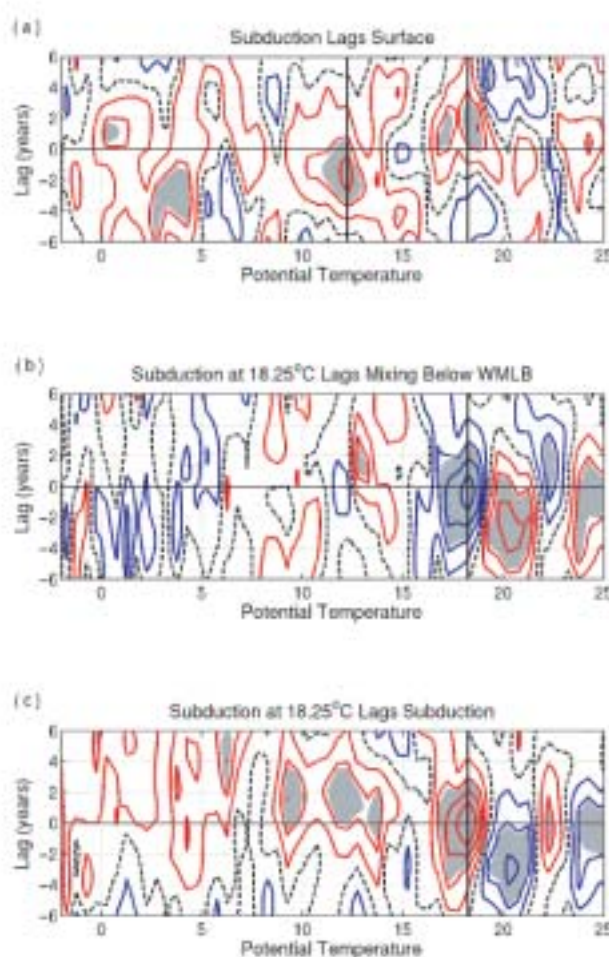

Figure 51. Lagged correlations of a) subduction against surface transformations, b) subduction at 18ºC against mixing below the WMLB at all temperatures, and c) subduction at 18ºC against subduction at all temperatures. The red contours indicate positive correlations, blue contours negative correlations, and black dashed contour zero correlation. The contour interval is 0.2. The grey shading highlights correlations with a statistical significance > 95%. The data were filtered using a 5-year Lanczos filter before correlating. See text for interpretation.

21ºC 3 years later. It can be shown that the strong mixing at higher temperatures in the mixed layer spreads the obducted anomaly so that its influence on surface transformations cannot be detected.

This methodology has produced a physically meaningful 5-year process pathway for the life cycle of 18ºC mode water anomalies. Anomalous surface fluxes produce a volume anomaly in the mixed layer that persists for 2 years before being subducted into the permanent thermocline. From here the anomaly is gradually mixed to warmer temperatures as it moves equatorward around the subtropical gyre, to be re-entrained into the mixed layer 3 years later, where it is spread out by mixing.

The 12ºC subpolar mode waters appear to be affected both by surface anomalies coming up from the subtropical gyre (see Sutton & Allen, 1997) and by obduction anomalies within the subpolar gyre (Figure 50). Recent promising results indicate that the above methodology can be used to unravel the more complicated subpolar mode water pathways. An understanding of anomalous subpolar mode water formation is important as it occurs in a region (western end of the NAC) where significant ocean-atmosphere feedback can occur.

References

Marshall, J., D. Jamous, and J. Nilsson, 1999. Reconciling thermodynamic and dynamic methods of computation of water-mass transformation rates. Deep-Sea Research I, 46, 545-572

Sutton, R., and M. Allen, 1997. Decadal predictability of North Atlantic sea surface temperature and climate. Nature, 388, 563-567

Walin, G., 1982. On the relation between sea-surface heat flow and thermal circulation in the ocean. Tellus, 34, 187-195

Towards a Refinement of the Boundary Forcing of HOPE

Scott Osprey, Rutherford Appleton Laboratory

Question

How does the nature of the persistence of SST anomalies during one winter affect their re-emergence the following winter?

Introduction

Observationally, large scale patterns of anomalous sea-surface temperature persist longer than those of smaller scale. This behaviour is inhibited in many ocean only models through the employment of strong relaxations to climatology to prevent model drift. The persistence of these patterns through one winter (together with the depth of the mixed layer) is thought influential in the re-emergence of these the following winter.

Method

An Empirical Orthogonal Function analysis (EOF) was performed on 100 years of sea-surface temperature (SST) output from the 1000 year HadCM3 control run. Decorrelation times were then calculated from the resultant principal component timeseries. Timescales representative of these decorrelation times were on the order of 10-15 months.

Three experiments were completed using the HOPE ocean model. For each experiment, the model domain comprised the North-Atlantic and utilised boundary forcing fields taken from the 100 years of HadCM3 output (above). To help eliminate model drift in the first experiment, a strong relaxation to climatological mean HadCM3 SST was imposed ($40\,\mathrm{Wm}^{-2}$). During the final year of integration, the monthly mean heat relaxation tendencies were logged.

The second integration ran following the conclusion of the first experiment but relaxed SST in two ways. SST anomalies were constructed by subtracted climatological monthly mean SST from the HadCM3 control run from instantaneous model values. These were then projected onto the set of EOFs constructed from the HadCM3 data (above) and the corresponding principal components were relaxed according to the decorrelation timescales calculated previously. The SST remaining which did not project onto the EOFs were relaxed strongly ($40\,\mathrm{Wm}^{-2}$).
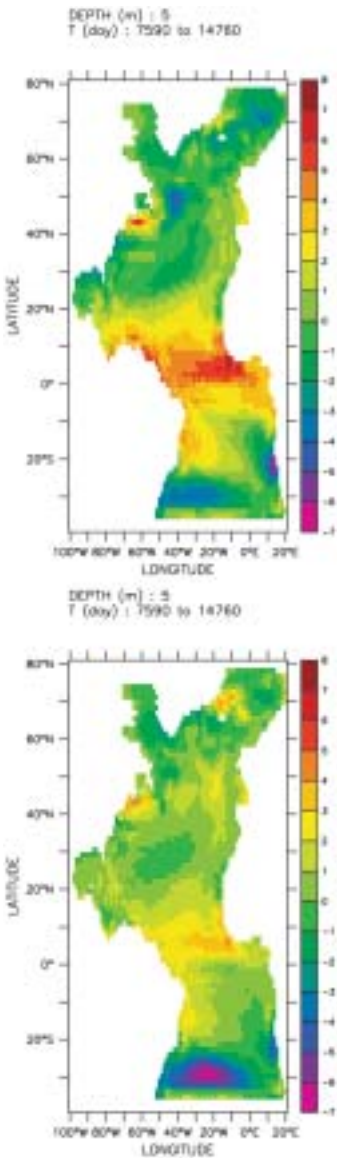

Figure 52. Deviations from the HadCM3 control run climatology of sea-surface temperature from experiment 2 (top) and 3 (bottom).

The third and final experiment also ran following the conclusion of the first but substituted the strong SST relaxation term in the boundary forcing with the mean field calculated at the conclusion of the first experiment. The scale dependent relaxation term was retained. The second and third experiments were run for 20 years following the end of the first experiment.

Results

It can be seen from Figure 52 that the inclusion of a scale dependent relaxation on model SST produces a mean field which differs appreciably from climatology. A conspicuous tongue of positive anomalous SST is apparent about the tropics while negative values occur about the extratropics. This tropical pattern is collocated with similar features seen in a number of the HadCM3 EOF fields (not shown). To a first approximation it should not be surprising that these patterns exist at all. The e-folding timescales for the strong relaxation term is about 11 days, which should be contrasted to the scale dependent timescales noted above. Thus, one could attribute these anomalies to the major change in nature of the heating budget. A second argument questions the existence of these patterns. The boundary forcing terms and climatological SST which is being relaxed to have each been taken from the same model run – the HadCM3 control run. The decorrelation times were also calculated using the timeseries from this control run. So, it could be argued (barring any significant difference between the two ocean models) that these patterns should not exist at all as they do not appear in the control run.

The bottom figure shows the SST difference field from experiment 3. The inclusion of a flux correction term has made a marked improvement in reducing both the tropical and extratropical anomalies. These anomalies persist, however and actually increase in value to the south of the model domain.

Concluding remarks

The introduction of a scale dependent relaxation to SST produces a mean field which differs markedly from climatology. On introduction of a flux corrected heating term an improvement is seen, but the anomalies are not removed and indeed are seen to increase in the southern domain of the model.

These discrepancies can be eliminated by modifying the flux correction heating term in one important way. If a scale dependent relaxation is used in experiment 1 together with a strong relaxation term which not only acts on residual SST but on the full SST anomaly, then by construction, such a flux correction should eliminate the mean anomalies seen in the other two experiments. This would have the desirable effect of allowing the scale dependent relaxations only to have an impact once interannual variability is introduced to the boundary forcing fields – their purpose is to act about the mean state

The influence of the persistence of SST anomalies during one winter on the re-emergence of these the following winter can be investigated in a couple of ways. Firstly, once interannually varying boundary fields are used, autocorrelation analysis can be used on a sufficiently long integration. The second method, complementing the first, involves the construction of the model adjoint to look at the re-emergence mechanism over a shorter timescales.

References

Deser, C. D., M. A. Alexander, M. S. Timlin; 'Understanding the Persistence of Sea Surface Temperature Anomalies in Midlatitudes', Journal of Climate, 16, 2003, 57-72
Timlin, M. S., M. A. Alexander, C. Deser; 'On the Re-emergence of North Atlantic SST Anomalies', Journal of Climate, 15, 2002, 2707-2712

The North Atlantic Oscillation and Coupled Ocean-Atmosphere Interactions in the Tropical Atlantic of HadCM3

Len Shaffrey and Rowan Sutton, CGAM, Department of Meteorology, University of Reading.

The North Atlantic Oscillation (NAO) is the dominant mode of wintertime atmospheric variability over the North Atlantic Ocean. When the NAO is said to be in its positive phase there is a strengthening of the surface westerlies over the midlatitude North Atlantic Ocean and a strengthening of the easterly trade winds over the subtropics. The winds associated with a positive NAO induce a tripolar SST pattern in the North Atlantic, with cooling in subtropics and at high latitudes and warming in the midlatitudes.

An interesting question that arises is, do the changes in SST induced by the NAO feedback onto the atmosphere at a later date? If so then the feedback of NAO induced changes in SST onto the atmosphere would provide a potential mechanism for extended predictability in the climate system. Such a mechanism is present in the Atlantic of HadCM3 where the cold subtropical SST induced by a positive wintertime NAO leads to a decrease in the following summertime precipitation in the subtropics. This is depicted in Figure 53 which shows the lagged regression of the summertime precipitation against the previous wintertime NAO

index. Vimont *et al.* (2001) studied a similar process in the North Pacific of the CSIRO CGCM (Coupled global climate model). They also found that the summertime subtropical atmosphere feels the SST 'footprint' induced by the North Pacific extratropical atmospheric variability from the previous winter.

The change in the summertime subtropical precipitation leads to changes in the equatorial Atlantic SST and the tropical atmosphere in the following winter (i.e. one year after the NAO event). The atmospheric circulation induced by the change in the summertime subtropical precipitation in Figure 53 leads to cross equatorial northerlies and so to westerly anomalous winds over the equatorial Atlantic. The westerlies then act to warm the ocean by reduced evaporation and tropical upwelling. The result is an SST dipole and a southwards shift of ITCZ (Intertropical convergence zone) towards the warmer waters. The SST dipole is depicted in Figure 54 which shows the following wintertime SST regressed against the previous winters NAO index. The SST dipole in Figure 54 is associated with stronger cross-equatorial northerlies and so to an
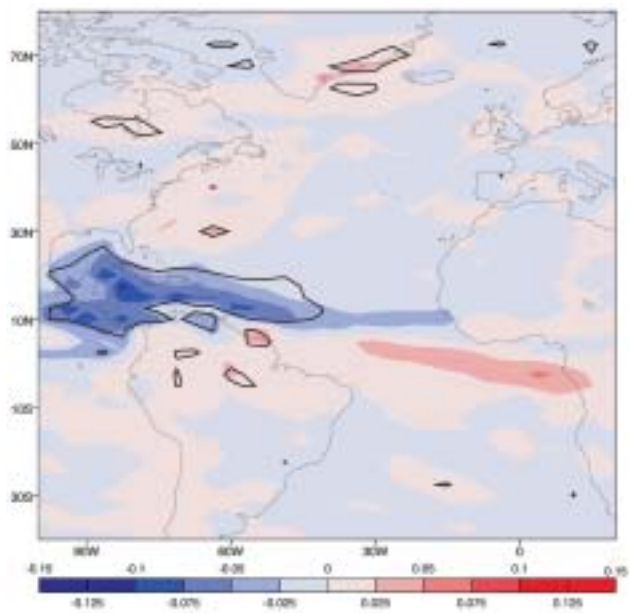
Figure 53. JJASON precipitation regressed against the previous DJFMAM NAO index. Contour interval is 0.025mm day^{-1} mb^{-1} and the bold lines denote regions that are 95% significant using a Student t-test.
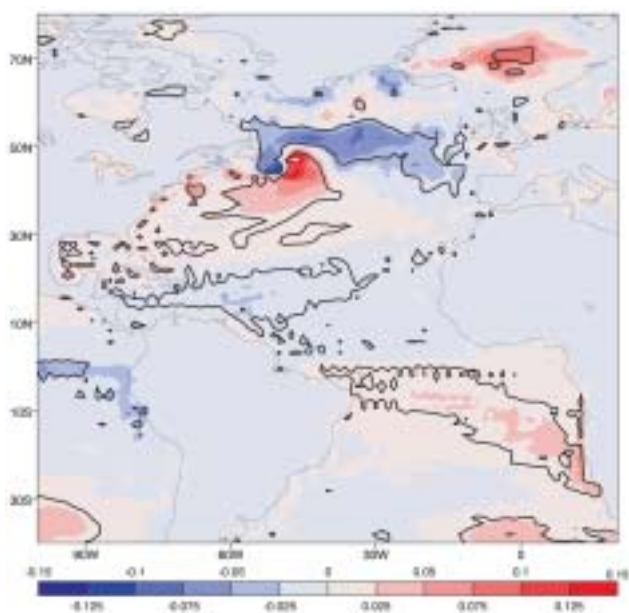

Figure 54. DJFMAM+1 SST regressed against the previous DJFMAM NAO index. The contour interval is 0.025K mb-1 and the bold lines denote regions that are 95% significant.

increase in the anomalous equatorial westerlies which further warm the SSTs. In this sense the tropical Atlantic SST dipole can be thought of self-maintaining coupled mode, an observation which has been previously made by Chang *et al.* (1997).

It is interesting to compare the results from HadCM3 with observations. In the NCEP reanalyses the 'footprint' of the wintertime NAO on the summertime subtropical precipitation and the SST can be clearly seen (not shown), but the tropical Atlantic SST dipole doesn't appear to be excited in the following winter. This suggests that the footprinting mechanism that is seen in

HadCM3 and NCEP appears to be a mechanism for extended predictability on seasonal timescales, but also that the tropical Atlantic SST dipole might too easily excited in HadCM3.

References

Chang P., J. Link and L. Hong (1997) A decadal climate variation in the tropical Atlantic Ocean from thermodynamic air-sea interactions. Nature, Vol 385, p 516-518.

Vimont D. J., D. S. Battisti and A. C. Hirst (2001) Footprinting: A seasonal connection between the tropics and the mid-latitudes. Geophys. Res. Letters, p 3923-3926

Great Salinity Anomalies in HadCM3?

Martin R. Wadley, University of East Anglia, Grant R. Bigg, University of Sheffield

Observations of salinity in the northern North Atlantic have revealed negative salinity anomalies which appear to propagate around the North Atlantic sub-polar gyre. The earliest of these commenced in the late 1960s, with an anomalously large export of low salinity water from the Arctic through Fram Strait. This anomalously low salinity water could be traced around the sub-polar gyre and back into the Nordic Seas some 10 years later. Dickson *et al.* (1988) suggested that the salinity anomaly had advected around the sub-polar gyre, whereas earlier it had been suggested that the eastward movement of water masses in the region west of Britain could account for the anomalously low salinity observed there in the mid 1970s (e.g. Ellett and MacDougall, 1983).

A hovmöller plot was constructed showing monthly salinity anomalies around the sub-polar gyre for a 100 year period within the HadCM3 coupled climate integration. This showed around seven salinity anomalies (both positive and negative) which 'moved' around the modelled sub-polar gyre with a time scale of

around 12 years, consistent with the observed Great Salinity Anomaly. The strongest negative anomaly event was chosen, and independent passive tracer parcels added at 2-monthly intervals for 5 years (30 releases) to the mixed layer in the modelled East Greenland Current during and after the passage of the negative salinity anomaly. If the salinity anomalies seen in the HadCM3 integration result from advection around the sub-polar gyre the passive tracer parcels will also propagate around the sub-polar gyre. The individual tracer parcels show very different evolutions with time. Those released during the passage of the low salinity anomaly mainly leave the Nordic Seas through the Denmark Strait, whereas later releases circulate around the Greenland Sea Gyre and spread into the Arctic.

Figure 55 shows the evolution of one tracer parcel released during the passage of the low salinity anomaly, over a 12 year period corresponding to the time scale of the Great Salinity Anomaly.
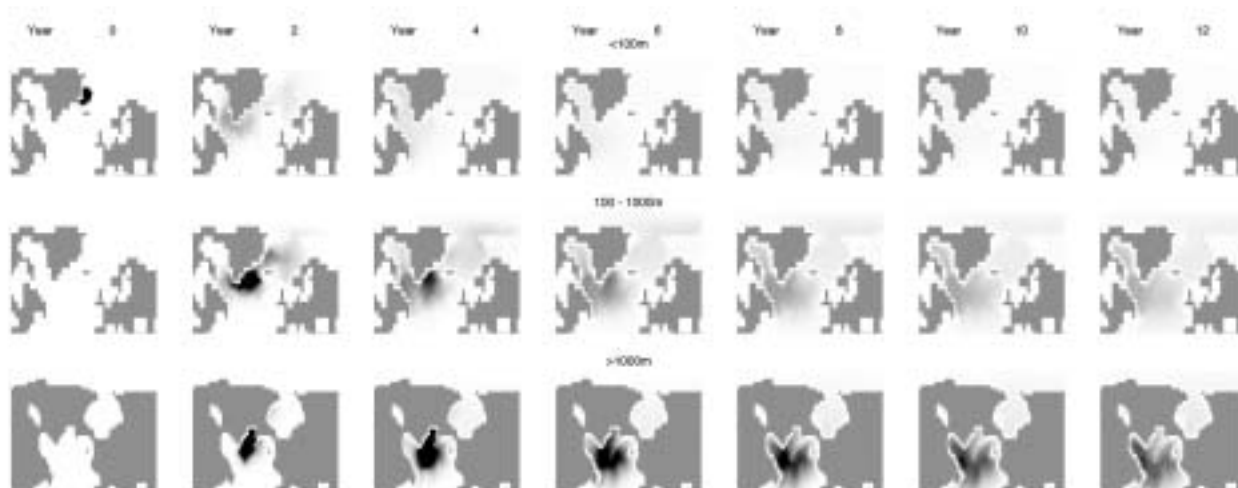
Figure 55. Relative depth-integrated concentration of passive tracer at 2-yearly intervals following release in the East Greenland Current.

It can be seen that the tracer advects firstly into the Labrador Sea, and then into the North West Atlantic, mostly at >1000m depth. Very little of the tracer remains in the mixed layer, where it could circulate around the sub-polar gyre in the manner described by Dickson *et al*. (1988), despite there being a surface signature of a low salinity anomaly which is consistent with Dickson *et al*.'s hypothesis.

In conclusion, the HadCM3 model is found to have Great Salinity Anomaly events which have a surface signature consistent with that observed during the 1970s. Dickson *et al*. proposed that this was the result of an initial low salinity anomaly advecting around the sub-polar gyre. However, in the HadCM3 model advection is not the cause of apparently propagating salinity

anomalies beyond the Labrador Sea. Work is under way to establish the cause of the anomalies in the north-east Atlantic, and it is speculated that changes in precipitation and evaporation may be responsible. It remains an open question as to whether advection was responsible for the Great Salinity Anomaly in the real ocean, and the HadCM3 model is behaving incorrectly, or whether the real Great Salinity Anomaly is more complex than has been suggested.

References

Dickson RR, Meincke J, Malmberg SA, Lee AJ, 1988: The Great Salinity Anomaly in the Northern North Atlantic 1968-1982. Prog. Oceanogr., 20, 103-151.

Ellett DJ, MacDougall N, 1983: Some monitoring results from west of Britain. IOC Technical Series Rept., 24, 21-25.

Does ocean gyre circulation affect storm tracks?

C.Wilson (c.wilson@liv.ac.uk) and R.G.Williams, Department of Earth and Ocean Sciences, University of Liverpool.

While the winter mean atmospheric flow may largely be set by orographically-forced standing waves (Seager *et al*. 2002), the ocean might still be important in locating the storm tracks and affecting its variability. The ocean influence might occur through the land-ocean temperature contrast, horizontal sea surface temperature (SST) gradient (possibly effecting boundary stability) and surface temperature differences between ocean and atmosphere (sustained by the high ocean heat content) inducing diabatic heat fluxes.

The large-scale ocean circulation has two components: a horizontal gyre circulation, which has typical periods of years to decades, and an overturning circulation in the meridional plane, which has associated timescales of decades to centuries within a basin. In the Atlantic, most of the ocean heat transport (typically 1 to 2 PW) is transported by the overturning circulation, while in the Pacific, the gyre circulation dominates. Given the importance of the upper ocean for interannual and decadal changes (such as those associated with the North Atlantic Oscillation), we consider how

artificial perturbations to the surface gyre circulation affect the atmospheric storm tracks.

We experiment with the FORTE global coupled model (Sinha and Smith, 2002), consisting of IGCM3 at T21 resolution with 22 levels and MOMA at 2 degrees with 15 levels. We spin-up for 40 years (currently being extended to 100 years) and then integrate for a further 10 years: a 'GYRE+' case, with the ocean surface drag coefficient artificially doubled, and a 'GYRE-' case with it halved. The last 5 winters are analysed and compared to the 'CONTROL' case.

By increasing the surface drag coefficient, we increase the gyre and Ekman transport, tending to transport more heat polewards in the ocean and leading to cooler equatorial SST and warmer extratropical SST. The response is most marked over the Pacific where the gyre circulation dominates over the overturning. The opposite response occurs when the drag coefficient is reduced.

We observe the strongest response in the storm tracks for the GYRE- case, where the 250 mb eddy kinetic energy (EKE) signal
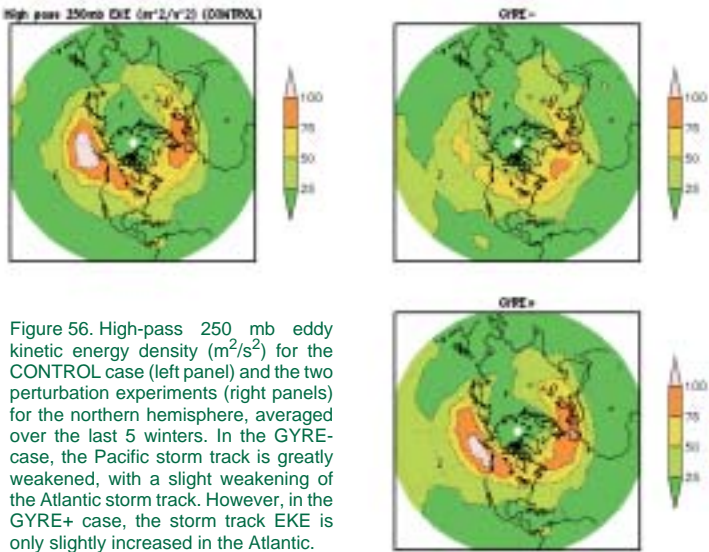
Figure 56. High-pass 250 mb eddy kinetic energy density (m^2/s^2) for the CONTROL case (left panel) and the two perturbation experiments (right panels) for the northern hemisphere, averaged over the last 5 winters. In the GYRE-case, the Pacific storm track is greatly weakened, with a slight weakening of the Atlantic storm track. However, in the GYRE+ case, the storm track EKE is only slightly increased in the Atlantic.
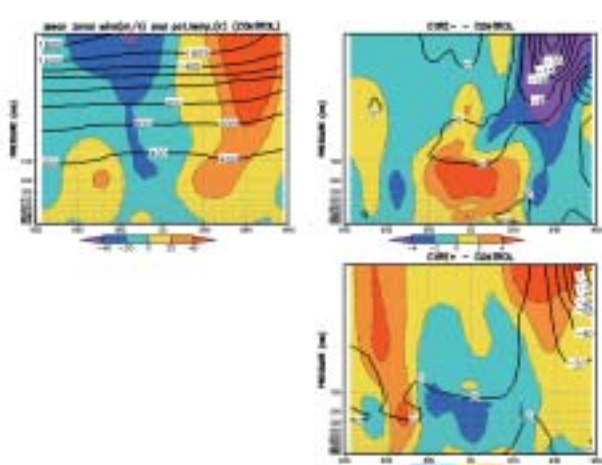

Figure 57. Mean zonal wind (m/s) (filled contours) and potential temperature (K) for the CONTROL case (left panel) and the differences between two perturbation experiments and the CONTROL (right panels), averaged over the last 5 winters. GYRE-shows a weakening of the tropospheric zonal jets and a marked weakening and cooling of the stratospheric jet at 60N. The GYRE+ case shows a strengthening of the stratospheric jet at 60N, but only a limited extension into the troposphere.

is destroyed over the mid-latitude Pacific (Figure 56) through an emergence of a cool anomaly in both SST and 750 mb temperature across the mid-latitude Pacific and equatorial Indian Ocean, associated with an atmospheric drying from reduced latent heating. While the GYRE- case stabilizes the storm track, there is an asymmetry as the GYRE+ case only provides a limited strengthening throughout the storm track.

The GYRE- case reveals a weakening of the mean zonal jets in the troposphere (Figure 57) and a marked weakening and cooling of the stratospheric jet at 60N. The 250mb E-vectors (not shown) suggest that there is reduced mean acceleration of the mean zonal jets by the waves. Conversely, the GYRE+ case shows a strengthening of the stratospheric jet in the winter hemisphere, but only a weak extension down into the troposphere.

While our perturbations involve an artificial change in the drag coefficient, they suggest that the ocean can play a direct role in modifying the strength of the storm tracks, (as suggested by Hoskins and Valdes, 1990). Our preliminary study will be

extended to identify the mechanisms by which the atmosphere and ocean alter, involving the combination of Ekman, boundary current and gyre circulations, as well as to assess the heat transport compensation between the atmosphere and ocean, and the angular momentum changes within them.

References

Hoskins, B.J., and P.J. Valdes, On the existence of storm-tracks. J.Atm. Sci., 47, 1854-1864, 1990.

Seager, R., D. S. Battisti, J. Yin, N. Gordon, N. Naik, A.C. Clement, M.A. Cane, Is the Gulf Stream responsible for Europe's mild winters? Q.J.ROY.MET.SOC. 128 (586): 2563-2586 Part B, OCT 2002.

Sinha, B. and R. Smith, Development of a fast Coupled General Circulation Model (FORTE) for climate studies, implemented using the OASIS coupler. SOUTHAMPTON OCEANOGRAPHY CENTRE Internal Document No.81, 2002.

Atmospheric Composition

Modelling Chemistry and Mixing During Trans-Atlantic Pollution Transport.

Steve Arnold and Martyn Chipperfield (School of Environment, University of Leeds, John Methven (Dept. Meteorology, University of Reading, Fiona O'Connor (Centre for Atmospheric Science, University of Cambridge)

Intercontinental transport of ozone and its precursors in the troposphere has been identified as an important factor in regional ozone budgets. The north Atlantic region displays such transport, where North American boundary layer pollutants are frequently exported to the European troposphere. This transport is facilitated by uplift of boundary layer mass to the upper troposphere in warm conveyor belts originating over the North American eastern seaboard. During the NERC part-funded EXPORT experiment (European eXport of Particulates and Ozone by long-Range Transport) in August 2000, extensive layers of enhanced ozone, CO and NOy were observed in the mid/upper troposphere over central Europe. Back-trajectory analysis indicated these air masses had origins over the North American continent.

A Lagrangian CTM (CiTTyCAT) and a global Eulerian CTM (TOMCAT) have been used to investigate the chemistry and transport of these air masses. Figure 58 shows a time series of flight observations and output from the models for the latter section of EXPORT flight A776 (Aug. 10 2000) in the European UT. Figure 59 shows the path of the aircraft through a cross section of ozone concentrations output from TOMCAT and through a cross section of a reverse domain filling trajectory simulation of ozone using the CiTTyCAT model. Fine-scale features in CO and ozone which correspond to transitions between air masses of distinct origins (West US UT and polluted; Eastern US PBL; SE

US coast) are smeared out by TOMCAT, since the advection and stretching of air masses during ascent from the US coast into the UT results in filaments and layers too narrow for the global CTM to resolve. The CiTTyCAT model produces structure on the same scale as the observations, however gradients are too strong, and are preserved where mixing appears to have diluted pollution into the North Atlantic UT (e.g. the Eastern US pollution) and mixed together air masses of diverse origins (e.g. observations between 13:15-13:45 UT).

Mixing has been introduced into the CiTTyCAT model by relaxing the modelled chemical species to interpolated 3D fields from the TOMCAT model, which are assumed to represent a well mixed 'background' atmosphere. The results demonstrate that a 5 day relaxation timescale reduces the over-estimated model signatures from the Eastern US pollution, while preserving the observed gradients at air mass boundaries. A 2.5 day relaxation timescale gives less structure during the homogeneous period between 13:15-13:45 UT, however the fast mixdown in TOMCAT appears to give the best simulation of this period, indicating rapid mixing. However, this faster relaxation timescale appears to erode the air mass gradients between 14:20 and 14:40UT in comparison with observations.
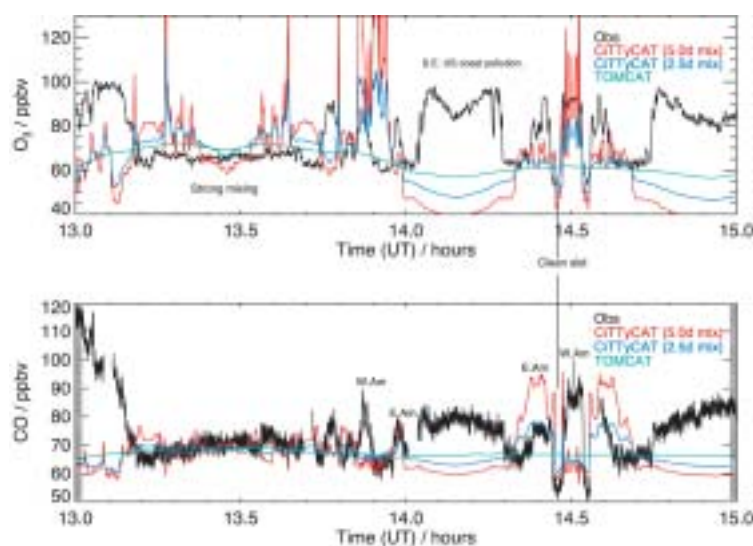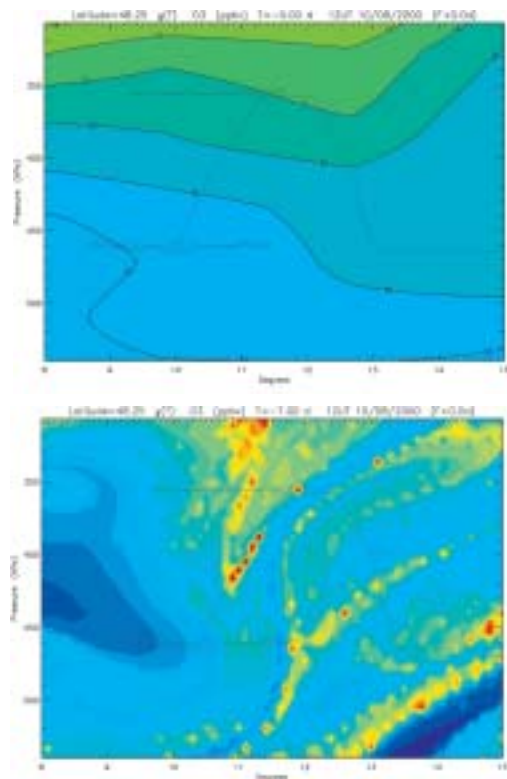
Figure 58. (above) Time series comparisons of the TOMCAT and CiTTyCAT CTMs with observed ozone and CO concentrations.

Figure 59. (right) Ozone model output from the TOMCAT CTM (top) and CiTTyCAT CTM (bottom) on vertical cross-sections in the plane of the aircraft flight track.
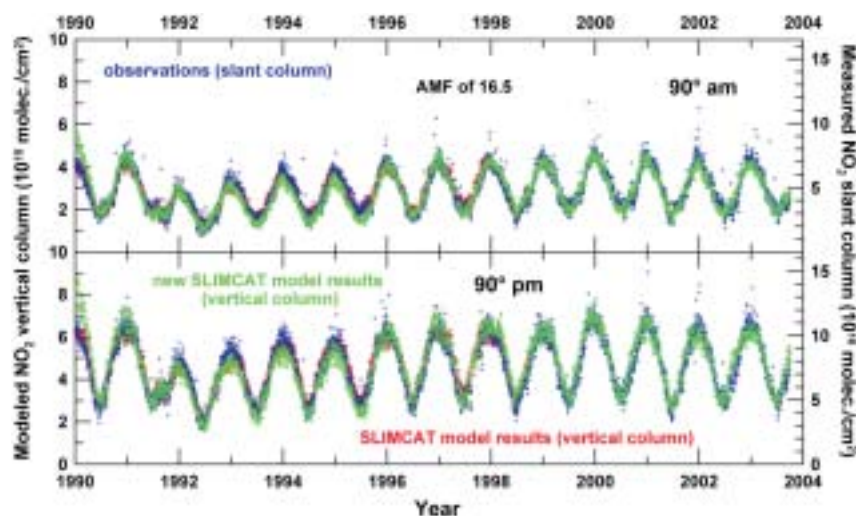
Figure 60. Comparison of observed (blue) slant column NO_2 at 90° am and pm at Lauder (45^oS) with corresponding vertical column from a long simulation of the SLIMCAT CTM (green) forced by ERA-40 analyses (ECMWF operational analyses after 2000). Data courtesy of Karin Kreher (NIWA) as part of EU QUILT project.

Multiannual CTM Simulations with the ERA-40 Analyses

Martyn Chipperfield, Institute for Atmospheric Science, School of the Environment, University of Leeds

Off-line chemical transport models (CTMs) are forced by meteorological analyses. Over the past few years the two sets of analyses that we have used to force long (multiannual) simulations of the SLIMCAT and TOMCAT off-line CTMs have been from the ECMWF and UKMO. The ECMWF ERA-15 analyses were available from 1979 but have an upper boundary at only 10 hPa. The UKMO 'UARS' analyses (Swinbank and O'Neill, 1994) extend up to 0.3 hPa but start in October 1991. Although these analyses are useful they both have limitations for forcing long-term simulations.

The ECMWF have recently completed the ERA-40 project. This provides forcing winds and temperatures from the surface to 0.1 hPa from 1957 on. This dataset will increase the range of stratospheric experiments that can be performed with the CTMs, notably simulations during the 1970s and 1980s when human activities were first seen to have a significant impact on the stratosphere.

We have used the ERA-40 winds to force the SLIMCAT CTM. Figure 60 shows the comparison of model column NO_2 with observations at Lauder, New Zealand during the 1990s. This dataset is one of the longest continuous records of stratospheric observations. The model clearly captures the observed annual cycle as well as the aerosol-induced variations (i.e. low values around 1992) and, apparently, most of the long-term trend (partly due to increases in N_2O). This comparison is very encouraging and illustrates the potential of using the ERA-40 analyses. Other preliminary comparisons with UKMO-forced runs show some differences which need to be further investigated. However, the ERA-40 analyses will provide a very important dataset for stratospheric modelling.

Reference

Swinbank, R., and A. O'Neil1, Mon. Wea. Rev., 122, 686-702, 1994.

Modelling water vapour and methane trends in the stratosphere

P. Hadjinicolaou and J.A. Pyle, Centre for Atmospheric Science, University of Cambridge, UK

We have used the 3-Dimensional chemical transport model SLIMCAT (Chipperfield, 1999) forced by the UK Met. Office (UKMO) analyses and including a simple methane oxidation scheme in a 10-year integration, in order to study the effect of year-to-year meteorological variability on stratospheric water vapour trends. The time-varying effect of source gases is not included in the chemistry so the modelled changes are solely due to the forcing winds and temperatures.

The chemical scheme is simply methane oxidation by OH, O^1D and Cl producing two water vapour molecules. The physical sink of H_2O through condensation at low temperatures is also included. The radiation scheme is not interacting with the chemistry and the bottom boundary at 330K is overwritten with monthly (but not annually varying) climatological HALOE data.

The methane and water vapour climatological fields from SLIMCAT for January (not shown) are in good agreement with those from HALOE, exhibiting the main characteristics of the Northern Hemisphere (N.H.) winter circulation. Quantitatively the model reproduces better H_2O than methane, where in the profile comparisons (not shown) the modelled methane is less than the observed, especially above 25 km.

Zonal mean trends for the 9-year period from April 1992 to March 2001 for the modelled species were derived using a multiple linear regression with a mean level and a trend term (no explanatory variables or noise were included). The global fields of the year-round trend are shown for the modelled methane (Figure 61a) and water vapour (Figure 61b). Very large (1-8%/year) negative trends throughout the stratosphere are calculated for methane, especially in the Southern Hemisphere (S.H.). Water
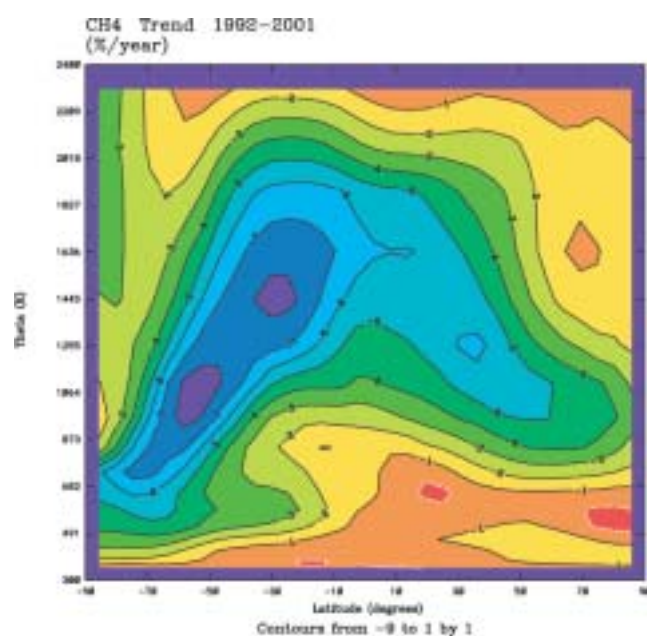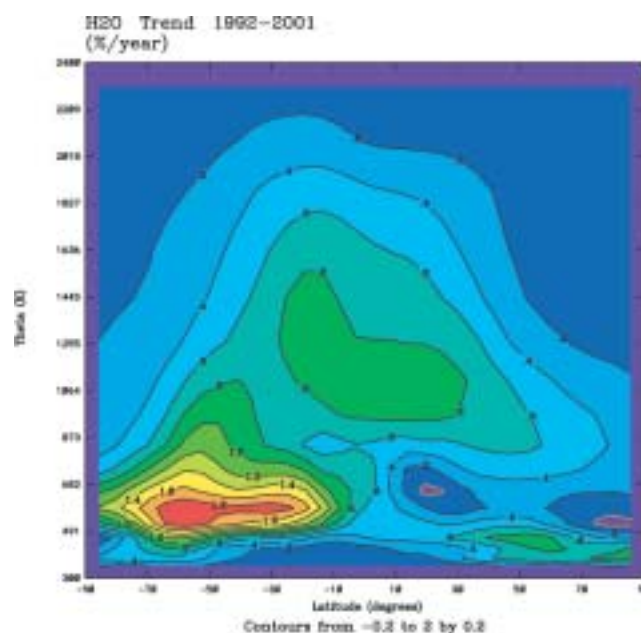
Figure 61. (a) Latitude-theta variation of modelled CH$_4$ year-round trends from April 1992 to March 2001.

(b) Latitude-theta variation of modelled CH4 year-round trends from April 1992 to March 2001.

vapour trends generally mirror spatially those in methane, and are positive and small (0-1%/year), maximising in the S.H. lower stratosphere (lower than the maximum methane trends appear).

These results are in some contrast with the recent study of Rosenlof (2002) on the trends in HALOE methane and water vapour measurements (over the same period and using a similar simple linear regression). The observed methane trend in that study is negative only above about 900K (~10 hPa) and much smaller (~ -2.5%) while is positive below. Note that the methane in our model does not have any sources (the increasing input of methane from the troposphere during the 1990s is not taken into account). In Rosenlof's work the HALOE water vapour increases and the methane decreases (in the upper stratosphere) are larger in the N.H. than the S.H., also opposite to our results.

Preliminary analysis reveals that the modelled trends in the S.H. winter mid-stratosphere can be attributed to changes in the cooling rates and the vertical transport. Further diagnostics (for example, the effect of temperature changes on the methane oxidation rate) are under way. A run with bottom boundary conditions from HALOE which vary annually will be carried out to take into account the interannual variability of methane and water vapour from the troposphere.

References

Chipperfield M.P., Multiannual simulations with a three-dimensional chemical transport model, J. Geophys. Res., 104, 1781-1805, 1999.
Rosenlof K.H, Transport changes inferred from HALOE water and methane measurements, J. Meteorol. Soc. Japan, 80, 4B, 831-848, 2002.

Multi-annual simulations of stratospheric ozone using the SLIMCAT model and the ERA-40 analyses

P. Hadjinicolaou and J.A. Pyle, Centre for Atmospheric Science, University of Cambridge, UK

The SLIMCAT stratospheric chemical-transport model (CTM), together with other CTMs within the CANDIDOZ EU project, will be used for 40-year stratospheric chemistry integrations forced by the new ERA-40 analyses, in order to quantify the contribution of chemical and dynamical changes to the observed ozone trend. These simulations extend the work of previous studies which used the ERA-15 analyses (Hadjinicolaou *et al*. 2002, Chipperfield 2003) in that the forcing ERA-40 data cover a longer period to study trends and include the whole vertical domain of the stratosphere. Here we present preliminary results from a 4-year test integration.

SLIMCAT was forced by the ERA-40 analyses from 1991 to 1995 using the model's full stratospheric chemistry scheme (Chipperfield, 1999).The horizontal resolution was 7.5 x 7.5 degrees with 17 isentropic levels from 340K to 2400K (approx.

from 10 to 55 km). The temperatures and horizontal winds are taken from the forcing ERA-40 analyses. The modelled ozone interacts with the MIDRAD radiation scheme in the calculation of the heating rates and the vertical motion. The most recent version of the model includes OpenMP parallelisation to take advantage of the multi-processor capabilities of the CSAR super-computing service.

Figure 61 show a comparison of the modelled column ozone in the Northern Hemisphere, against the TOMS satellite data and a similar SLIMCAT run forced by the UKMO analyses. A tropospheric contribution was added to the model column to facilitate comparison with TOMS. This added tropospheric ozone column (1000-286 hPa) varies with latitude and month and is taken from a 1985-89 UGAMP climatology. At 83N the model ozone (with both ERA-40 and UKMO forcing) captures accurately the
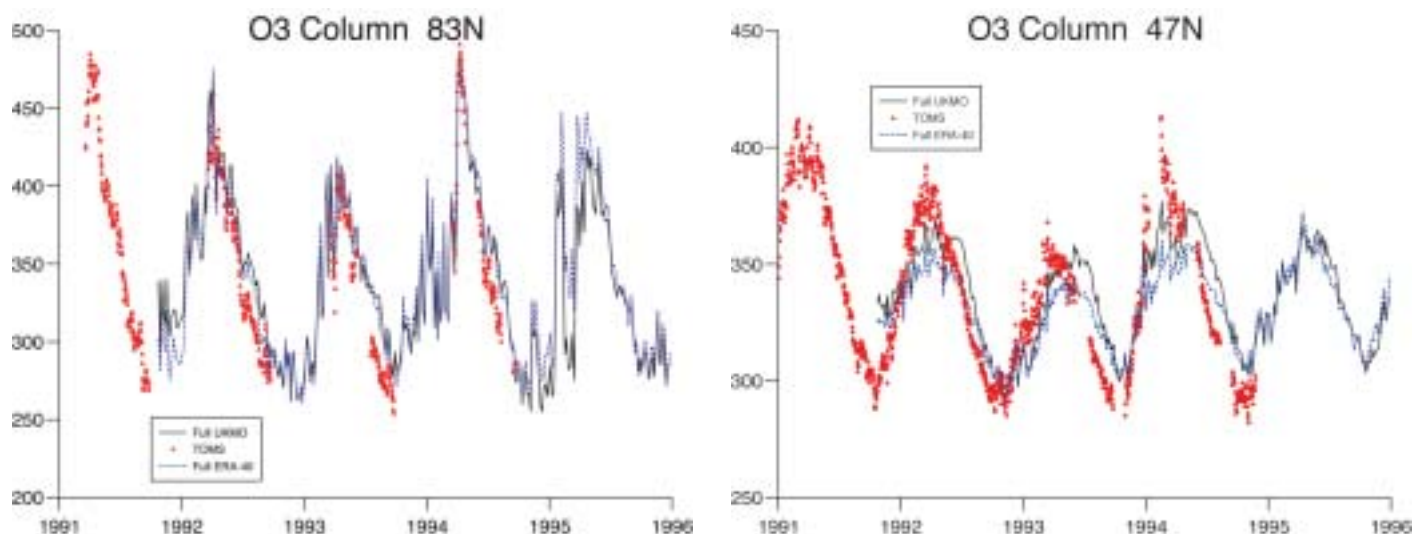
Figure 62. Zonal mean total ozone from the full chemistry SLIMCAT runs forced by ERA-40 and UKMO analyses (5-day output) compared with TOMS data (daily, Meteor3/Nimbus) at 83N (a, left) and 47N (b, right).

interannual variability and the annual cycle (winter/spring maxima, summer minima). At 47N, the observed year-to-year variations are well reproduced by the model and the agreement of the ozone maxima and minima is satisfactory although not exact. The comparison is also good in the Southern Hemisphere (not shown) where the Antarctic ozone hole is reproduced, but with differences in the southern middle latitudes. The model performance appears very satisfactory and that should allow the 40-year experiment to be carried out next.

References

Chipperfield M.P., Multiannual simulations with a three-dimensional chemical transport model, J. Geophys. Res., 104, 1781-1805, 1999.
Chipperfield M.P., A three-dimensional model study of long-term mid-high latitude lower stratosphere ozone changes, Atmos. Chem. Phys., 3, 1253-1265, 2003.

Modelling the Impact on Ozone from Cruise Altitude Perturbations applied to the Global Subsonic Aircraft Fleet

M.O. Köhler, H.L. Rogers, and J.A. Pyle, Centre for Atmospheric Science, Chemistry Department, University of Cambridge, U.K

Nitrogen oxide emissions from the global subsonic aircraft fleet result in a significant increase in ozone mixing ratios in the upper troposphere and lower stratosphere. Options are investigated on how to reduce the impact of the fast growing air traffic, and current investigations include changes to operational practices. In this study the TOMCAT chemistry transport model has been used to perform sensitivity studies on how UTLS ozone levels respond to cruise altitude perturbations of the global aircraft fleet.

The TOMCAT model has performed one pair of integrations (s3a and s3b) with cruise altitudes lowered by 6000 feet, and one pair of integrations (s5a and s5b) with cruise altitudes raised by 2000 feet. These changes have been made with respect to a reference scenario (s1), representing present-day cruise altitude conditions. For each pair of the cruise altitude perturbation experiments a normalised scenario, where the location of cruise altitude has been changed without globally altering the total amount of emissions (s3a and s5a), and a non-normalised experiment, which additionally accounts for a change in the Emission Index of NOx, due to the changes in operational procedure (s3b and s5b), have been performed.

Identical boundary conditions have been used for all experiments in order to achieve optimal comparability. All integrations have been performed for one year and were forced by ECMWF meteorological analyses of the year 1995. Both the initialisation of the chemical model fields as well as a 7-month spin-up have been performed identically for each of the experiments. The surface emissions used represent conditions appropriate for the year 2000 and for each experiment specifically developed aircraft emission inventories, also appropriate for the year 2000, have been used reflecting the corresponding cruise altitude perturbations. These aircraft emission inventories have been provided within the framework of the EC funded TRADEOFF project.

Changes in cruise altitude will lead to perturbations in the geographical distribution of aircraft emissions. Due to the large variability in atmospheric dynamics and chemistry, the shift in the location of aircraft emissions has potentially large implications for atmospheric chemistry. The results have shown that changes in cruise altitudes can lead to significant differences in ozone mixing ratios. The transport of aircraft emissions by atmospheric motion is highly dependent upon the geographical location and the altitude

at which the emissions are released. The amount of emissions released, in combination with the NOx mixing ratio of the ambient air, determine the amount of ozone produced from aircraft emissions.

In order to evaluate the total impact of the ozone changes in the northern hemisphere, both the annual mean tropospheric ozone column (from the surface to the tropopause) and the annual mean stratospheric ozone column (between the tropopause and 20 hPa, approximately 27 km altitude) have been calculated, both averaged over the northern hemisphere only. The altitude range of the stratospheric ozone column was chosen as a suitable domain to represent the region of perturbation due to subsonic aircraft. Figure 63 displays the average value for the northern hemispheric ozone column under present-day conditions (s1) and the perturbations for both higher (s5a, s5b) and lower (s3a, s3b) cruise altitudes.

In the stratosphere the ozone column below 20 hPa exhibits an almost linear relationship with the change of cruise altitude (Figure 63a). The magnitude of ozone column change due to a 2000 ft rise in cruise altitudes is approximately a third of that resulting from a 6000 ft fall in cruise altitudes. The difference in ozone column change between the normalised scenarios (s3a, s5a) and the non-normalised scenarios (s3b, s5b) is negligible and as such indicates that the ozone column change in the stratosphere is independent of the total amount of aircraft emissions.

The tropospheric ozone column shows a substantial difference between the normalised and non-normalised scenarios (Figure 63b). In the experiments with normalised aircraft emissions the magnitude of the ozone column change for a reduction in cruise altitude by 6000 ft is approximately 30% smaller than the change in ozone column due to an increase in cruise altitude by 2000 ft. The relationship between the perturbed ozone column and the change in cruise altitude is therefore non-linear. In the non-normalised experiments, where the total emitted NOx varies, both cruise altitude perturbations lead to an increase in tropospheric ozone column. This shows that the tropospheric ozone column is sensitive to the total amount of aircraft emissions. This difference between normalised and non-normalised scenarios in the troposphere and stratosphere could be explained by the low background NOx mixing ratios in the troposphere in comparison with the lower stratosphere. An increase in NOx due to aircraft emissions in the troposphere (where background values are low) could result in a higher chemical ozone production rate compared to the stratosphere.

The total ozone column up to 20 hPa shows that an increase in cruise altitudes leads to an increase of ozone column and lower cruise altitude lead to a reduction in total ozone for both scenarios (Figure 63c). In each case the main effect occurs around the tropopause region where increased NOx will increase ozone in the model. For scenarios with normalised emissions the relationship between ozone column and cruise altitude appears again to be almost linear. For non-normalised emissions the reduction of ozone column due to lower cruise altitudes is decreased by approximately 30% relative to the normalised emission scenario. Similarly, the increase in ozone column at higher cruise altitudes
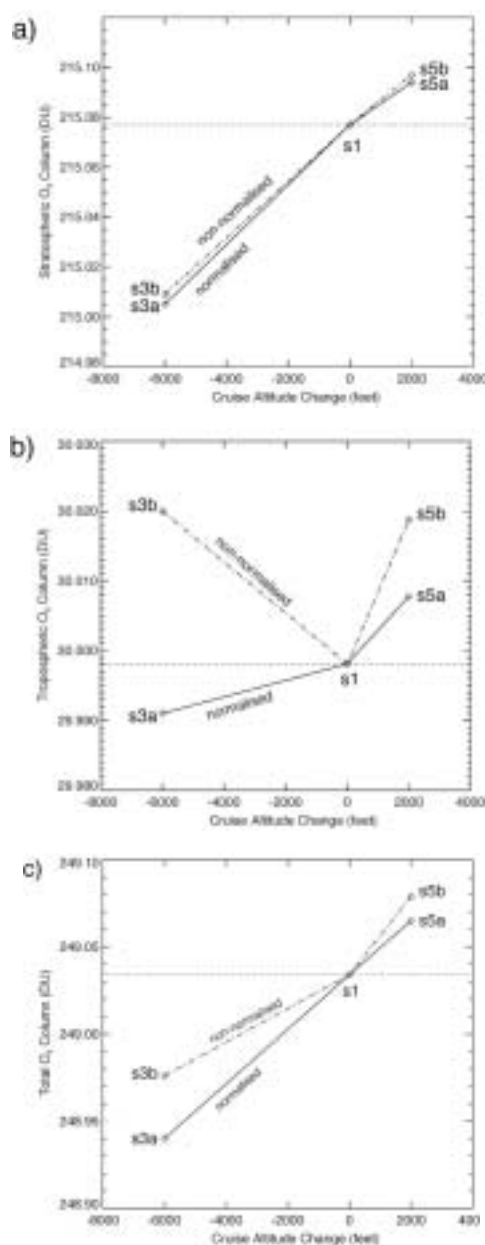

Figure 63. Ozone column (DU) for the northern hemisphere, averaged over the year 1995. The figures show the stratospheric ozone column between the tropopause and 20~hPa (a), the tropospheric ozone column (b), and the total ozone column below 20~hPa (c), for the reference scenario s1 and perturbations to cruise altitudes (s3a, s3b, s5a, s5b).

is further enhanced by nearly 30% relative to normalised emissions.

Summarising, it can be said that changes to cruise altitudes affect the total ozone column (below 20 hPa) in the northern hemisphere. The troposphere and the lower stratosphere respond in significantly ways different to small perturbations in the total amount of emitted NOx. Lower cruise altitudes lead generally to a decrease, and higher cruise altitudes lead generally to an increase in the total ozone column. This work has been performed within the European TRADEOFF project (EVK2-CT-1999-00030) and the authors would like to express their gratitude towards all participants of this project. MOK also acknowledges funding from NERC and the Cambridge European Trust.

Air trajectories in the South-European UTLS: implications for the impact of air traffic emissions

P. Leigh[1], A. R. MacKenzie[1] and S. Borrman[2],
[1]Department of Environmental and Natural Sciences, Lancaster University, Lancaster, UK.
[2]Johannes Gutenberg-Universität, D-55099 Mainz, Germany.

This article presents initial statistical analysis and aircraft data for meridional and vertical transport in the region of the tropopause (UTLS) during the APE-INFRA 2002 and Geophysica-ENVISAT satellite test and validation campaigns from Forli, Italy during July and October 2002. To date, in-situ observations of air traffic corridors have focused on the North America, central Europe and North Atlantic flight sectors (Schlager et al., 1996). The APE-2002 ENVISAT test and validation campaigns provide an ideal opportunity to carry preliminary investigations of the state of the upper troposphere-lower stratosphere (UTLS) in and around southern Europe. Rome is a major international hub for air traffic, placed at the southern edge of the European maximum in the geographical distribution of aviation fuel usage (IPCC, 1999).

Five day back trajectory modelling over 3 isentropic surfaces (340K, 360K, 380K) was carried out for July and October 2002 during the campaigns over the region shown in Figure 64. In addition to the above, a twenty-three-year climatology (July and October, 1980-2002) is also under study, for comparison and to build a climatology of the region. The back trajectories used for this analysis were obtained from the ECMWF analysis of vertical and horizontal wind data using the offline 3-D trajectory code of Methven (1997). The 5 day back trajectory modelling has shown that a number of air parcels have descended from the lower stratosphere into the emissions zone (UTLS); while a smaller number have risen through the mid-tropospheric layer to the upper troposphere. Rapid cross-isentropic transport and/or dispersion is reported in the UTLS in a number of cases (Figure 64B, (bulls-eye effect)). This rapid vertical transport is unsurprising in the troposphere, but the cause of rapid vertical transport in the lower stratosphere is still under investigation. Since, we would expect air from high latitudes to be chemically different to air originating in the sub-tropics in the lower stratosphere, we suggest that the relative abundance of high and low latitude air in the region of air traffic emissions will influence the likely impact of these emissions.

Figure 65 shows a section of the return leg of the NERC sponsored flight of the Geophysica during the ENVISAT validation campaign during October 2002. The figure shows a number of signatures in the data from both the SIOUX (NO and NOy) (Schlager et al. 1996) and COPAS (Non-volatile and total particle counts), (Borrmann *et al.*, 2000) instruments. It is believed a number of these peaks are associated with aged aircraft plumes. Work by Schlager et al. (1996), showed similar perturbations in signals from the SIOUX and CN instruments during flights across the north Atlantic. Other instruments such as H_2O vapour and O_3 on board the Geophysica show similar patterns to Figure 65. The flight path for this particular flight followed the Adriatic coastline of Italy (Figure 64). The flight altitude was 10,000m and this particular route crossed a number of flight paths; this, along with suitable contrail forming meteorological
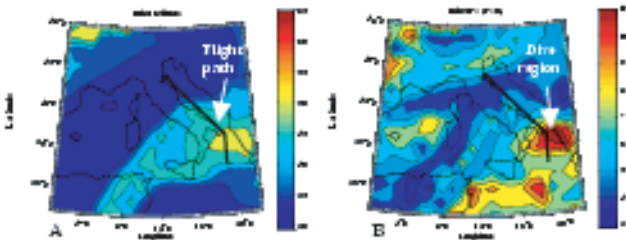

Figure 1: Plots of final latitude against initial latitude (A); initial latitude (B); initial PV for the 380K level, (130mb, 14km) for the NERC flight on 17-10-2002.

Figure 64. Plots of final latitude against initial latitude (A); initial latitude (B); initial PV for the 380K level, (130mb, 14km) for the NERC flight on17-10-2002.

Figure 65. SIOUX and COPAS comparison plot of time series data for Geophysica flight on 17-10-02, Forli.
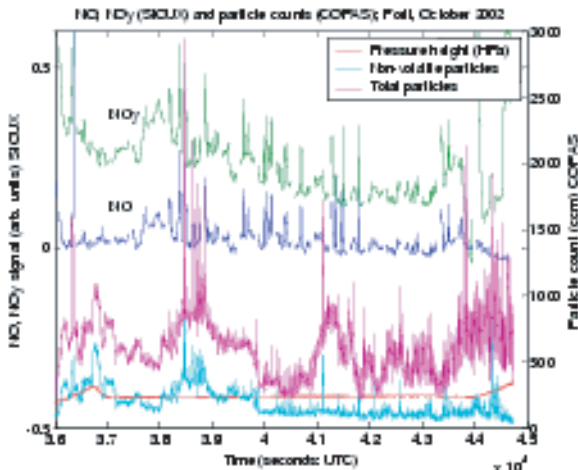

Figure 2: SIOUX and COPAS comparison plot of time series data for Geophysica flight on 17-10-02, Forli.

conditions (i.e. cold and humid air around 10-12km) points to the probability of aircraft condensation trails being present.

Here we have mentioned some of the analytical tools being developed for the analysis of the origin of air masses within a defined grid. Further analysis of the chemistry and particle count of these air masses within the emissions region during the Geophysica and Falcon flights of July and October 2002 is expected to reveal further aged aircraft plumes. This should help us to further understand both the climatic and pollution implications of allowing air traffic levels to increase. Preliminary conclusions include:
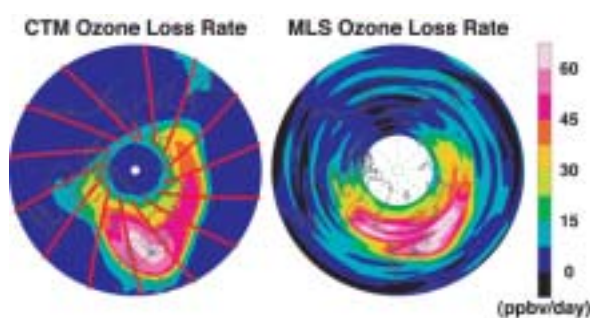
Figure 66. Northern polar stereographic maps of daily ozone loss on February 20. Left: results from the CTM. Right: results recreated from the simulated EOS MLS ClO retrievals (including added noise). Red dots on the CTM map mark the location of the daylight ClO retrievals used for the off-line calculation.
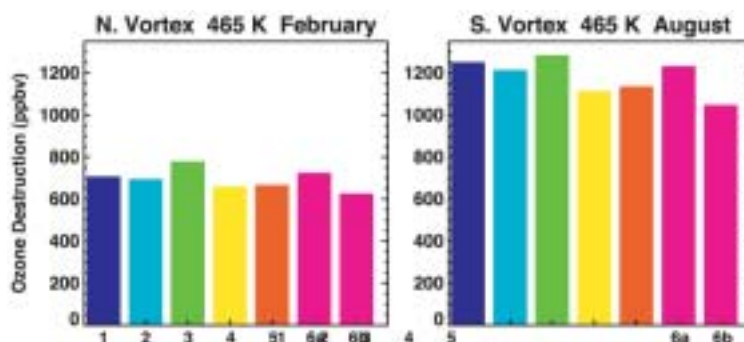

Figure 67. Vortex-averaged ozone destruction at 465 K integrated over a period of one month in the northern (February) and southern (August) polar vortices. See enumerated list in text for an explanation of the individual bars.

i) Trajectory studies of a region of the mid-latitude UTLS show the expected transport of air from widely separated latitudes into the region.

ii) Vertical transport of air entering the region usually approximates a random walk, with a mean 6-hour step size of about 2K at 380K. However, small numbers of outlier vertical-step sizes occur frequently. It remains to be determined whether these outlier steps are physically meaningful.

iii) Pollution from air traffic emitted into the region will encounter air of different chemical characteristics, due to the meridional and vertical transport of air into the region.

References

BADC, EMCWF analysis: http://www.badc.rl.ac.uk.
Borrmann, S., et al., (2000), In-situ aerosol measurements in the northern hemispheric stratosphere of the 1996/7 winter on the Russian M-55 Geophysica high altitude research aircraft, Tellus, 52B, 1088-1103.
IPCC, 1999. Aviation and the Global Atmosphere.
Methven, J., 1997 Offline trajectories: Calculation and accuracy, Tech. Rep. 44, U.K. Univ. Global Atmos. Modelling Programme, Dept. of Met., Univ. of Reading, UK.
Myasishchev Design Bureau, 2002: High Altitude M55 Geophysica Aircraft, Investigators Handbook, Russia.
Schlager et al., 1996, In situ Observations of air traffic emission signatures in the north Atlantic flight corridor. J. of Geophysical Research.

Polar Ozone Loss Inferred from EOS MLS ClO

I. A. MacKenzie (iam@met.ed.ac.uk), Institute of Atmospheric and Environmental Science, The University of Edinburgh

The second Microwave Limb Sounder (MLS) is due for launch in early 2004 aboard the Earth Observing System (EOS) Aura satellite. It will measure a number of trace gases in the upper troposphere, stratosphere, and mesosphere, including stratospheric ClO and ozone. The expected precision of the ClO retrievals is sufficiently high that meaningful individual measurements will be obtained from within the winter polar vortices while the reactive chlorine is enhanced by mixed-phase reactions on polar stratospheric clouds. It is planned to use these ClO measurements to infer the ongoing rate of chemical ozone destruction within the vortices. The approach taken involves using chemical equilibrium arguments to derive the total reactive chlorine ($ClO + 2Cl_2O_2$) at each measurement location and thence, on the assumption that this value remains constant over the course of one day, the diurnal cycle of ClO. This then allows the local daily ozone loss due to the ClO+ClO, ClO+BrO, and ClO+O catalytic cycles to be evaluated (the diurnal cycle of O is inferred from the retrieved ozone, and the BrO cycle from the ClO cycle and an assumption of total inorganic bromine).

Prior to the launch of EOS MLS the method has been tested within the known environment of a chemical transport model (CTM). The SLIMCAT CTM was run for one northern and one southern winter forced by analysed dynamical fields. In running,

detailed information was collected on the full chlorine and ozone chemistry occurring at each model grid point, but additionally the model atmosphere was sampled as it would appear to EOS MLS, outputting the appropriate instantaneous values of ClO. The ozone loss calculation was then performed on these MLS-like data and the results obtained compared with the true chemical ozone behaviour occurring within the model. Figure 66 shows example results for a single day; the magnitude and complex morphology of the polar ozone loss within the model are well reproduced by the simplified calculation, notwithstanding the limited vortex sampling and imperfect precision of the EOS MLS ClO

A number of further validation tests were performed aimed at identifying individual sources of error within the overall procedure. The results of these tests are summarized in Figure 67, with the origin and significance of the individual bars explained below.

1. The net chemical change in ozone occurring within the CTM taking into account all ~50 reactions involving ozone – this represents the "correct" answer for the ozone change. The remaining bars show the results produced as successive simplifications and uncertainties are added to the ozone loss calculation.

2. Consideration of only three cycles: the ozone loss occurring

within the CTM due only to the ClO+ClO, ClO+BrO, and ClO+O catalytic cycles – these three cycles account for virtually all the chemical ozone change within vortex.

3. Simplified chemistry: The ozone loss due to same three cycles as (2) but now calculated by the simple treatment assuming an MLS ClO measurement at every model grid point at the appropriate local time – the simplified chemical treatment leads to a slight overestimate of the true ozone destruction.

4. Sampling density: as (3) but performing the simplified calculation only at the actual measurement locations instead of at the model grid points – the incomplete sampling of vortex by EOS MLS leads to an, on average, underestimate of the total vortex ozone loss.

5. Measurement precision: as (4) but with the expected random

noise added to the simulated ClO retrievals prior to performing the calculation – the measurement precision and sampling density are sufficiently high that the effect of noise is virtually eliminated in the vortex average.

6. Measurement accuracy: as (5) but with biases of plus (a) and minus (b) 5% added to the ClO retrievals – small biases in retrieved ClO translate into similar sized biases in the calculated ozone loss.

Overall, these results show that the various errors and uncertainties inherent in performing the ozone loss calculation on the EOS MLS retrievals are individually small, and that application of the method to real data will produce sensible estimates of the ongoing chemical ozone change.

Comparison of modelled and observed Arctic ozone loss rates

G.A.Millard[1], J.A.Pyle[1], M.P.Chipperfield[2]
[1]Centre for Atmospheric Science, University of Cambridge, U.K. [2]School of the Environment, University of Leeds, U.K.

The Match technique consists of launching two ozonesondes into the same air mass a few days apart. The illustration left shows a typical air mass trajectory being sampled as it passes over ground stations. Forward trajectory clusters are calculated checking for divergence and proximity to the vortex edge. Air parcel descent is included from the MIDRAD radiation scheme calculated by SLIMCAT. Air parcels which do not remain isolated are discarded so that changes in ozone between the ozone sondes along a trajectory can be attributed to ozone loss. The individual ozone change values are then put into groups of ± 7 days at 7 day intervals. A linear regression of ozone change against the time the air parcel is exposed to sunlight provides the ozone loss per sunlit hour. At zero sunlit hours, the ozone change is assumed to be zero due to isolation within the measurements.

The 3D chemical transport model SLIMCAT was initialised each November at T31 (3.75° latitude by 3.75° longitude) over 17 isentropic levels from 340 K to 3000 K, from a low resolution full chemistry integration started in 1991. The model was run using 60 level ECMWF operational analyses for 1999 to 2003, or ECMWF ERA40 analyses for the winters before 1999. SLIMCAT ozone was sampled at the Match ozonesonde sampling points and analysed with the same linear regression technique used by Match. These results are shown in the comparison against Match in Figure 68a to e.

A box model with SLIMCAT chemistry was run along the Match trajectories. Each box model integration was initialised from the 3D chemical field at the Match trajectory location 10 days prior to the first ozonesonde measurement. The chemistry included within the box model was the same scheme found in the 3D SLIMCAT model, although the temperatures, pressure and solar zenith angle used by the box model came from the Match trajectory. The box model ozone was again sampled at the ozonesonde points and was
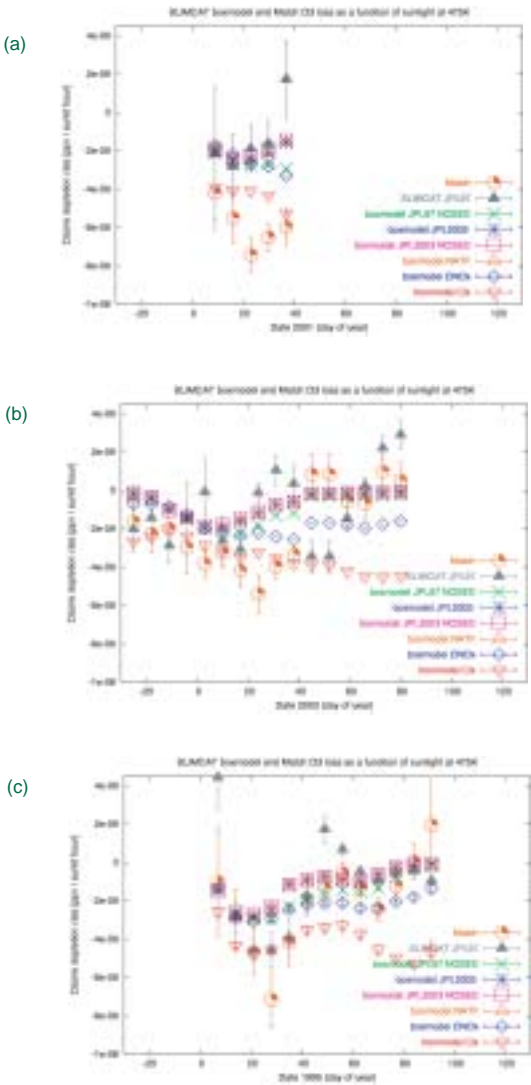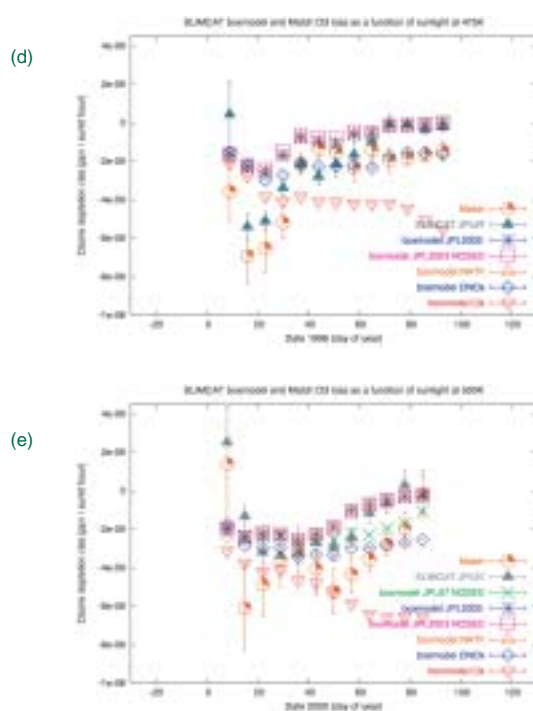
(a)

(b)

(c)

Figure 68. Comparison of Match ozone loss rates to those modelled by SLIMCAT and box model sensitivity tests for the Arctic winters; a) 1994/1995, b)1995/1996, c) 1999/2000, d)2000/2001, and e)2002/2003.

(d)

(e)

particles of diameter >10 μm if temperatures along the trajectory remain less than the NAT threshold for more than 6 days (study NATF). Full denitrification with complete conversion of $ClONO_2$ to ClO_x and NO_x set to zero was investigated in the DNOx study. Finally, the effect of maximum Cl_y activation and activation of $BrONO_2$ on ozone loss rates was also investigated in the Cl_x study, where all box model $ClONO_2$, HCl and $BrONO_2$ was activated to Cl_x and Br_x respectively.

In almost all of the winters it is clear that the 3D SLIMCAT model is better able to reproduce the high ozone changes diagnosed by Match in the early winter. The box model integrations which do not force chlorine and bromine reservoirs to active species fail to reach these high values in 1995, 1996 and 2003. This may indicate that vortex inhomogeneity or mixing is important for the model to successfully compare to the Match results. However, the 3D model still fails to produce the high ozone loss rates seen by Match in January 1995, January 2000, 2001 and late January 2003.

The box model experiment with full activation of the HCl, ClONO2 and BrONO2 reservoirs does better at reaching the high January ozone loss rates in the 1995, 2000, 2001 and 2003 winters without the inclusion of mixing. This sensitivity study does lead to too great an ozone loss rate in the late winter for all the years studied. So perhaps an activation reaction from these reservoirs which depends on PSCs or low sunlight conditions is required, like the heterogeneous reaction of BrONO2 with HCl to form BrCl and HNO3. This reaction is not presently in the heterogeneous chemistry scheme and so further work is required.

It is likely that the high January ozone change rates observed by Match will require both a 3D chemical transport model approach and some additional activation of the chlorine and bromine reservoirs in the early winter cold polar vortex.

then analysed in the same way as Match. The box model benefits from having isolated air parcels throughout the trajectory as the validation checks attempt to ensure with the Match data. The initial box model experiment, JPL 1997, compared the basic box model data against Match ozone loss rates using reaction rate data recommended by DeMore *et al*. 1997. Sensitivity studies were then carried out on updating the reaction rate data to 2003 recommendations with no PSC sedimentation (JPL 2002 NOSED) and allowing PSCs to sediment out of the bottom box boundary (JPL 2003).

The maximum ozone loss rates attainable with different scenarios was also investigated. The sensitivity of ozone loss to NAT rocks was investigated by allowing NAT PSCs to fall as

Reference

DeMore, W. B., S. P. Sander, C. J. Howard, A. R. Ravishankara, D. M. Golden, C. E. Kolb, R. F. Hampson, M. J. Kurylo, and M. J. Molina, Chemical kinetics and photochemical data for use in stratospheric modelling, Eval. 12, JPL, Publ. 97-4, Jet Propul. Lab., Calif., 1997.

High Resolution Tropospheric Chemistry Modelling: First Results

F.M. O'Connor[1], G.D. Carver[1], N.H. Savage[2], and C. Bridgeman[3]
[1]NCAS-ACMSU, Centre for Atmospheric Science, University of Cambridge, UK.
[2]Centre for Atmospheric Science, University of Cambridge, UK. [3]School of the Environment, University of Leeds, UK.

Introduction

Aircraft observations indicate that fine-scale structures are ubiquitous throughout the troposphere. However, the inability of coarse resolution global models to resolve these small-scale features has implications for the accuracy of model-calculated chemical rates due to the sensitivity of chemical evolution to mixing. Furthermore, low resolution model integrations do not make optimum use of the spatial resolution of the global emission inventories which are currently available. As a result, there is a strong need to fully investigate the impact of model resolution on the integrity of model calculations. High resolution integrations using the parallel version of the 3D chemical transport model,

p-TOMCAT, are now possible; some first results will be presented here.

Results

Figure 69 shows modelled ozone on the 383 mbar surface at 12 UT on 19 May 2000 and the black line represents a flight track of the UKMO C-130 aircraft during the UTLS ACTO campaign. Panel a was produced by advecting a low resolution ozone field from p-TOMCAT for one day at low resolution (T42L31: T42 is 2.8^o horizontal resolution) while panel b was produced by advecting the same field but at higher resolution (T106L44: T106 is 1.1^o horizontal resolution). On this timescale, the advection of a long-lived species, such as ozone or carbon monoxide, is valid.

In both cases, a stratospheric intrusion over western Scotland is evident. However, in panel b, the intrusion is narrower in horizontal extent with higher peak ozone concentrations within the intrusion. In addition, the stratospheric intrusion is separated from the neighbouring uplifted boundary layer air on both its western and eastern fringes by sharp gradients in the high resolution simulation.

The validity of these model simulations can be assessed by comparison with the aircraft observations. Figure 70a and b show the measured ozone and carbon monoxide concentrations along the flight track in comparison with the low resolution modelled fields. They indicate that the low resolution simulation cannot accurately capture the spatial variation observed on the C-130 flight track. By contrast, the higher resolution advection shows a marked improvement in terms of capturing the observed concentrations both within the stratospheric intrusion and in the neighbouring air masses (Figure 70c and d). Furthermore, the timescale of the advection can be increased to at least four days without appreciable degradation of the flight track comparison. This is in sharp contrast to a Lagrangian simulation which tends to produce too much detail at small scales.

Conclusions

Preliminary integrations of the parallel 3D chemical transport model, *p*-TOMCAT, at high resolution indicate that the model is capable of resolving the fine-scale structures associated with stratosphere-troposphere exchange and frontal uplift from the boundary layer. In addition, once the model is fully operational at high resolution, it will be capable of a more accurate estimate of the stratospheric influence on the tropospheric ozone budget, which is currently highly uncertain.
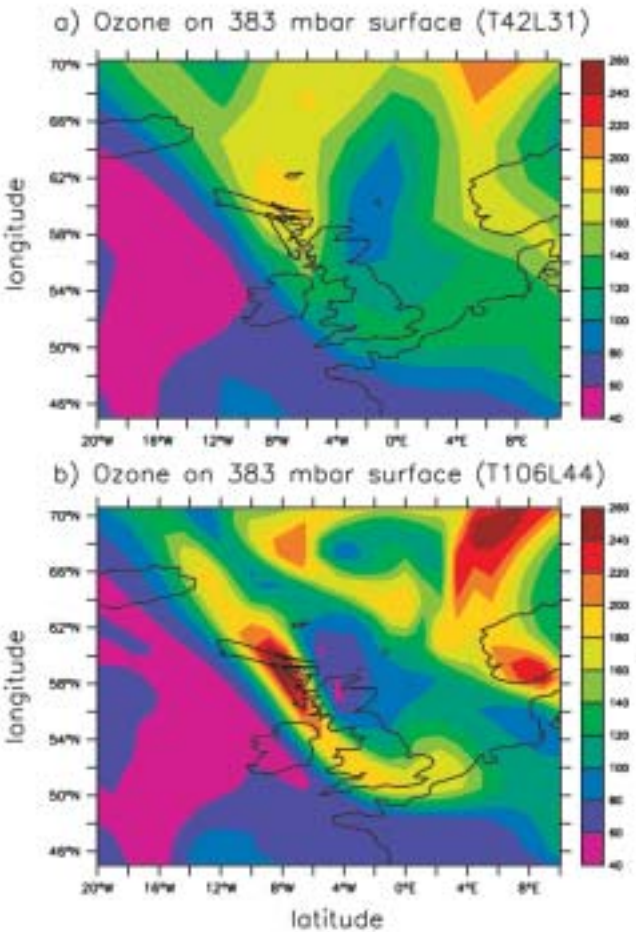

Figure 69. Ozone on the 383 mbar surface at 12 UT on 19 May 2000 simulated at a) low resolution (T42L31) and b) high resolution (T106L44). The black line superimposed on the plots indicates the flight track of the UKMO C-130 aircraft relative to the modelled ozone fields.
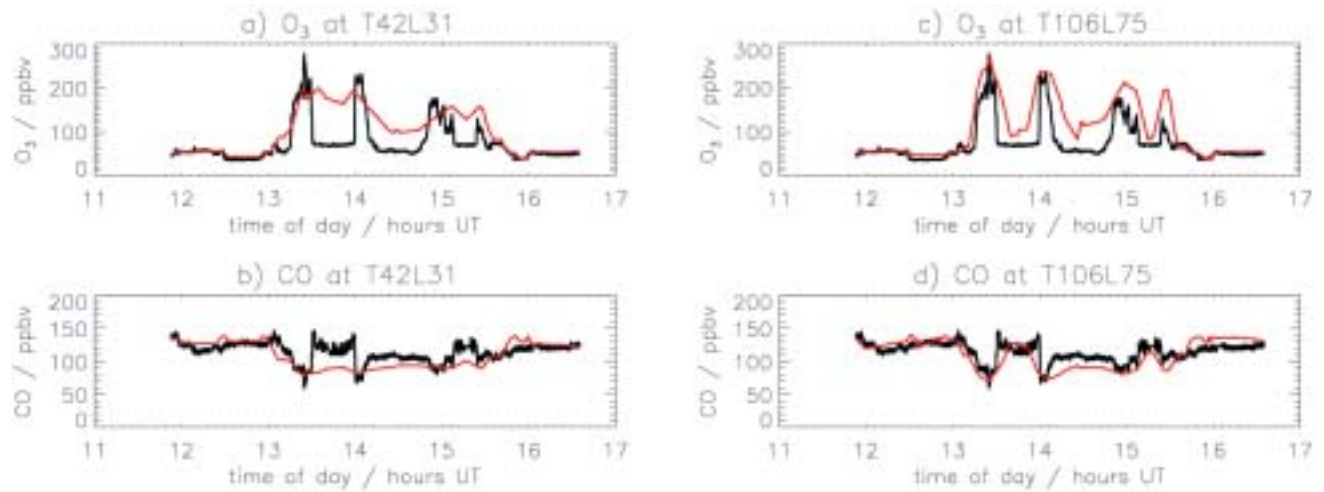

Figure 70. Flight track comparisons between modelled and measured ozone and carbon monoxide at low resolution in a) and b) and at high resolution in c) and d). Measured concentrations are shown in black and modelled concentrations are shown in red.
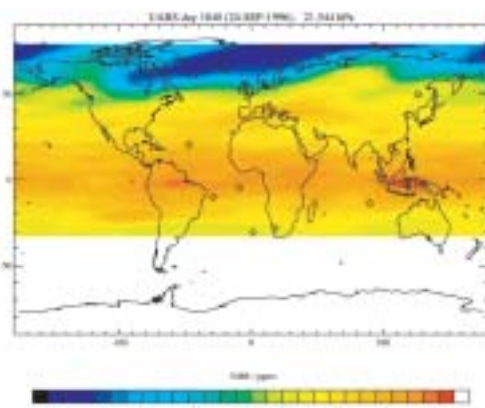
Figure 71. MLS ozone field at 21 hPa on an arbitrary day in September 1996, with diamonds marking the locations of 10 observed profiles to be assimilated.
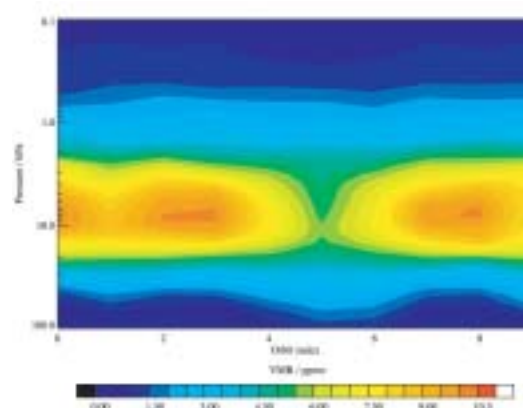

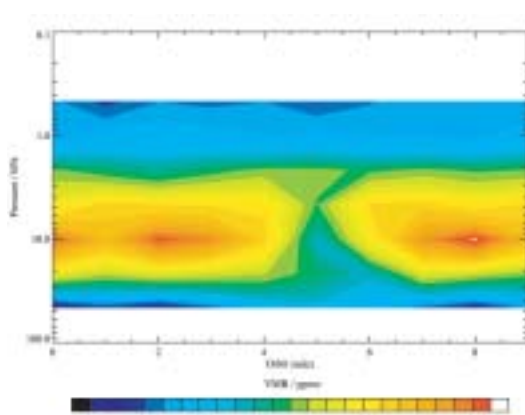Figure 73. Cross-section of the UM ozone field along the MLS orbit-track.

Figure 72. Cross-section of the MLS ozone as a function of pressure along the orbit-track of the MLS instrument.
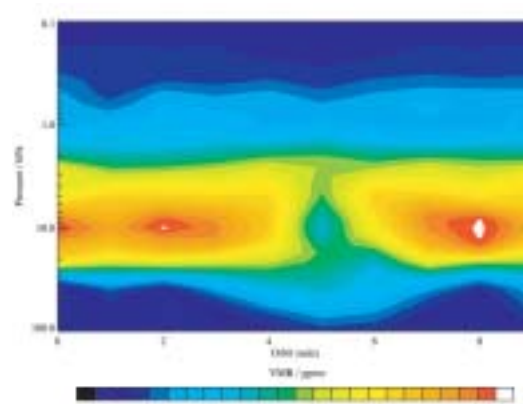

Figure 74. Combination of the observed field with the modelled field performed by the Kalman filter and shows how the two fields are adjusted relative to each other.

Chemical Data Assimilation in the Unified Model

Mark Parrington (Mark.Parrington@atm.ch.cam.ac.uk), Peter Braesicke, John Pyle and Hamse Mussa,
Centre for Atmospheric Science, University of Cambridge

Introduction

Chemical data assimilation provides an optimal tool for exploiting the wealth of data available from satellite instruments such as those on, for example, the UARS and Envisat-1 platforms. Selected data will be assimilated into a version of the Unified Model running a comprehensive stratospheric chemistry scheme to assess the potential of improving the model forecast skill through the assimilation of, e.g., ozone and to furthering our understanding of chemistry-climate interactions and the distribution of trace gases in the atmosphere.

Model description

For chemical data assimilation experiments at the University of Cambridge, a version of the Unified Model (UM) with comprehensive stratospheric chemistry is to be used. The model grid has a resolution of 3.75 degrees longitude by 2.5 degrees latitude, with 58 levels in the vertical (1000 to 0.1 hPa). Chemistry in the stratosphere is provided by the ASAD chemical integrator

(Carver *et al*., 1997). The ASAD chemistry setup includes 22 tracers (37 species) and 4 families (Ox, NOx, ClOx and BrOx). The time step of the model is 15 minutes. At each time step, the model output is an estimate of trace gas concentration at each model grid point, based on the advection of the trace gas concentrations estimated at the previous model time step. The equation

$$x^f(t_i) = M_{i-1}[x^a(t_{i-1})] \qquad (1)$$

shows that the forecast output is some function of the analysis at the previous time step (the operator M represents the UM).

Data Assimilation

Data assimilation provides the optimal approach to combining observations with theory. The data assimilation scheme to be used for assimilation experiments is the suboptimal Kalman filter developed by Khattatov *et al.* (2000). The advantage of this approach to data assimilation compared to other methods (e.g. 3D- or 4D-Var) is in the propagation of the background error

covariance. Evaluation of the full Kalman filter approach to data assimilation is computationally expensive, and simplifications are required in order to make an analysis feasible. For the suboptimal Kalman filter, the off-diagonal elements of the forecast error covariance are parameterised. The equation

$$y_i^o = H_i(x^f(t_i)) + \varepsilon_i^o$$

shows the relationship of trace gas observations to the forecast values, via the observation operator H. At each model time step, the analysis values are computed using the equation

$$x^a(t_i) = x^f(t_i) + K_i(y_i^o - H_i[x^f(t_i)])$$

where K is the Kalman gain. The Kalman gain weights the difference between the observed and forecast values by combining the forecast (P) and observation (R) error covariances, and is given by

$$K_i = P^f(t_i)H_i^T[H_iP^f(t_i)H^T + R_i]^{-1}$$

Finally, the analysis error covariance is calculated with

$$P^a(t_i) = (I - K_iH_i)P^f(t_i)$$

The analysis values are incorporated into the model output to estimate trace gas concentration at the subsequent model time step via equation 1.

Off-line Assimilation of Ozone

To illustrate how data assimilation may be used to update chemistry at a particular instance, ozone data from the Microwave Limb Sounder (MLS) instrument on UARS have been assimilated into a 3-D UM ozone field in an off-line (i.e. not incorporated in the UM) example. Figure 71 shows the MLS ozone field at 21 hPa on an arbitrary day in September 1996, with diamonds marking the locations of 10 observed profiles to be assimilated. Figure 72 shows the cross-section of the MLS ozone as a function of pressure along the orbit-track of the MLS instrument. Figure 73 shows the cross-section of the UM ozone field along the MLS orbit-track. Figure 74 shows the combination of the observed field with the modelled field performed by the Kalman filter and shows how the two fields are adjusted relative to each other.

Summary

The suboptimal Kalman filter code produces an analysis field which is a combination of the observed and modelled fields weighted by their error covariances. The computed analysis field is sensitive to the error covariance of the forecast, the forecast error covariance in the figures shown is 100% and in reality would be considerably smaller. The Kalman filter codes is currently being integrated into the UM with experiments proposed to investigate the benefits of data assimilation to chemical modelling and understanding chemistry-climate interactions. Data for assimilation experiments are and will be available from a variety of sources in the coming years (UARS MLS, Envisat MIPAS, EOS Aura etc.). Assimilation experiments will be performed for approximately 10 day integrations of long-lived tracers (ozone and water vapour) with and without feedback into the radiation scheme.

References

Braesicke, P. and Pyle, J. A., Changing ozone and changing circulation in northern mid-latitudes: Possible feedbacks?, Geophysical Research Letters 30 (2): 1059, doi:10.129/2002GL015973, 2003

Carver, G. D., Brown, P. D. and Wild, O., The ASAD atmospheric chemistry integration package and chemical reaction database, Computer Physics Communications 105: 197-215, 1997

Khattatov, B. V. et al., Assimilation of satellite observations of long-lived chemical species in global chemistry transport models, Journal of Geophysical Research 105 (D23): 29,135-29,155, 2000

The freeze-drying of ensembles of air parcels in determining stratospheric water

Chuansen Ren (c.ren@lancaster.ac.uk), and A. Robert MacKenzie, Environmental Science Department, Lancaster University

Dehydration processes occurring near the tropical tropopause are known to be crucial in determining the global distribution of lower stratospheric water vapour. Dehydration there must be through the sedimentation of condensed water – i.e. ice crystals in cloud events – thus controlling the dryness of the stratosphere, but substantial uncertainty remains over the mechanisms by which dehydration takes place. In this study, we combine microphysical modelling with trajectories to assess the dehydration more directly.

A Lagrangian, partial-column, microphysical model has been established to simulate the nucleation, growth, and sedimentation of ice crystals in an air parcel (Ren and MacKenzie, 2003). The model agrees well with existing box models in test scenarios without sedimentation, and, with sedimentation, shows some features of APE-THESEO observations, such as the number and size of ice crystals in tropopause cirrus clouds. Homogeneous nucleation appears to provide a sufficient number of ice particles to match cirrus cloud observations, even though supersaturations of about 0.6 with respect to ice are required (Koop *et al.*, 2000). A model run, with imposed notional gravity waves, shows that supersaturation produced by the wave dwarfs the supersaturation hurdle for homogeneous nucleation, and consequently influences later cloud events.

To increase the number of cases it is possible to study, a simplified parameterisation has been developed. The parameterisation is based on the e-folding time for a cloud to relax water vapour towards saturated conditions assuming a uniform size of ice crystals. All microphysical variables are determined by the thermodynamic history of an air parcel, so the parameterisation maintains more of the essential cloud physics, without significantly increasing calculation-time, than current parameterisations, e.g., the Gettelman *et al.* (2002) parameterisation, which prescribes three time-scales as known parameters and fixes the supersaturation hurdle at 10%. Our parameterisation also has a dehydration behaviour similar to the detailed model. Using this parameterisation, ensemble runs of large (i.e. space-filling) trajectory sets are carried out to estimate the influence of large-scale condensation on the transport and
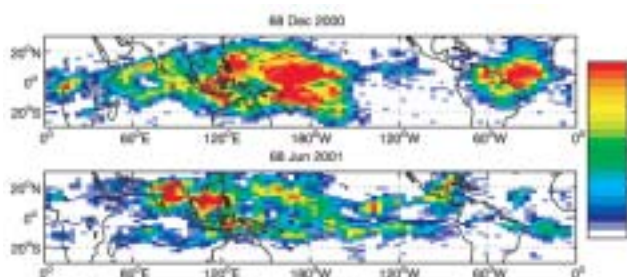
Figure 75. The frequencies of optically thin clouds in the TTL. For each case, 12 sets of space-filling backward trajectories, upon which the Ci-dehydration parameterisation was applied, were generated at 6hr-intervals. The frequency at a point was calculated by counting how many times there was ice water out of the 12 snapshots. The red and yellow in the figure represent the regions where cirrus clouds are most likely to appear, while the white means no appearance of clouds on any of the three levels of 360, 370, and 380 Kelvin potential temperatures. Please note, the blank areas figure in 2 mean that no reliable data are available.
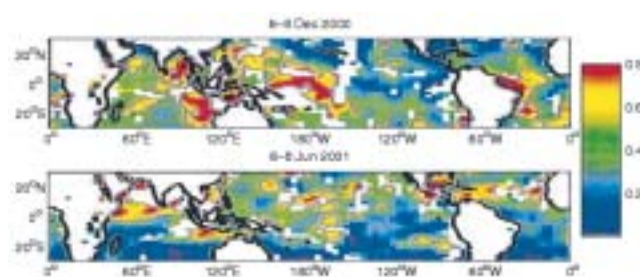
Figure 76. Fraction of observations (colour scale) between latitudes 30N and 30S and longitudes 0 to 360E during the (a) 6¨C8 Dec. 2000 and (b) 6¨C8 Jun. 2001 time periods whose optical depth \tau exceeded 0.02. White indicates less than 1000 measurements in the box. The fields have been smoothed to emphasize the large-scale structure. Gray contours indicate the 30% frequency contour for \tau > 0.03.(Reproduction of figure 2 of Dessler and Yang (2003), by the courtesy of the authors and AMS)

distribution of water vapour in the tropical tropopause layer (TTL). A boreal winter case and a summer case are discussed here. Figure 75 shows the presence frequencies of optically thin clouds in the TTL (please see the caption for further details). These results compare well with MODIS satellite results retrieved by Dessler and Yang (2003) (reproduced by Figure 76). The frequencies shown in Figure 75 generally match the fraction of Figure 76 in positions. Since both studies are "first attempts", the results support each other. In the winter case (Figure 75a and Figure 76a), the stratospheric 'fountain' region shows high occurrences of cirrus clouds. In contrast, in the summer case (Figure 75b and Figure 76b), the high-frequency region is less well defined. More

water is allowed to enter the stratosphere in summer than in winter, but dehydration has removed more water from the TTL.

References

Dessler, and Yang, 2003: The distribution of tropical thin cirrus clouds inferred from Terra MODIS data. J. Climate, 16, 1241-1247.
Gettelman et al., 2002: Transport of water vapour in the tropical tropopause layer. Geophys. Res. Lett., 29, 10.1029/2001GL013818.
Koop et al., 2000: Water activity as the determinant for homogeneous ice nucleation in aqueous solutions. Nature, 406, 611-614.
Ren, and MacKenzie, 2003: Modelling cirrus and dehydration in the tropical tropopause layer: a Lagrangian, partial-column, approach. Submitted to J. Atmos. Sci.

A Modelling Study of Transport into and out of the Tropical Lower Stratosphere

D.E.M. Ross (debbie.ross@atm.ch.cam.ac.uk), A.D. Robinson, J.A. Pyle, Centre for Atmospheric Science, Chemistry Dept., Univ. of Cambridge

Introduction

The Subtropical Barrier hinders isentropic transport between the tropics and midlatitudes. This barrier is more permeable at lower altitudes. Transport from the tropics to the midlatitude lower stratosphere is an important issue for midlatitude ozone decline. Transport in the reverse direction may increase the pollution effects of aviation, as chemical species will be incorporated into the general circulation and transported to regions where their damaging effects are enhanced. More measurements will improve understanding of the transport rates, and lead to more accurate meteorological analyses.

The HIBISCUS Campaign

In preparation for the HIBISCUS Campaign of 2004, several stratospheric balloon flights were launched from Bauru, Brazil (22°S 48°W) in February 2003. Two GC based instruments were deployed on these flights. DIRAC and DESCARTES measurements from a flight on 19th February 2003 are shown in Figure 77. In support of these measurements, a 3D chemical transport model (SLIMCAT) has been used to investigate transport along isentropes in the tropical lower stratosphere.

SLIMCAT was initialised on 7th January 2003 and run for 60 days with a horizontal resolution of 3.75^o x 3.75^o. There are 18 vertical levels from 335-2700 K. The model is forced using ECMWF winds and temperatures, and tracers are advected horizontally using the 2nd order moments scheme of Prather. Each box has a value of 1 inside and 0 everywhere else. The mixing ratio
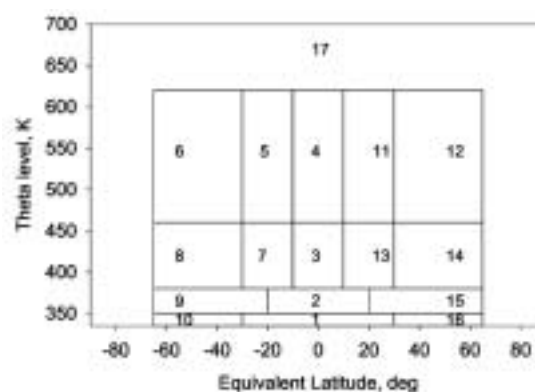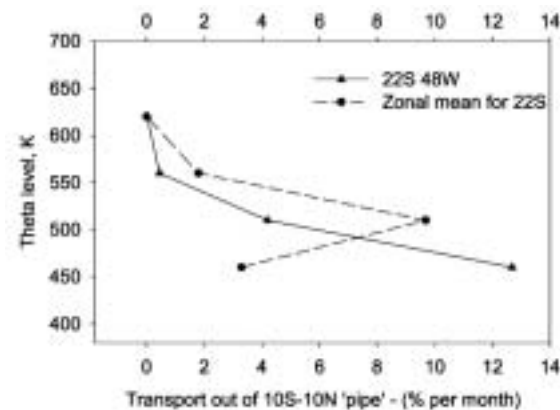
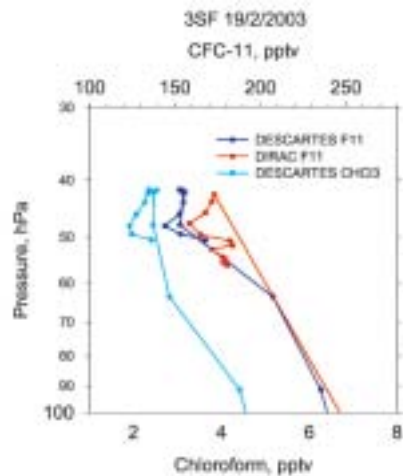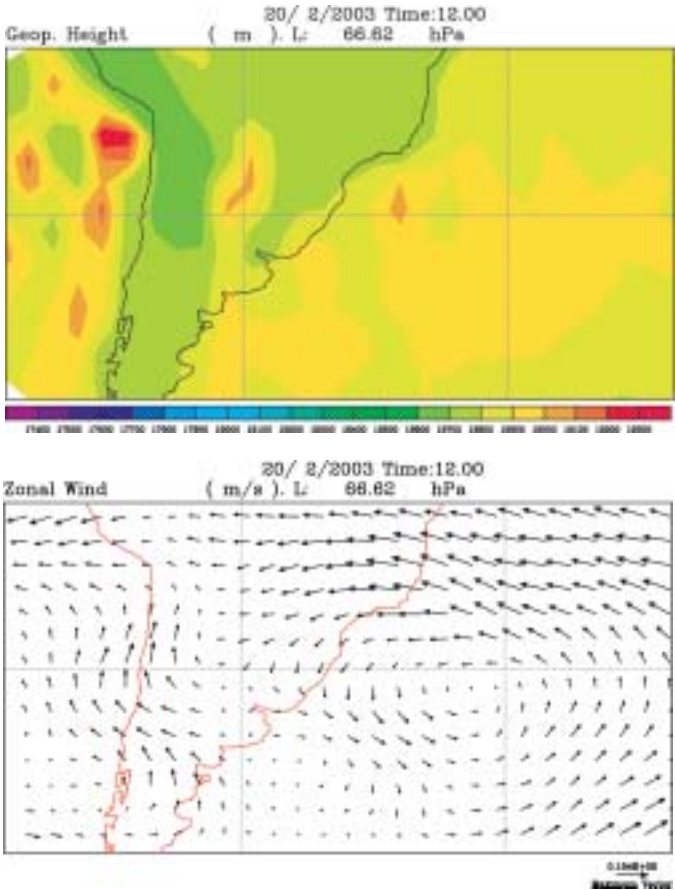

Figure 77.

Figure 78.

Figure 80.

Figure 79. (top) Geopotential height at 460K. (bottom) zonal wind at 460K

of a box out with the box boundary is then the percentage of air transported from that box. The boxes are advected for 60 days, and a time series of tracer evolution obtained on each vertical level above the Bauru site. A best-fit straight line is applied to the tracer evolution. The gradient is then used to evaluate the rate of transport of that tracer (% per month). This is also done for the zonal mean tracer evolution at 22°S.

Transport from the 'deep tropics' to 22°S

There is more transport out of the 10°S-10°N region to 22°S for the site over Bauru than for the zonal mean and the 460 K isentrope (Figure 78). Upper tropospheric disturbances and increased wave activity lead to meridionial flow and transport out of the tropics (Dunkerton 1995, Chen 1994)

Maps of geopotential height (Figure 79a) and zonal wind (Figure 79b) at 460 K, taken from ECMWF analyses, show disturbances extending from the upper troposphere. These are probably associated with the South American monsoon. The maps are taken from ECMWF on 20th February 2003. We propose this circulation is the cause of increased transport out of the deep tropics to the Bauru site.

The data indicate an equatorial feature was indeed sampled in the lower stratosphere over Bauru (sharp minimum at ~50 hPa in Figure 80).

References

Dunkerton, T., J.Geophys.Res., 100, 16675, (1995).
Chen, P., J.Atmos. Sci., 51, 3006, (1994).

Quantifying Maximum Controllable Contributions to Global Ozone Budgets

N.H.Savage and J.A. Pyle Centre for Atmospheric Science, University of Cambridge

Tropospheric ozone is a greenhouse gas and also an air pollutant which frequently exceeds air pollution criteria across the European Union. It also plays a central role in controlling the oxidising capacity of the atmosphere. However it is also a major challenge to try and attribute ozone to any given source region or process because it is a secondary pollutant and is chemically produced from other gases. In addition a significant source of tropospheric

ozone is the downward transport of ozone from the stratosphere or ozone layer.

Using the chemistry-transport model TOMCAT a study has been performed to quantify the maximum controllable contribution of emissions on the global atmosphere from 3 parts of the world. TOMCAT is a global CTM and in this experiment was driven with 1997 ECMWF winds at a resolution of 2.8 x 2.8 degrees with 31

levels from the ground to 10 hPa. The emissions inventory used was from the FP5 project POET. Anthropogenic emissions were based on EDGAR 3.2 scaled to 1997 emissions.

In the experiment performed here we simulated the effect of reducing all anthropogenic emissions to zero in 3 regions: Western Europe, North America, Asia. It should be noted that this is not same as the impact of those pollutants on the ozone budget. This is due to the non-linearity of ozone production.

Figure 81 shows the results of the turning off of Western European emissions for June. The impact on ozone of European emissions is greatest at high latitudes (2-5ppb), with an effect of 1-2 ppb over most of the Northern Hemisphere. North American emissions have an impact of 2-5 ppb in Western Europe. Asian emissions have an impact of 2-5 ppb on ozone over West Coast US and Canada.
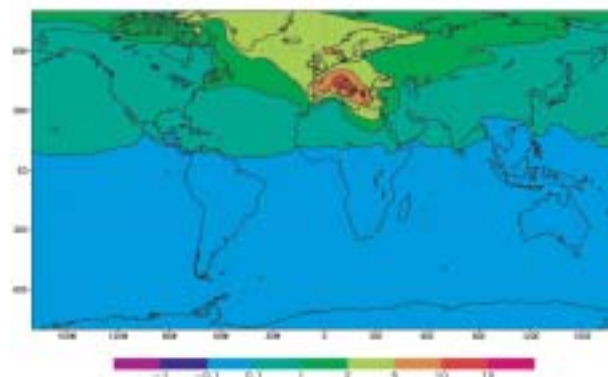
Figure 81. The maximum anthropogenic contribution of European emissions to the global surface ozone concentration. European emissions have their greatest impact over Europe and high latitudes to the north of Europe.

Trends and variability in the future tropospheric ozone budget

David Stevenson[1] (davids@met.ed.ac.uk), Ruth Doherty[1] and Colin Johnson[2]
[1]Institute of Atmospheric and Environmental Science, The University of Edinburgh, [2]Hadley Centre for Climate Prediction and Research

Future projections of tropospheric ozone (O_{3T}) rely on models of atmospheric chemistry and climate, driven by emissions scenarios. The IPCC 2001 assessment included a model inter-comparison for 2000 and 2100, using time-slice experiments following the SRES A2 scenario (see Gauss *et al*., 2003). This study did not consider any effects of climate change on chemistry. Johnson *et al*. (2001) presented results from a coupled transient climate-chemistry integration of HadCM3-STOCHEM from 1990 to 2100, also following the A2 scenario, in both climate and chemistry sub-models. By comparison with a control run with an unforced climate, a significant negative feedback of climate on O_{3T} was identified, mainly driven by increased ozone destruction through

the O^1D+H_2O reaction in the warmer, more humid, climate change scenario. Further results from this climate change simulation are presented here, to analyse trends and variability in components of the ozone budget.

Figure 82 shows the annually smoothed global O_{3T} budget from 1990 to 2100. The O_{3T} budget consists of stratospheric input (SI), in-situ net chemical production (NCP), surface dry deposition (DD), and a residual term, representing the change in tropospheric burden. The troposphere is taken to be everywhere modelled ozone concentrations (monthly averages over the whole run) are less than 150 ppbv. Modelled O_{3T} is used to calculate the net change in burden; DD and NCP fluxes are taken directly from the model. The
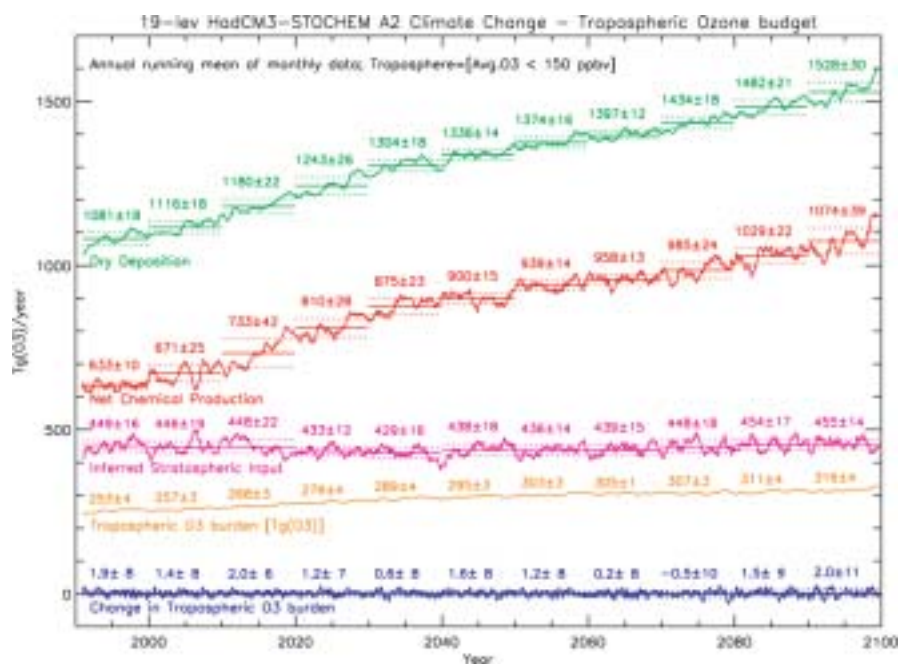

Figure 82. The global O_{3T} budget (fluxes in Tg (O_3) yr^{-1}) from 1990 to 2100, for the SRES A2 scenario, in both the chemistry and climate sub-models. Thick lines are running annual means of monthly data. Decadal means (thin lines) and standard deviations (dashed lines) are also plotted and given as numbers. The O_{3T} burden (Tg(O_3)) is also shown. The chemistry model extends into the lower stratosphere; the stratosphere has been masked off in these results using a threshold of $O_3 > 150$ ppbv, using a monthly O_3 field calculated from the mean of all months in the experiment.

SI term is calculated as the residual of the other budget terms. Note that NCP (+630 Tg (O_3) yr^{-1} in the 1990s) is the residual of large production and destruction terms, each around 4000 Tg (O_3) yr^{-1}. Also note that the projected growth in the O_{3T} burden (from 253 Tg in the 1990s to 316 Tg in the 2090s) averages less than 1 Tg (O_3) yr^{-1}, so reflects a very small (but significant) imbalance in the overall budget.

The most obvious feature of Figure 82 is the growth in NCP and DD: both show increases of ~450 Tg (O_3) yr^{-1} between the 1990s and 2090s. This growth is driven by increases in ozone precursor emissions in the A2 scenario. The SI term remains approximately constant, at ~440 Tg (O_3) yr^{-1}. The constancy of SI is at odds with subsequent experiments using a version of HadAM4 with higher vertical resolution (Collins *et al.*, 2003), where climate change significantly increased SI. Other studies with the 19-level HadAM3 model using an Eulerian chemistry formulation (Zeng and Pyle, 2003) also indicate increased SI with climate change. A UGAMP inter-comparison of this model with HadAM3-STOCHEM (which uses a Lagrangian approach) is underway, in an attempt to understand these and other differences.

The variability of the change in O_{3T} burden is less than the variability in all of the other budget terms, indicating that there is significant buffering, or compensation, between terms. We examined the relationship in the variability amongst different fluxes by correlating de-trended time-series. The variability in NCP and SI is inversely related (r=-0.67), whilst NCP and DD are directly related (r=0.63). These correlations make physical sense: an increase in stratospheric input leads to more O_3 destruction; higher O_3 production leads to more deposition. We also find a

relationship between O_3 burden and the Niño-3 index (r=-0.49); see the accompanying article (Doherty and Stevenson, 2003) for further discussion. Sources of variability are probably underestimated in these runs: e.g., natural emissions from lightning and vegetation remain fixed. A new model version (Sanderson *et al.*, 2003) now generates natural emissions linked to climate model variables, such as convective cloud height and photosynthetically available radiation, which will introduce additional ozone variability.

References

Collins, W. J., R. G. Derwent, B. Garnier, C. E. Johnson, M. G. Sanderson and D. S. Stevenson, The effect of stratosphere-troposphere exchange on the future tropospheric ozone trend, J. Geophys. Res., 108 (D12), doi: 10.1029/2002JD002617, 2003.

Doherty, R., and D. Stevenson, ENSO direct and indirect effects on tropospheric ozone over the Indonesian region, UGAMP Newsletter (this issue), 2003.

Gauss, M., et al., Radiative forcing in the 21st century due to ozone changes in the troposphere and the lower stratosphere, J. Geophys. Res., 108 (D9), doi: 10.1029/2002JD002624, 2003.

Johnson, C. E., D. S. Stevenson, W. J. Collins, and R. G. Derwent, Role of climate feedback on methane and ozone studied with a coupled Ocean-Atmosphere-Chemistry model, Geophys. Res. Lett. 28, 1723-1726, 2001.

Sanderson, M. G., C. D. Jones, W. J. Collins, C. E. Johnson, and R. G. Derwent, Effect of climate change on isoprene emissions and surface ozone levels, Geophys. Res. Lett. 30(18), 1936, doi:10.1029/2003GL017642, 2003.

Zeng G., and J. A. Pyle, Changes in tropospheric ozone between 2000 and 2100 modelled in a chemistry-climate model, Geophys. Res. Lett. 30(7), 1392, doi:10.1029/2002GL016708, 2003.

Global Modelling of Methyl Bromide

N.J. Warwick[1], D.E. Shallcross[2] & J.A. Pyle[1]
[1] Centre for Atmospheric Science, University of Cambridge, [2] School of Chemistry, University of Bristol

Methyl bromide is the most abundant species containing bromine in the free troposphere and is one of the largest carriers of bromine atoms to the lower stratosphere (Schauffler *et al.*, 1993; Kourtidis *et al.*, 1998; Cicerone *et al.*, 1988; Dvortsov *et al.*, 1999). The catalytic destruction of stratospheric ozone which ensues has led to an international agreement under the Montreal Protocol of 1995 to reduce anthropogenic methyl bromide emissions by restricting future sales and consumption of CH_3Br. To successfully verify reductions in anthropogenic emissions, the surface fluxes and environmental interactions of methyl bromide need to be fully understood. At present, mid-range estimates of known sinks exceed known sources by approximately 45 Gg/yr (WMO, 2002). This difference in source and sink magnitudes is inconsistent with the observed small growth rates of atmospheric CH_3Br. An additional terrestrial source is therefore required to bring simulated values in line with atmospheric measurements. A modelling study by Lee-Taylor *et al.* (1998) derived an apparent terrestrial missing source of 89-104 Gg/yr by comparing simulated CH_3Br distributions to atmospheric observations. It was estimated that 50-70% of this 'missing' source is located in the Southern Hemisphere and is likely biased towards tropical regions.

In this study, the 'missing' source identified by Lee-Taylor *et al.* (1998) was replaced by a double strength biomass burning source and a combination of vegetation sources which were grouped into six model scenarios (see Table). These prescribed emission

Table 2: The six CH_3Br prescribed emission scenarios. Each emission scenario contains anthropogenic emissions from cars and fumigation, plus different combinations of vegetation and biomass burning emissions with a prescribed seasonal variation.

Scenario	Description	Global Emissions (Gg/yr)
LBNV	Low Biomass Burning, No Vegetation	66
LBGV	Low Biomass Burning, Global Vegetation	141
HBNV	High Biomass Burning, No Vegetation	86
HBV40	High Biomass Burning, Vegetation 40°N-40°S	131
HBV60	High Biomass Burning, 60°N-60°S	150
HBGV	High Biomass burning, Global Vegetation	161

scenarios were incorporated into a version of the global chemistry-transport model (TOMCAT) including a simple chemistry scheme with methyl bromide tracers (coloured by source) and 10-day mean prescribed OH fields taken from the full chemistry version of TOMCAT. The sinks of atmospheric methyl bromide in the model include reaction with OH, photolysis (values taken from Cambridge 2D model), and loss to the ocean and soils (prescribed deposition velocities). The lifetime of atmospheric CH_3Br in the model with respect to each of these processes is described in the Table. The model was run for a spin-up period of 7 years using perpetual ECMWF meteorological analyses for the year 1998. The results presented here are the last year of this model integration.

Both the inclusion of a vegetation source, and increasing emissions from biomass burning substantially improved the agreement between model simulations and measurements relative to the control scenario (see Figures). A comparison of observed and modelled methyl bromide seasonal cycles in high northern latitudes indicated that vegetation in this region is unlikely to be a large CH_3Br source. Results from this study suggest that the 'missing' source is most likely to consist of increased emissions from biomass burning and a strong vegetation source in the tropics and mid-latitudes (i.e. as scenario HBV40, but with increased vegetation emissions in northern low latitudes). The existence of a large CH_3Br source from vegetation and various terrestrial ecosystems is supported by a variety of measurements which suggest peatlands, wetlands, salt marshes, shrublands, forests, and some cultivated crops are all sources of CH_3Br) (Gan *et al*., 1998; Varner *et al*., 1999; Lee-Taylor and Holland, 2000; Rhew *et al*., 2000, 2001; Dimmer *et al*., 2001; Youkouchi *et al*., 2002). Observations of Youkouchi *et al*. (2002) suggest that the vegetation source may be concentrated in the tropics. However, measurements that are currently available are insufficient to distinguish between the relative likelihoods of the model scenarios containing additional tropical vegetation sources and increased biomass burning emissions. Model simulations indicate that future CH_3Br measurements performed in continental mid-to-high latitudes, central-southern Africa and South America would be of particular benefit in constraining the sources of methyl bromide
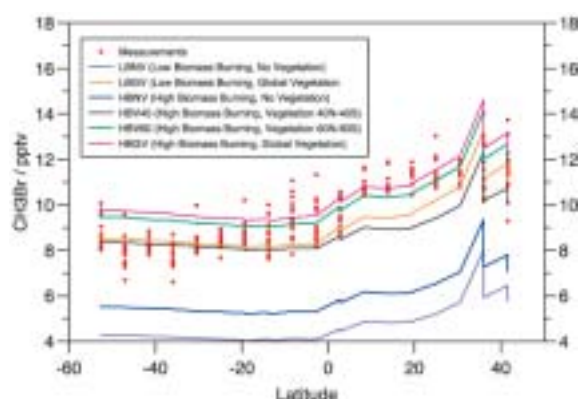

Figure 83. Modelled CH_3Br concentrations compared with the observed latitudinal methyl bromide distribution obtained from the BLAST 94 cruise data (Lobert *et al*., 1995).
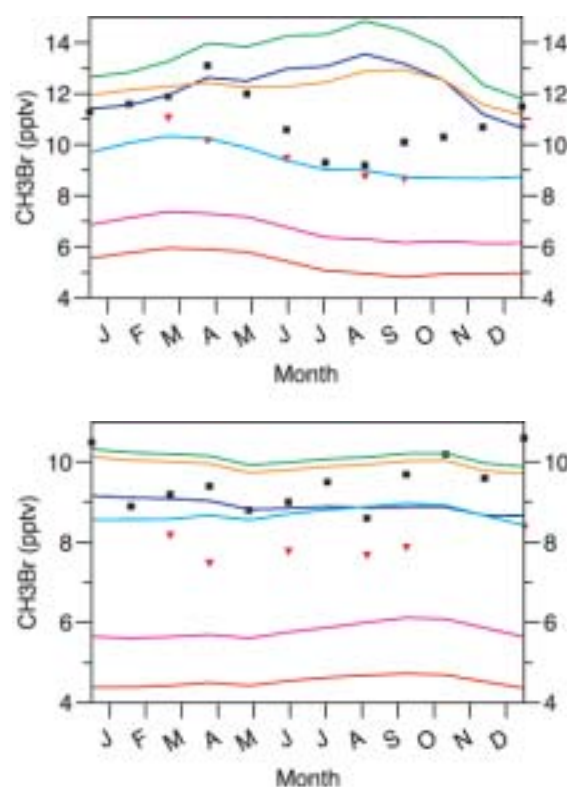

Figure 84. A comparison of modelled monthly means with CH_3Br measurement data from Cicerone *et al*. (1988) and Wingenter *et al*. (1998). (top) Point Barrow (157˚W, 71˚N) (bottom) New Zealand Coast (37˚S to 47˚S)

Radiative Forcing by Sulphur Hexafluoride

Wenyi Zhong and Joanna Haigh, Imperial College London, UK

SF_6 is widely used in electrical transmission and distribution, and many other industries. It has a long lifetime (3200 years) and could significantly contribute to the enhanced greenhouse effect owing to its strong absorption in the mid-infrared region. This has been recognized by the Kyoto Protocol in which SF_6 (along with CO_2, CH_4, N_2O, HFCs, PFCs) has been targeted for a reduction in emissions. Recent measurements have provided data on SF_6 absorption bands over a much wider spectral region than that (925-955cm^{-1}) represented in the standard HITRAN-2K spectral line database. In this note we present preliminary estimates of the

potential additional contribution of the newly-measured spectral bands in the 590-640cm^{-1} and 900-1800cm^{-1} regions to SF_6 radiative forcing.

The spectral measurements used in this work include SF6 cross-sections in the HITRAN-2K database (Rothman *et al*., 2003) and new measurements of SF_6 transmission spectra recorded by Lacome and Boudon (personal communications, 2003). The former covers nine temperatures from 180K-295K but only for ν_3 band centre (925-955cm^{-1}) with spectral resolution of 0.1-0.3 cm^{-1}; the latter covers a wider spectral range (590-640cm^{-1} and
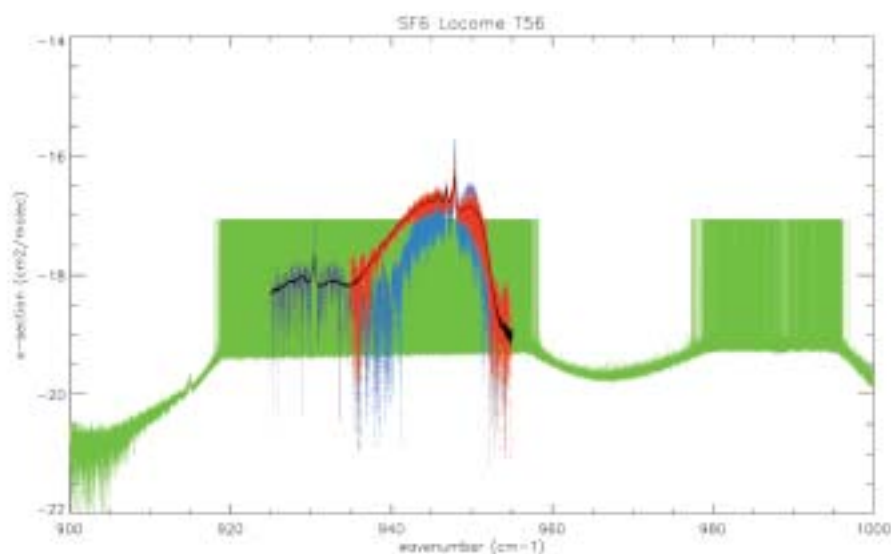
Figure 85. SF_6 absorption cross-sections: HITRAN-2K 295K (solid line, black); HITRAN-2K 180K (dotted line, purple); Lacome 297K (dash-dotted, red); Lacome 207K (dash-dotted, light blue); Lacome 296K (solid, light green).

900-1800cm^{-1}) with much higher spectral in terms of the resolutions (~0.002cm^{-1}) but only recorded for one or two temperatures. Figure 85 shows the comparison between HITRAN-2K SF_6 cross-sections and Lacome's measurements. It can be seen that in the spectral region of 935-955cm^{-1} Lacome's spectra measured for lower SF_6 amounts (red and blue curves) agree with HITRAN-2K data (black and purple curves). Unfortunately, the Lacome's measurements for higher SF_6 amounts (light green curve) are saturated in the ν_3 band wings and the $\nu_2 + \nu_6$ band. In order to obtain an approximate estimate of the radiative forcing contributed by these regions we assume the cross-sections of the saturated records as 0.4x10^{-18} (cm^2/molec) according to the values of the cross-sections in their adjacent regions.

GENLN2 line-by-line model (version 4.0, Edwards 1995), HITRAN-2K line parameters and CKD2.2 water vapour continuum (Clough *et al*., 1995) are used for the calculations. A global mean atmospheric profile (Forster, personal communication) is employed which has 19 layers and the tropopause defined at 105mb. The concentration of CO_2 is 356ppmv and that of SF_6 from 0 to 1 ppbv. Overlap of SF_6 with the three major greenhouse gases (water vapour, CO_2 and O_3) is

considered. HITRAN-2K SF_6 IR cross-sections and Lacome's measurements are included in the respective calculations and the results compared.

Table 1 gives the results of radiative forcing calculated for five spectral regions. Comparison between the radiative forcings due to HITRAN-2K (H2K in the table) and Lacome's data in the 935-955cm^{-1} region is also given. The difference may be caused by two factors: (1) Lacome's data are only for two temperatures (297K and 207K) but HITRAN-2K have 9 temperatures so represent more accurate temperature dependence in the calculation; (2) Lacome's data are of much higher spectral resolution than HITRAN-2K therefore the calculated radiative forcing may be more accurate in terms of the spectral integration.

From our calculations and comparison it can be concluded that omitting ν_3 band wings and $\nu_2 + \nu_6$ band (e.g. HITRAN-2K) may result in about 10% underestimation of SF6 radiative forcing. We are expecting new measurements for these regions from Lacome in the near future and the uncertainty in SF6 radiative forcing caused by the saturated records will be reduced. We will use these results to construct accurate band models to estimate the radiative forcing of the SF6 emissions from North Sea oil fields.

Table 3: Radiative Forcing of SF$_6$ Bands

Spectral Band	ν_3	ν_3	ν_3	ν_3 wings	$\nu_2 + \nu_6$	ν_4
Region (cm^{-1})	925 - 955	935 - 955	935 - 955	900 − 925 + 955 - 965	965 - 1030	590 - 646
Data source	H2K	H2K	Lacome	Lacome	Lacome	Lacome
Forcing (Wm^{-2})	0.50	0.42	0.39	~ 0.03	~ 0.03	0.01

References

Clough, S.A. and Iacono, M.J. 1995: Line-by-line calculation of atmospheric fluxes and cooling rates. 2. application to carbon-dioxide, ozone, methane, nitrous-oxide and the halocarbons. J. Geophys. Res., 100, 16519

Edwards, D.P. 1995: GENLN2: A general line-by-line atmospheric transmittance and radiance model. NCAR Technical Note TN-367.

Rothman, L.S. *et al*., The HITRAN molecular spectroscopic database and HAWKS (HITRAN Atmospheric Workstation): 2000 edition, JQSRT, 82, 5-44, 2003.

Climate Dynamics

Downward influence of stratospheric signals

Maarten Ambaum & John Methven, Department of Meteorology, University of Reading

Recent work by Charlton and others at the University of Reading has highlighted the possibility of extended predictability using stratospheric vortex anomalies as a precursor to certain tropospheric anomalies. This extended predictability appears to have the form of patterns (essentially manifestations of a local zonal index) propagating downward through the stratosphere on a time-scale of about two weeks. The present work points out the limitations of more traditional ideas on the mechanisms for such a downward propagation and suggests that we should be interpreting these propagating signals as non-linear wavepackets. Here we provide observational and theoretical evidence for this picture.

Traditionally it was thought that upward propagating Rossby waves "deposit momentum" when they break at a critical line just below the stratospheric jet maximum and thereby lower the jet maximum. However, this could only propagate strong jet anomalies downward; weak jet anomalies would propagate upward in this picture. Furthermore, observations show that in fact mainly weak jet anomalies, associated with stratospheric warmings, propagate downward. For such highly non-linear events – the break up of the whole vortex – the ideas of critical lines appear not very applicable anyway.

We propose the downward propagation of non-linear Rossby wave packets as a possible mechanism: after the barotropic break up of the vortex the associated PV anomalies would induce anomalous winds at lower levels. These can perturb the vortex there. For a linear perturbation this is the Charney-Drazin mechanism of vertical Rossby wave propagation. However, for the non-linear events under consideration the downward propagation is associated with an advective timescale on which the anomalous winds may modify the local vortex sufficiently. A back-of-the-envelope calculation shows that this mechanism has the correct time-scale.

Figure 86 shows Lagrangian measures of anomalous vortex strength (left panel) and non-linear wave activity (right panel) for a particular stratospheric warming event in the ERA40 data set. Over time the wave activity maximum (blue/green colours) is seen to move downward, leaving a weak jet anomaly (blue colours)
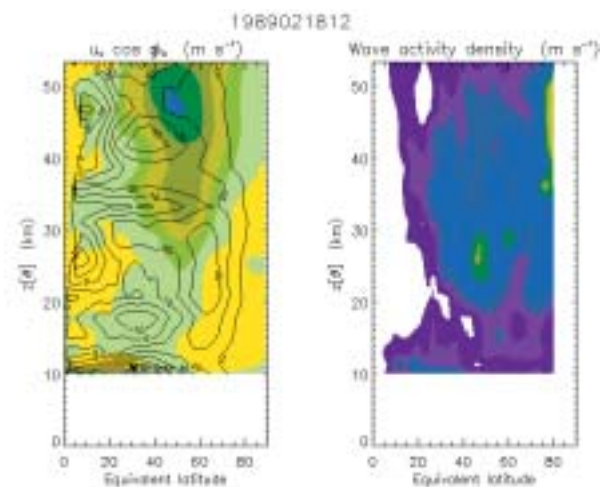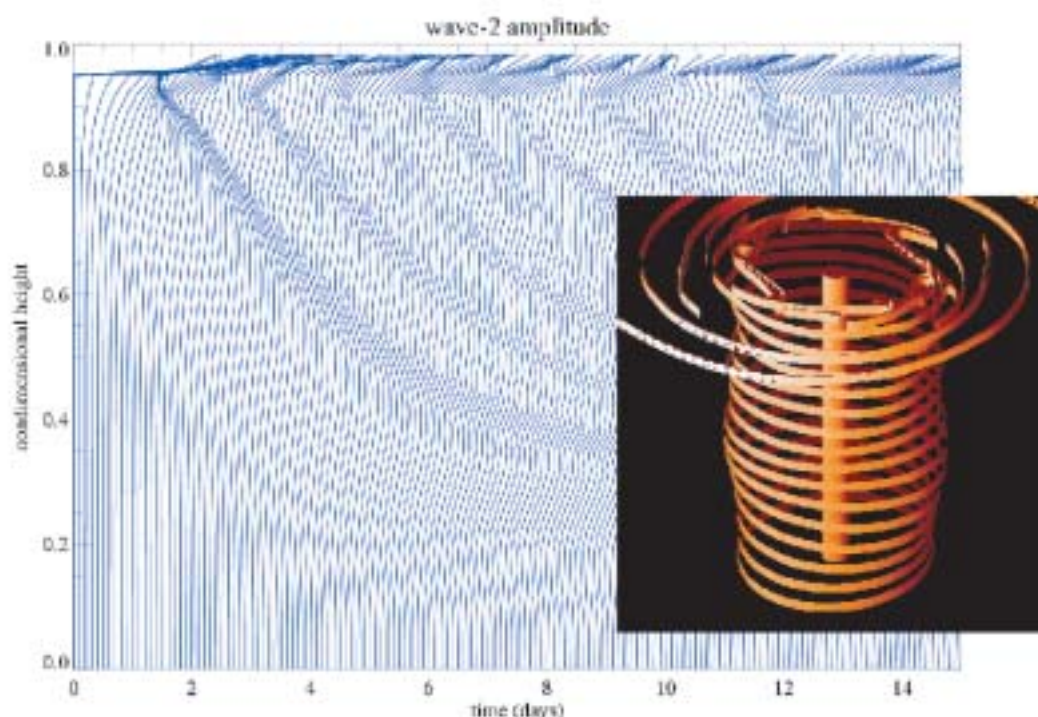

Figure 86.

Figure 87.

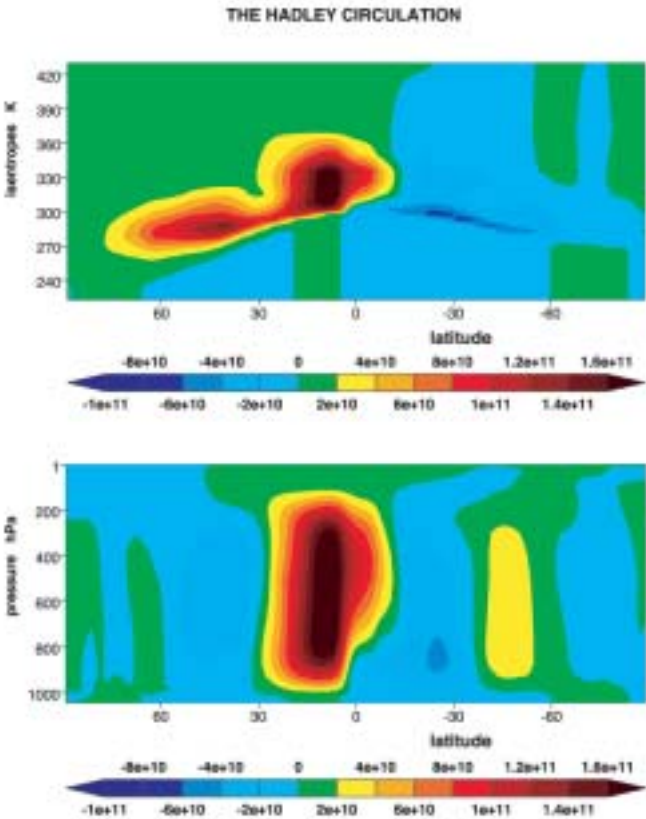THE HADLEY CIRCULATION

THE BREWER-DOBSON CIRCULATION

Figure 88. The mean meridional streamfunction in the troposphere. The upper plot shows the isentropic view while the lower plot shows the pressure level view. Units Kg/s.
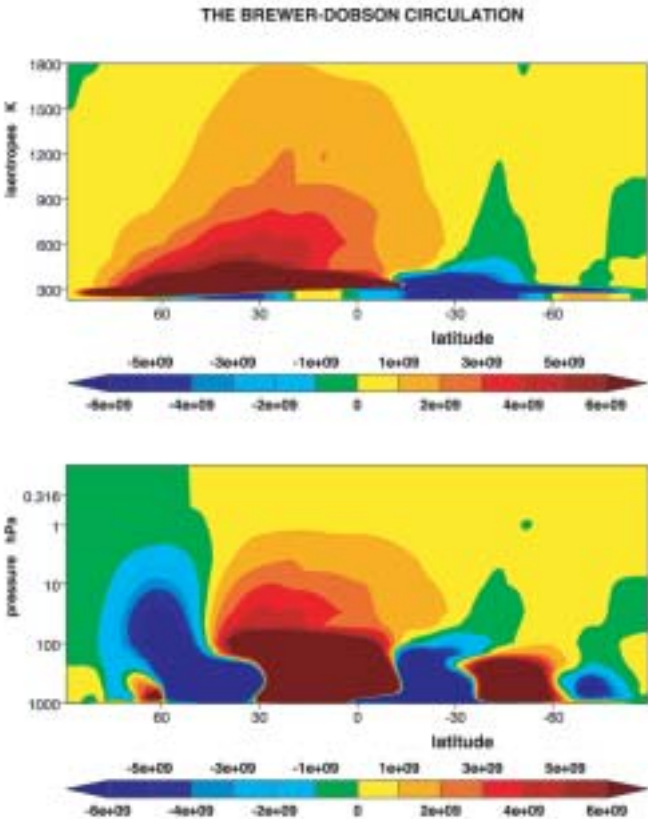
Figure 89. The mean meridional streamfunction in the stratosphere. The upper plot shows the isentropic view while the lower plot shows the pressure level view. Units Kg/s.

behind. This demonstrates how the eventual dissipation of non-linear wave packets lead to permanent changes to the vortex strength.

The Figure 87 shows results from an idealized contour dynamics simulation of the polar vortex. It is seen how a non-linear measure of wave activity (the wave-2 amplitude of the vortex at a particular level) will propagate downward with the group speed. The linear wave-like perturbations move down much quicker than the wave-2 amplitude maximum; the latter can only increase with substantial deformation of the vortex.

The mean meridional circulation as seen in ERA-40

Paul Berrisford, CGAM, University of Reading, Brian J. Hoskins. University of Reading

The mean meridional mass streamfunction is a description of the meridional mass transport. Given that the latter can depend on many dynamical and physical processes, such as the strength of the tropical heating and the activity in the mid-latitude storm tracks, it can usefully be used as one representation of the global climate. Here, we investigate the meridional circulation by using analyses and forecasts from the ECMWF 45 year re-analysis dataset (ERA-40). To date, we have analysed one month, January 1958, but the work is on-going.

Using methodologies from Juckes *et al.* (1994) and Boer (1982) the problem is formulated in both the traditional pressure co-ordinate framework and also the more novel isentropic framework. In both cases we are able to derive the mean meridional streamfunction from both the vertical and meridional motion.

Figure 88 and Figure 89 show the streamfunction, computed from the analysed meridional motion, in both the pressure and isentropic frameworks. Figure 88 emphasizes The Hadley Circulation in the troposphere, while Figure 89 emphasizes The Brewer-Dobson Circulation in the stratosphere. In both figures it can be clearly seen that the two viewpoints give a markedly different picture. The isentropic viewpoints show direct circulations that extend from the tropics to the northern polar region. The pressure level viewpoints limit these direct circulations to about 30N in the troposphere and 45N in the stratosphere and further north you can see reverse (indirect) circulations. Given that the isentropic framework captures Lagrangian motion much better than the pressure level framework (see for example, Karoly *et al.* (1997)), it is thought that the isentropic picture is the more physically meaningful summary of the circulation.
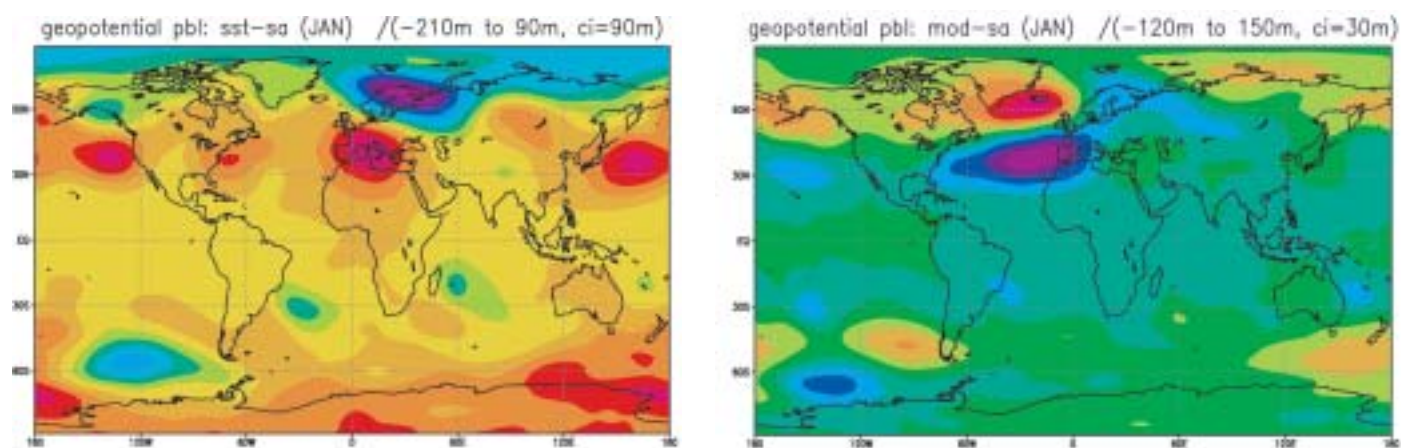
Figure 90. Geopotential differences for: "sst-sa" (a: left) and "mod-sa" (b: right); the contour interval (m) is specified for each figure; on abscissa there is the longitude, on ordinate the latitude.

A good test of self-consistency of the data is to use the streamfunction above, as computed from the meridional motion, to compute the vertical motion, and then compare that with the given vertical motion. Apart from some noise near the bottom boundary, which is thought to be due to inadequate vertical resolution used in the computation of the streamfunction, such a test works well in pressure co-ordinates where both vertical and meridional motion are available from the analyses. Unfortunately, it is not possible to make such a meaningful comparison in isentropic co-ordinates because the vertical motion, or heating, is produced by the forecast model and not the analyses.

We have also computed the Brewer-Dobson Circulation from the meridional motion from various forecast steps, as well as from the analysed motion which was used for Figure 89. In the tropical lower stratosphere, in particular, the exact form of The Brewer-Dobson Circulation is sensitive to whether analysed or forecast data is used. The circulation even appears to be sensitive to the range of the forecast. This indicates that from ECMWF data there is currently significant uncertainty in the quantification of the Brewer-Dobson Circulation.

Clearly, in order to make the results more robust, this work should be applied to the entire 45 year period of the ERA-40 dataset. We are currently engaged in doing that. This will also enable us to study the temporal variability of the tropospheric mean meridional circulation. In the stratosphere the dependence of the computed Brewer-Dobson circulation on the data available to the analysis system will be assessed.

References

Boer, 1997: Similarities of the Deacon cell in the Southern Ocean and Ferrel cells in the atmosphere.Q. J. R. Meteorol. Soc., 123, 519-526.

Ocean feedback on wave propagation during post-volcanic eruption winters

M. Caian, J.D. Haigh, Imperial College, London

A modulation of stationary waves by interaction with transient waves has been suggested (Kodera, 1994; Graf, 1995) to be responsible for the distribution of tropospheric temperature perturbations in winters following large volcanic eruptions. This distribution consists of a surface warming over Northern Hemisphere (NH) continents. Although the average post-eruption response, a global tropospheric cooling and stratospheric warming, was shown to be directly due to a radiative response, the surface and boundary layer heating was shown to be a dynamical response to the increased temperature gradient in the lower stratosphere.

In a similar experiment using the UK Met. Office Unified Model (UM) we found that transience can be an important source of triggering the difference during such an event between the responses of a coupled atmosphere-ocean and an uncoupled system. This study aims to analyse the direct role of the ocean in a system which is forced diabatically at the tropopause and its feedbacks through the response induced in the climate system.

The role of the ocean is analysed by comparing the results of a simulation incorporating an interactive atmosphere-ocean ("sa") with one in which the sea surface temperatures were specified from climatology ("sst"). Two parallel 90 day (DJF) integrations were performed for these configurations, starting from same initial conditions and both forced in a same way by intrusion of observed (Sato, 1993) stratospheric aerosol. Continental warming in post-eruption winters is favoured by a strong polar vortex - positive AO anomaly (AO+). We show that in the system diabatically forced by the aerosol the ocean role is very important in guiding the system between this state and the opposite (weak polar vortex - negative AO anomaly: AO-). An increase in the horizontal gradient of surface temperature at baroclinic latitudes can induce a transient change in the preferential regime (from the
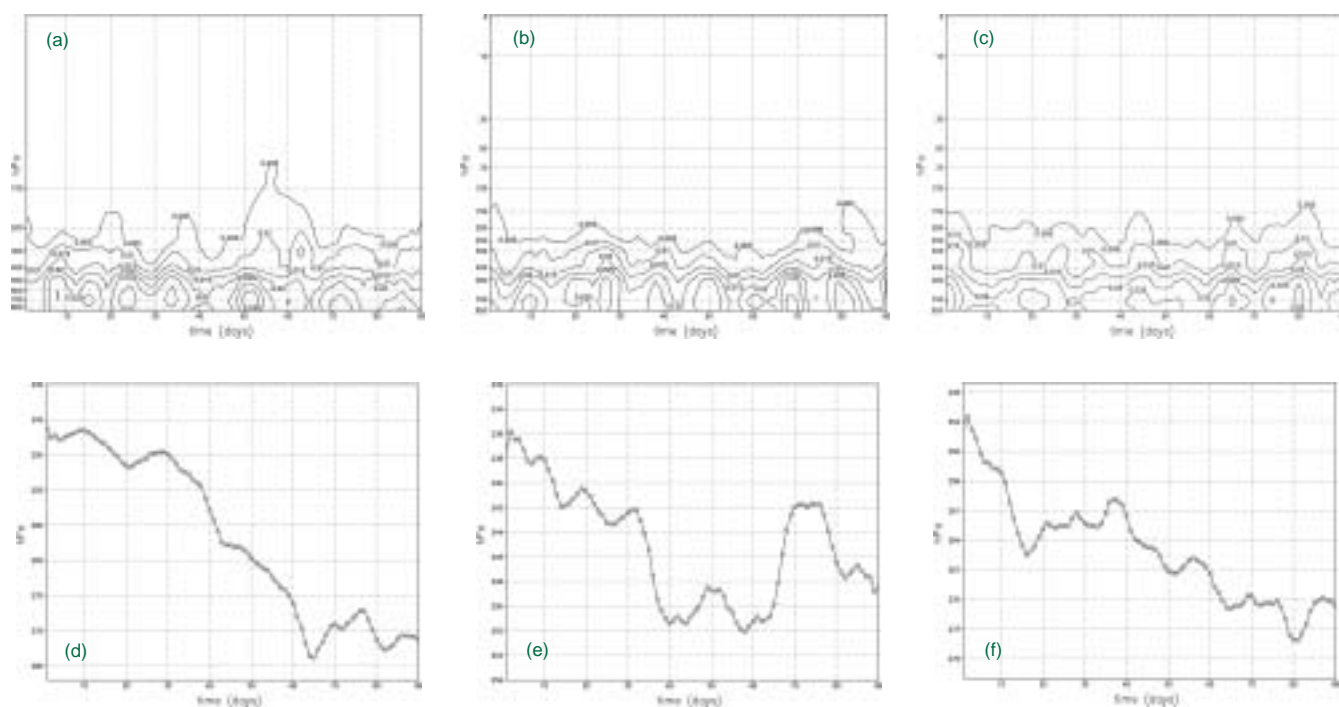
Figure 91. Time evolution, December 1991-February 1992, of Fp (the vertical component of Eliassen-Palm Flux, as defined by Edmon et.al., 1980) averaged over 41-71°N for simulations: a) with stratospheric aerosol and interactive sea surface temperatures, b): without aerosol but with interactive SSTs and c) with aerosol but with specified (climatological) SSTs. Above 300hPa the flux component has been magnified by a factor 1.8 to enhance features. The lower row shows the time evolution of the tropopause pressure for each simulation, respectively.

AO+ to AO- in our diabatic forcing case, Figure 90a) that amplifies leading to a stratospheric warming.

The atmosphere-ocean feedback was analysed in a further experiment ("mod") in which the longwave radiative contribution of clouds to surface heating was not allowed over the ocean: clear sky fluxes were used instead, without removing the clouds from the system. The cloud-surface interaction acts through (at least) two feedbacks on ocean heat transport: a positive feedback related to gradients in surface temperature, and another feedback due to eddy heat transport. The cloud-SST feedback is shown to be negative in the transient response to the aerosol as a negative SST anomaly leads to increased wave amplification and an AO- anomaly in the coupled system forced by the aerosol (Figure 90b). The system evolves according with the time scale and strength of

each feedback until reaching the equilibrium of the equivalent gain function.

Acknowledgements: This work was funded by the NERC UGAMP programme.

References
Graf, H.F. *et.al*, Clim Dyn, 9, 81-93, 1993, "Pinatubo eruption winter climate effects: model versus observations"
Kodera, K., JGR, 99, 1273-1282, 1994, "Influence of volcanic eruptions on the troposphere through stratospheric dynamical process in the Northern hemisphere winter"
Sato, M., JGR, 98, 22987-22994, 1993, "Stratospheric optical depths, 1850-1990"
Wang, C. *et.al*., GRL, 28, 1635-1638, year "The tropical western hemisphere warm pool"

Eddy activity in the presence of stratospheric aerosol

M. Caian J.D. Haigh, Imperial College, London

We have investigated the dynamical changes in the stratosphere, the troposphere and the interaction between them, induced by a dipolar diabatic forcing at the tropopause. The atmospheric response to this forcing, similar to that acting in the case of strong volcanic eruptions, was studied through numerical simulations using both the UK Met Office Unified Model, in coupled atmosphere-ocean format, and a linear primitive equation model.

The dynamical features of the stratosphere-troposphere interaction are correlated with regions of production/destruction of potential energy available for conversion through eddy heat fluxes. We show that a significant increase of eddy poleward heat flux can result as a consequence of the system being diabatically forced by

a tropospheric cooling and a stratospheric warming about the tropopause (Figure 91). In a more general context we show that second order variations of the static stability at the tropopause play an important role in triggering a dynamical instability and leading to wave amplification in quasi-stationary conditions of non-zero circulation at the tropopause. The dipolar thermal anomaly is important in sharpening variations of the vertical gradient of potential temperature at the tropopause, which intensifies the residual circulation and relaxes the control of the basic state on the propagation of longer waves. Considering a mechanism for the wave propagation we show that the presence of the stratospheric aerosol induces at global scale valid conditions for enhanced wave

transmission about the tropopause layer. The dominance of the baroclinic component in the exchange at the tropopause is shown to be important in triggering the initiation of the mechanism, allowing wave guidance towards higher latitudes and the amplification of longer-wavelength transient waves. The zonally asymmetric transient heating allowed by an interactive ocean-atmosphere system is better able to reproduce these non-linear features.

References

Edmon, H.J.Jr., B.J.Hoskins and M.E.McIntyre, 1980, "Eliassen-Palm cross sections for the troposphere", J.Atmos.Sci., Vol.37, Dec. 1980, pp.2600-2616.
O'Neill, A. and C.E. Youngblut, 1982, "Stratospheric warmings diagnosed using the Transformed Eulerian-Mean Equations and the effect of the mean state on wave propagation", J.Atmos.Sci., 39, 1370-1386.
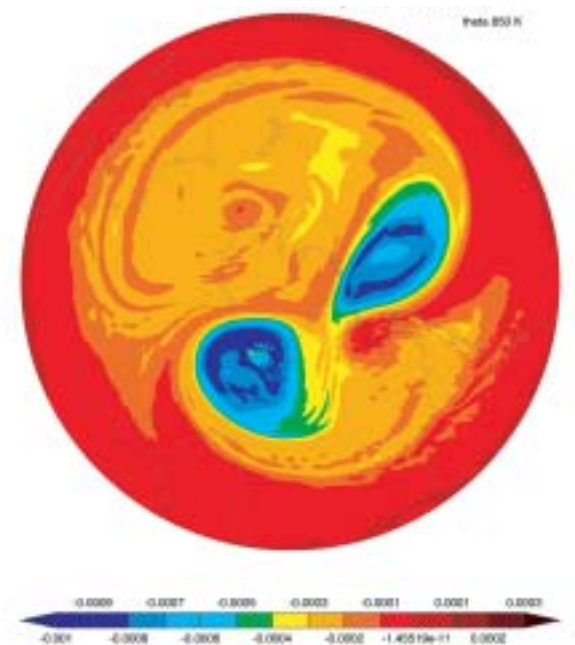
The September 2002 Southern Hemisphere Sudden Warming Event

Lesley Gray, Warwick Norton, CGAM, Reading University, U.K.
Charlotte Pascoe, Rutherford Appleton Laboratory, Chilton, U.K.
Andrew Charlton, Meteorology Department, Reading University, U.K.

In September 2002 the atmosphere gave us yet another of it's surprises – just to remind us that this natural world of ours is incredibly complicated and chaotic. Normally, the Southern Hemisphere (SH) vortex is relatively undisturbed and the air inside it, where most of the chlorine activation and ozone depletion occurs, is relatively isolated until the vortex breaks down in late winter / spring (October / November). However, throughout the whole of 2002 the SH winter stratosphere was more disturbed by planetary wave activity than usual and this culminated in a sudden warming event in mid-September in which the vortex elongated and split, as shown in Figure 92. This is generally known as a wave-2 warming because of the presence of the two lobes. This type of behaviour is common in the Northern Hemisphere (NH) but has not been observed in the SH before, at least not since observations of the upper stratosphere became routinely available.

The 2002 SH warming event was unexpected for two reasons. Firstly, planetary wave activity in the Southern Hemisphere is usually very weak. Secondly, the warming occurred in a west-phase of the quasi biennial oscillation (QBO) in the lower stratosphere. This is unexpected because warmings are usually considered to be more likely in the east-phase of the QBO, when a zero wind line is present in the winter subtropics and hence confines planetary wave propagation to higher latitudes closer to the polar vortex. At first, this evidence suggests that the sudden warming must be simply a result of anomalously strong planetary wave forcing from the troposphere. However, recent model studies have suggested that the mid-winter polar vortex may also be sensitive to the equatorial winds in the upper stratosphere, the region dominated by the semi annual oscillation. Examination of the time-series of equatorial zonal winds from two different data sources, the ECMWF 40-year reanalyses (ERA) and the UK Met Office assimilated dataset, show that the equatorial winds in the upper stratosphere above 10 hPa were anomalously easterly in 2002.

Using an idealised model of the stratosphere / mesosphere region of the atmosphere we have examined the possible influence of this easterly anomaly. The modelled equatorial winds were relaxed towards observations for various years to examine whether the anomalous easterlies in 2002 could influence the timing of a

Figure 92. Distribution of potential vorticity on the 850 K surface on September 25th 2002 showing the dramatic splitting of the vortex.

warming event. We find that the 2002 equatorial winds speed up the evolution of a warming event in the model. This suggests that the anomalous easterlies in the region 1-10 hPa may have been a contributory factor in the development of the observed SH warming. However, we also conclude that the anomalous equatorial winds on their own cannot explain the 2002 warming event. Relaxing the model's equatorial winds towards the 1999 observations also speeds up the evolution of the modelled warmings, but that winter did not display a warming event. It seems likely, therefore, that the warming was a result of a combination of unusually large planetary wave fluxes from the troposphere together with unusually strong easterlies in the upper equatorial stratosphere. The question of why the tropospheric wave forcing was unusually strong and the equatorial winds unusually easterly remains open.

Low-Frequency Midlatitude Variability in a Quasi-Geostrophic Coupled Model

Andrew McC. Hogg (A.Hogg@soc.soton.ac.uk)[1], William K. Dewar[2], Peter D. Killworth[1], Jeffrey R. Blundell[1],
[1]James Rennell Division, Southampton Oceanography Centre, [2]Department of Oceanography, Florida State University

As a complement to numerous coupled GCM studies, in which ocean variability is inaccurately computed, an idealised coupled climate study is presented that highlights ocean dynamics. The simulated ocean uses high spatial resolution with low viscosity, and produces low-frequency variability due nonlinear processes (see, for example, Berloff and McWilliams, 1999 for a demonstration of low-frequency variability in idealised ocean models). Variations in ocean circulation leads to oscillations in heat transport, and hence the climate of the coupled model.

We use a high resolution coupled process model called Q-GCM (Hogg *et al.*, 2003), which employs nonlinear quasi-geostrophic (QG) dynamics to efficiently solve for flow in an ocean basin coupled to a QG midlatitude atmosphere. Q-GCM is forced only by meridional variations in incoming radiation and produces a realistic simulation of the midlatitude climate. The atmospheric circulation is dominated by a baroclinically unstable westerly storm track, and forces a double gyre circulation in a rectangular ocean. Mesoscale variability in the ocean is well represented, and ocean eddies, as well as Rossby waves, can be identified.

The ocean used in this study is a large (3840 x 5000 km) three-layer box ocean, in which viscous dissipation is minimised by using biharmonic viscosity with a small coefficient ($A_H = 1 \times 10^{10}$ m^4/s). The ocean is driven only by wind, and has no overturning component. The wind stress forces a double gyre ocean circulation upon which a strong ocean eddy field is superimposed. The eddy field acts to increase variability on short (monthly) scales, as well as on longer (decadal scales).

Figure 93 shows the mean transport streamfunction (black contours) for two different cases: (a) case A is the default case and (b) case B with the viscosity coefficient doubled, which acts to damp eddy activity. Both cases have similar circulation over much of the basin, but case A has a stronger jet separating from the Western boundary of the ocean, and also larger nonlinear inertial gyres close to the region of Western boundary current separation. For each case we show two panels. These panels are the real (left) and imaginary (right) components of the first mode from a Hilbert EOF analysis of the transport streamfunction, along with the percentage of total variance represented by the mode (see von Storch and Zwiers, 1999, for the definition of the Hilbert EOF). Model data has been filtered with a 2 year FFT filter before applying the EOF analysis. In both cases shown here, the first statistical mode has a tripole in one phase of the oscillation, and a dipole in the other phase. The spatial extent of the modes is a function of the jet strength, so that in case A (where eddy activity is stronger) the spatial pattern of the statistical mode is larger, and it therefore represents a greater proportion of the variance. Importantly, the spectra (Figure 93c) of the first mode shows a peak in the interdecadal range which is largest when eddy activity is strongest.

Experiments with Q-GCM over a wide range of parameters have shown that the intrinsic ocean variability shown in Figure 93 is found over a wide parameter range. In addition, diagnostics from
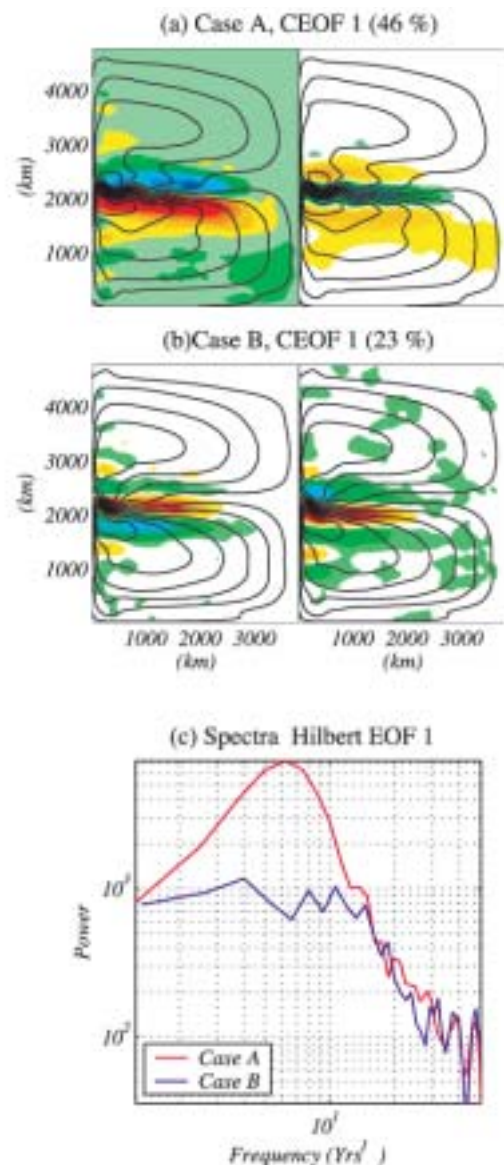

Figure 93. (a) Mean transport streamfunction (black contours) for case A, which real (top) and imaginary (middle) components of the first Hilbert EOF, with the percentage of total variance expressed by this mode shown in the caption; (b) Same for case B; (c) Spectra of the timeseries associated with the first Hilbert EOF of cases A and B.

coupled, partially coupled and uncoupled simulations (not shown here) demonstrates that this ocean generated variability can alter the variability of the whole coupled system. It follows that the low resolution, viscous oceans used in most GCM studies may be missing climate variability which is produced by instability in the wind driven gyres of the oceanic circulation.

References

P. S. Berloff & J. C. McWilliams (1999), Large-scale, low-frequency variability in wind-driven ocean
gyres, J. Phys. Ocean., 29, 1925-1949.

A. McC. Hogg, W. K. Dewar, P. D. Killworth & J. R. Blundell, (2003). A Quasi-Geostrophic Coupled Model (Q-GCM). Mon. Weather Rev., 131, 2261-2278.

H. von Storch & F. W. Zwiers (1999), Statistical analysis in climate research, Cambridge University Press.

How many storm tracks are there?

I.N. James, Dept. of Meteorology, University of Reading,
U. Burkhardt, DLR-Institut fuer Physik der Atmosphaere, Oberpfaffenhofen, D-82234 Wessling, Germany

Introduction

Since the work of Blackmon (1967), the "term "stormtrack" has referred to maxima of high frequency transient variance or covariance located in the midlatitudes of both hemispheres. In the northern hemisphere, the principal storm tracks are found above the Atlantic and Pacific Oceans. The term "storm track" was coined because the major axes of the elongated maxima of height or wind variance were similar to the mean tracks followed by the centres of individual cyclone systems. This somewhat subjective observation was confirmed by work such as Hodges (1997) who used an automatic feature tracking algorithm.

The interpretation of these storm track observations was based on the pioneering work of Hoskins & Simmons (1978) on the life cycles of idealised baroclinic waves. The variation of eddy variances and covariances as cyclones grew, matured and decayed followed closely the spatial variation of the same quantities along each storm track. This work was consolidated by the Eliassen-Palm diagnostic of Edmon *et al.* (1980), suggesting that the lifecycle could be understood in terms of the excitation, propagation and ultimate dissipation of Rossby waves.

According to this view, each storm track may be thought of as a "hyper-weather system", the accumulation of many cyclone events each going through its life cycle locally. Feedbacks between the high frequency transients and the larger scale, lower frequency flow help to maintain the storm track in its characteristic location (see, for example, Hoskins et al. 1983). The implied corollary is that each storm track is a more or less autonomous system, interacting locally with the orography, land-sea distribution and surface fluxes in its vicinity.

This paper sets out to examine critically this conceptual model, making use of our improved ability to handle large four dimensional datasets, to slice them in many different planes and to examine their time evolution. A fuller account will be published elsewhere.

Data

The work in this paper is based on the 40 year ECMWF Re-analysis data (ERA 40). Fields of wind, temperature, pressure, etc., were generated on a 1.75^o latitude longitude grid, at 17 variably spaced pressure levels. Data were recorded every 6 hours. This long dataset uses a consistent analysis-forecast assimilation system which generates consistent dynamical fields, along with reliable estimates of unobservable fields, such as that of vertical velocity. The data have been filtered using various filter cut-offs, in the manner of Blackmon and many others. The data discussed in this paper have been filtered using a 2-6 day band pass filter, based on a 31 point Lanczos filter.

Fields of variances and co-variances

Some interesting perspectives emerge when modern graphical algorithms are used to generate three dimensional views of the distribution of mean high pass filtered variances and covariances. These are not shown here in the interests of brevity. The variances
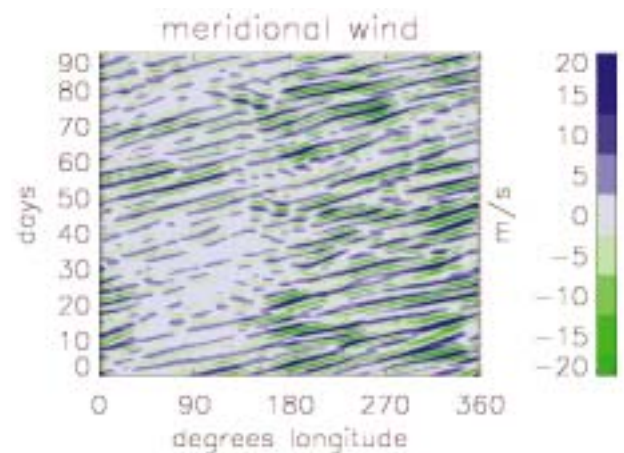

Figure 94. Hovmoeller plot of v' at 30 kPa for 34°N to 66°N, December 1984 to February 1985.

of wind ("eddy kinetic energy") and geopotential height are largest near the tropopause and smaller in the lower troposphere. However, the division into two storm tracks is most pronounced at 50 kPa and below. At tropopause levels, around 25 kPa, there is a single maximum of eddy kinetic energy, with some variations with longitude. The lowest values are found over Eurasia and the largest over the western, ocean hemisphere.

Co-variances such as the poleward and upward temperature fluxes, in contrast, are largest in the lower troposphere and over the oceans. They are suppressed over North America and Eurasia. In terms of the E-vector of Hoskins *et al.* (1983), it is as if there is a single broad belt of large eddy activity in the Northern Hemisphere, fed by two low level sources over the oceans.

Hovmoeller plot

The previous section was based on what have become standard diagnostic techniques, in which the spatial structure of the average seasonal mean structure was displayed. At the expense of reducing the spatial detail, this section concentrates upon the time evolution of the dynamical fields, examining how individual transient events accumulate to form the time-mean "storm track".

Figure 94 is a Hovmoeller plot, that is, a longitude-time plot, of the high-pass filtered poleward component of wind at the 30 kPa level, averaged over the mid-latitudes between 34°N and 66°N. This plot is for a single winter season, from December 1984 to February 1985. Zeroes in the field correspond to troughs and ridges. The generally eastward procession of troughs and ridges is clearly seen. Largest values of v' are seen in mid-winter over the Atlantic, but are largest in late Autumn and early spring over the Pacific. Several points of interest can be seen. It is notable that the

total number of synoptic events contributing to the seasonal mean
storm track is not large, generally less than 10. More germane to
the theme of this paper is that individual disturbances may have
their larger amplitudes in the storm track regions, but they can be
followed around large parts of the northern hemisphere, both
before and after their involvement with the storm track. In
particular, virtually without exception, every major disturbance in
the Atlantic storm track can be traced back to a precursor in the
Pacific storm track.

Re-ignition of active systems

Movies have been produced, showing the time evolution of the
filtered v' fields in the mid-latitudes. A strong poleward
temperature flux is associated with a westward tilt with height of
the troughs and ridges in the systems (see for example James 1995,
p 122 et seq). The movies reveal relatively little variation of the
amplitude of the v' wave in the lower troposphere as disturbances
move from the Pacific storm track to the Atlantic storm track.
However, a marked increase in the phase tilt is seen as many
disturbances cross the Atlantic coast of North America. This phase
tilt is a precursor of the intensification of the upper level
disturbances in the Atlantic storm track.

This process of "re-ignition" of eddies, restarting the baroclinic
energy conversion processes and ultimately intensifying the upper
level disturbances, appears to be a crucial element of the storm
track dynamics. It involves the interaction of finite amplitude
disturbances moving into the storm track region and the low level
temperature and potential vorticity fields.

Conclusions

This study has shown that the "lifecycle" model of storm tracks
is an oversimplification. So too is the notion that each stormtrack
is a more or less autonomous system, interacting with its local
environment. Other authors have pointed out the importance of
finite amplitude disturbances at the start of the stormtracks (see,
for example, Chang *et al.* 2002). As far as we are aware, this work
is the first to demonstrate just how long lived some of the high
frequency transients appear to be. This result has important
implications for predictability, and for the need to represent the
global circulation adequately even for simulations of a single
storm track region. In terms of modelling storm tracks in global
circulation models, this work suggests that it is as important to
focus on the processes that suppress the low level transients over
north America as on the processes which enhance them over the
oceans.

Figure 95. Land-atmosphere coupling strength in HadAM3 for (a)
precipitation and (b) evaporation. See Koster et al. (2002) for details
on coupling strength diagnostic. Small values indicate that soil
moisture has weak influence on variable, large values indicate
strong soil moisture influence. (c) Soil moisture availability factor
averaged over June-August for HadAM3.

References

Chang, E.K.M, S. Lee & K.L. Swanson (2002): Storm track dynamics.
Journal of Climate 15 2163-83.

Edmon, H.K., B.J. Hoskins & M.E. McIntyre (1980): Eliassen-Palm cross
sections for the troposphere. J. Atm. Sci., 37, 2600-16 (see also
corrigendum, ibid, 38, 1115).

Hoskins, B.J., I.N. James & G. H. White (1983): The shape, propagation
and mean-flow interaction of large scale weather systems. J. Atm. Sci. 40,
1595-1612.

James, I.N. (1995): Introduction to circulating atmospheres. Cambridge
University Press, 422pp.

Simmons, A.J. & B.J. Hoskins (1978): The life cycles of some baroclinic
waves. J. Atm. Sci. 35, 414-32.

Land-Atmosphere Coupling Strength in HadAM3

David Lawrence, CGAM, Dept. of Meteorology, University of Reading

Land-atmosphere coupling strength, defined here as the extent to
which a precipitation-induced soil moisture anomaly influences
the overlying atmosphere and thereby the evolution of weather and
the generation of precipitation, is not well quantified or understood
in climate models. However, climate models are often used to
address questions such as: Do and by how much do land-surface
state anomalies affect weather and / or seasonal forecast skill? or
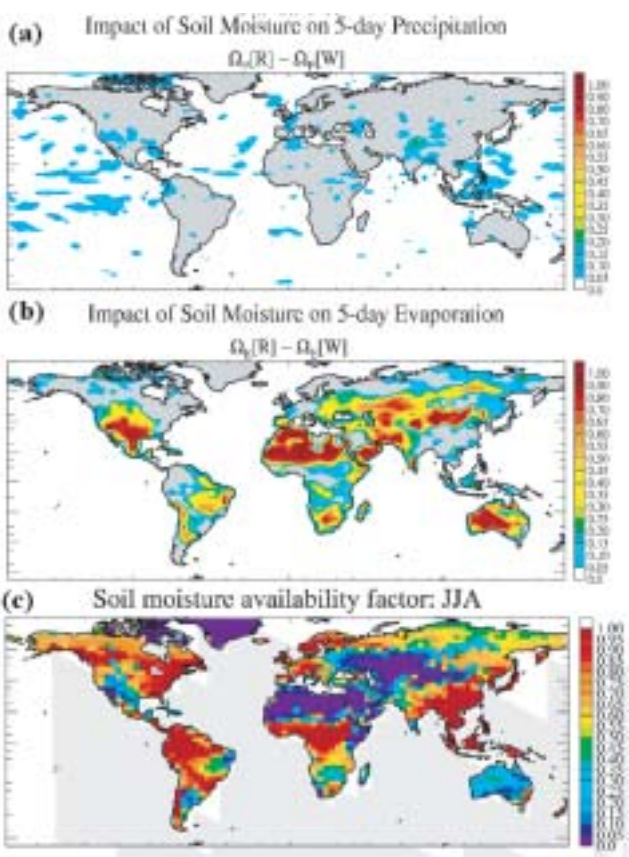What are the feedbacks associated with drought or flood

conditions?   The answers to such questions are often model-
dependent, strongly reducing their significance. Part of the
problem is that every climate model has a unique inherent
land-atmosphere coupling strength. A recent pilot model
intercomparison study by Koster *et al.* (2002) revealed that
land-atmosphere coupling strength in HadAM3 was the lowest
among the four models tested, only negligibly larger than zero,
which effectively says that weather and precipitation are

Theory developed by Betts and Ball (1995), Betts et al. (1996), Eltahir (1997), and Schär et al. (1999) supported by observations from FIFE, 1-d models, and regional climate models.

Over wet soil:

- lower Bowen ratio (SH/LH) → shallower and wetter boundary layer

- darker soil ($\alpha \Downarrow$) and cooler surface temperatures → enhanced net surface radiation → larger total heat flux into boundary layer

- two factors combine to increase Moist Static Energy per unit mass of Boundary Layer air
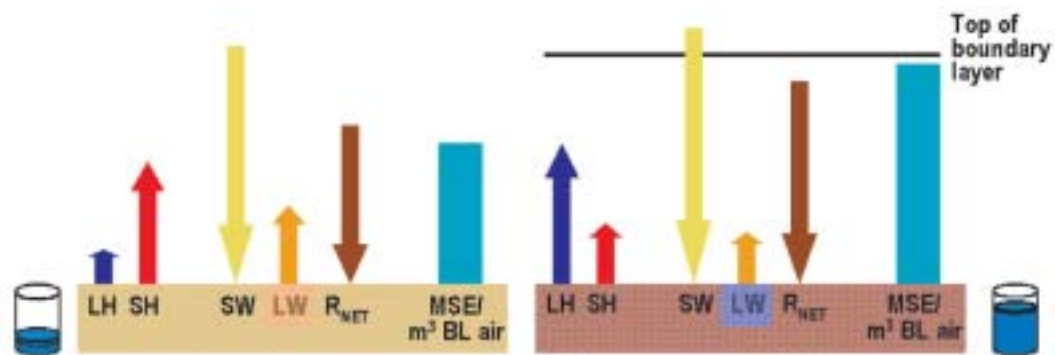

Figure 96. Schematic depicting theoretical indirect soil moisture-precipitation feedback mechanism.

essentially uninfluenced by land surface soil moisture conditions. The original Koster *et al.* study is being repeated with a slightly improved experimental design and with more participating climate-modelling groups (Global Land-Atmosphere Coupling Experiment, GLACE). Land-atmosphere coupling strength remains low in HadAM3 despite interim improvements to the land-surface scheme in the intervening years (see Fig. 1).

The reasons for the low land-atmosphere coupling strength are investigated in this study. The degree with which soil moisture influences evaporation is a key component of overall land-atmosphere coupling (see Fig. 2 for schematic describing the theoretical land-atmosphere feedback mechanism). As seen in Fig. 1, soil moisture conditions exert considerable influence over evaporation (and consequently latent and sensible heat fluxes) in arid regions but do not exert much influence in other regions. When one compares the map showing the influence of soil moisture on evaporation with a map of soil moisture availability (SMA, the degree to which plant transpiration is water stressed), it is clear that areas of low evaporation coupling are coincident with areas where SMA is high and level 1 soil moisture variability is low (not shown). Rerunning the GLACE experiment with soil

configuration designed to increase the dependence of evaporation on soil moisture (adjusting θ_{wilt} and θ_{crit} so that SMA is always < 1, reducing top layer soil depth from 10cm to 4cm, and increasing soil albedo dependence on level 1 soil moisture) does not demonstrably increase evaporation (or precipitation) coupling, a result that implies, but doesn't prove, that errors and uncertainties in soil moisture parameterizations are not generating the low land-atmosphere coupling strength.

Previous experience with the model suggests that precipitation frequency is considerably larger than in the real world (supported by cursory analysis not shown here). Our current, but as yet not fully tested hypothesis, is that the overly frequent precipitation is preventing the model from experiencing a realistic range of soil moistures and thereby land-atmosphere coupling is being circumvented. For example, level 1 soil moisture never drops below 60% of saturation in the SE United States. The reasons for the overly frequent precipitation are not presently understood.

Reference

Koster, R. D., P. A. Dirmeyer, A. N. Hahmann, R. Ijpelaar, L. Tyahla, P. Cox, and M. J. Suarez (2002). Comparing the degree of land-atmosphere interaction in four atmospheric general circulation models. J. Hydromet., 3, 363-375.

Large warming trends over the Antarctic Peninsula associated with blocked winds and changes in zonal circulation

Andrew Orr[1], Gareth Marshall[2], Julian Hunt[1] and Doug Cresswell[1]
[1]Centre for Polar Observation and Modelling, University College London, [2]British Antarctic Survey

Introduction

Observations from stations on the Antarctic Peninsula show that over the past 50 years this region has experienced a warming trend in near-surface air temperatures significantly greater than the global mean (e.g. Vaughan *et al.*, 2001). However the Peninsula warming is far from uniform, being more pronounced on the western side (see Figure 97). Recently research has focused on the trend towards the high-index polarity of the Southern Hemisphere Annual Mode (SAM) (e.g. Thompson and Solomon, 2002), beginning in the mid-1960s, as a contributory factor to this enhanced warming trend. The SAM, the principal mode of variability in the Southern Hemisphere, is essentially an annular structure with synchronous anomalies in pressure of opposite signs above Antarctica and the mid-latitudes. The result of this recent trend in the SAM is a strengthening of the circumpolar (predominately low-Froude number ($F < 1$)) westerly flow (see Figure 98) around Antarctica, as observed in northern Peninsula radiosonde data (Marshall, 2002).

It is demonstrated here, using numerical mesoscale modelling of westerly flows over the Peninsula and laboratory simulations using the Coriolis platform, Grenoble, France, that the warming trend

Figure 97. Warming trends in °C per century complete with 95% confidence intervals, the significance (if any) is given in parenthesis and the period over which the trend is produced is also shown.
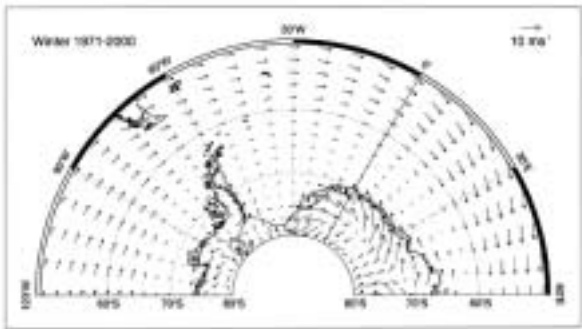

Figure 98. Climatological mean surface wind around Antarctica. From NCEP/NCAR data.

can be associated with the interaction of the stronger zonal winds and blocking over the (2km high) Antarctic Peninsula. The advection of warm maritime air from the south eastern Pacific Ocean to the western Antarctic Peninsula increases with stronger zonal winds. King (1994) showed that annual temperatures along the western coast are more highly correlated with meridional rather than zonal flow (in line with blocked air being directed southwards through Coriolis forces), meaning enhanced warm air advection to this region. Warm air is less likely to reach the surface of the eastern side of the Peninsula because of the tendency for the flow to be low-Froude number and because of the presence of very stable air over the ice-covered western Weddell Sea.

Critical to developing this theory was to understand how mesoscale flows (i.e. on a horizontal scale 30-100km) respond to being blocked by the Peninsula. Much of this originated from the idealised shallow-layer model of Hunt *et al.* (2003) for stable mesoscale atmospheric flows incident to a "cape" (which also discusses the limitations of numerical weather/climate prediction models, frequently used in climate change research, in capturing (or parameterizing) these important mesoscale processes).

Laboratory simulation

The modelling of the interaction of westerly zonal winds with the Antarctic Peninsula was conducted in a linearly rotating stratified experiment using the Coriolis turntable (13m in diameter and fluid depth of 60cm), Grenoble, France. The Antarctic Peninsula was represented by a simple "cape" (see Figure 99) placed on the tank bottom. Westerly and easterly flows over the cape of 1-10 cms^{-1} ($0 < F < 2$) were driven by either impulsively increasing or decreasing the turntable rotation rate (Orr *et al.* 2003).

Figure 99 shows horizontal streamline patterns of near-surface, low-Froude number ($F \approx 1/3$), westerly flow relative to the cape (Orr *et al.* 2003). The upstream circulation diverges when blocked by the cape, with the flow towards the base of the cape recirculating upwind and the flow towards the tip flowing around the cape and forming a jet extending downstream and a circulation cell in the lee of the cape.

The proportion of the flow recirculating upwind appeared to depend on the mean flow speed, with more circulating at higher upstream speeds (not shown). Also evident was upper-level flow passing over the cape with little deflection (not shown). High-Froude number flow ($F \geq 1$) when blocked by the cape was shown to travel over the obstacle and descend the other side (not shown).

Numerical mesoscale modelling

The numerical model used in this study is the UK Met. Office Unified Model version 4.5 (UM 4.5). The simulations use a nested limited-area domain with horizontal resolution of 12km and 38 vertical levels centred over the Antarctic Peninsula. Use of a rotated coordinate pole achieves uniform resolution. Lateral boundary conditions are generated initially from the global model.
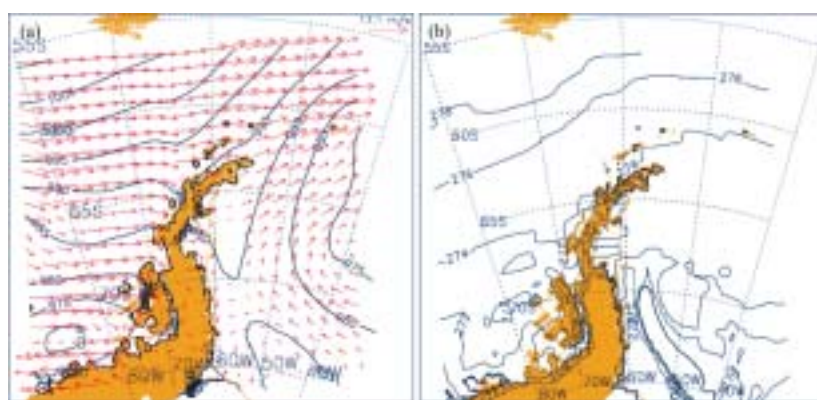
Figure 99. (left) Horizontal streamline photograph of near-surface, westerly, low-Froude number flow (left to right) around a cape in the Southern Hemisphere.
Figure 100. (above) Atmospheric westerly flow over the Antarctic Peninsula at 06Z 23 Jan 2002. Computed using UM 4.5 with a horizontal resolution of 12km. Shown are (a) 10m-wind speed (ms^{-1}) vectors (every 8 gridpoints) and surface level pressure (mb), & (b) surface temperature (K).

Figure 100(a) shows the 10m-wind speed and surface pressure (mb) over the Antarctic Peninsula for 23 January 2003 06Z computed using UM 4.5. The flow is a well defined and relatively strong westerly flow (velocity approximately 10ms^{-1}, giving F≈1/2). Evident is upstream flow divergence as the flow is blocked by the cape, with some recirculating upwind and some flowing around the cape and forming a jet extending downstream. Figure 100(b) shows the surface temperature at 10m, illustrating that relatively warm northerly air at near surface level is being transported to the Peninsula. At upper-levels the flow passes over the cape with little deflection (not shown). The blocking in Figure 100(a) and Figure 99 is broadly similar, with some differences perhaps explained by the different Froude numbers involved.

Discussion

The laboratory and numerical simulations show that near-surface, low-Froude number, westerly flow diverges when blocked by the Antarctic Peninsula, with some recirculating upwind and some flowing around the cape and forming a jet extending downstream and a circulation cell in the lee of the cape. The simulations showed that upper-level flow is relatively undeflected by the obstacle and that high Froude number flow when blocked by the Peninsula can travel over the obstacle and descend the other side. (Certainly the sensitivity of the blocking mechanism to the Froude number requires further investigation.) However, this behaviour does provide a possible mechanism to link the trend for stronger westerlies with the enhanced near-surface warming over the Antarctic Peninsula, particularly over the western side where winds are blocked at near-surface level, giving rise to more northerlies and greater transport of relatively warm air into this region. The increase in the strength of the westerlies also makes the probability of high-Froude number flow more likely, meaning the possibility of greater amounts of warm westerly air at both near-surface and upper-levels being transported over the Peninsula to the eastern side and influencing the near-surface warming trend over the region.

It should be noted that other factors, which are often closely coupled, are thought to contribute to the warming trend, mainly, atmosphere-ice-ocean interaction, changes to the regional oceanic circulation, and other changes to the atmospheric circulation.

Observational evidence for the circulation change and the resulting warming is strong. Marshall *et al*. (2002) showed that above Faraday station the upper-air temperature trend was approximately half that recorded at the surface and not statistically dissimilar to that observed globally. (If a contribution to the near-surface warming trend is a blocking mechanism, then it follows that the enhanced warming is found at the near-surface and not at upper levels.) The temperature records analysed by Vaughan *et al*. (2001) show a warming trend which increases further south along the Peninsula – consistent with the laboratory evidence for increasing upwind recirculation as the upstream velocity strengthens. At Bellingshausen station the meridional component of the 850hPa wind is predominately northerly, while the 500hPa component is predominately southerly (Marshall 2002).

References
Hunt, J. C. R., Orr, A., Cresswell, D. and Owinoh, A., "Coriolis effects in mesoscale shallow layer flows", Proceedings of the International Symposium on Shallow Flows, Delft, 16-18 June, 117--124, 2003.
King, J. C., "Recent climate variability in the vicinity of the Antarctic Peninsula", Int. J. Clim., 14, 357-369, 1994.
King, J. C. and Harangozo, S. A., "Climate change in the western Antarctic Peninsula since 1945", Ann. Glacol. 27, 571-575, 1998.
Marshall, G. J., "Analysis of recent circulation and thermal advection in the northern Antarctic Peninsula", Int. J. Clim., 22, 1557-1567, 2002.
Marshal, G. J., Lagun, V. and Lachlan-Cope, T. A., "Changes in Antarctic Peninsula tropospheric temperatures from 1956 to 1999: A synthesis of observations and reanalysis data", J. Climate, 22, 291-310, 2002.
Orr, A., Cresswell, D., Hunt, J. C. R., Owinoh, A. Z. and Sommeria, J., "Rotating stratified flow over rough orography", Report on experiment using the Coriolis turntable, Grenoble, France, 2003.
Thompson, D. W. J. and Solomon, S., "Interpretation of recent Southern hemisphere climate change", Science, 296, 895-899, 2002.
Vaughan, D. G., Marshall, G. J., Connolley, W., M., King, J., C. and Mulvaney, R., "Climate change – devil in the detail", Science, 293, 1777-1779, 2001.
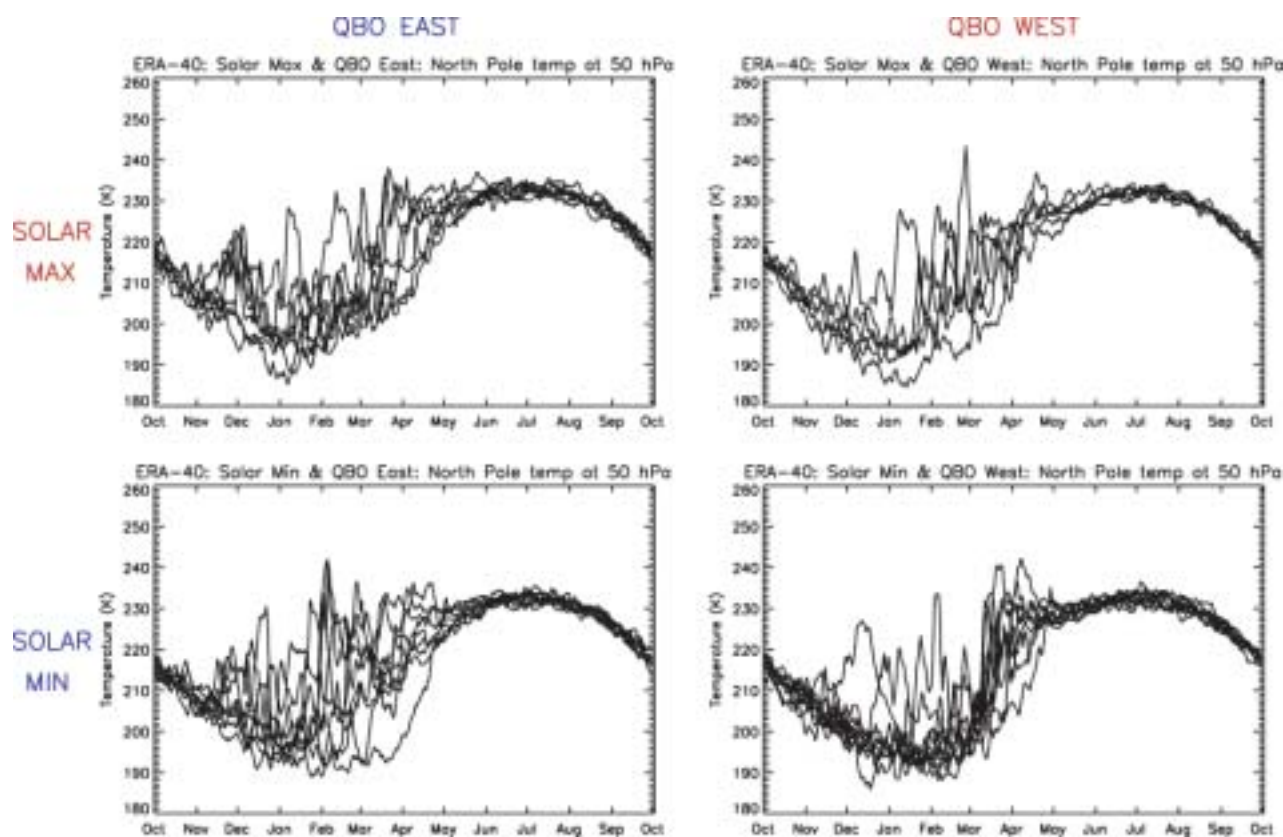
Figure 101. Time series of daily North Pole temperatures at 50 hPa for each of the four categories: Solar Max QBO East, Solar Max QBO West, Solar Min QBO East and Solar Min QBO West.

Analysis of the ERA-40 data: Examining the link between equatorial QBO winds and the flow regime of the wintertime polar stratosphere

Charlotte Pascoe, Rutherford Appleton Laboratory, Lesley Gray, University of Reading and Agathe Untch ECMWF

The vertical and meridional propagation of planetary waves in winter stratosphere is influenced by the phase of the quasi-biennial oscillation (QBO) (Holton and Tan, 1980, 1982). This behaviour is such that one would expect warm (cold) North Pole temperatures to occur during the east (west) phase of the QBO. Studies of the Holton-Tan relationship between equatorial winds and polar temperatures usually use winds in the lower stratosphere around 40-50 hPa to define the phase of the QBO (Baldwin and Dunkerton, 1998) and in this study we do the same.

Winters have been stratified according to the phase of the QBO at 44hpa in December (QBO East, QBO West), the mean January February North Pole temperature at 30hPa (Warm North Pole, Cold North Pole) and the solar irradiance during the winter season from November to March (Solar Max., Solar Min.). The average January February zonal mean zonal wind has been used as a measure of the strength of the winter polar vortex. The maximum difference between polar vortex strength of Cold and Warm winters is 35 m/s. The maximum difference for QBO West minus QBO East is just 10 m/s. Therefore the Holton-Tan relationship is able to explain 29% of polar vortex variability. However when we stratify according to Solar Min/Max we find that for solar minimum winters the maximum difference of QBO West minus QBO East is 35 m/s.

Figure 101 shows time series of daily North Pole temperatures at 50 hPa for each of the four categories: Solar Max QBO East, Solar Max QBO West, Solar Min QBO East and Solar Min QBO West, from this one can clearly see that Solar Min QBO West years have far fewer sudden stratospheric warming events than Solar Min QBO East years which exhibit greater variability throughout the entire winter season. Solar Max QBO East years are more variable than Solar Max QBO West years in the early winter (November and December) but there is little to distinguish between the two solar maximum categories in the later winter months from January onwards.

The equatorial QBO of zonal wind has a three fold vertical structure with westerly (easterly) anomalies in the lower stratosphere overlaid by easterly (westerly) anomalies in the mid-stratosphere and westerly (easterly) anomalies in the upper stratosphere. In solar minimum winters the magnitude of this third upper stratospheric QBO anomaly is greater than that found in solar maximum winters by approximately 5 m/s. Hence periods of solar minimum experience greater QBO zonal wind anomalies in the upper stratosphere than periods of solar maximum.

A numerical experiment to test the sensitivity of Northern Hemisphere winter stratospheric flow to equatorial winds in the upper and lower stratosphere performed by Gray (2003) with a

stratosphere mesosphere model suggested that the lower stratospheric QBO may influence the early winter but later in the winter when the flow is highly non-linear the greatest influence may come from variations in the equatorial winds in the upper stratosphere. This assumption appears to have been confirmed by the present QBO-Solar analysis of ERA-40 North Pole temperatures.

References

Baldwin, M. P., and T. J. Dunkerton, 1988: Biennial, quasi-biennial, and decadal oscillations of potential vorticity in the northern stratosphere, J. Geophys. Res., 103, 3919-3928.

Gray, L. J., 2003: The influence of the equatorial upper stratosphere on stratospheric sudden warmings, Geophys. Res. Lett., 30(4), 1166, doi:10.1029/2002GL016430.

Holton, J. R., and H.-C. Tan, 1980: The influence of the equatorial quasi-biennial oscillation on the global circulation at 50 mb, J. Atmos. Sci., 37, 2200-2208.

Holton, J. R., and H.-C. Tan, 1982: The quasi-biennial oscillation in the Northern Hemisphere lower stratosphere, J. Meteorol. Soc. Japan., 60, 140-148.

The Equatorial Stratospheric Response to Stochastic Gravity-wave Parameterizations

Claudio Piani, Oxford University, Atmospheric, Oceanic and Planetary Physics, Clarendon Laboratory

Motivation

In Global Climate Models (GCMs), contributions to the forcing by subgrid-scale (unresolved) flows are generally represented, if at all, by deterministic parameterizations. A deterministic parameterization rests on the assumption that subgrid-scale flows are in some form of statistical equilibrium with the resolved fields and that such a statistical equilibrium can be adequately represented by the mean of their statistical distribution alone.

In the past some studies have suggested (Salby and Garcia, 1987) that representing higher order moments in parameterizations of subgrid-scale flows may improve GCMs. Buizza et al. (1999) showed how the skill of the probabilistic prediction of weather observables in the European Center for Medium-Range Weather Forecast ensemble Prediction System (ECMWS EPS) could be improved simply by adding an arbitrary amount of variance to the total parameterized forcings. Palmer (2001) used a low-order simple dynamical system, commonly known as the Lorenz Attractor, to show that some of the remaining errors in climate prediction may have their origin in the neglect of the 2nd order moments of unresolved flows. Here we will use the same dynamical model to show that further improvements may come from also considering higher order moments of the statistical distribution of unresolved flows. We will then implement a version of the Hines gravity wave scheme with a stochastic source strength distribution in the unified model and test the effects on the simulated climate of the equatorial stratosphere. Particular interest is given to the annual cycle and quasi-biennial oscillation of the mean zonal winds.

Exploratory results with a simple dynamical model

Figure 102 presents the results from simple numerical experiments with the Lorenz Attractor. Following Palmer *et al.*, 2001, the attractor is rotated so that the 'Z' variable is responsible for only 4% of the variance. Figure 102a shows a single trajectory obtained by integrating the full 3D equations. Figure 102b shows the trajectory obtained from the same initial conditions as in Figure 102a by integrating the full 'X' and 'Y' dynamical components of the Lorenz equations but using a deterministic parameterization for the 'Z' component. In Figure 102b, at every time step, 'Z' is given the value of the mean of the 'Z' distribution from the
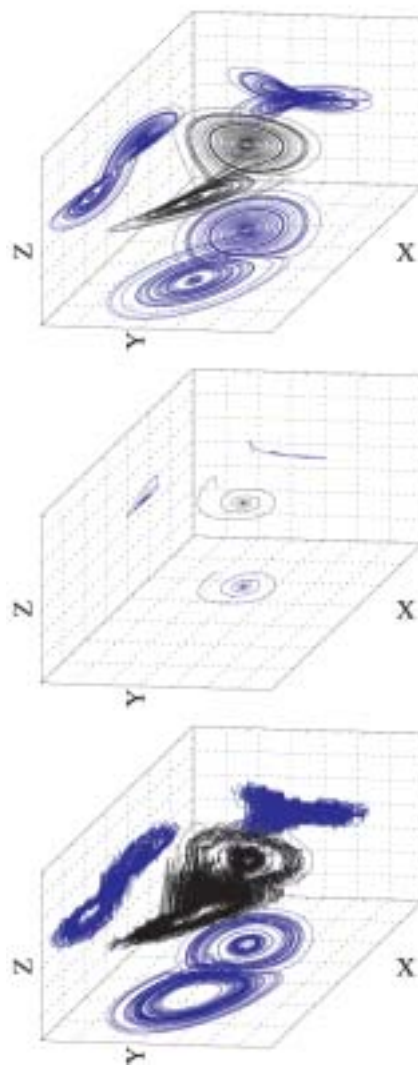

Figure 102. Numerical simulation of a rotated Lorenz attractor. A single trajectory is calculated using:
(top) the full 3D set of prognostic equations;
(middle) a deterministic parameterization for the `Z' variable;
(bottom) a stochastic parameterization for the `Z' variable that takes into account all order moments of the observed distribution.

trajectory shown in Figure 102a associated with the relevant values of 'X' and 'Y'. Palmer showed that although deterministic parameterizations of 'Z' could not reproduce chaotic behaviour, adding a simple random component to the 'Z' equation can reproduce such behaviour (not shown). Such a model however does not produce a climatology similar to that shown in Figure 102a. Figure 102c shows the trajectory obtained as in Figure 102a,b but with a full stochastic parameterization for 'Z'. Here, at every time step, 'Z' is given a random value that follows the observed distribution of 'Z' from the trajectory shown in Figure 102a associated with the relevant values of 'X' and 'Y'. The improvements are evident. The climatology of 'Z' is constrained to be correct and the chaotic behaviour is reproduced.

Results from the Unified Model

Three simulations with different distributions of the source strength parameter in the gravity wave scheme were examined. In the first simulation the source strength parameter (hereafter referred to as RMS) follows a delta function distribution. This is tantamount to using a deterministic parameterization and has been done for comparison with previous work. In the second simulation RMS follows a uniform distribution from 0 to a given RMSmax. A uniform distribution is the simplest choice when no information on the observable source strength is available. In the third simulation RMS follows an exponential distribution.

An exponential distribution was chosen to represent a hypothesized distribution of the intensity of convection in the tropics. Since, to our knowledge, there is no global observational dataset of convection intensity we adopted two proxy sources as models for the distribution. The first is a histogram of daily precipitation on grid points between 13.75N and 13.75S from a 30 year simulation of the coupled ocean-atmosphere version of the Unified Model referred to as HadCM3 (courtesy of Pardeep Pall, email:pall@atm.ox.ac.uk, and not shown). For equally sized bins the histogram is exponential in nature with highest occurrences associated with the smallest bin value. The second is an observational dataset, compiled by Mohr and Zipser (1996) (hereafter MZ96), of Mesoscale convective systems (MCSs). Fig.~2 shows the normalized size distribution of MCS for 18 different regions. These regions cover all longitudes between 35N and 35S without overlapping and are extremely divers in nature, including areas such as the Maritime Continent and Equatorial Africa. It is therefore quite surprising that the 18 curves on fig.~2 should overlap so well.

Conclusions

Al simulations produced a realistic QBO not unlike the one produced by Scaife et al., 2000 (not shown). Also simulations 1 and 2 show no relative improvements in there ability to reproduce the observed annual cycle in mean zonal winds. A visible improvement is however present in the annual cycle produced by the third simulation with an exponential source strength distribution. The differences between the simulated and Observed annual cycles, for the first and third simulations, is shown in fig.~3. The three maximums in fig.~3a, two negative in April and
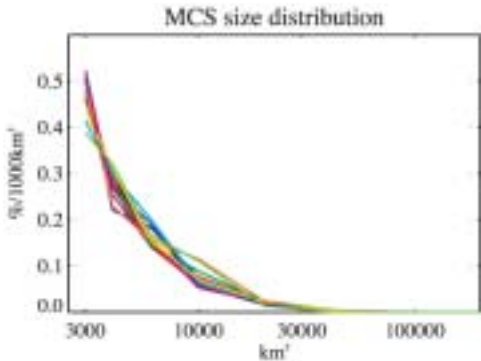

Figure 103. Size distribution of tropical Mesoscale Convective Systems, produced with data obtained from Mohr and Zipser (1996). Different colours represent different areas of the tropics.
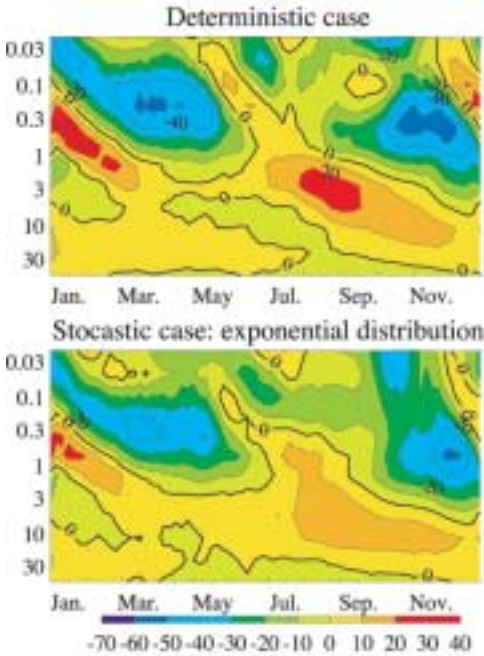

Figure 104. Difference in the equatorial annual cycle of zonally averaged zonal winds between observations an simulations with the Unified Model using: a) a deterministic source strength parameter: b) a stochastic source strength parameter with an exponential distribution.

November and one positive in September, are all visibly reduced in fig.~3b. Hence the simulation with a stochastic source strength distribution derived from observations gives the best combined results.

References

Buizza, R., M. J. Miller, and T. N. Palmer, Stochastic simulation of model uncertainties in the ECMWF ensemble prediction system. Q. J. Meteorol. Soc., 125, 2887-2908, 1999.

Lin, J. W.-B., and J. D. Neelin, Influence of a stochastic moist convective parameterization on tropical climate variability. Geophys. Res. Lett., 27,3691-3694, 2000.

Lin, J. W.-B., and J. D. Neelin, Considerations for stochastic convective parameterization. J. Atmos. Sci., 59, 959-975, 2002.

Lin, J. W.-B., and J. D. Neelin, Towards stochastic deep convective parameterizations in general circulation models. Geophys. Res. Lett., 30(4), 1162, 2003.

Mohr, K. I., and E. J. Zipser, Mesoscale convective systems defined by their 85-GHz ice scattering signature: size and intensity comparison over tropical oceans and continents. Mon. Wea. Rev., 124, 2417-2437, 1996.

Palmer, T. N., A nonlinear dynamical perspective on model error: A proposal for non-local stochastic-dynamic parameterization in weather and climate prediction models. Q. J. R. Meteorol. Soc., 127,279-304, 2001.

Salby, M. L., and R. R. Garcia, Transient response to localized episodic heating in the tropics. Part I: Excitation and short-time near-field behaviour. J. Atmos. Sci., 44, 458-498, 1987.

Scaife A. A., N. Butchart, C. D. Warner, D. Stainforth, and W. A. Norton, Realistic Quasi-Biennial Oscillations in a simulation of the Global Climate. Geophys. Res. Lett.,26, 3481-3484, 2000.

Estimating the magnitudes of "missing forces" induced by gravity waves in the atmosphere

Chris Warner, Björn Haßler and Michael McIntyre, Dept. of Applied Mathematics and Theoretical Physics, University of Cambridge.

We are working on the problem of <u>estimating the magnitudes of "missing forces" induced by gravity waves in the atmosphere</u>. These missing forces – hitherto unrecognized in the standard paradigm on which gravity-wave parametrization is based – are persistent or cumulative forces which depend not on wavebreaking or other dissipative processes, but on changes in the horizontal wavevector due to horizontal refraction. They may depend significantly on the time-dependence as well as on the horizontal refraction of the background. Ray tracing numerical experiments are under way to investigate the importance of horizontal refraction and the consequent missing forces, and to attempt to answer to the question of whether such forces can continue to be ignored in gravity wave parameterizations.

A start on the underlying theory can be found in a paper by Bühler and McIntyre (2003, J. Fluid Mechanics 492, 207-230), and it is planned to report further progress at the Chapman Conference in Hawaii next January.

Impact of Climate Variability and Change

Climate Variability and local markets

Mike Bithell, Dept. Of Geography, University of Cambridge,
Richard Washington, Bill Macmillan, Mark New, School of Geography and the Environment, Oxford,
Edmund Chattoe, Dept. Of Sociology, University of Oxford
Sukaina Bharwani, Gina Ziervogel, Tom Downing, Stockholm Environment Institute, Oxford,
Matthew Swann, Alex Haxeltine, School of Environmental Sciences, University of East Anglia

What are the effects of coupling market processes in a subsistence farming community to the a system that can provide seasonal forecasts? In a previous newsletter we reported the first results from a model that coupled a simple parametrization of crop planting and harvest to an agent based representation of African farmers (part of the Tyndall centre project "Climate outlooks and agent based simulation of adaptation in Africa"). At that stage no process was available in the model to allow the farmers to buy food or sell their crops. Such an ability might allow them to compensate for climate fluctuations by setting aside capital for purchase of food in future deficit years. The model now incorporates a simple market that permits this to take place.

The preliminary implementation allows farmers to buy and sell as much as they wish. In practice this means that they sell all surplus over the current years needs, or buy just what is required to survive the current year. The market has fixed prices that do not change with time, and the farmers have to take the price as given, whether buying or selling. Although this is a very simple case, when combined with seasonal forecasts, it supplies some insight into how markets might interact with climate information. Forecasts alone can only make a limited impact upon this situation, and with seasonal forecasts that are correct 65% of the time, 8 member households are still liable to run out of food as a consequence of yearly fluctuations in rainfall (see Figure 105).

Similarly, the ability to trade on its own is not necessarily helpful. Although there is a threshold for consumption below which a steady income is possible, for an 8 member household with a single 1ha field, this means eating approximately 20% less

food than would comfortably be needed for survival. However, when the forecasts are combined with the ability to trade, the situation is much improved. The effect of bad years can be overcome by trading, even for farmers that only take into account conditions for the current year. However, the farmers in this case still are not quite able to consistently generate income. Further development will incorporate markets where prices can fluctuate with time, and will generalize to farmers with a wider range of behaviour, including the ability to plant more than one crop type.

Reference

"Agent-based social simulation: a method for assessing the impact of seasonal climate forecasts applications among smallholder farmers" by Gina Ziervogel, Mike Bithell, Richard Washington and Tom Downing accepted for publication in Agricultural Systems
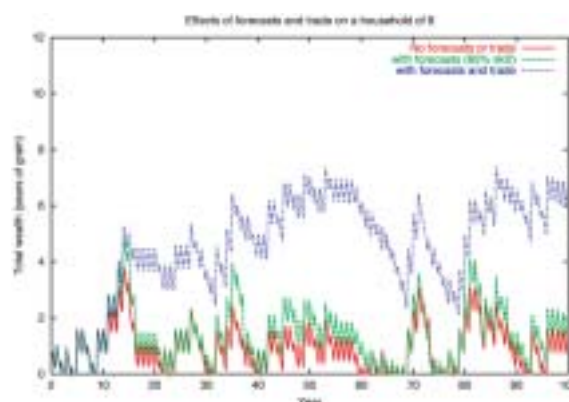

Figure 105.

Large-area simulations of crop productivity using atmospheric circulation model output.

Andrew Challinor, Julia Slingo, CGAM, Dept. of Meteorology, University of Reading,
Tim Wheeler, Peter Craufurd, Dept. of Agriculture, University of Reading.

The development of numerical crop and weather simulation models is ongoing. Increasing skill in both areas presents an opportunity to combine these models into a single forecasting system. Such a system could contribute to the forecasting of food provision on seasonal to inter-decadal timescales. The seasonally arid tropics provide excellent conditions for the development of a combined forecasting system: there is a strong seasonal signal in weather, and much of the agriculture is rainfed crops, with yields that depend upon weather. One key design issue is that of spatial scale: General Circulation Models (GCMs) operate on relatively

large spatial scales (tens to hundreds of kilometres), and there is an uncertainty associated with downscaling GCM output. Crop models, however, tend to have greater skill at small scales (tens to hundreds of metres), where non-linear physiological processes and responses to local environment may be accurately represented. Hence the choice of the spatial scale at which to operate a combined system is of paramount importance.

Consideration of these issues at The University of Reading has lead to the development of the General Large-Area Model for annual crops (GLAM; Challinor *et. al.* 2002,2003). The model is

sufficiently process-based to simulate crop productivity over a range of tropical environments, whilst being simple enough to avoid the need for large amounts of location-specific input data or calibration. In this way, the model aims to combine the benefits of more empirical modelling methods (low input data requirement, validity over large areas such as the grid-scales of general and regional circulation models and re-analysis) with the benefits of a process-based approach (the potential to capture variability due to different intra-seasonal weather patterns, and hence increased validity under future climates). The model is intended for annual crops, and uses crop parameters which can be estimated from the literature. Some key crop characteristics can be varied in order to explore their effect on productivity in the context of climate variability across a range of time scales.

Recently, GLAM has been used to investigate the impact of climate variability on groundnut production in India, using ERA40 data as input. Precipitation biases in ERA40 have a significant impact on the accuracy of yield simulations. Where there is a strong climate signal in yields and ERA40 simulates the seasonal rainfall cycle well, a simple mean bias correction improves accuracy. The impact of high temperatures at critical crop phenological stages is also being investigated. In groundnut, high temperatures near anthesis can cause pegs to abort, and this can drastically reduce yields (Wheeler *et. al*. 2000). Initial results using the ERA40 data suggest that temperatures in India during the growing season between 1966 and 1989 have not seriously threatened yields in this way. A similar study using a HadRM3 scenario for 2041-2060 (courtesy of the Indian Institute of Tropical Meteorology) suggests that this situation may change (Figure 106).

Climate change can impact crop productivity in various ways: changes in rainfall intensity and distribution have an obvious impact, mean temperature increases shorten crop duration (and therefore tend to reduce yields), and higher CO_2 levels mean that photosynthesis rates rise, and biomass and yields rise also (the so-called CO_2 fertilisation effect). GLAM simulations have been used to assess the   relative importance of these effects and the uncertainties associated with them. The key parameter for assessing the CO_2 effect is Transpiration Efficiency, and uncertainty in its estimation under increased CO_2 contributes significant uncertainty in yield estimation for these simulations (Figure 107).

There are many sources of error and uncertainty in the use of atmospheric circulation models to simulate yields. Errors coming from the atmospheric models can be assessed in terms of their impact on the errors in the yield simulations. Despite these sources of error and uncertainty, modelling approaches can fruitfully explore the sensitivity of crops to weather and climate. Many of the impacts of climate change will be regional and a combined weather and productivity prediction system such as the one being developed here is a useful way of assessing potential impacts on a pragmatic spatial scale, without the need for downscaling weather data.
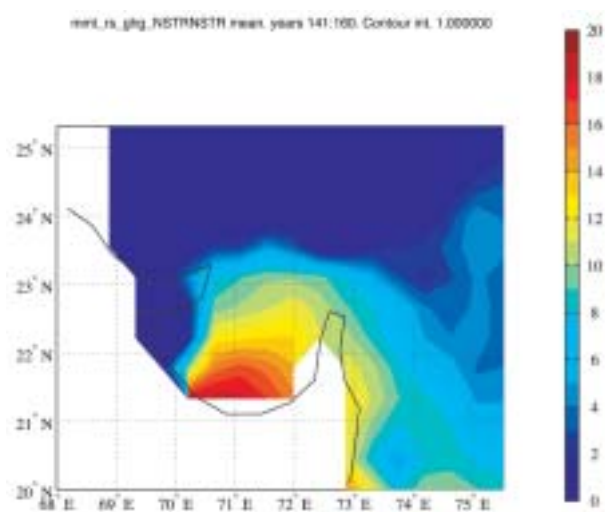

Figure 106. The number of stress-days during anthesis (flowering) for a groundnut crop in Gujarat, as simulated by GLAM with HadRM3 input weather data for the period 2041-2060 with 1% per annum (compound) greenhouse gas (GHG) increase (IS92a). Stress periods of just one day can have a serious impact on yields (depending on the timing).
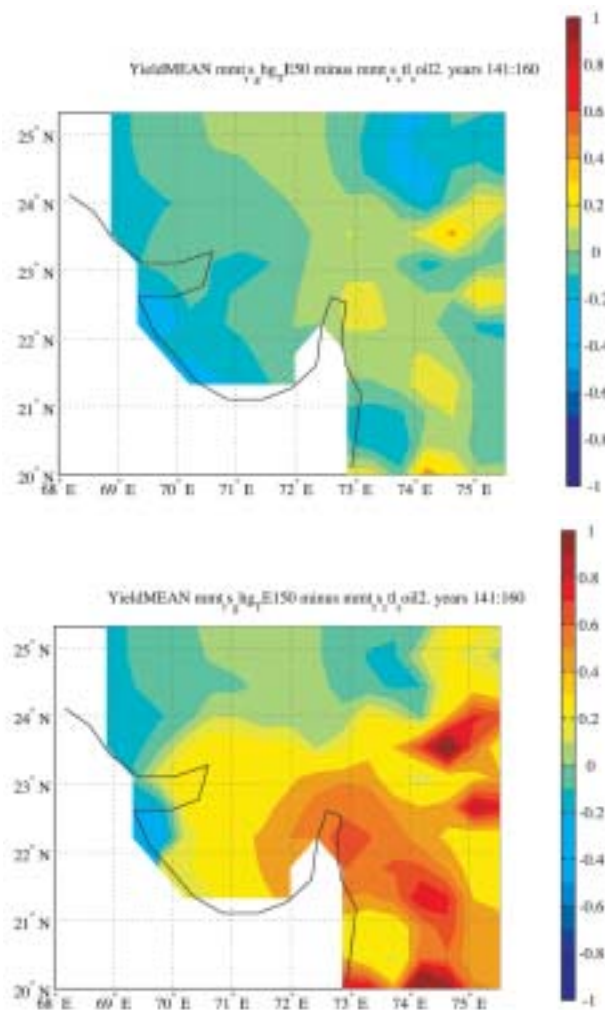

Figure 107. Fractional mean yield changes for IS92a scenario from control simulation (current GHG levels) for the period 2041-2060 using a) lower (1.5 * control) and b) upper (2.5 * control) estimates of Transpiration Efficiency.

References

Challinor, A.J., J. M. Slingo, T.R. Wheeler, P.Q. Craufurd and D. I. F. Grimes, 2003: Towards a combined seasonal weather and crop productivity forecasting system: Determination of the working spatial scale. Journal of Applied Meteorology 42, 175-192

Challinor, A.J., T.R. Wheeler and J. M. Slingo, 2002: Large-area crop modelling techniques for use with GCMs. UGAMP Newsletter 26, 9.
Wheeler, T. R., P. Q. Craufurd, R. H. Ellis, J. R. Porter, P. V. Vara Prasad, 2000: Temperature variability and the annual yield of crops, Agric. Ecosyst. Environ. 82, 159-167

Climate and health indices for use in a health forecasting model over monthly to seasonal time scales

Michelle Cox and Glenn McGregor, University of Birmingham

From 1976-1983, 55% of excess winter mortality in the UK was due to circulatory disease (Curwen *et al*., 1990). The aim of this study is to develop a climate-based health forecast model for winter to assist the UK health sector with winter capacity planning. Monthly and seasonal climate indices have been calculated to describe the relationship between Ischaemic heart disease (IHD) mortality and climate in four UK counties. Daily IHD mortality (International Classification of Diseases classes 410.0-414.9) from 1974-1999 was obtained from the Office for National Statistics for four UK counties Hampshire, West Midlands, West Yorkshire and Tyne and Wear. The mortality data were divided into five categories (all, male, female, under 65 years and 65 years and over). Daily surface maximum (max) and minimum (min) temperatures were obtained from The British Atmospheric Data Centre (BADC) for meteorological stations within these counties. Where available, multiple station data were averaged to construct a maximum and minimum temperature series for each county.

The highest significant correlations between total mortality and average monthly temperature (max and min) were found for January for the counties Hampshire, West Midlands and Tyne and Wear. For West Yorkshire the most significant correlations were found in February. The rates identified using linear regression

(errors using delete-1 Jackknife method; Duchesne and MacGregor, 2001) for the number of deaths (65 years and over) per degree over January were –11 with error 4 (Hampshire), -21 with error 4 (West Midlands) and –10 with error 2 (Tyne and Wear). The rates found for West Yorkshire (over 65 age group) in February were –18 deaths per degree with an error of 3. The small error relative to the total mortality rate suggests that these indices may be applied as parameters in a health forecast model. For one degree temperature intervals covering the range of max/min temperatures for each county, the number of days below these temperature thresholds were calculated. The temperature threshold 'day count' with the most significant correlation with total winter mortality was identified for each county. The thresholds identified for the over 65 year age group were maximum temperatures below 9ºC (Hampshire), 7ºC (West Midlands), 5ºC (Tyne and Wear) and 4ºC (West Yorkshire). This suggests acclimatisation plays a part in determining the temperature sensitivity of these groups.

References

Curwen M., 1990: Excess winter mortality: a British phenomenon? Health Trends 22(4):169-175.
Duchesne C., J.F. MacGregor, 2001: Jackknife and bootstrap methods in the identification of dynamic models. Journal of Process Control 11:553-564.

Constraining Sea Ice Model Parameters Using Sea Ice Thickness and Concentration Data

Paul Miller (pm@cpom.ucl.ac.uk), Douglas Cresswell, Seymour Laxon, Daniel Feltham, Robert Potter, Centre for Polar Observation and Modelling, University College London, Gower Street, London WC1E 6BT, United Kingdom. (www.cpom.org)

Introduction

Change in Arctic sea ice represents one of the largest uncertainties in the prediction of future temperature rise (1,2) and an improved understanding of ice pack variability is critical to determine whether observed and predicted changes are natural or anthropogenic in origin (3,4). It is therefore important to improve the representation of sea ice in general circulation models (GCMs), and to arrive at a better understanding of the underlying physics and feedback effects which determine its variation.

We use a stand-alone sea ice model with prescribed atmospheric and oceanic forcing to simulate observed changes in Arctic sea ice. The simulations are then compared with observed sea ice thickness and sea ice extent. This will allow us to pinpoint those processes it is most necessary to include in future GCMs.

Data Sets

The sparseness of sea ice thickness observations until now has meant that our understanding of the regional, and inter-annual,

variability of sea ice thickness was entirely based on numerical models of the Arctic (5-8) with little or no validation of the model predictions.

In this project we use a new time-series of Arctic ice thickness over the 8-year period 1993 to 2001, derived from satellite altimeter measurements of ice freeboard (9), to validate our model. The region of coverage (ROC) extends to 81.5N, covering more than half of the permanent sea ice cover, and includes the Beaufort, Chukchi, East Siberian, Kara, Laptev, Barents and Greenland Seas. The data are available from October to April each year and offers us the first opportunity to study Arctic sea ice on basin scales.

The second data set we use is a time series of sea ice extent since 1994 derived from measurements of ice concentration using passive microwave data (10). This data set extends to 87.6N and is available daily, but We average the data into monthly estimates of sea ice extent to validate our model.
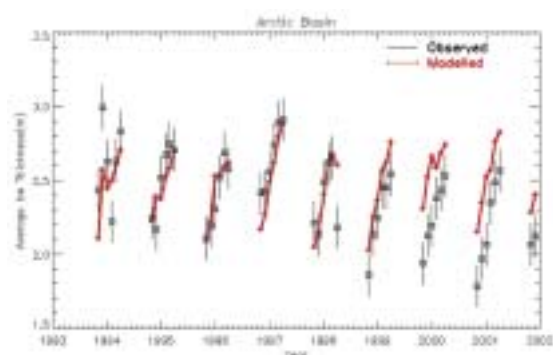
Figure 108. Monthly-averaged ice thickness plotted against the observed ice thicknesses from Nov. 1993 to Dec. 2001. (The area considered is the Arctic Basin below 81.5N, so the Kara, Barents and Greenland Seas are excluded.)
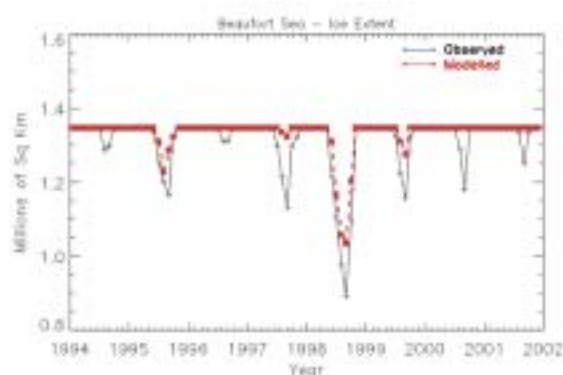

Figure 109. The observed and modelled ice extent in the Beaufort Sea from Jan. 1994 to Dec. 2001.

Model Description

The model we use is CICE: the Los Alamos Sea Ice Model (version 3). It has multiple ice thickness categories at the sub-grid scale and calculates ice thermodynamic growth and decay for each thickness category explicitly. It also simulates the ice ridging processes which redistribute ice among the various thickness categories. The ice pack has a grid size of 100km and is assumed to have an elastic-viscous-plastic (EVP) rheology (11).

To force the model we use surface winds, temperatures and humidity, as well as longwave and shortwave radiation fluxes and snowfall from the ECMWF's first ERA-40 reanalysis.

In each case the model was run from 1980 to 2001 after a 10-year spin-up period.

Results

Figure 108 shows the model's monthly-averaged ice thickness plotted against the observed ice thicknesses from Nov. 1993 to Dec. 2001. (The area considered is the Arctic Basin below 81.5N, with the Kara, Barents and Greenland Seas excluded.) The model and data agree closely (to within ~30cm) during the 1990s, but diverge after 1999.

Figure 109 shows the observed and modelled ice extent in the Beaufort Sea. The Beaufort Sea is covered with ice during the winter, but the extent to which it retreats each summer is very variable. In particular, the summer of 1998 saw a record minimum sea ice extent in the whole Western Arctic (12), and this is evident here. The model does capture this large signal, but once again overestimates the extent (and thickness) in the summers since 1999.

Discussion

It is important to validate the predictions of sea ice models against as many data sets as possible. We have used two data sets in this study, of Arctic basin-scale ice thickness and extent, and shown that the model captures both the inter-annual and seasonal variations well. However, there is room for improvement, and the first step is to vary those parameters in the model which are poorly known but strongly influence the modelled ice thickness and extent, such as the ice strength and reflectivity (6).

Some parameters may also be optimized against other data sets, for example ice motion fields (6).

There are also improvements that could be made to the model physics. We could using a better albedo parameterisation, for example, refine the model of the ridging processes, or model summer melt ponds explicitly.

Parameter optimisation and model refinement, in tandem with comparisons with multiple observational data sets, should result in a better parameterisation of existing processes in GCMs, and identify new processes which should be included in future GCMs in order to simulate those properties of the ice pack which influence the climate.

References

Carson, D. J. Climate modelling: Achievements and prospects. Q. J. R. Meteorol. Soc. 125, 1-27 (1999).

Rind, D., Healy, R., Parkinson, C. & Martinson, D. The role of sea ice in 2xCo2 climate model sensitivity: Part II: hemispheric dependencies. Geophys. Res. Lett. 24, 1491-1494 (1997).

Houghton, J. T. et al. Climate Change 2001: The Scientific Basis (Cambridge University Press, 2001).

Rothrock, D., Zhang, J. & Yu, Y. The arctic ice thickness anomaly of the 1990s: A consistent view from observations and models. J. Geophys. Res. 108, 28-1 - 28-10 (2003).

Polyakov, I. V. & Johnson, M. A. Arctic decadal and interdecadal variability. Geophys. Res. Lett. 27, 4097-4100 (2000).

Chapman, W. L., Welch, W. J., Bowman, K. P., Sacks, J. & Walsh, J. E. Arctic sea ice variability: Model sensitivities and a multidecadal simulation. J. Geophys. Res. 99, 919-935 (1994).

Zhang, J. L., Rothrock, D. & Steele, M. Recent changes in Arctic sea ice: The interplay between ice dynamics and thermodynamics. J. Clim. 13, 3099-3114 (2000).

Zhang, Y. X. & Hunke, E. C. Recent Arctic change simulated with a coupled ice-ocean model. J. Geophys. Res. 106, 4369-4390 (2001).

Laxon, S. W., Peacock, N. R. & Smith, D. Inter-annual Variability of Arctic Sea Ice Thickness. Nature (2003), in press.

Cavalieri, D., C. Parkinson, P. Gloerson, and H.J. Zwally. 1999, updated 2002. Sea ice concentrations from Nimbus-7 SMMR and DMSP SSM/I passive microwave data. Boulder, CO, USA: National Snow and Ice Data Center. CD-ROM. nsidc.org

Hunke, E. C. & Dukowicz, J. K. An Elastic-Viscous-Plastic Model for Sea Ice Dynamics. J. Phys. Oceanography 27, 1849-1867 (1997).

Maslanik, J. A., Serreze. M. C. & Agnew T On the Record Reduction in 1998 Western Arctic Sea-Ice Cover. Geophys. Res. Lett. 26, 1905-1908 (1999).
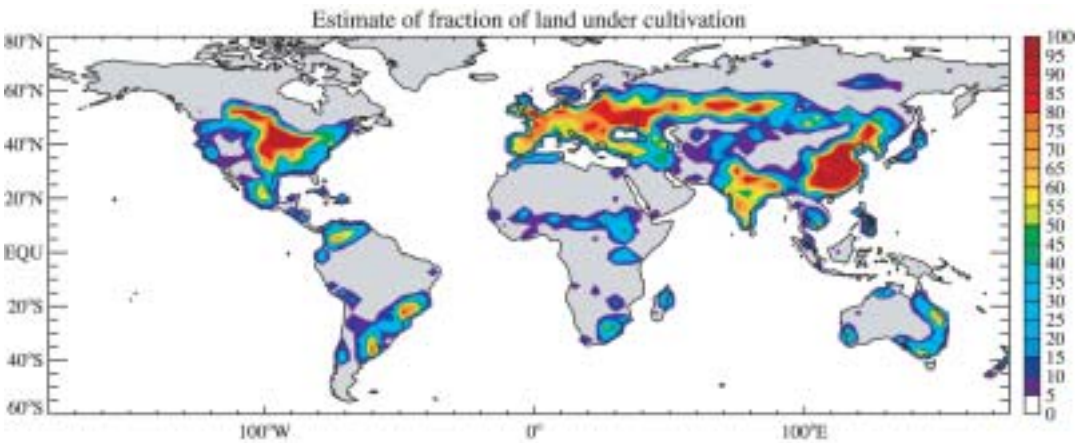
Estimate of fraction of land under cultivation

Investigating the interaction of crops and climate

Tom Osborne, Julia Slingo, Tim Wheeler, David Lawrence, Andrew Challinor, CGAM, Dept. of Meteorology, University of Reading

Feedbacks between the land surface and the overlying atmosphere have been investigated extensively since the hypothesis of Charney (1975) that changes in vegetation cover in Sub-Saharan Africa could alter the interannual variability of Sahelian rainfall. Numerous other examples of vegetation – atmosphere interactions, such as deforestation, have been investigated with modelling and/or observational studies. In a recent study, Osborne et al. (2003) examined the sensitivity of tropical climate in HadAM3 to vegetation. Vegetation plays a key role in the hydrological cycle. On the shorter timescale, the vegetated canopy intercepts rainfall, which is re-evaporated into the boundary layer. On a longer timescale, deep-rooted vegetation can access sub-surface soil water used for transpiration and is thus evaporated from the leaf surface. Therefore, vegetation alters the partitioning of available energy at the surface between sensible and latent heat fluxes (i.e. decreases the Bowen ratio). The authors found that the tropical rainforests and the predominantly grassland vegetation of China significantly influenced the local climate.

It is possible to study these interactions with atmospheric GCMs due to the sophistication of their land surface schemes. The Met Office Surface Exchange Scheme (MOSES) is typical of such schemes. It explicitly models the surface hydrological cycle, the movement of water through the soil layers and calculates the rate of photosynthesis of vegetation, which is dependent on the vegetation type and the climate. The latest version of MOSES uses a tiling scheme to represent heterogeneous vegetation in a gridbox. A gridbox is represented by fractions of nine surface tiles (5 plant functional types, ice, water, urban and soil). For each tile, fluxes of momentum, moisture and energy are calculated which are then aggregated together with respect to their fractional coverage to give gridbox mean values to the atmospheric model. The characteristics of each plant functional type (e.g. canopy height, leaf area index) are held constant throughout the year in the standard set-up of the model. Lawrence and Slingo (2003) have shown recently, however, that prescribing a realistic annual cycle of vegetation characteristics (plant phenology) can significantly influence the climate.

Figure 110 shows that crops extensively cover certain areas of the Tropics. If the cultivation of crops replaces areas of tropical rainforest then most of the Tropics would be covered with crops.
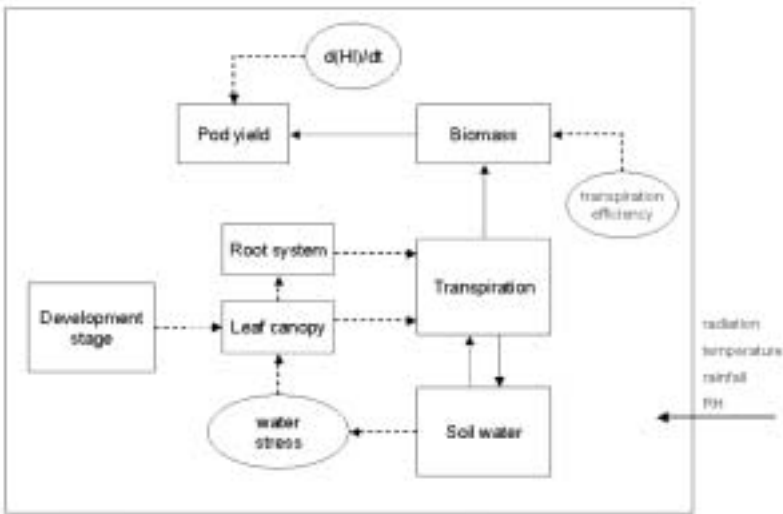
Therefore, it is important to have a realistic representation of crops in the land surface schemes. Crop growth and development is strongly coupled to the environment, therefore, the prescription of an annual cycle is not applicable. The influence of weather and climate on growth and development for the major crops is well understood due to a large amount of experimental work. This understanding is used to formulate crop models, which are used to aid farmers' decision making. Crop models, therefore, are developed for use at the field scale and include many crop and soil type parameters. Challinor et al. (2003) have developed the General Large Area Model (GLAM) for annual crops to work in regions where there is a strong correlation between the weather and crop yield. GLAM has fewer parameters than conventional crop models and can operate over areas equivalent to a GCM gridbox.

Figure 111 shows the variables and processes modelled by GLAM. The aim of this work is to incorporate GLAM into MOSES resulting in a crop tile that can grow in response to the climate of the atmospheric. This work differs to offline simulations of crop growth because the influence of the crop itself on the climate will also be influenced. Once the coupled system is complete we aim to investigate this complicated feedback further.

References

Challinor, A.J., J.M. Slingo, D.I.F. Grimes, T.R. Wheeler and P.Q. Craufurd. 2003: Design and optimisation of a large-area process-based model for annual crops. Submitted Agric. And Forest. Meteor/.

Charney, J.G., 1975: Dynamics of deserts and droughts in the Sahel. Quart. J. Roy. Meteor. Soc.,101,193-202.

Lawrence, D.M., and J.M. Slingo, 2003: Incorporation of an annual cycle of vegetation into a GCM. Part II: Global impacts on climate and hydrology. Accepted Clim. Dyn.

Osborne, T.M., D.M. Lawrence, J.M. Slingo, A.J. Challinor and T.R. Wheeler 2003: Influence of vegetation on the local climate and hydrology in the Tropics: Sensitivity to soil parameters. Accepted Clim. Dyn.

Advances in modelling and techniques

APE - the Aqua-Planet Experiment project
http://www-pcmdi.llnl.gov/amip/ape

M. Blackburn and B. J. Hoskins, The University of Reading, UK;
R. B. Neale, NOAA-CIRES Climate Diagnostics Center, Boulder, USA;
D. L. Williamson, National Center for Atmospheric Research, Boulder, USA;
P. J. Gleckler, Program for Climate Model Diagnosis and Intercomparison, Livermore, USA.

Introduction

CGAM, together with partners at NOAA, NCAR and PCMDI, is coordinating a new atmospheric model intercomparison project endorsed by the World Climate Research Programme. This is APE, the Aqua-Planet Experiment, in which modelling groups perform a series of atmospheric GCM integrations on a water covered planet using simple prescribed distributions of sea surface temperature. The project aims to compare the simulated climates of these idealised planets, focusing on the distribution and variability of convection in the tropics and the behaviour of the storm-tracks in mid-latitudes. APE spans the gap between dynamical core experiments, used to test new numerical schemes for the resolved fluid flow in GCMs, and existing intercomparison projects such as AMIP and CMIP, which include the radiative and moist parameterisations in the GCMs and apply them to the real Earth, with all its complexities of land-sea contrast, orography and SST variability.

The concept of an Aqua-Planet Experiment project arose from the work of Neale and Hoskins (2000a), although such idealised scenarios have been used for many years to aid understanding of tropical convection, its variability and its parameterisation in GCMs. One of the first such experiments, by Hayashi and Sumi (1986), used a globally uniform SST to investigate the propagation of organised convection in the Madden-Julian Oscillation.

Experimental Design

APE consists of a series of eight, 3.5 year, GCM integrations, forced by idealised SST distributions. The first five SSTs (Figure 112) are zonally symmetric and vary the latitudinal profile in the tropics.

These experiments aim to span a range of behaviour of the inter-tropical convergence zone (ITCZ), from a single equatorial peak through to a tropical radiative-convective equilibrium regime in the case of the "flat" SST profile, for which theory suggests that a Hadley circulation cannot be maintained. The fifth profile shifts the SST maximum to 5degN, to investigate an asymmetric tropical regime. The remaining three SST distributions (Figure 113) add tropical anomalies to the control profile, with limited or global extent in longitude. Both the local convective-dynamical response and remote wave-induced teleconnections will be of interest here.

The experimental protocol for APE is specified in a similar manner to AMIP, comprising a set of experimental requirements and recommendations. A symmetrised ozone distribution is provided in addition to the prescribed SSTs. North-south
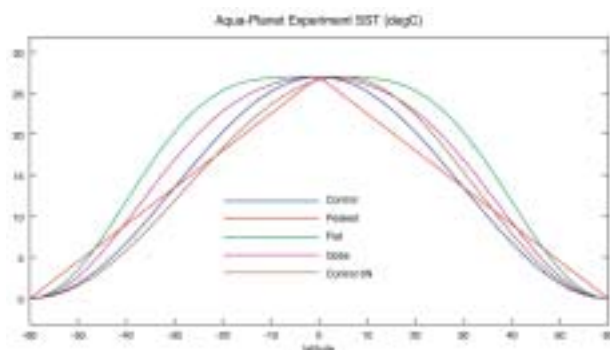

Figure 112. Zonally symmetric SST distribution specified for the Aqua-Planet Experiment

symmetry of the radiative forcing is achieved either by using perpetual equinoctial conditions or (preferably) by simplifying the planet's orbital geometry. Full details can be found at the APE website.

Current Status and Future Plans

The last year has involved a detailed planning phase and launch of the computational phase of APE. 16 modelling groups from 7 countries are currently participating. Specified data from the experiments will be collected and quality controlled at PCMDI, with access open to all APE participants for comparative diagnosis. A workshop for participating groups will be held in Reading in early June 2004.

Results already published using the APE SSTs have documented aspects of the climate and convective variability in the UK Met Office model HadAM3 (Neale and Hoskins, 2000b), and revealed an unexpected dependence of ITCZ behaviour on the choice of dynamical core in the NCAR Community Climate Model (Williamson and Olson, 2003), due primarily to a timestep-dependence of the dynamics-parameterisation coupling in the model.

APE aims to provide a benchmark of current model behaviour and, more importantly, to stimulate research to understand the causes of inter-model differences, arising from different subgrid-scale parameterisation suites, different dynamical cores, and different methods of coupling the two. The current experiment is hopefully only a beginning, prompting further diagnostic and experimental work using the participating models. There is already
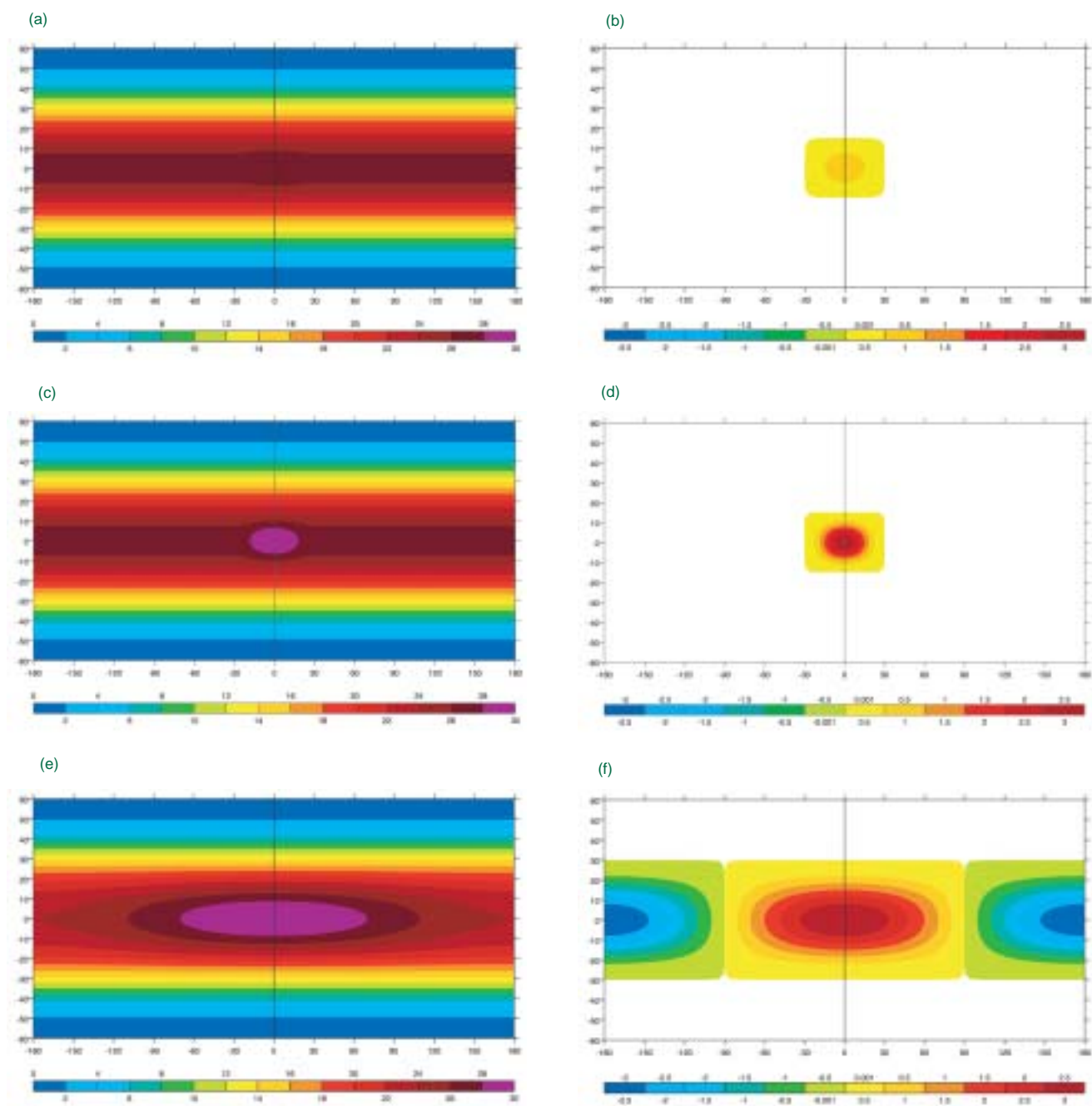
(a)

(b)

(c)

(d)

(e)

(f)

Figure 113. Global distributions of SST and their departures from zonal symmetry, for the tropical SST anomaly experiments in APE.

interest in aqua-planet experiments in which the atmospheric GCMs are coupled to a slab ocean.

At Reading the aqua-planet scenario is being used to study the diurnal cycle of tropical convection and it will be used as the starting point for projects on tropical – extratropical interaction and on the hydrological budget and climate change.

References

Hayashi, Y.-Y. and Sumi A. 1986 The 30-40 day oscillation simulated in an 'aqua-planet' model. J. Meteorol. Soc. Japan, 64, 451-4677.

Neale, R. B. and Hoskins B. J. 2000 A standard test for AGCMs and their physical parameterizations. I: The proposal. Atmos. Sci. Letters, 1, 101-107.

Neale, R. B. and Hoskins, B. J. 2000 A standard test for AGCMs and their physical parameterizations. II: Results for The Met. Office Model. Atmos. Sci. Letters, 1, 108-114.

Williamson, D. L. and Olson, J. G. 2003 Dependence of aqua-planet simulations on time step. Q. J. R. Meteorol. Soc., 129, 2049-2064.

Introducing UMCET, the Unified Model Climate Ensemble Toolkit

Paul Burton (paul@met.rdg.ac.uk), Computational Scientist, CGAM. Web: http://www.cgam.nerc.ac.uk/~paul/

In late 2002 EPSRC and NERC took delivery of one of the world's fastest supercomputers, a 1280 processor IBM known as "HPCx". This machine was procured in order to provide a "world-class service for world-class research" to the UK's scientific community. One year later it is clearly starting to deliver on its promises in many areas of research, but what about atmospheric and climate science?

UGAMP has been using the UK Met Office's Unified Model (UM) for many years now as its primary tool to investigate basic climate processes in the atmosphere-ocean system, and to better understand and predict climate change. Although the UM is written to take advantage of massively parallel processor (MPP) machines, such as HPCx and the Met Office's Cray T3E and NEC SX-6 systems, it is not able to run efficiently on large numbers of processors. This is especially true for the low-resolution configurations typically used for climate prediction work. At large processor counts the amount of work per processor becomes vanishingly small, and the computational costs become dominated by the synchronisation and communication between processors rather than the real work done on them.

The HPCx system is specifically aimed at "capability" computing – these are computational jobs which require vast computational resource, in contrast to "throughput" computing, where individual jobs require only a modest computational resource. The most widely used UGAMP climate configurations of the UM currently fit into "throughput" model, rather than the "capability" model. The charging model and job scheduling policies employed by HPCx directly favour "capability" jobs, and as such, do not make it the best platform for running typical UGAMP UM jobs on.

If we want to take full advantage of the world-class facilities offered to us by HPCx then it is obvious that we will need to take a new approach. There are a number of ways that the UM can be made to become more of a "capability" job, which also give real benefit to the scientists using it, such as:

Increasing the resolution. A doubling of resolution (i.e. halving of grid lengths) results in approximately a sixteen-fold increase in computational cost (2x2x2 for the three spatial dimensions, and a further factor of 2 for the halving of timestep required).

Improving the science and numerical solvers. Experience tells us that improved physical parameterisation schemes and numerical solvers often increase the computational cost of the model.

Coupling to other models. Obviously, including additional models within the UM system will increase its computational cost.

Although all of these will give real benefit to scientists using the UM, there is one fundamental problem. That is that these all require a large amount of effort to research, develop and implement. The good news is that the Met Office and various UGAMP groups are making this effort, all three of these improvements to the UM are being actively investigated and developed.

This, however, is not so useful to UGAMP if we want to be able to take full advantage of HPCx today. For this reason, another approach has been taken, which should also offer real benefit to scientists using the UM whilst ensuring that it becomes sufficiently "capability" to run on HPCx.

Instead of just "improving" the model itself, another approach is to investigate and better understand the sensitivities of the model and the system it is modelling, so that we can objectively quantify the confidence we have in the evolution and outcome of a model, and the effect of the many and varied forcings of the climate system. Such an approach has been used for many years in weather forecasting – ECMWF for example use a 51 member model ensemble to generate their 10 day forecasts.

This approach has the benefit that it is relatively easy to implement, requiring little change to the model itself, just an infrastructure harness to allow multiple ensemble members to run simultaneously. While being easy to implement, it has the positive effect of generating UM jobs which require very large computational resource, and are real "capability" jobs, suitable for running on HPCx.

Over the past few months CGAM have developed such an "infrastructure harness" called the "Unified Model Climate Ensemble Toolkit" (UMCET). Using UMCET it should be relatively easy for a scientist to run a large (typically we expect many tens of members) ensemble of UM jobs on HPCx. We hope that the principles we have applied to the design and implementation of UMCET can be easily applied to other numerical models, enabling them also to take advantage of the facilities offered by HPCx.

Whilst forecast ensembles typical work by perturbing the initial conditions of each member, climate ensembles need some additional, more sophisticated types of "perturbations" for members:

Forcing: For example we may want to vary the amount of CO_2 in the atmosphere of each member to investigate the response of the climate system to increasing amounts of the gas.

Parameterisation: The climate system is potentially highly sensitive to some of the model parameterisations. By varying certain constants and parameters within these schemes in different members, we could start to better understand these sensitivities.

The current functionality offered by UMCET provides:

Infrastructure to allow multiple UM jobs (ensemble members) to run as a single job on HPCx.

Automatic generation of all the necessary job control files to run an UMCET ensemble based on a simple user configuration file.

Ability (via the configuration file) to vary any UM namelist variable (or introduce new variables), allowing the parameterisations to be perturbed between ensemble members. The values of these variables for each member can be exactly described by the user, or randomised within defined limits.

Ability (via the configuration file) to allow each ensemble member to use a different model executable, which could potentially include different parameterisations or numerical solvers.
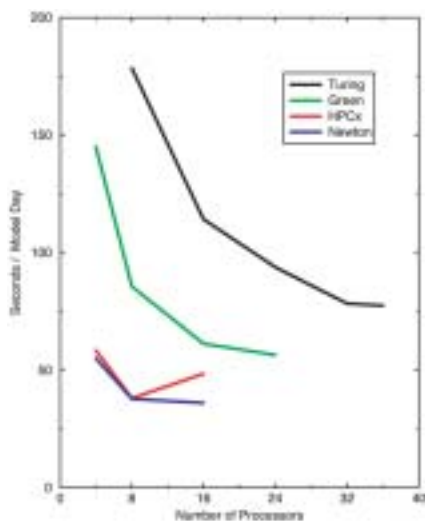
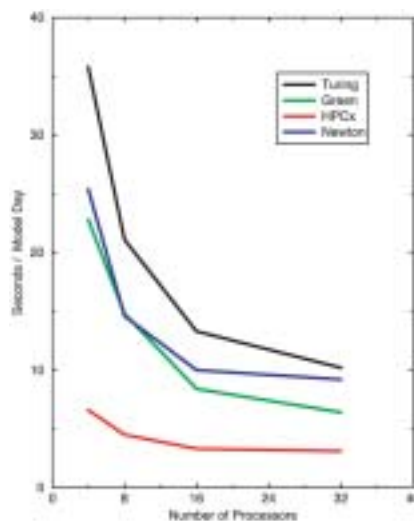Figure 114. A 30 day HadAM3 (96x73x19) atmosphere only run.

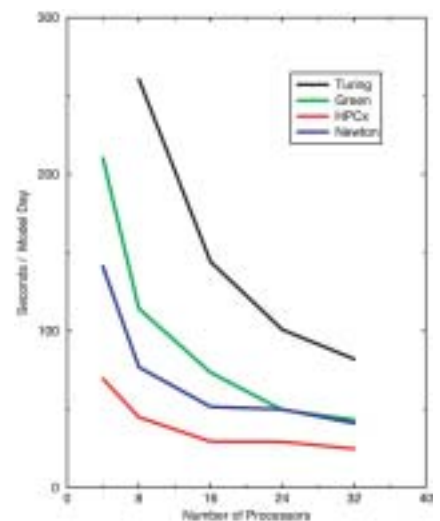Figure 115. A 30 day HadOM2 (98x73x20) ocean only run.

Figure 116. A 10 day HadCM3 (96x73x19 atmosphere, 190x144x20 ocean) coupled run.

Ability (via the configuration file) to allow each ensemble member to use different input files. This gives the potential for the user to vary initial conditions between members and/or vary forcings (which are supplied via ancillary files) between members.

Ability to vary more than one variable/input file within an ensemble, such that the effect of the individual perturbation can be identified as well as its interactions with other perturbations.

We hope to add to the functionality offered by UMCET in the future. Specifically we plan to provide:

• Tools to allow perturbation of UM data sets (such as start dumps and ancillary files).

• Diagnostic tools to aid the analysis of the vast amounts of data that will be produced by large ensembles.

For this development to proceed, we need your help. If you are interested in using UMCET, then please read the information provided on the web page (see links below). Please email me and let you know what functionality you require (especially in the two areas highlighted previously).

We hope that you will find UMCET to be a useful and productive tool. Our aim is that it will start to enable the atmospheric science and climate research community within the UK to make good use of our world class computing facilities at HPCx.

Links

HPCx: http://www.hpcx.ac.uk/
UMCET: http://www.cgam.nerc.ac.uk/~paul/UMCET

Running the Unified Model after Turing Retirement

Jeff Cole (jeff@met.rdg.ac.uk), CGAM, Dept. of Meteorology, University of Reading.

Currently the main national HPC service used for running the Unified Model is Turing. This service is due to end on Midnight 31st December 2003, and all of the UM modelling done on this machine will need to transfer elsewhere. There are 3 alternative platforms available, a pair of SGI Origins (Fermat and Green), a SGI Altix (Newton) and an IBM p690 (HPCx). HPCx is designated to be a capability service and has incentives in place to encourage this type of job, whereas capacity jobs are discouraged. A capability job is one that is defined to use at least 512 processors (out of 1280), whereas a capacity job is defined to be one that uses less than 32 processors for more than one hour. The type of jobs that are currently run on Turing are definitely capacity jobs and are therefore unsuitable for running on HPCx. The type of jobs that are suitable for running on HPCx are high resolution, new dynamics, coupled UM runs and large ensemble UM runs, see separate newsletter article by Paul Burton on a framework for ensemble modelling. Therefore the most appropriate option for the current Turing jobs is to transfer them to one of the CSAR SGI machines.

One impediment to transferring code from Turing was the fact that ocean runs, including the coupled model, would give incorrect results when run on more the 10 processors. The cause of this problem was tracked down to the ocean Fourier filtering code, which is done at the Polar Regions. The error occurred when the filtering done at the South Pole spanned more than one processor on the MPP grid decomposition. On Turing a load balancing version of the Fourier filtering had been used, which did not have this bug, unfortunately this code was written using the T3E specific SHMEM routines and couldn't be used on other machines. A decision was made to modify the code to use a load balancing scheme using the standard UM message passing library GCOM, instead of just fixing the bug, so that the performance of the UM would be improved when run with a large number of processors. In fact NEC had written some code to do this when they were benchmarking the UM for the Met Office, this was taken and used as the basis for the new code.

Several short runs of typical UM configurations were performed on Turing, Green, HPCx and Newton, to give a general idea of the
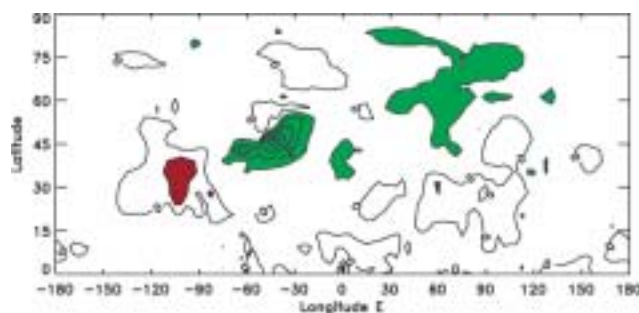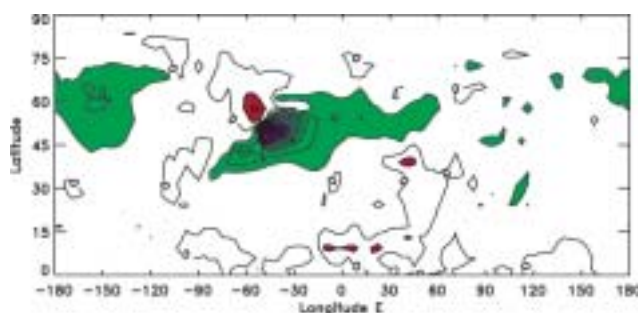
Figure 117.

Figure 118.

performance of the new machines compared to Turing. See Figure 114 to Figure 116 for the timings on different numbers of processors. One thing to note is the scalability of the runs on the faster machines (HPCx and Newton) depends to large extent on the amount of STASH diagnostics selected in the run. For the HadAM3 runs there was a large amount of diagnostics selected and scalability suffers as a result, on 8 processors STASH

processing accounts for about 40% of the run time and on 16 processors it account for more than 70% of the run time. The HadCM3 run has slightly less diagnostics selected and it scales slightly better than the HadAM3 run. The Newton results are preliminary and may be improved with further optimisation, especially the ocean results, which look very poor compared to the atmosphere.

A new coupled model for studying North Atlantic atmosphere-ocean interaction

Manoj Joshi (m.m.joshi@reading.ac.uk), David Marshall, Brian Hoskins and Maarten Ambaum, Department of Meteorology, University of Reading

Conventional ocean models used to study coupled atmosphere-ocean processes in the North Atlantic region have resolutions of O(1-2) degrees, which are insufficient to resolve phenomena such as western boundary currents and eddies, which are an important component of the system. We have developed CARGO (Coupled Atmosphere Reduced Gravity Ocean) in order to investigate the effects that resolving these smaller scales may have on climate.

The atmospheric part of CARGO is the IGCM (Intermediate Global Circulation Model), which has most of the complexity associated with a GCM, but with less computational cost (Forster *et al*. 2000). Here the IGCM is run at a resolution of T31, with 15 layers in the vertical up to approximately the 20 hPa level.

We have circumvented the computational problems associated with running the ocean at high resolution by sacrificing vertical resolution and global coverage. The oceanic part of CARGO is a reduced gravity shallow water model of the Atlantic with boundaries at 45S and 65N (Johnson and Marshall 2002), and presently has a resolution of 1/6 degree. This is equivalent to a grid box having longitudinal length 14 km at 40 degrees north, which is adequate to resolve the Gulf stream. Using appropriate lateral boundary conditions, a North-South flow can be set up along the western boundary, which represents the meridional overturning current (MOC). The dynamic depth of the ocean is 500m, while the thermodynamic depth is 100m.

As a first comparison of CARGO with other models, we have performed two model integrations: a control with a 17 Sv MOC, and another with the MOC turned off. Figure 117 shows the difference in ocean temperature between the control and the zero-MOC integration 10-20 years after the MOC has been turned off. The response is quite localised in the North Atlantic region when compared to other models (Dong and Sutton 2002).

We have repeated the above experiment, but with a horizontal diffusion increased 20 times to 1E4 m^2/s, mimicking the impact of using a lower, more usual, ocean resolution. The temperature response shown in Figure 118 is larger in amplitude and horizontal scale, and more similar to that in Dong and Sutton (2002). This suggests that the smaller response seen in Figure 117 may partly be because of the resolved small scales in CARGO.

In the future we intend to investigate these results more fully, as well as conduct other studies into the role of small-scale processes on the North Atlantic climate system.

References

Dong B-W and Sutton RT (2002): Geophys. Res. Lett., 29, 10.1029/2002GL015229.
Forster PM De F, Blackburn M, Glover R and Shine KP (2000): Clim. Dyn., 16, 833-849.
Johnson HL and Marshall DP (2002): J. Phys. Oceanography, 32, 1121-1132.

Figure 119. Each participant is supplied with a simple visualisation package (see following article by Heaps), allowing them to follow the development of weather patterns on their unique world. A more complex IDL based visualisation package is being developed to allow interested users to learn about the climate.

Figure 120. (above) Over 30,000 users registered within the first week from all over the world
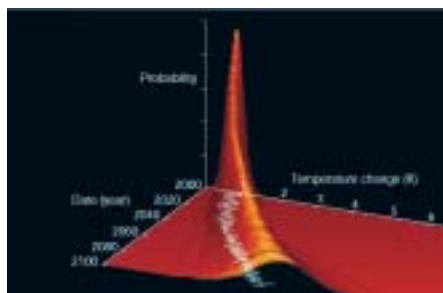

Figure 121. Results from the experiment will allow a fully probabilistic forecast of 21st century climate to be made.

climateprediction.net goes live!

S. Knight[1], T.Aina[1], M. Allen[1], C. Christensen[1], M. Collins[2], N. Faull[1], D. Frame[1], E. Highwood[3], J. Kettleborough[4] and D. Stainforth[1]
[1]AOPP, University of Oxford, [2]The Met Office, [3]The Meteorology Department, University of Reading, [4]The Rutherford Appleton Laboratory

The climateprediction.net distributed computing experiment was successfully launched at the BA festival of science in Salford and the Science Museum, on the 12th September. The launch attracted a huge amount of media interest and despite some initial technical glitches (we strained the JANET backbone on the night of the launch!), 30,000 users registered within the first week, from many countries across the world (although the UK, with almost 10,000 users, leads the way).

Funded by the Natural Environment Research Council and the Department of Trade and Industry, the project consists of a core of climate scientists, computer scientists and support staff based at the University of Oxford, the Open University and the Rutherford Appleton Lab., as well as affiliated scientists and development staff from a number of other institutions such as CGAM, the University of Reading and the Met Office.

The climateprediction.net project began in 1999, with a commentary article in Nature (Allen 1999) describing how a very large perturbed physics ensemble forecast could help quantify uncertainties in climate forecasts. By distributing hundreds of thousands of uniquely perturbed versions of the Unified Model to the general public around the world to run on home, school and work PCs, the project aims to produce the most comprehensive probability based forecast of 21st century climate (see also Allen 2003).

The experiment aims to "Improve methods to quantify uncertainties of climate projections and scenarios, including long-term ensemble simulations using complex models", identified by the IPCC in 2001 as a high priority. Climateprediction.net is working closely with the Hadley Centre QUMP project, and hopes to be able to contribute to the IPCC's Fourth Assessment Report in 2007.

As David Stainforth presented at the Royal Meteorological Society's recent conference in Norwich, results from the beta test (in itself probably the largest GCM experiment to date) look very promising.

The educational side of the project is now being developed. The Open University will be running a short course on climate prediction based on the project. To facilitate this, Andy Heaps at CGAM has been developing an IDL user interface, which will be supplied to any interested participant without cost. This should also be an extremely useful resource for schools, allowing the experiment to be used for coursework in a range of subjects.

To join the experiment or find out more, go to http://www.climateprediction.net/.

References

Myles Allen (1999), Do it yourself climate prediction, Nature, 401, pp642.
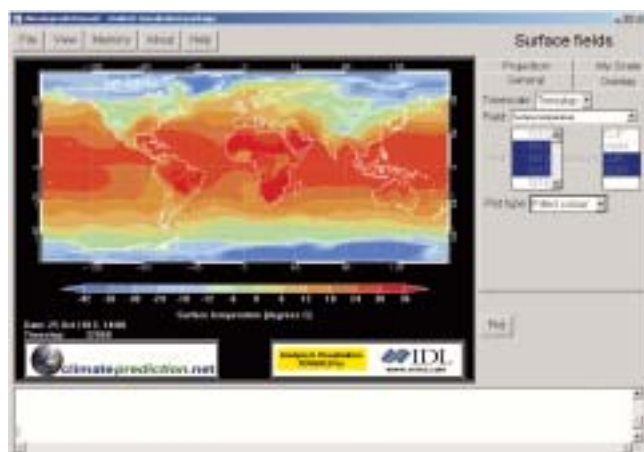Myles Allen (2003), Possible or probable?, Nature, 425, pp242.

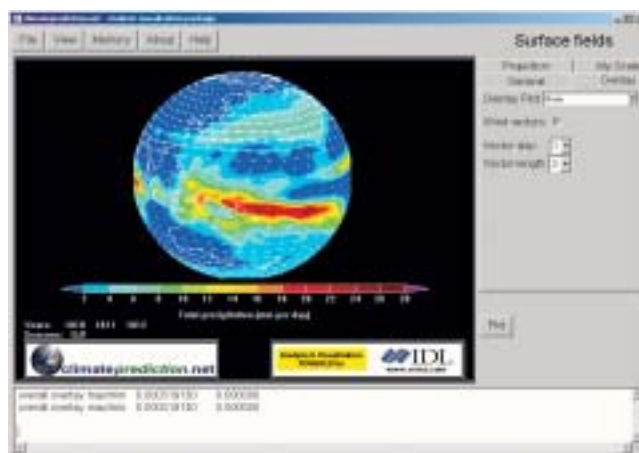Figure 122. The timestep surface temperature for 2pm on the 25th October 1812.

Figure 123. Precipitation and winds for the DJF season for the years 1810 – 1812.

Development of a student visualization package for the Open University and schools

Andy Heaps (andy@met.rdg.ac.uk), NCAS Centre for Global Atmospheric Modelling, Dept. of Meteorology, University of Reading.

A visualization package is being developed for use by schools and college students to allow simple research projects to be undertaken using the output of participants' runs under the climateprediction.net experiment. IDL (Interactive Data Language) was the natural choice of graphics language for this package because of its cross platform capabilities and extensive widget groups allowing a point and click style interface to be developed.

Data selections will be available on a timestep, seasonal and yearly basis. On these timescales the student will be able to plot surface, zonal, time-height and surface area average fields. Output

of data and images to files will be available, including on a timestep basis allowing the creation of movies.

Initially the package is being developed for the Windows platform as this is the platform that most students will have available. Porting the package to other platforms such as Linux, Solaris and Mac OSX will only entail the changing of a few lines of code in the file input/output section.

The plots and interface layout presented Figure 122 and Figure 123 are provisional, as beta testing has just started. An Open University short course using this package is scheduled to begin in February 2004.

The development and application of a global model of aerosol processes (GLOMAP)

Dominick Spracklen, Kirsty Pringle, Ken Carslaw, Martyn Chipperfield, School of Environment, University of Leeds.

GLOMAP is a global aerosol microphysics and chemistry transport model within an existing offline CTM. GLOMAP aims to model all the processes affecting global aerosol size distribution and chemical composition from emission of aerosol to removal. It is designed to fill the 'model sophistication gap' between highly detailed box models and simpler aerosol parcel models.

GLOMAP will be used to examine the processes controlling the global aerosol lifecycle, representing simultaneously the effects of microphysics, chemistry and long-range transport that cannot be achieved in a box model nor captured by necessarily simplified GCMs. We expect GLOMAP to be an important tool in support of field campaigns, as a benchmark model for developing parameterisations for GCMs and for identifying the key processes affecting aerosol radiative forcing.

GLOMAP is based on the existing 3-D chemical transport model, TOMCAT. The aerosol size spectrum is distributed over a moving centre geometric size bin structure. GLOMAP includes the major

aerosol processes in the atmosphere: nucleation, condensation, hygroscopic growth, coagulation, dry deposition, below-cloud scavenging, in-cloud nucleation scavenging and also the chemical transformation of sulfur species in clear air and in clouds and the emission of sulfur species and primary emission of sea salt. Chemical oxidant fields are calculated offline using 'full' tropospheric chemistry TOMCAT simulations. At present GLOMAP treats sulfate and sea salt aerosol in a single distribution. Further development of GLOMAP will allow multi component aerosol to be treated.

Our first global simulations over the period of one month, spun up from an aerosol-free atmosphere, are encouraging (Figure 124 and Figure 125). Simulations are on a 2.8 x 2.8 degree grid, with 19 levels (surface to 10hPa) and 20 aerosol size bins spanning dry radius of approximately 2nm to 25 micrometres. Initial comparisons with aerosol climatologies show reasonable agreement with measurements. The results show peak aerosol
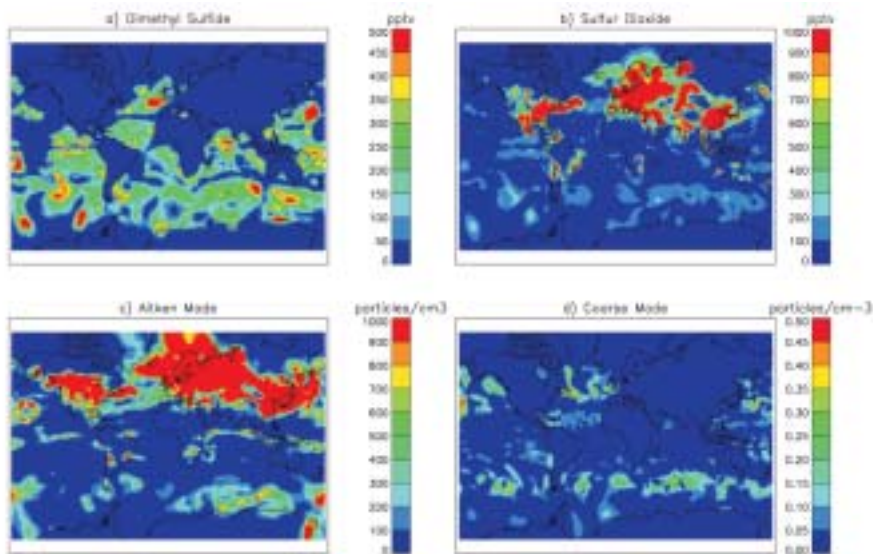
Figure 124. Simulated surface global fields of a) dimethyl sulfide (pptv), b) sulfur dioxide (pptv) and aerosol number density (particles cm-3) c) aitken mode particles and d) coarse mode particles.
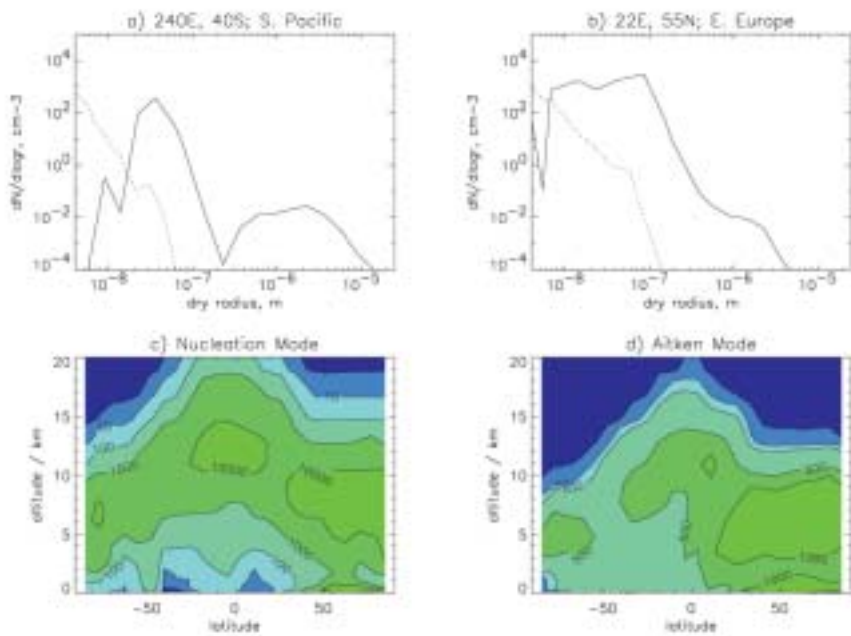

Figure 125. Simulated number size distribution over a) the South Pacific b) Eastern Europe. Bold line is surface concentration, dashed line at 10km altitude. Zonal mean (particles cm-3) as a function of altitude and latitude of c) nucleation mode and d) Aitken mode particles.

nucleation in the upper troposphere and transport downwards, as has been observed. The aerosol size distributions show evidence for characteristic aerosol classes, such as nucleation mode, accumulation mode and coarse mode. An important part of our work will be to test our understanding of how these canonical aerosol classes arise in the atmosphere.

GLOMAP will be tested against a wide variety of aerosol gas precursor and aerosol measurements including aerosol climatologies and aerosol field campaigns. Initially GLOMAP will be used to investigate the effect of nucleation, aqueous chemistry and wet deposition on global aerosol distribution.

Interactions between the Numerical Modelling of Tracer Advection and Chemistry Reactions in Global Atmospheric Models

B.M.-J. Walker and N. Nikiforakis, Laboratory of Computational Dynamics, DAMTP, University of Cambridge (Blandine.Walker@centraliens.net)

The accuracy of the chemical output of Global Atmospheric Models (GAMs) is greatly tributary to the choice of the numerical techniques for the advective transport of chemical species in these models (see Rood, 1997). If improving the modelling of advective transport is essential to the physical relevance and accuracy of

GAMs results, a deeper understanding of the profound numerical interactions between the different algorithmic parts of a GAM is fundamental for the interpretation of these results. The specific challenge we set ourselves for this project was therefore to investigate the coupling mechanisms between simple chemistry
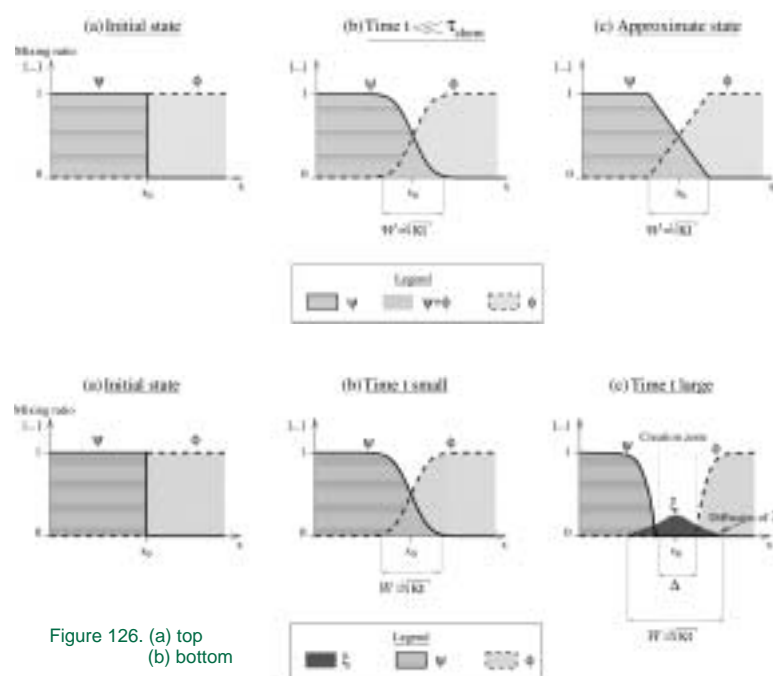
Figure 126. (a) top
(b) bottom

field, with initially complementary step distributions for Φ and Ψ and no Ξ (see Figure 126a) and with $Da_2^{num} \ll 1$, a simple scaling analysis suggested that the overall quantity of Ξ increases proportionally to $\Delta x^{1/2} t^{3/2}$ approximately, where Δx represents the discretisation cell size and t, time. On the other hand, a similar analysis carried out for the same problem albeit with $Da_2^{num} \gg 1$ indicated the apparition of a two-phase behaviour: for $t \ll \tau_{chem}$, the same law in $\Delta x^{1/2} t^{3/2}$ was approximately followed by the total quantity of Ξ produced, whilst this increase was found to follow a $\sqrt{\Delta x t}$ law for large times ($t \gg \tau_{chem}$), and the scaling analysis further suggested the apparition of a 'creation zone' for Ξ (see Figure 126b) where the mixing ratios of Φ and Ψ are both close to zero; the width W of this creation zone was further estimated through dimensional analysis. These analysis results were confirmed by (numerical) experimental evidence.

We thus finally considered a simplified ozone-loss problem over the globe: the trace chemical composition of the stratosphere was reduced to four species ClO, NO_2, $ClONO_2$ and O_3 (see Anderson *et al*., 1989, Dessler *et al*., 1996, for example): we were therefore confronted by a problem of competing chemical reactions (Dessler, 2000). The concentrations for these species were simplified too, so that the mixing ratios of ClO, NO_2 and O_3 were prescribed as 1.5 ppbv, 0 and 2000 ppbv respectively in the Polar Vortex, and as 0, 5 ppbv and 2000 ppbv respectively outside the Vortex, as illustrated in Figure 127 (see Anderson *et al*.,1989, Brune *et al*., 1989, Proffitt *et al*., 1990).

Solutions for this problem, corresponding to different times and resolutions, were computed with a CTM based on a previous model developed in the CAS, in Cambridge. Numerical diffusion was found to profoundly affect the ozone loss rate (see fig:ozone). A comparison between the qualitative and quantitative results suggested by the – now complex – scaling analysis for this problem and the computational observations confirmed again the validity, both of the formalism chosen to account for the numerical diffusion inherent to advection schemes and of the dimensional and scaling analysis following. This approach revealed the development of genuine coupling and feedback processes between the advective and the reactive parts of GAMs, as well as their vital importance in explaining the observed behaviour of chemistry budgets as discretisation choices or time change.

More complex chemistry will be included in our CTM for our future investigations; we also intend to extend our study to numerical schemes found in other GAMs used in UGAMP, such as in TOMCAT or SLIMCAT, for instance.

reactions and numerical advection techniques, and to quantify their impact on GAM results for simplified chemistry scenarios.

Four principal ways by which numerical advection schemes can influence the chemical output of Chemistry and Transport Models (CTMs) have been identified: data averaging within computational cells – an unavoidable side-effect of space discretisation – numerical mixing consecutive to the inherent numerical diffusion of advection schemes, inaccurate estimation of the surface area or interface length of the contact surfaces between reacting species' distributions and distortions of pre-existing correlations between the mixing ratios of chemical species (see Plumb & Ko, 1992, and Thuburn & McIntyre, 1997, for example) can all contribute to changes in the creation or loss rates and budgets of chemical tracers (see Walker, 2003).

The issue of numerical diffusion was selected for in-depth investigation, through the exploration of coupling mechanisms, the quantification of the resulting straying from exact estimates of the physical budgets considered, and the study of the behaviour of these errors with time advances and resolution improvements.

To understand the coupling developing between the scheme-induced numerical diffusion and chemical reactions, a parallel has been drawn between diffusive tracer transport equations and the expressions formalising the equations truly solved by the numerical advection schemes considered, numerical diffusion included, also known as the *modified equations* (see J.D. Anderson, 1995 or Laney, 1998, e.g.). Based on these modified equations, a numerical *second Damköhler number* Da_2^{num} expressing the ratio of the characteristic time for numerical diffusion τ_{chem}, to the characteristic time for a given chemical reaction was defined (cf. Oran & Boris, 2001 for example).

Reformulating the modified conservation law for a given numerical advection scheme and for different reacting species revealed the emergence of very different regimes of coupling, depending on the values found for Da_2^{num}. For instance, for the simple three-species problem $\Phi + \Psi \rightarrow \Xi$ in a given velocity

References

J.D. Anderson Jr., Computational Fluid Dynamics, McGraw-Hill International Editions, Mechanical Engineering Series, 1995.

J.G. Anderson, Free Radicals in the Earth's Atmosphere: Measurements and Interpretation, Ozone Depletion, Greenhouse Gases, and Climate Change Proceedings of a Joint Symposium, Chapter 7, pp.56-65, 1989.

J.G. Anderson, W.H. Brune and M.J. Proffitt, Ozone Destruction by Chlorine Radicals in the Antarctic Vortex: the Spacial and Temporal

Chlorine oxide (ClO) and nitrogen dioxide (NO2)
on 24 January 1992 at 02.00 GMT.
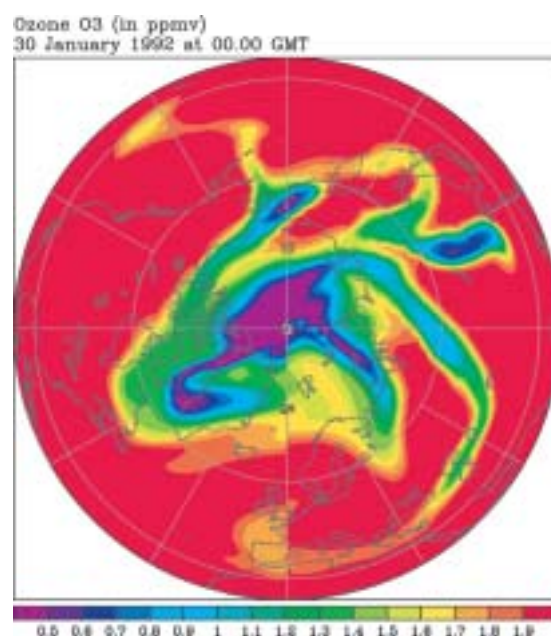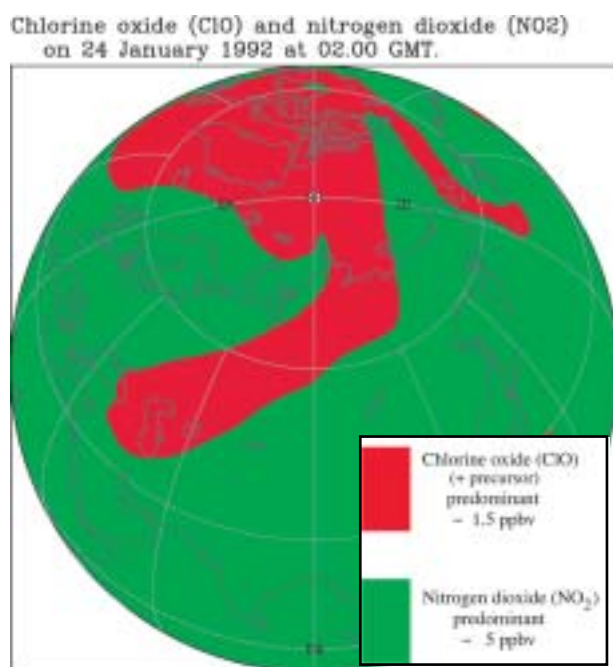
Ozone O3 (in ppmv)
30 January 1992 at 00.00 GMT

Figure 127.

Evolution of Anticorrelation based on in situ ER-2 Data, Journal of Geophysical Research (JGR), Special Issue on Antarctic Ozone, 1989.

J.G. Anderson, W.H. Brune, S.A. Loyd, W.L. Starr, M. Loewenstein and J.R. Podolske, Kinetics of Destruction by and within the Antarctic Vortex: an Analysis based on in situ ER-2 Data, JGR, Special Issue on Antarctic Ozone, 1989.

W.H. Brune, J.G. Anderson and K.R. Chan, In situ Observations of in the Antarctic: ER-2 Aircraft Results from 54°S to 72°S Latitude}, JGR, Special Issue on Antarctic Ozone, 1989.

A.E. Dessler, S.R. Kawa, A.R. Douglass, D.B. Considine, J.B. Kumer, A.E. Roche, J.L. Mergenthaler, J.W. Waters, J.M. Russell and J.C. Gille, A Test of the Partitioning between and using Simultaneous UARS Measurements of and, JGR, 101, pp.12,515-12,521, 1996.

A.E. Dessler, The Chemistry and Physics of Stratospheric Ozone, Academic Press AP, International Geophysic Series, Volume 74, 2000.

C.B. Laney, Computational Gasdynamics, Cambridge University Press, 1998.

E.S. Oran and J.P. Boris, Numerical Simulation of Reactive Flows, CUP (First Edition: 1987, Elsevier Science Publishing), 2001.

R.A. Plumb and M.K.W. Ko, Interrelationships between Mixing Ratios of Long-Lived Stratospheric Constituents, JGR, 97, pp.10,145-10,155, 1992.

M.H. Proffitt, J.J. Margitan, K.K. Kelly, M. Loewenstein, J.R. Podolske, and K.R. Chan, Ozone Loss in the Arctic Polar Vortex Inferred from High-Altitude Aircraft Measurements, Nature 347, 1990.

R.B. Rood, Numerical Advection Algorithms and their Role in Atmospheric Transport and Chemistry Models, RG, 25, 1987.

J. Thuburn and M.E. McIntyre, Numerical Advection Schemes, Cross-Isentropic Random Walks and Correlations between Numerical Species, JGR, 102, pp.6775-6797, 1997.

B.M.-J. Walker, The Impact of Computational Techniques on Tracer Interrelations in Atmospheric Chemistry and Transport Models, Ph.D. thesis, 2003.